NPS AA-92-001CR

NAVAL POSTGRADUATE SCHOOL
Monterey, California

CONTRACTOR REPORT

AN EXPERIMENTAL AND ANALYTICAL STUDY OF TIP CLEARANCE EFFECTS IN AXIAL FLOW COMPRESSORS

Ian N. Moyle
Exotech Pty. Ltd.
2625 Cabot Court
Fremont, CA 94538-1405

December 1991

Approved for Public Release; Distribution is unlimited

Prepared for: Naval Air Systems Command
Washington, D.C. 20361

and

Naval Postgraduate School
Monterey, CA 93943-5000

NAVAL POSTGRADUATE SCHOOL
Monterey, California

RADM R. W. WEST, JR.
Superintendent

H. Shull
Provost

The reported study was carried out in large part at the Turbopropulsion Laboratory of the Naval Postgraduate School. The work was initiated under the sponsorship of Naval Air Systems Command, as part of the Air-Breathing Propulsion Research Program under the cognizance of George Derderian (AIR 931E), and was completed under the NPS Direct Funded Research Program. The project was carried out in association with the University of Tasmania, Australia, where the author was a Ph.D. candidate under the co-supervision (with Professor R. P. Shreeve) of Dr. G. J. Walker. Dr. Walker was the Naval Air Systems Command Research Professor in Aeronautics at NPS in 1986.

This report was prepared by:

I. N. MOYLE
Exotech Pty. Ltd.
2625 Cabot Court
Fremont, Ca 94538-1405

Reviewed by:

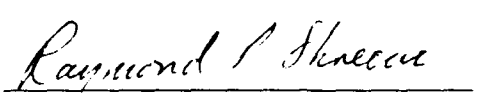

RAYMOND P. SHREEVE
Professor
Department of Aeronautics
and Astronautics

D. J. COLLINS
Department of Aeronautics
and Astronautics

Released by:

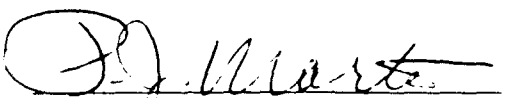

PAUL [illegible]
Dean of Research

AN EXPERIMENTAL AND ANALYTICAL STUDY OF TIP CLEARANCE EFFECTS IN AXIAL FLOW COMPRESSORS

by

Ian N. Moyle, B.Eng.(Hons.), M.Sc.(Eng.)

Department of Civil and Mechanical Engineering

Submitted in fulfillment of the requirements for the degree of

Doctor of Philosophy

University of Tasmania

December, 1991

I hereby declare that this thesis contains no material which has been accepted for the award of any other higher degree or graduate diploma in any tertiary institution and that, to the best of my knowledge and belief. this thesis contains no material previously published or written by another person except when due reference is made in the text of this thesis.

Ian N. Moyle
December 15, 1991

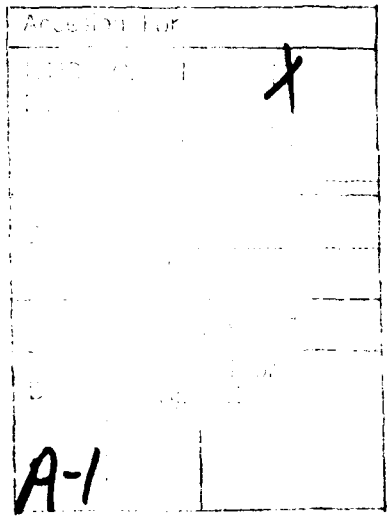

Abstract

An analytical and experimental study of the performance changes and flow effects of rotor tip clearance variation in axial flow compressors is presented. The analyses demonstrate that previously unrecognized loss characteristics and flow behavior trends can be identified in a wide range of published tests of clearance effects. The performance and flow data are correlated at constant power conditions or non-dimensionally in terms of the test compressor's geometry and wall flow conditions to observe the trends.

Flow field changes caused by increasing the tip seal clearance of a low speed, large scale axial compressor having a symmetric velocity diagram were examined experimentally. The measurements were made at several clearances for one rotational speed. Synchronized blade-to-blade measurements of case wall static pressure and skin friction under the rotor tip of the second stage were collected.

The detailed surveys showed the tip local blade-to-blade flow pattern to be dependent on the rotor blade's position relative to the upstream stator. Preliminary case wall skin friction traces showed a similar dependence and indicated a region of stagnant flow several blade thicknesses wide exists on the case wall beside the blade suction side. The stagnant region's position corresponds with a minimum wall static pressure trough standing off the blade suction surface. The blade loading at the tip was found to alter its form depending on the passage throughflow, stator relative position and tip clearance height. Detailed measurements and correlative results are presented.

The detailed measurements were evaluated in the context of the flow mechanisms causing the efficiency losses, the models typically used to quantify tip clearance effects, computations of the tip local flow field and the possibilities for improved tip local blade and case wall geometry design for axial flow compressors.

Acknowledgements

Many people have assisted this program of research. The author especially wishes to mention the efforts of the Technical Staff of the Naval Postgraduate School at Monterey. The assistance and interest of K. Harris, and J. Morris (blade fabrication and testing), P. Hickey, D. Harvey, R. Raymaker, G. Middleton, and T. Moulton (machining and models), T. Dunton, J. King, and A. McGuire (systems and instrumentation) and M. Odell and T. Best (builds and testing) are gratefully acknowledged.

The provision of tabulated performance data on previously published stage tests by Prof. M. Inoue of Kyushu University, Japan and Drs. D. C. Wisler and B. F. Beacher of the General Electric Company, United States is also acknowledged with thanks. Their data are included in the analysis of Part 2.

This work was conducted as part of an axial compressor tip clearance research study at the United States Naval Postgraduate School, Monterey, California sponsored by the United States Naval Air Systems Command, Air Breathing Propulsion Research Program under the cognizance of G. Derderian. The author wishes to express his particular gratitude to Prof. R. P. Shreeve of the Naval Postgraduate School and Dr. G. J. Walker at the University of Tasmania for their instruction, criticism, encouragement and patience. My final thanks go to Valerie Fintel-Moyle, who survived the experience.

Table of Contents

List of Figures

List of Tables

Nomenclature

a	axial chord
A	annulus or section area
AA	aspect ratio based on axial chord (b/a)
AR	blade aspect ratio
b	blade height or span
c	constant or chord
$c^{\#}$	friction velocity, (τ_w/ρ)
C_f	wall friction coefficient, $\tau_w/1/2\rho(\Phi U_t)^2$
C_L	lift coefficient
C_{Di}	induced drag coefficient
C_D	drag coefficient
C_{10}	camber (NASA convention)
C_p	specific heat at constant pressure
C_P	pressure coefficient
C_{pu}	pressure coefficient
D	diffusion factor
D_{eq}	equivalent diffusion factor
e	clearance gap
e"	effective clearance gap
Ek	Ekman Number, $\mu/(\rho R^2\Omega)$
F(.)	correlation
f(.)	function
f	friction, friction force
g	staggered spacing
G_w	functional dummy for casing treatment parameters
G^*	$AR/(1\text{-}HR)$
HR	hub to tip radius ratio
$\underline{i}$	unit vector
L	lost work rate
m	mass flow rate
M	torque coefficient
n	exponent depending on model
P	power coefficient
p	pressure static
P	pressure total (' relative total)
P	shaft power coefficient
q	dynamic pressure
r	radius of axisymmetric stream surface
$r^{\#}$	theoretical degree of reaction
R	radius ratio (r/rt)
R	tip radius
R	gas constant
R_u	Reynolds Number term, $\rho U_t c/\mu$
s,S	entropy
s	blade spacing or pitch
t	profile section thickness
T	temperature
Ta	Taylor Number
u	velocity dummy term (V_a)
U	wheel velocity on stream surface

v	specific volume
V	velocity in absolute frame
W	velocity in relative frame
WS	wall shear factor ($1/2\ \Phi^2\ C_f\ R_u\ AR/(1 - HR)$
x	distance in circumferential or tangential direction
x	profile chordwise distance
X	work coefficient
X	work coefficient, Pwr/Φ
y	distance radially inward from case wall
y	profile thickness distribution
z	axial distance
z	profile leading or trailing edge radius
Z	number of stages

Greek Symbols

α	flow angle from axial or skew, absolute frame
β	flow angle from axial, blade relative frame
Δ	incremental change in a quantity
δ^*	displacement thickness
ε	ratio of drag to lift (C_D/C_L)
ϕ	flow pitch angle
Φ	section average flow coefficient ($m/\rho A U_t$)
γ	stagger angle,direction from axial, absolute frame
η	adiabatic efficiency, $\Phi\Pi/P$
φ	flow coefficient on an axisymmetric surface, V_a/U
μ	viscosity
Π	pressure rise coefficient, $\Delta p/\rho U_t^2$
ν	kinematic viscosity
ρ	density
σ	blade solidity
$\Sigma[\ ]$	integration operator
τ	shear local
Ω	angular velocity, rotor
ω	loss coefficient $\Delta P/(P-p)$
ξ	profile camber angle

Other Symbols

$\surd$	square root
$\propto$	proportional to
∇	gradient operator
∂	partial differential operator
$\rightarrow$	approaches, tends to

$\|\alpha\|$	modulus, absolute value of α
^{o}	angle in degrees
?	data value could not be established

Subscripts

$_{a}$	in axial direction
$_{av}$	area averaged
$_{M}$	model scale
$_{F}$	full scale
$_{e}$	in tip gap
$_{m}$	at mid radius
$_{r}$	in radial direction, at arbitrary radius
$_{R}$	applicable to rotor
$_{S}$	applicable to stator
$_{s}$	streak line
$_{t}$	at tip radius
$_{w}$	at or on wall
$_{0}$	at zero clearance
$_{2D}$	two dimensional, planar or cascade blade element
$_{3D}$	three dimensional, radially varying or annular
$_{u}$	in tangential direction

Acronyms and Abbreviations

NPS	Naval Postgraduate School, Monterey, California
LSMSC	Low speed multistage compressor test facility
AEDC	Arnold Engineering Development Center, Tullahoma, Tenessee
NACA	National Advisory Council for Aeronautics (now NASA)
CC	Compressor characteristic surveys
RS	Radial or spanwise surveys
WP	Wall pressure surveys
WS	Wall shear surveys
HW	Hot wire spanwise surveys
B-B	Blade-to-blade
A42	Low flow coefficient throttle setting, ($\Phi = 0.60$)
54	Design flow coefficient throttle setting, ($\Phi = 0.64$)
53	High flow coefficient throttle setting, ($\Phi = 0.68$)
-A	Clearance A, ($e/b = 0.0025$, 1 Stage or $e/b = 0.0035$, 2 Stage)
-B	Clearance B, ($e/b = 0.006$, 2 Stage)

Introduction

Turbomachines use rotating components and flow deflection to transfer energy to or from a fluid. The typical machine consists of a rotor of many cantilevered blades which spins at high speed within a concentric casing. The flow effects of the small running clearance between the cantilevered blades and the casing are the primary concern of this study. The restriction on flow through the running clearance caused by the blade end and the adjacent wall is often thought of as a seal and the consequences of changing the clearance, blade end or wall are discussed in terms of sealing and its effectiveness. Often the wall consists of a hoop of abradable material and the blade tip end may be coated with a cutting compound. The entire assembly has been referred to as a seal in the present discussion. The seal clearance is considered to be an aerodynamic dimension of the blade or passage in this study, like chord or thickness, and its flow effects are considered accordingly. The running clearance is often referred to as the tip gap or tip clearance.

Changes in the dimension of this clearance on pumping capacity, thrust, power consumption or fuel usage can be very significant in terms of the turbomachine's overall performance. Generally speaking, the observed results of tip gap changes are the consequence of ineffective flow control between the moving and stationary parts of the machine. The stationary parts of the machine are usually the case (outer) and hub (inner) walls. Partial or complete rings or hoops of material which are sometimes attached to the blading are referred to as shrouds in the present study.

The study particularly addresses the influence of the clearance at the tip of an unshrouded rotor in an axial flow compressor and the degradation of compressor efficiency and pumping performance that it may produce. Motivation for the work lies in the strong effects that small tip clearance changes can have on the overall performance of aircraft gas turbine engines. The subject, however, is relevant to any unshrouded turbomachine.

Preceding research by other workers has, over a period of time, defined general features of the tip local flow and the typical magnitude of the efficiency decreases to be expected. The nature of the physical mechanisms causing the changes is by no means resolved, however, and there is still no generally accepted method of designing the outer span of the blade or the extremity at the blade tip or the case wall at the tip to account for the presence of the clearance gap. As a consequence, this study was initiated with an emphasis on increasing fundamental understanding of the local flow at a blade tip with a running clearance and how this flow influences the overall compressor performance. The format of the document and key aspects of the work are described below.

The investigation is discussed in seven parts. Part 1 introduces the subject and reviews the experimental and theoretical literature on the topic. The general applicability of the analytical tip flow models developed in earlier work was addressed due to their lack of consistent prediction, when applied, for the same geometry and flow conditions.

Part 2 presents analyses of two aspects of the tip clearance mechanism(s) or physical modelling problem. These analyses developed from examination of the literature and recognition that the published test data formed a database for exploration, identification and isolation of tip flow mechanisms over a wide range of conditions. Usually the published data are only used for validation of *analytical* models of the tip flow.

Attempts to use the data for mechanism identification have not previously been published. The result of this work is an extremely simple quantitative correlation of the change in compressor efficiency with a change in clearance when the compressor characteristic is mapped in terms of lines of constant power. However, more importantly the analysis shows that blade shapes and passage geometries, tested to date, do not influence the efficiency decreases. This is an important observation in the context of current research on end-bends and tailored blade profile sections. Such tip local designs are thought to hold promise of lower compressor sensitivity to tip clearance. This conclusion is then examined in the context of the passage secondary flow and the total pressure gradients that are typically observed when clearance is increased. The influences of rotational flow are considered and a new similarity parameter, developed in terms of a wall friction coefficient, throughflow, Reynolds Number and passage geometry, is shown to be a significant term in an expression for the wall local pressure gradient. The significance of the term, particularly regarding the contradictory tip local secondary flow results obtained by other investigators, is examined in the discussion.

Part 3 describes an experimental investigation of the tip clearance and tip local flow in the second stage of a multistage compressor and the data that were developed. This work extends the analytical themes in an experimental program and particularly emphasizes the blade-to-blade case wall static pressure patterns. These patterns are shown to depend on the position of the rotor blade relative to its upstream stator. Data of this type have not been previously available in the literature in the context of tip clearance flows. Major features of the flow were the tip unloading behavior, the location of the blade-to-blade pressure minimum some distance from the blade suction side and large fluctuations observed in the pressure gradient on the suction side of the rotor near the leading edge of the blade. The fluctuations occur as the rotor passes through a cycle of one stator pitch. These measurements introduce new considerations regarding the mechanisms of loss production associated with tip clearance changes. Measurements of case wall blade-to-blade skin friction, which delineated a region of stagnant flow extending into the passage from the suction side, also are presented in a preliminary form.

Part 4 discusses the experimental results obtained in the context of the observations made in the literature discussion (Part 1) and the analyses (Part 2). Part 5 summarizes the conclusions that were reached from the investigation.

Supporting information and references are set out in the remaining parts. Part 6 is a compilation of the references consulted and cited in the text. Part 7 comprises attachments and appended information related to the thesis. One area of concern in this study was the consequences of a wide range of blade passage geometries and flow conditions, found in practice, on the tip local flow field. A review of this subject is included in Appendix A. Appendix B describes the experimental program development, instrument calibration and computational aspects of the research program.

Part 1

Tip Clearance and its Literature

Aircraft gas turbines have a large number of locations where leakage of working fluid in the gas path can occur. The accumulated effect of the many leaks on power, thrust and fuel usage is substantial and usually detrimental in terms of overall engine performance.

A typical airbreathing engine is made up of five major component subsystems which act on the internal gas flow. The sequence and action of the subsystems consists of a deceleration of the gas in an inlet system, a compression of the gas, heat addition in a combustor, expansion of the hot and high pressure gas through a turbine and further expansion of the gas through a nozzle or power turbine. All of these components utilize seals to regulate the leakage of the working fluid within the subsystem. Most of the seals attempt to minimize leakage. However, under certain circumstances leakage may be desirable, so the technical issue, in a particular sealing situation, is how to use the working fluid to best advantage rather than solely leakage minimization or elimination.

Of these components, the performance of unshrouded compressors and turbines is known to be particularly sensitive to clearance changes at the blade tips. Consequently, compressor and turbine tip seal design continues to receive research attention. Many of the mechanical design and (transient) operational aspects of the tip seal arrangement are similar in both components. However there are major aerodynamic and heat transfer differences. From a flow viewpoint, these differences are fundamental. The dissimilarities start with the fact that compressors decelerate the flow whereas the flow accelerates in a turbine. The consequences of this difference are evident in the amount of turning the blade can achieve, the side of the blade (pressure or suction) which leads the blade motion and the characteristic blade section profiles for the rotor. Turbine blade section profiles are typically much thicker than those of a compressor and are able to support much higher flow turning. These aerodynamic differences alter the magnitude of the performance changes that occur with mechanically similar seal arrangements and cause the aerodynamic research to divide into two areas of study.

The present study is concerned with the aerodynamic effects of tip seal clearance in the compression subsystem. In compressors the flow decelerates and adverse pressure gradients can be large. In a decelerating flow, boundary layers typically thicken and flow turning is limited due to the onset of separation or stall. Compressors, therefore, have lightly cambered and slender blade section profiles which are able to support moderate turning. The type of compressor and blading arrangement is usually described by the amount of radius change of the flow path through the component and distinctions are made between radial, mixed and axial designs. Whenever compression efficiency is of paramount importance in the engine cycle economics, axial compressors tend to be favoured over mixed or radial compressors due to the typically higher efficiency of axial stages in series. Differentiating the tip effects in axial compressors from those in radial compressors is largely a matter of the seal geometry description, rather than any fundamental differences in the flow character or governing equations. Axial compressors normally involve many stages of blading with moderate changes in mean line radius through the machine. Radial compressors typically involve a very large radius change in a single stage. Because the machines differ so much in blading layout, radial compressor flows are often treated as a separate area of

aerodynamic study from those of axial compressors. In the present study the emphasis is placed on tip seal clearance effects in axial compressors.

A typical compressor layout for an axial design is shown in Figure 1.1-1. Small changes of tip seal clearance dimensions affect both efficiency and stall margin in such a configuration. A blade tip seal may exist at both the hub and case wall in unshrouded (cantilevered) designs. Minimum seal clearances mechanically depend on the cycle steady state design point, structural arrangement and material selection (Mahler 1972, Eqn. 1, p. 17).

In operation the tip seal clearances depend on the relative temperature differentials of the engine components under transient conditions, the materials used, forces on the engine structure and accumulated effects of assembly tolerances and operational wear and tear. The magnitude of the dimensional changes seen in operation can usually be determined with confidence from structural analyses and simulations. Because the compressor blade tip seal clearances vary during transient operation, the *sensitivity* of the compressor's efficiency and stall margin to small clearance changes is of particular interest. Correspondingly, an ability to design the blading, blade end or the seal wall to minimize the sensitivity, at a specified level of clearance, is highly desirable.

While stall sensitivity to tip clearance is of interest, in reality, stability or stall margin is a property of the whole compression system rather than an exclusively tip seal induced flow phenomenon. In the present study stall and stability will not be of primary concern. This study will concentrate on efficiency. The aerodynamics of the clearance's influence on efficiency very quickly reduces to understanding the detailed flows in and around the tip gap and their effect on the whole flow in the blading passages.

The subject of the present study is therefore rather narrowly defined in the context of an entire gas turbine engine flow path. However, small changes in the clearance of core compressor rotor tip seals have a very strong effect on overall engine performance. The study, therefore, will confine its attention to the aerodynamic effects of blade tip seal flows in axial compressors and how those effects may be used to advantage in improving compression efficiency.

1.1 Seal Clearance as an Aerodynamic Design Problem

From a cycle *design* and compressor operating point perspective, tip clearance enlargement lowers overall efficiency and poses a gas path design problem.[1] The performance impact of clearance changes is indicated in Figure 1.1-2. The figure shows the decrease in isentropic efficiency with pressure ratio for a compressor with a uniform clearance along its gas path. The decrease is shown over the typical range of efficiency decrement divided by gap-to-blade height ($\Delta\eta/\Delta(e/b)$) found in the literature. The impact of the sensitivities become more significant as pressure ratio is increased and the penalties associated with a high sensitivity design are pronounced. It has been generally accepted as a "rule of thumb" that increasing rotor tip clearance reduces compressor efficiency by approximately 1% for each 1% increase of gap-to-blade height (e/b). Freeman (1985, p. 2) points out that a 2% (e/b) change at this sensitivity is equivalent to the performance of one stage in a six stage machine. Operation at minimal clearances would appear to be aerodynamically desirable from this information, but the structural difficulties and costs of very small clearances begin to outweigh the aerodynamic gains. As a consequence, the design problem is directed toward minimizing the aerodynamic effects of a finite tip clearance through blade profile design, blade and case treatments, abradable seal strips and their related design improvements.

It is relevant to note that tip clearance is often uniform along sections of an axial compressor case wall while blade heights reduce with increasing pressure level. This results in tip seal clearance effects becoming more significant in the rear stages of the high pressure compressor due to the relative enlargement of the gap with respect to the height (or working surface) of the blade. As a result, clearance effects constrain developmental growth of an engine. In order to boost (or grow) overall compressor pressure ratio it is usually cheaper to upgrade or add to the rear stages rather than develop a completely new compression system. As the rear stages are the most affected by tip seal clearance, gains in pressure ratio are increasingly offset by tip seal losses as pressure level rises.

A related problem exists for small engines at lower pressure ratios. Due to the mechanical difficulties of scaling running clearances to extremely small values in order to match the small blade heights, tip clearances become proportionally larger and their effects more significant in small engines. Mahler (1972, Fig. 2) provides gap-to-blade height data for different sized production engines and describes the seal scaling problem.

1.1.1 Means of Designing for Tip Clearance

The blading design problem associated with clearance effects reduces to knowing how to camber, twist, and distribute the loading on the outer blade span to control the flow.

---

[1] Seal clearance changes throughout an engine are known to cause significant shifts in overall performance. Of these shifts only a certain amount can be attributed to the tip clearances. For example, airline data on performance degradation suggest bypass engine specific fuel consumption (SFC) increases on the order of 1 to 1.5% per year. Of that, an unrecoverable 5 to 10% increase in SFC over a sequence of periodic overhauls is typical of the magnitude of all permanent degradation effects (Ludwig, 1978 p. 1-1). Military engines show a more rapid performance degradation in the between-overhaul interval. Ten percent thrust decrease in 800 hours is not uncommon (Moyle, 1979, Sec. 4.5). Between overhaul degradation can be attributed to a number of factors (hot section distress, blade erosion, fouling). After overhaul the unrecoverable performance is often related to less effective sealing in the gas path. This includes changes in tip clearance. The cost of these performance changes are not insignificant in terms of overall operating costs (Maki and Moyle, 1978 p. 3-30) and encourage continued interest in tip clearance and leakage control.

A method is required, for a clearance variation range, that can define a blade shape which produces minimum end wall losses and a desirable outflow angle distribution from the blade row. A solution to this problem is preferable in a closed (design) form. Generally speaking, however, there is no known way to predict the loss and outflow analytically. Consequently, a proven (analysis) method to reliably predict blade-to-blade distributions of loss, velocity, and flow angle near the wall from blade section profile data would be a substantial advance over current methods. Without such an analysis method, design development relies on experiment and empiricism and, more recently, simulation.

It is pertinent to note that the order of magnitude of clearance induced losses is similar to that measured for boundary layer thickness variations and casing treatments. Unfortunately, this implies that it is not an easy problem to isolate the clearance effects in an informative way or disassociate them from the particular compressor arrangement in which they are observed. It also implies that loss modelling can be approached from several viewpoints. Approaches to analyzing and designing for tip clearances have generally focussed on two major activities in recent years:

Experiments or Testing The issues of isolation and experimental control in simulating the stage flow, especially near the case walls, has emphasized the concept of "repeating-stage" testing in tip clearance research. In this technique several (usually two) stages are required to produce inflow profiles that are representative of the real flow the stage experiences in a compressor. The physical basis for the repeating-stage concept is shown in Figure 1.1-3. If measurements are made in the third stage, with the expectation that they will be representative of an embedded stage flow, it is also usually necessary to have a following stage to establish a repeating exit condition. Performance measures for the blading, when embedded, can then be developed (on average) from the repeating-stage test performance. By comparing the performance measures for different stage designs in such a standard repeating-stage arrangement, the best or better designs can be identified. General Electric four stage test data (Wisler, 1985) in Figure 1.1-4 show the magnitude of clearance change effects on pressure rise and efficiency observed in a *repeating-stage* test. The data of Fig. 1.1-4 also show a very substantial decrease in stage range as clearance increases.[2]

Flow Field Simulation Computational solutions for the complete flow in a turbomachine stage are increasingly being used for design insight into the flow field. Implementations of the Navier Stokes equations using interacting grids or similar schemes are typical examples. These solutions can provide very detailed pictures and representations of the flow's behavior. Unfortunately, the computational method's utility depends, to a large extent, on the accuracy of the turbulence models for the local flow regime and geometry.[3] The turbulence models are, in turn, usually geometry sensitive, so it is be premature to conclude such computations will always be able to produce reliable end wall loss predictions for untested design geometries. However, the computational methods exist, as viable tools, and provide qualitative and

---

[2] There are a number of counter observations to this trend reported in the literature. The results of McDougall (1989, Fig. 1) show a 1.2% clearance to chord gap having better range than a sealed tip, 0.5% and 3.0%. Freeman (1985, p. 7.3) discusses (the same) or similar results.

[3] While the viscous influences are of second order importance in terms of the pressure distributions in well ordered flows, such as at mid-passage, they have a first order effect on loss predictions or estimates for the profile. Because pressure distributions can be estimated reasonably well from potential flow methods a major incentive for Navier Stokes computations is to calculate the losses comprehensively and accurately. In corner flows where there are interacting shear layers, the Navier Stokes codes, with robust turbulence models, may be required just to calculate the pressure distributions.

increasingly quantitative insight regarding the whole flow field and how it is influenced by tip leakage or seal dimensions.

1.1.2 State of the Art

An overall breakdown of the factors contributing to compressor inefficiency was proposed by Rains (1954) and is shown in Figure 1.1-5. Considerable effort has been expended since that time to refine our understanding and design control of the mechanisms that produce these flow zones or effects. Progress since 1954, however, has been modest in terms of comprehensive modelling or global flow description. For example, in 1982 Robinson, regarding the tip clearance loss models, stated that;

> "The published, semi-empirical, attempts at correlating the efficiency loss were all found inadequate in the light of the data collected in this report".

In terms of the flow field, Chen, Greitzer, Tan and Marble (1990), observed that;

> "There is little need to give a detailed background on the flow in turbomachinery end wall regions. It is well known that: 1) the fluid mechanics of the end wall region are critical in developing performance prediction methods and 2) *in spite of over forty years of research on this topic, the flow in this region is not very well understood.*"

Commenting on the models, Senoo states in his 1990 paper;

> "In 1987, the present author reviewed the literature on the tip clearance and he was quite embarrassed on the inconsistent presentations of the tip clearance loss by different authors. ... These different relations have been derived based on different hypotheses on the mechanics of pressure loss due to the tip clearance. *Obviously all of these equations cannot be correct, but all of these empirical equations are widely used by adopting empirical correction coefficients and by limiting the range of application to near the design condition.*"

Dissatisfaction with the consistency, or predictive capability of the prior models is well documented in the tip clearance literature. Thus, while the sensitivity of efficiency and pressure rise to tip clearance levels have been known for many years, the source(s) and mechanism(s) of the loss increase have not been captured in a widely accepted model. Several mechanisms have been proposed to explain the flow effects and efficiency changes observed. These are discussed in more detail in the following section. The fact that several competing propositions based on fundamentally different mechanisms are used as a basis for predicting the effects observed, in itself, indicates that our understanding of the problem is not complete.

Features

A. Minimized Seal Cavities

B. 3 Tooth CDP Seal

C. Dovetail Sealing

D. Recessed Rotor Blade Tips

E. Active Clearance Control

F. Customer Bleed

G. Start Bleed

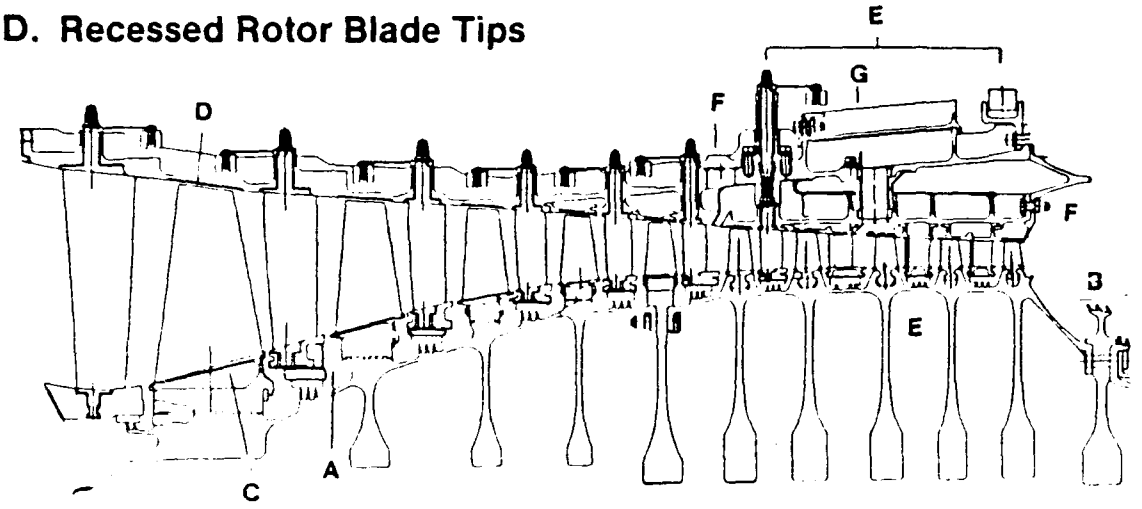

Fig. 1.1-1 A typical multistage axial compressor design (from Wisler (1985, Fig. 9)) showing the tip clearance (D), active clearance control region (E) and other features of a modern design.

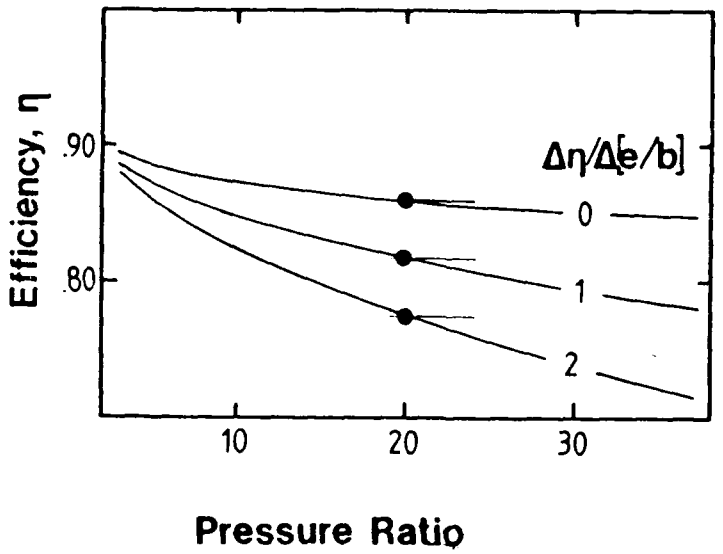

Fig. 1.1-2 Changes in compressor efficiency as a function of pressure ratio showing the impact on efficiency due to increased sensitivity to tip clearance, $\Delta\eta\%/\Delta(e/b)\%$ (from Moyle (1988)).

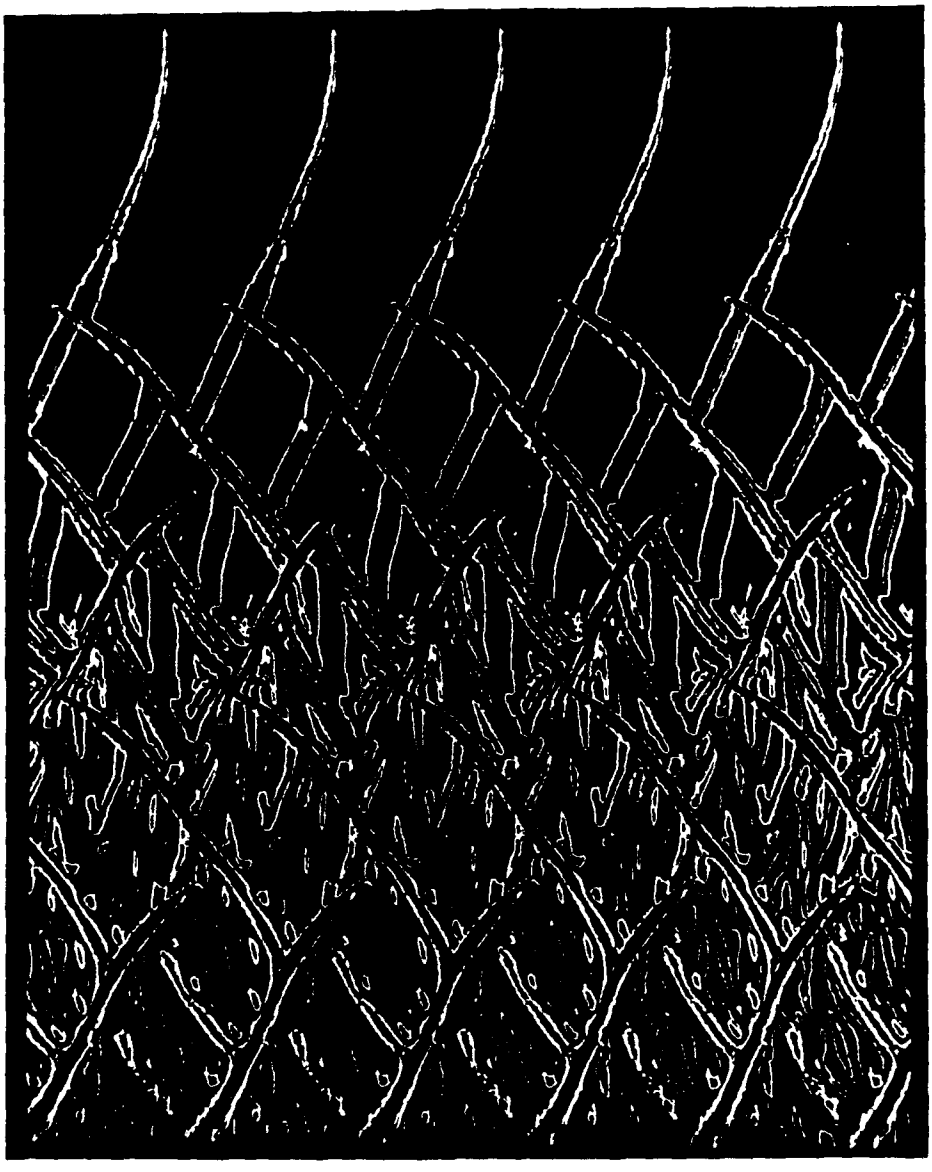

Fig. 1.1-3 A two-dimensional computational prediction of the interaction of the wakes on the mean line of a multistage compressor showing the differences in the flow field in the first and second rotors. Reprinted with permission from Gundy-Burlet et al. (1989).

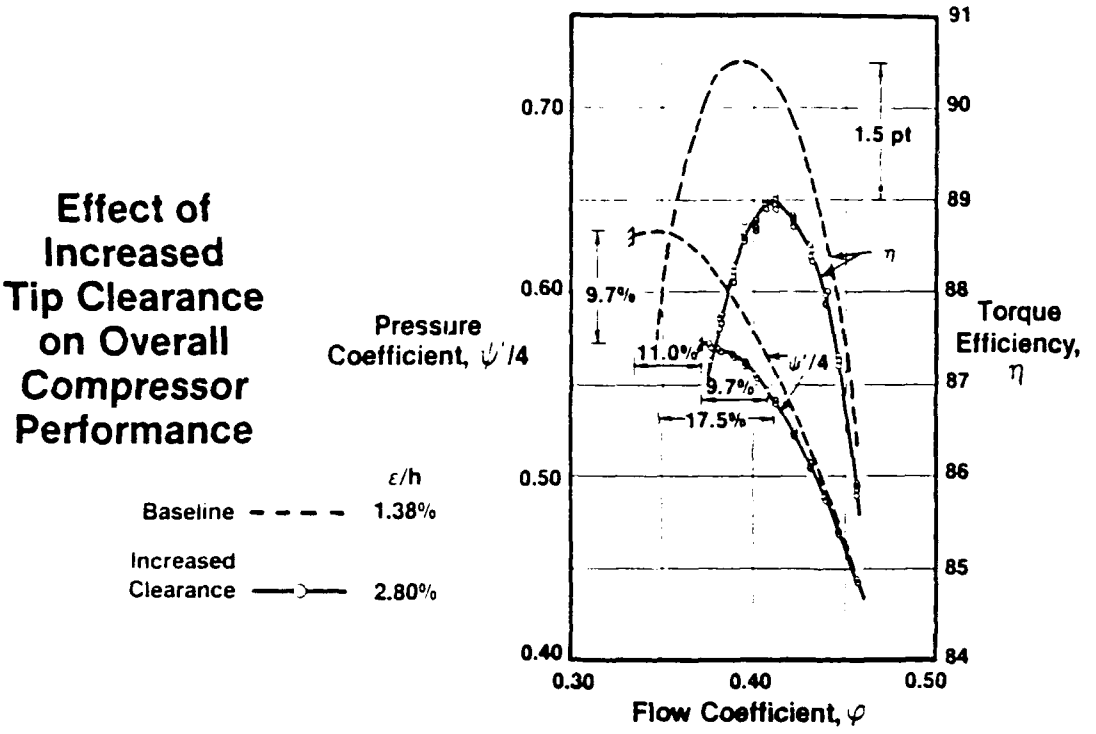

Fig. 1.1-4 The magnitude of typical tip clearance gap effects on the characteristics of a stage tested in a repeating stage configuration (from Wisler, (1985, Fig. 9)). The data show an efficiency decrease and a decrease in stall margin.

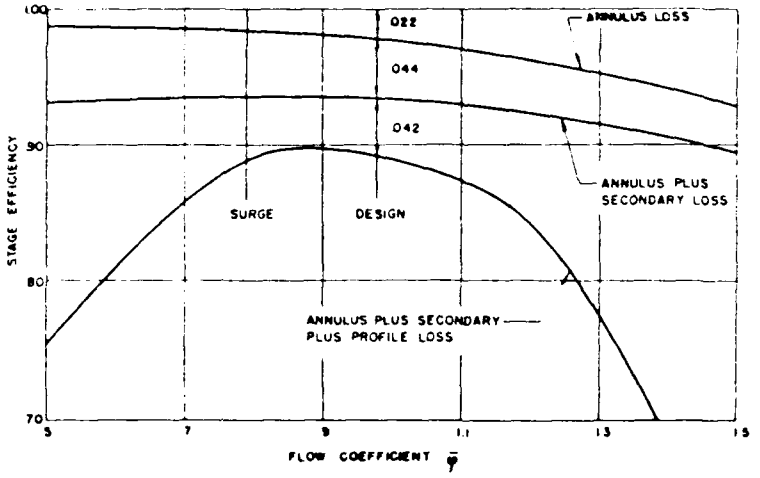

Fig. 1.1-5 Approximate breakdown of the factors affecting compressor efficiency by Rains (1954, Fig. 2). Tip clearance changes typically affect the zone of secondary loss.

1.2 Conclusions of Previous Research

Previous basic research of the tip seal flow has led to a number of fundamentally different methods of describing the significant flow features at or near the tip. These descriptions have developed over a period of time and are compared in several reviews. Such reviews, include those of Reeder (1968), Peacock (1981, 1982, 1983 and 1989) and discussions by Robinson (1982), Senoo (1987) and Schmidt et al. (1987). There is also an extensive compilation of relevant lecture material by Lakshminarayana, Booth, Wisler, Freeman and Hennecke in the von Karman Institute Lecture Series, No. 5 (1985). The descriptions of the mechanisms can be loosely grouped in three main categories:

(1) The arguments of Fickert (1946), Rains (1954), Vavra (1960, p. 380) based on Rains and Senoo (1986) are relevant if the dominant flow mechanism is considered to be one of momentum loss due to fluid passing (leaking) through the tip gap. The leakage, it is argued, is driven by the pressure difference across the tip due to the difference in pressure on the blade surfaces.

(2) The approaches of Betz (1926), Vavra (1960, p. 379) based on Betz and Lakshminarayana (1970) formulate a second approach based on the nature of the circulation shed at the blade tip. Lakshminarayana and coworkers (1982-1988) have evaluated such a description, both computationally and experimentally, in an extended series of papers and reports. This work stresses the additional influence of spanwise flows in the blade surface boundary layers. They were also concerned with the shed circulation. The circulation actually shed, the approach argues, is only part of the circulation at the tip. A component of the tip circulation is retained due to the viscous forces in the gap. The retention mechanism was proposed by Lakshminarayana and Horlock (1967). Loss increase or entropy production is attributed to viscous dissipation of the flow energy bound in the shed vortex. This process is augmented by spanwise blade boundary-layer flows. While this flow behavior seems to be readily demonstrated in cascades with stationary walls, firm proof of the same behavior in a compressor had been elusive until the recent work of Inoue (1986). Despite the clarity of the vortex detected by Inoue, it is not clear that the proposed flow pattern is universal.

The leakage and circulation descriptions argue for a flow pattern which involves a kinetic energy *loss* due to either fluid passing through a viscous or shear region under the blade and near the tip suction corner or increased induced drag due to shed circulation. The models derived from these descriptions generally depend on flow coefficient and passage geometry parameters, i.e., gap-to-blade height ratio, aspect ratio and solidity.

However *inherent loss* flow patterns are not the only ones that have been considered by previous researchers. There is evidence to suggest that there may not be a significant blade relative mass or energy transport of passage fluid from pressure side to suction side in the tip gap of a compressor rotor. Herzig, Hansen and Costello (1954, Fig. 39(a)) using smoke traces in a linear cascade showed conditions where no smoke went under the blade tip, at the wall, when the wall moved from pressure to suction side. These tests were conducted in a cascade of low stagger with a moving wall at laminar conditions and have to be treated carefully in extrapolating to a rotating machine; however, the smoke paths are often scraped up the pressure side of the blade and do not clearly pass through the tip gap. A well defined vortex on the blade suction side was also found to disappear when the wall was moving. This flow behavior is

indicative of a passage wall boundary layer influencing the tip flow more strongly than the passage throughflow velocity field.

(3) The third fundamental description of the flow effects of clearance changes concentrates on this case wall boundary layer influence on the tip flow. Researchers of clearance losses in compressors who stress case wall boundary layer flow patterns are Mellor (1953), Smith (1970) and Bettner and Elrod (1982). Smith (1970) applied a force defect correlation based on boundary layer thicknesses to large body of experimental data. The philosophy of his approach does not define the flow details but concentrates on flow effect correlation and predictive utility. Such descriptions do not inherently involve losses and resemble *blockage* in formulation. The correlation derived by Smith is expressed in terms of normalized pressure rise (i.e., degree of diffusion) and tip gap normalized by staggered spacing (g), see Fig. A.1-1, rather than conventional cascade passage dimensions.

The significant flow features influencing the inefficiency for each approach may be summarized as;

(1) Flow passing through or pressure driven leakage through the tip gap depleting the momentum of the pressure side throughflow and mixing with the suction side throughflow.

(2) Circulation shed at the tip gap forming a vortex which entrains and dissipates flow energy.

(3) Case wall boundary layers, thickened due to the lack of work on the fluid at the tip gap. The thicker layers reduce the overall stage performance.

These flow descriptions encompass the main thrust of the established arguments concerning the tip effect mechanisms. The concepts involved are fundamentally different and the arguments have never been superseded by a more comprehensive flow description which could reconcile them satisfactorily.

1.2.1 Approach To The Literature Discussion

After considering the large body of previous work and the divergent flow mechanism descriptions which resulted, the style and approach of much of the previous work was not adopted for the present study. Many of the earlier studies followed a somewhat fixed approach. Typically, the investigator proposed a flow pattern for either the flow in the tip clearance gap or for the secondary flow adjacent to the gap. The proposed flow pattern was usually based on observations of the flow field in a device which represented a compressor stage in some way. This proposed flow pattern was then attributed to one or more mechanisms which were approximated in a model. The model typically accounted for the main parameters which were expected to effect the proposed flow pattern. The investigators most frequently attempted to predict loss or efficiency changes associated with clearance gap changes. The model was usually calibrated and shown to be in reasonable agreement with a limited selection of experimental data.

Over a period of time, the tendency of previous investigators to select a particular aspect of the flow pattern, model and evaluate has led to a large number of tip loss models and algorithms. These many models are based, however, on a relatively small

number of mechanisms. Unfortunately, little or no insight into the general applicability[4] of their proposed or underlying mechanisms has been developed.

Extensive comparisons of models of efficiency change due to clearance have been published in the recent past by Yamamoto (1982) for turbines and Robinson (1982) for compressors. Their model comparisons are substantial compilations of model equations, experimental data and predictions. Most models in the literature are covered. Neither Yamamoto or Robinson were particularly satisfied with the outcome of such an exercise and both proposed new models. Consequently, the present study has not emphasized extended or detailed comparison, one to another, of the many models that have been proposed. Instead it has favoured a broader approach to the tip local flow field and losses and looked more to the general applicability of the flow mechanism descriptions.

The following sections, which discuss the literature in more detail, therefore examine the prior work at a more collective level than is typical of earlier clearance studies. The subject is approached by considering the experiments and then the models in order to provide a review of the subject. Appendix A also includes a broad overview of the flow field and other mechanism considerations which are relevant to the tip clearance effect on efficiency.

[4] The overall nature and presumed contribution, or allocation, of the inefficiencies in a compressor stage is shown in Figure 1.1-5. It can be seen that the contributions to the losses or inefficiency are not uniform over the flow coefficient range and would be expected to change from stage to stage. The capability of the models to account for changes in overall efficiency distribution from one stage to another is not at all proven or well established. It is also apparent that wall and tip clearance produce a very significant component of the total inefficiencies. However, the total inefficiencies are relatively small and large reductions in clearance losses are required to produce significant improvements in overall efficiency.

1.3 Experimental Observations of Clearance Effects

Tip seal flows and effects originate in a region which is at the confluence of several distinct flow regimes in the blade passage. The regimes include the blade surface flow, the case wall flow and the passage throughflow. These flow regimes are not readily modelled when combined in a rotating passage and each flow is known to depend on a wide variety of parametric design influences (Appendix A.1). In such a situation experimental data are essential for design purposes. It is also desirable that the experimental machine be as representative of the actual machine as possible to ensure the fidelity of the data.

From an analytical viewpoint, however, experimentation with the simplest configuration that demonstrates the tip clearance effects is the most desirable. What constitutes a minimum experimental configuration has by no means been resolved (at any point in time) in the literature. Rather, a process of gradual upgrading of the experimental configurations toward rotating, multistage flows seems to have taken place.

1.3.1 Cascades (Linear and Annular)

Linear cascades had not been used for some time to study tip seal effects in compressor rotor flows until the recent work of Storer and Cumpsty (1991). Consequently, much of the literature regarding compressor cascades has been previously surveyed in some depth. For example, Peacock (1982) presents an overview discussion of the limited cascade tip clearance literature up to 1982.[5]

Although cascade studies of tip clearance effects are not extensive (Moyle, 1981 p. 11), the relative simplicity of making measurements in cascades permits the flow surveys to be more detailed than is usual in compressors. While this is a great advantage in terms of examining a flow, the principal difficulty with interpreting cascade test results, *in terms of rotor tip flows*, lies in the lack of the centrifugal forces, the relative skew at the wall, the wall curvature stability conditions (App. A.1.4) and the shear distribution near the wall. The quantitative impact of these factors is shown by the present author in discussing Storer and Cumpsty's (1991) results.[6] Comparison of wall pressures from their cascade with the measurements from a rotating blade row, examined in this study, show marked discrepancies in placement of pressure contours relative to the blade suction surface. The differences noted would be expected to substantially alter the blade loading and flow in the tip gap.

With construction of more mechanically complex cascades, simulation improves, somewhat. For example, moving wall linear cascades capture a skew effect, but the approaching flow conditions to the tip gap in a moving wall linear cascade are not representative of the stability due to wall curvature. This problem is not overcome in a moving (outer) wall annular cascade. The flow on the wall in that case is stable. If examined closely, moving wall cascade simulation of rotor tip flows is not really possible without accepting some compromise. This has probably contributed, in part, to the trend toward rotating tests.

---

[5] Conversely, linear cascades have become more widely used for tip seal clearance research in turbines since Peacock's (1982) review. Papers by Sharma and Butler (1987, pp. 229-236) and Dishart and Moore (1989) and Yaras and Sjolander (1991) provide overviews of recent turbine cascade work that include representative selections of references.

[6] Present author's discussion of Storer and Cumpsty (1991) in the ASME Journal of Turbomachinery

Simulation of cantilevered stator tip flows, on the other hand, is an exact simulation in an annular cascade with a moving inner wall. An annular cascade was recently used for investigation of compressor stator clearance effects at the hub wall in a time varying flow (Schulz et al., 1989). The emphasis of their study focussed on unsteady flow effects rather than clearance changes, but their results show that time varying flows reduce the magnitude of corner separations relative to those of a steady flow. This is of some importance in interpreting flow results from studies in cascades to those of rotors. A flow study at the tip of a cantilevered stator in a linear cascade (without wall motion) was also completed by Storer (1989) and will be discussed further in Part 4. Storer's results were of some interest due to their delineation of a gradual change in vortex structure in the tip wall corner as clearance increased.

1.3.2 Rotating Devices

In contrast to cascades, clearance experiments using compressors provide greater flow field fidelity. However, measurements are often made in scaled, low speed machines and the experiments rarely map the entire flow field. To fully survey blade-to-blade pressure and velocity field data for a single stage over a wide range of conditions requires substantial resources. Consequently, complete surveys of multistage flows are even more limited. A summary is shown in Table 1.3-1 of test data the author could identify and their leading characteristics. The table covers experiments where a case wall boundary layer or clearance variation was a parameter and the flow effects of tip clearance were being studied.

It can be seen in Table 1.3-1 that the blade tip gap was mainly varied in early experiments but the more recent experiments combine more than one variable. In addition to the different geometries and speeds shown, stage whirl distributions of both free vortex and solid body rotations are present in the test cases of the table. As the blade relative velocities tend to be high at the case wall for free-vortex compared to the relatively low velocities of solid-body rotations near the wall, the tip pressure loadings will vary in the test machines due to whirl (App. A.1.2).

Experimental data from the test programs shown in Table 1.3-1 usually fall into one of two overall categories. The distinction made between the categories is based on the type of results produced.

(1) *Performance Decrement Testing* In the first type of experiment performance quantities are typically acquired. The results are usually presented in the form of pressure coefficient vs. flow coefficient and work coefficient vs. flow coefficient for the stage. Not all experiments provide both characteristic curves. In some cases efficiency changes were determined but not pressure coefficient, or vice versa. The performance data is by no means consistently derived in terms of instrumentation or technique and the experiments cannot be considered of uniform quality. Occasionally a particular aspect of the detailed flow is also measured along with the performance data. For example, Bettner and Elrod (1982) measured boundary layer thickness growth in the interblade spaces and examined the influence of wall roughness.

(2) *Secondary Flow Measurement* In the second format of experiment, the major emphasis is on measuring the passage flow velocity field, total pressure, wall local flows or thicknesses and deriving the secondary velocity pattern. The detailed velocity studies are tabulated in Table 1.3-2. With the exception of Inoue's (1988) study none of these detailed flow researches have also published a complete set of overall performance quantities. This is a major difficulty in interpreting, or attempting to correlate, the detailed flow pattern's changes with performance of the stage.

Table 1.3-1

Experimental Compressors used for Flow Studies with Tip Clearance or Case Wall Boundary Layer Parameter Variation (Z=No. Stages, Z=0 indicates an isolated rotor, ?=data value could not be established).

Investigator(s)	Z	*HR*	*AR*	R (m)	Ut (m/s)	Varied
Ruden (1937)	1	0.5	1.27	.250	?	Blade tip
Williams (1960)	1	0.6	2.00	.178	4	Blade tip
Holman & Kidwell (1975)	1	0.39	1.11	.059	474	Blade tip
Moore & Osborne (1977)	1	0.5	2.40	.250	423	Wall diam.
Dring (1980)	0	0.8	1.00	.762	41	B/L profile
Moore (1982)	1	0.5	2.40	.250	423	Wall diam.
Bettner & Elrod (1982)	1	0.8	1.06	.610	56	Blade tip-wall roughn.
Hunter & Cumpsty (1982)	0	0.4	3.00	.762	42	Blade tip-B/L profile
Cumpsty (1985)	4	0.78	2.00	.185	58	Blade spacing
Dring (1983)	2	0.8	1.50	.762	52	Blade tip
Lakshmin. et al. (1982-8)	1	0.5	1.52	.469	52	- [7]
Inoue et al. (1986)	0	0.6	0.76	.225	35	Wall diam.
Wisler & Beacher (1986)	4	0.7	1.90	.762	71	Blade tip/Wall diam.
Schmidt et al. (1987)	0	0.6	2.63	.254	39	Blade root
Inoue et al. (1988)	0	0.6	0.76	.225	35	Wall diam./solidity

The performance studies all show similar results for the fall-off or decrease in efficiency with enlarging tip gap. Data from a constant speed throttle line at the same throttle condition (constant flow) show an approximately linear decrease in efficiency over a clearance gap-to-blade-height (e/b) range of 0.007 to 0.04. The slope of the fall-off varies from compressor to compressor with a slope ($\Delta\eta/\Delta(e/b)$) range of 0.75 to 2.00. Typical test results are shown in Figure 1.3-1.

The efficiency decrement is frequently treated as a linear correlation and extrapolated to zero clearance and the curves are compared from one compressor the another by examining the slope ($\Delta\eta/\Delta(e/b)$). Tests where the (e/b) range has been less than 0.007 tend to show much larger efficiency fall-off and large clearances (e/b > 0.04) have a tendency to lower slopes. These trends suggest the linear fall-off range may be only an approximately linear region of a more general non-linear relationship. Mahler (1972, Fig. 4), for example, presents a non-linear correlation for a range of experimental and production compressors. Mahler's data are reproduced in Figure 1.3-2. A review of the general applicability of models at the extremes of the range suggest the processes are non-linear near the tip. This implies models which reflect those processes are more likely to be representative of the flow physics.

Comparisons of the secondary flow field from different studies can be quite complex. For example, Moyle (1989) demonstrates some of the difficulties of a quantitative comparison of secondary flow field measurement patterns from four different

[7] Lakshminarayana et al. (1982-1988) did not actually vary the passage or tip geometry at all in an extended series of studies with many co-workers. Lakshminarayana's investigations concentrated on detailed measurements of the flow field in and around the tip gap. His work is the notable exception to the general tendency of investigators to measure the flow field at different clearance conditions. However, other investigators measured the stage flow far less comprehensively. See Sec. 1.3.2.2 for more comprehensive discussion.

compressors. An advance in quantitative comparison is made in Part 2, Sec. 2.2, however, the process still remains largely qualitative. The most dominant feature of the secondary flow pattern linked to the clearance gap is the near wall total pressure defect core. Establishing the movement, magnitude and growth rate of this core, as tip gap is enlarged, is a fundamental output of the detailed surveys. Typical total pressure surveys at the rotor exit are shown in Figure 1.3-3. The development of the total pressure field is examined in more detail in Moyle (1989) and Part 2.

Table 1.3-2

Experimental Compressors used for Flow Studies with Tip Clearance or Case Wall Boundary Layer Parameter Variation which included Rotor Exit Secondary Flow Velocity Mapping (Z=No. Stages, Z=0 indicates an isolated rotor).

Investigator(s)	Z	*HR*	*AR*	R (m)	Ut (m/s)	Varied
Dring (1980/1)	0	0.8	1.00	.762	41	B/L profile
Hunter & Cumpsty (1982)	0	0.4	3.0	.762	42	Blade tip-B/L profile
Lakshmin. et al. (1982-8)	1	0.5	1.52	.469	52	-
Inoue et al. (1986/8)	0	0.6	0.76	.225	35	Wall diam./solidity

The data in the tables show that a range of passage geometries have been tested in terms of hub-to-tip ratio and aspect ratio. Tip speeds of about 50 m/s are typical of most tests and multistage configurations are relatively limited. The blading arrangements may also differ between experiments for the same number of stages. For example, interblade spacings vary considerably in the single stage experiments. Some of the stages in the table have been highly expanded to permit instrumentation access.

The combination of all these factors (different geometries, spacings, type of data acquired, etc.) makes it impossible to directly compare one set of results with another without first developing some form of correlation procedure or approach. New efforts with correlation are discussed in Part 2, Sec. 2.1 while the following section (1.4) sets out some of the previous modelling, analytical and correlation work.

A coherent view of the tip flow problem can be developed by viewing the experiments as a collection of information or database and this point is addressed later in this section. There is some value in grouping the tests by number of stages and looking more closely at how different stage configurations are tested and the flow situation they represent. The typical test configurations (Z parameter) represent quite different flow conditions at the tip.

1.3.2.1 Fans or Isolated Rotors (Z = 0)

Fans or isolated rotors provide an idealized flow environment in which a flow can be studied. The inflow velocity field is axial, circumferentially uniform and has a low turbulence level. The case wall boundary layers, which have developed on the upstream walls, are not skewed relative to axial. This flow situation is not representative of an embedded stage environment, however, it is representative for a fan stage. The configuration is well suited to rotor exit flow surveys (only one radial survey is required at one circumferential location) and results can be readily correlated with upstream boundary layer thickness variations. A data baseline for a rotor tested in isolation can be used to estimate the impact of stage matching by testing the same rotor in an embedded configuration. This has not been routinely attempted in clearance studies, however. Most experimental observations of clearance related effects have

also been made with only one rotor design per experiment. An exception is Inoue (1988), who has tested two rotors of different solidity using the same blading and made the same measurements on both rotors. His results are presented in the form of a qualitative comparison of the secondary flow patterns. The results indicate the total pressure defect crosses the passage at the same rate for either solidity as it is convected in the passage. In the higher solidity case the defect collides with the pressure side of the adjacent blade rather than cleanly exiting from the passage.

1.3.2.2 Single Stages with and without Inlet Vanes (Z = 1)

Single stages form the largest group of tested configurations. Stages without inlet vanes are similar to isolated rotors in terms of inflow conditions. The presence of a stator alters the flow considerably in the rotor if the stator is close to the rotor. The stator pressure recovery and efficiency reflect the flow in the rotor and matching effects come into play in the stage flow. Performance of stages with inlet vanes (Ruden (1944), Williams (1960), Lakshminarayana et al. (1982-91)) reflect the influences of upstream wakes and boundary layer skewing relative to axial depending on the degree of blade row separation. The experimental data that result are more representative of an embedded stage flow. Inlet guide vanes are accelerating blade rows, however, and do not present the rotor with an inflow which is typical of a stator exit flow. The number of flow regimes being handled by the rotor (wakes, wall boundary flows, skewing) has grown, compared to an isolated rotor configuration. The accessibility of the flow for surveys also diminishes and many circumferential locations for radial surveys are required to define the flow field leaving the blade rows.

A very comprehensive study of this type of flow has been completed by Lakshminarayana, Pouagare and Davino (Parts I and II) (1982) in an expanded stage with inlet guide vanes (Table 1.3.2). The flow in the rotor was examined using a probe traversing system mounted *on the rotor*. This system permitted Kiel, hot-wire or five-hole probes to be traversed circumferentially in the blade passage or through the blade wake downstream of the rotor in the relative frame. Probes could survey radially from the hub side of the passage to within 1-2% of the case wall radius. They could also be positioned at different yaw angles. The survey probe used in the experiments was a tri-axial hot wire. Part I of the paper describes mean velocity profiles and case wall boundary layer properties in the tip region of the rotor passage (0.88 to 0.98 of radius) and also includes corresponding static pressure data on the blade surface near the tip. Part II presents the turbulence properties of the flow (which are discussed further in Part 4). The flow condition surveyed ($\Phi = 0.56$) was near design and the tip clearance was 2.5 to 3.0 mm[8] corresponding to e/b = 0.008 to 0.013. The results provide a detailed picture of the velocity field development through the passage from 0.88 to 0.98 of radius. The velocity field changes gradually from 0.88 to 0.975 of radius but shows a rapid change in streamwise velocity from 0.975 to 0.980 of radius, i.e., very close to the wall.

Exploration of this outer region of the flow with a "V" type hot-wire probe (in addition to surveys of the inner region with the tri-axial wire) was reported in Lakshminarayana, Murthy, Pouagare, and Govindan (1983). The "V" probe permitted axial and circumferential components of velocity to be surveyed from 0.970 to 0.997

[8] Lakshminarayana, Zaccaria and Marathe (1991) state that contrary to reports of clearances of 5 mm in papers in 1990, the largest clearance ever employed in the Penn. State Program was 3.5 mm. This corresponds to e/b = 0.0152. Another clearance level seem to have measured at Penn. State in 1990 (see footnote to Table 1.3.1). It would appear that prior to 1989 the clearance level was e/b = 0.011 and in 1990 the clearance increased to e/b = 0.0152. The authors do not indicate whether the earlier reported clearance levels (i.e., 1982-8) should be corrected.

of radius. The radial component could not be obtained with this probe. The relative flow was swept circumferentially towards the pressure side of the passage sharply as the probe penetrated into the tip clearance zone of the annulus. These results are compared with similar surveys from other sources in Moyle (1989). The authors also provided data on the thickness development of the boundary layer through the passage and compared their results with multistage compressor data. Figure 18 of the paper shows the displacement thickness of this flow to be substantially lower than in the multistage case. The thicknesses were compared at a similar proportion peak pressure rise. The difference is attributed to the machine configurations, i.e., Z = 1 compared to Z > 1.

Losses for the same situation were addressed by Lakshminarayana, Sitaram and Zhang (1986) using a Kiel probe mounted in the rotor traverse mechanism discussed above. The flow was surveyed at two flow coefficients (Φ = 0.50 and 0.56) to examine the effects of loading on the losses. The outermost surface surveyed was at 0.9864 of radius. A region of high loss was seen in Fig. 3 to develop from the upstream suction side of the passage and move toward midpassage as the flow moved downstream. The strength and size of the loss core were increased at the lower flow condition. Secondary (velocity) flow patterns in the tip region are shown in this paper for the (Φ = 0.56) condition. These results appear to have been acquired by Lakshminarayana, Pouagare and Davino (Parts I and II) (1982) and are used in conjunction with the loss data to interpret the sources of the case wall profile losses. The secondary flow pattern is compared with similar data from other sources in Moyle (1989). The data from the Lakshminarayana paper are unique, however, in showing the secondary flow development within the rotor passage at three axial stations. Other data of this type have been acquired downstream of the rotor.

The same rotor flow (Φ = 0.56) was then studied using a single component LDV system and reported in Murthy and Lakshminarayana (1986) and Lakshminarayana and Murthy (1988). Axial and circumferential velocity components were measured between 0.902 and 0.980 of radius. The Kiel probe data from the prior study were remeasured and used in conjunction with the LDV measurements to analyze the flow. The main thrust of the study was to present the annulus wall boundary layer profiles within the passage and interpret the data. Figure 16 of the paper shows that the blade tip is approximately 70% unloaded in the outer 5% of the span compared to the lift derived from blade element theory. The results are generally interpreted in the context of a leakage vortex generating the observed losses and velocity field in the flow.

The conclusions reached in the preceding papers regarding the mechanism at work in the flow were substantially revised in Lakshminarayana, Zaccaria and Marathe (1991) due to another survey of the same rotor (at Φ = 0.51) using a miniature five hole probe in the tip region. This probe provided radial velocity components near the case wall. These measurements led the authors to conclude a strong shear layer interaction occurs as the leakage flow traverses the passage case wall. This represented a significant change from the conclusions of Lakshminarayana and Murthy (1988) concerning the presence of a vortex structure based on the LDV measurements (Conclusion 8). The results of Lakshminarayana, Zaccaria and Marathe (1991) are discussed further in Part 4 in the context of the measurements of Part 3.[9]

[9] It should be noted that Lakshminarayana, Zaccaria and Marathe (1991) refer to results of the present study (discussed in Moyle, Walker and Shreeve (1991)) in their paper and comment that their work confirmed a number of the observations discussed in Parts 3 and 4.

1.3.2.3 Embedded Stages and Multistage Machines (Z > 1)

The flow field for an embedded stage in a multistage machine has been surveyed by Dring (1983). Dring's data are based on blade-to-blade surveys with both a rotating traversable probe and probes traversed in the absolute frame. Unfortunately, performance of the configuration is not discussed from a tip clearance viewpoint. In a multistage machine configuration, stage performance data are more commonly generated by averaging the performance of the whole configuration. Usually little or no information on the flow within the stage is available.

In the multistage configuration the overall tip and case wall flows are produced in a manner which is representative by definition. The main difficulty in using multistage test results is that they are usually averages and cannot be easily related to flow details. The measurements by Dring seem to be the only comprehensive *detailed* measurements of tip local flow in the open literature derived from a *multistage* machine stage. In terms of analysis or a database this is a serious limitation.

1.3.3 The Experimental Observations as a Database

The high level of interdependence of many influences on the flow regime at the tip-wall suggests the data analysis is best approached with a multivariable philosophy from the outset. If one looks at the problem from this viewpoint, it is apparent that the range of parametric variation provided in one experiment is very small. However, the test programs collected as a whole show some range of parametric variation. This database is still sparse, however, it does provide a multidimensional space to work with.

Using data from the collection of tests one can appraise our understanding of certain aspects of the general tip flow problem. For example, Fig. A.1-2 shows the database in terms of passage geometry variations tested. It can be seen that solidity has not been varied widely. Thus it is unlikely that any model proposed including a solidity parameter has any basis in experimental experience. When the solidity parameter appears in a model it is really related to the proposer's use of the lift coefficient (see Sec. 1.4.1).

By adopting such a multivariable view, it becomes clear from the database that:

(1) There is very little redundant testing in the database in terms of passage geometry, so consistency of the data is thus hard to verify or confirm (Table 1.3-1).

(2) The database is sparse and the most thoroughly tested dimension is aspect ratio variation at unit solidity (Fig. A.1-2).

(3) Except for Dring's (1983) testing there are no data available on embedded (Z > 1) stage secondary flow patterns (Table 1.3-1 and 1.3-2).

(4) The only intersection of performance test results, clearance variation and secondary flow survey data occurs in Inoue's (1988) test program on isolated rotors.[10]

[10] It would be a most valuable addition to understanding of the subject to see a reconciliation of Inoue's loss distribution surveys with the overall rotor performance data. Such a reconciliation over a range of clearances would greatly aid in refining the contributions to the overall inefficiency of Fig. 1.1-5.

This overall situation is far from what one would like to see in an multivariable analysis sample. In addition, it is relatively easy to raise questions about the statistical quality of the database due to bias in the experimental definition and data acquisition.

If the state of the art, discussed in Sec. 1.1.2 and Appendix A.1, are considered, it is clear that the experimental database is not comprehensive enough to validate any model confidently.

1.3.4 The Experimental Basis for Modelling

There are also notable distinctions in the treatment of experimental data which need to be recognized in the tip clearance literature. Philosophical differences arise between the *comparability* of data and its *representativeness*. These distinctions are discussed in Appendix A.1.2.5. The point to be noted is that the experimental data are not exclusively generated for the purpose of developing models and in some cases are not well suited to use in model development. As a rule, the tip flow *models are based on limited observations*. It is also reasonable to say they cannot be verified or discounted while the experimental database described above is so sparse. In fact, there is a reasonable probability that *all the models may be adequate descriptions of the flow under certain conditions.*

The sparseness of the database of tests (at present) does not mean that the database cannot be used to examine a number of hypotheses about the nature of the tip flow. Consequently, the present author spent some time compiling the data so that it could be analyzed as a database of tests. The hypotheses and analyses conducted are discussed in Part 2. In discussing the test data, it is worthwhile examining what is typically considered to be a tip clearance effect.

1.3.4.1 Isolation of the Clearance Effect

As the tip gap dimension is a geometric parameter, perturbing the gap dimension while all others remain unchanged is not, in fact, geometrically possible, its conceptual desirability notwithstanding. For example, the changes observed in a compressor flow due to reducing blade height in a constant annulus is the combined effect of an enlarged clearance, a reduced blade height and a total system adjustment to the new flow.[11]

In the context of a repeating stage and the comments on matching made in App. A.1.2.3, the flow will adjust to both the clearance enlargement, the work input reduction and the resulting pressure distribution in the duct system and other blading. Unscrambling the factors involved in the combined effect, on a constant speed throttle line, is aided by noting that if efficiency is defined, incompressibly, for a control volume as

$$\eta = \Phi\Pi/P \qquad 1(1)$$

then a differential change in η can be expressed by

$$d\eta = (\Phi/P).d\Pi + (\Pi/P).d\Phi - (\Phi\Pi/P^2).dP \qquad 1(2)$$

If the efficiency change ($d\eta$) is examined at constant flow ($d\Phi = 0$) then

---

[11] Comparison of the performance of geometrically similar compressors at different clearances is not possible because the clearance is a geometric variable. The performance of two different compressors at similar flow conditions is what is, in fact, compared. This subject is discussed further in Sec. 2.1

$$d\eta = (\Phi/P).d\Pi - (\Phi\Pi/P^2).dP$$

1(3)

and it is clear that the efficiency change involves more than just the change in pressure rise coefficient ($d\Pi$). If the efficiency change is determined at constant power input ($dP = 0$) then

$$d\eta = (\Phi/P).d\Pi + (\Pi/P).d\Phi = d(\Phi\Pi)/P$$

1(4)

Note that if the flow is constant ($d\Phi = 0$) and the power is constant ($dP = 0$) then the efficiency for the control volume resembles the blade element efficiency definition

$$d\eta = (\Phi/P).d\Pi = (1/X).d\Pi = d\Pi/X$$

1(5)

More generally the condition that

$$(\Pi/P).d\Phi - (\Phi\Pi/P^2).dP = 0$$

which implies

$$dP = (P/\Phi).d\Phi = X.d\Phi$$

1(6)

is the condition where the blade element efficiency is equivalent to the control volume efficiency.

These relationships are utilized further in Part 2, Sec. 2.1, however, for the purposes of the present discussion, the nature of the problem of isolating the clearance effect becomes clearer. Using efficiency decrement data determined at constant flow (Eqn. 1(3)) when calibrating a model, that only predicts changes in Π with tip gap (e), will include an error of $(\Phi\Pi/P^2).dP$ in the calibration. Similarly, Eqn. 1(5) is frequently used as a basis for modelling efficiency changes and, in so doing, assumes an efficiency change occurred at constant flow and power. This not usually the case in experiments which might be used for calibration of the model.

Modelling attempts to describe an isolated clearance effect in terms of efficiency changes also need to be scrutinized carefully in terms of the definitions of quantities being determined. Note that equation 1(2), above, is formulated in terms of total derivatives ($d\Pi$, $d\Phi$ etc.). Generally, models that have been developed from considerations of the flow physics only involve partial derivatives ($\partial\Pi$, $\partial\Phi$ etc.). This is primarily due to the modelling not accounting for *all* the parameters that affect the variable. For example, using an isolated aerofoil, a model might be developed for pressure loss as a function of tip gap as

$$\partial\Pi/\partial e = f(e/b, AR)$$

and for correlation purposes, an assumption will be made that

$$d\Pi = (\partial\Pi/\partial e)de$$

1(7)

Such an assumption is clearly very restrictive considering the number of parameters that are known to be involved in the passage flow description.

Industrial methods seem to be more empirical in dealing with this problem of isolation in a multiple parameter situation. Mahler (1972, p. 11) alludes to an industrial efficiency decrement model that includes blade loading, thickness/clearance, gap/chord, hub/tip and aspect ratios as secondary effects in a correlation based primarily on gap/span (e/b). In a similar style, Koch and Smith (1976) provide a review of losses in axial compressors which includes trends for the many factors to be considered in a design point efficiency prediction. Their tip gap effect correlation follows Smith (1970). Figure 5 of Koch's (1981) paper also shows a normalized change in stalling pressure rise correlated with a gap/staggered spacing (e/g) for a range of aspect ratios. The slope of this curve shows a roughly 1.5% decrease in pressure rise per 1% increase in e/g at small clearances. A lower slope is shown at larger clearances. By compiling rate-of-change data of this type, and arguing that such data might be generally representative of $\partial\Pi/\partial e$, one could develop analysis methods to isolate the clearance effects by cross correlation using experimental data. This is obviously a cumbersome approach requiring extensive testing or test data evaluation, however, it is consistent with the tendencies of published industrial methods.

1.3.4.2 Tip Local Design Experience

It is evident that geometric parameters, rather than flow variables, are the desirable variables to be included in any model or experiment. The parameters of interest include axial chord, staggered spacing, stagger angle, lean and blade camber and thickness distribution. These quantities can be varied locally within the overall design constraints of throughflow and the blade element velocity diagrams. Often the designer develops the aerofoil by twisting, thickening and shaping the blade using the experience of model tests or computer predictions to reach a suitable design. Despite advanced computational techniques, these methods have produced less than the desired results when applied to tip section profiles experimentally (Wisler, 1985, p. 68), Figure 1.3-4. At a more detailed level the shape of the tip gap and wall under the blade may also be varied with a wide variety of treatments, see Figure 1.3-5.

Attempts to design for, or at least reduce, clearance loss effects have been reported in the literature with mixed results. Reeder's (1968) review describes a number of approaches. The methods frequently tailor the tip geometry or section profile. Examples of some designs are shown in Figure 1.3-5. Isolated investigations of this type often originate in industrial development research and may be limited to a particular blading or a blade family design.[12] In general, claims of radical improvements in performance due to singular tip modifications do not appear in the literature. Studies by Wisler (1977) and Wisler and Beacher (1986) involving changes to both blade profile and case wall profile (recesses or trenching), respectively, provide good examples of the typical study. They also show the difficulties of interpreting a performance change when the net effect is modest.

At the other extreme of the spectrum of modified tip design approaches, Beknev (1961) attempted to comprehensively arrive at an optimum design for a stage by allowing for several different regimes of the passage flow across the span. The tip local design extended radially inward about 10% of span. The stage showed quite

[12] The initial level of efficiency demonstrated by a stage is also of concern in interpreting the results of isolated design modifications. A stage design with a relatively low efficiency (unmodified) may have much more potential to show marked improvement than a highly developed design with a relatively high (unmodified) efficiency.

high efficiency (η = 0.945) when tested but the results suffer from the interpretation problems encountered above, except in this case, the issue was one of allocation of the improvement to any of the several features of the design across the span.

1.3.5 Experiments Summarized

This section has provided an overview of a selection of the prior experiments which emphasized compressor performance changes caused by tip clearance variation or examinations of the flow in or near the tip clearance gap. This work was addressed by examining cascade testing (Sec. 1.3.1) and rotating testing (Sec. 1.3.2). While many experiments have been conducted on this subject, most of the data document one compressor's overall performance change as the tip clearance was varied. Data of this type provide very limited insight into the flow field changes that occur. From the discussion it was clear that many more detailed surveys of passage secondary flows with corresponding compressor performance data for a range of tip clearances are required to have a global description of the flow field.

These data need to be acquired consistently, over a wide range of compressor geometries to arrive at a broad based verification sample which could be used for model validation. Because such experiments would absorb enormous resources, it is most unlikely that they will ever be conducted. Therefore, analyses which can draw upon or utilize prior experimental results are of major value in this subject. Consequently, the collection of tests from many different compressors was considered as a whole (Sec. 1.3.3) and issues related to the definition and isolation of flow effects caused by tip clearance was addressed in Sec. 1.3.4. Both these subjects are relevant to the analyses of Part 2, which utilize data from many experiments to identify behavioral trends with tip clearance changes. In that context it is valuable to examine how the tip losses have been previously defined, modelled, correlated and analyzed. The following section examines the prior models and correlations.

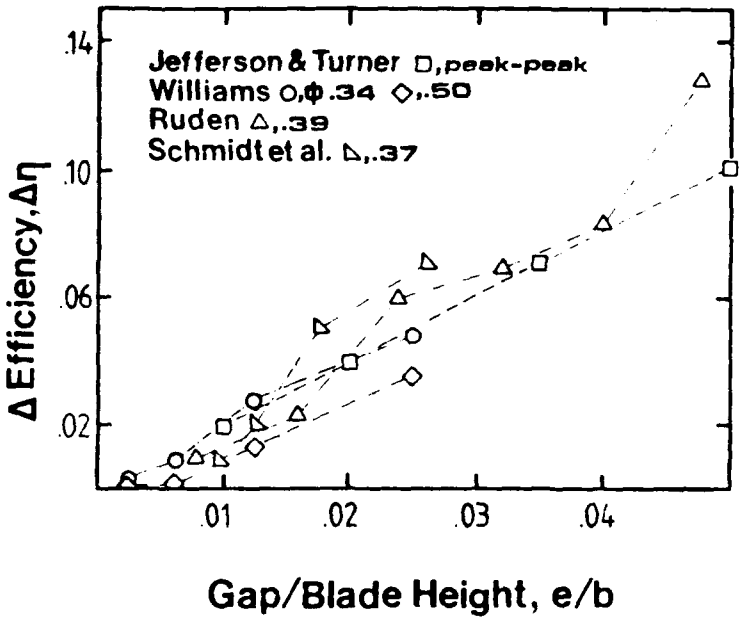

Fig. 1.3-1 Data from a variety of experimental studies showing approximately linear efficiency *change* as a function of gap over blade height (e/b). Data in this format are frequently used to verify models (from Moyle, 1988).

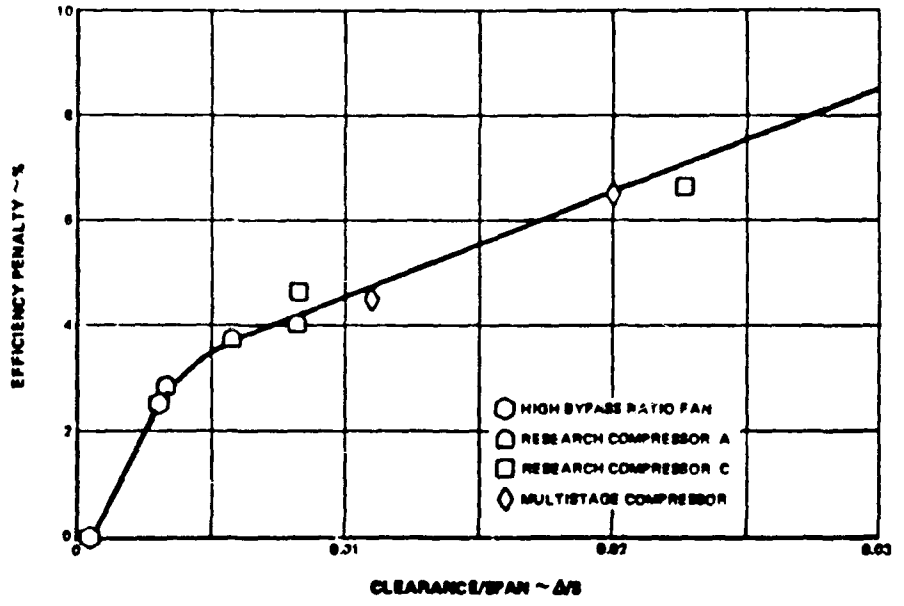

Fig. 1.3-2 Efficiency decrement data from Mahler (1972, Fig. 4) showing a non-linear form of the decrement with increasing gap over blade height.

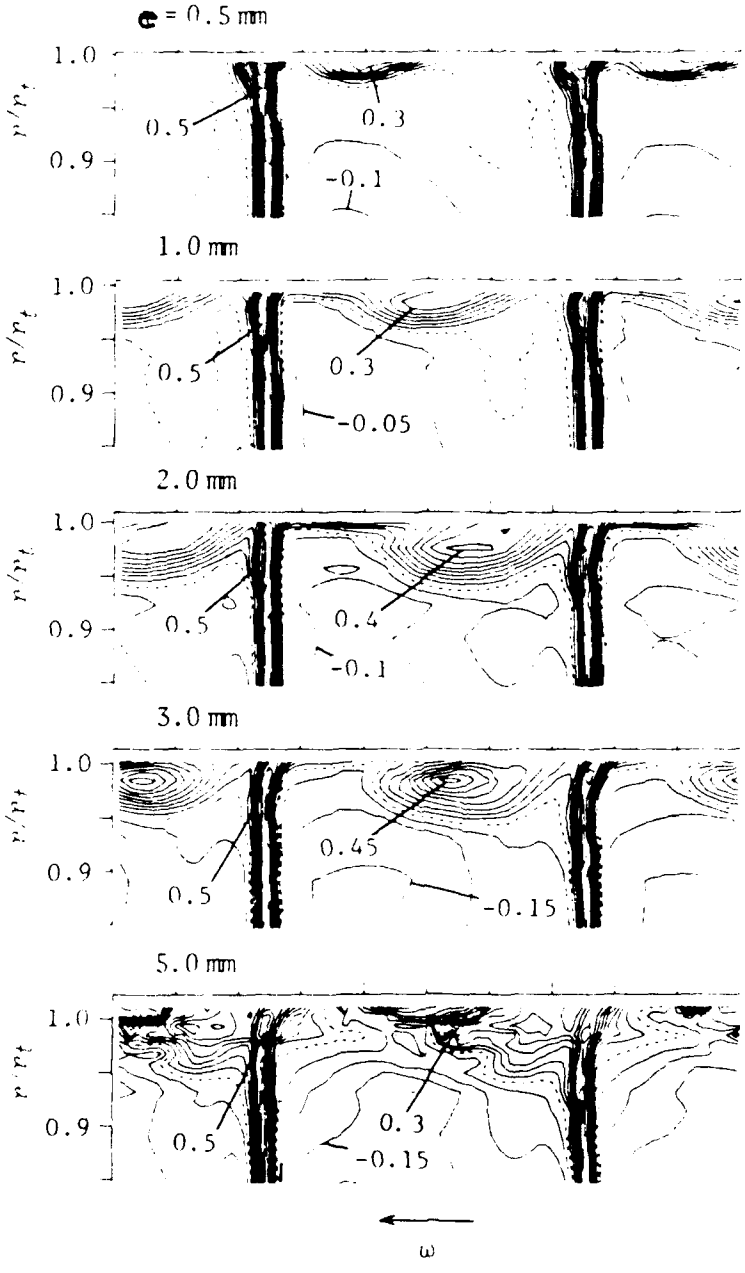

Variation of relative kinetic energy defect with tip clearance

Fig. 1.3-3 Typical total pressure surveys at the rotor exit showing the growth of the case wall total pressure defect due to increasing tip gap (from Inoue and Kuroumaru, 1988, Fig. 10b). Data of this type from several compressors are compared in Moyle (1989).

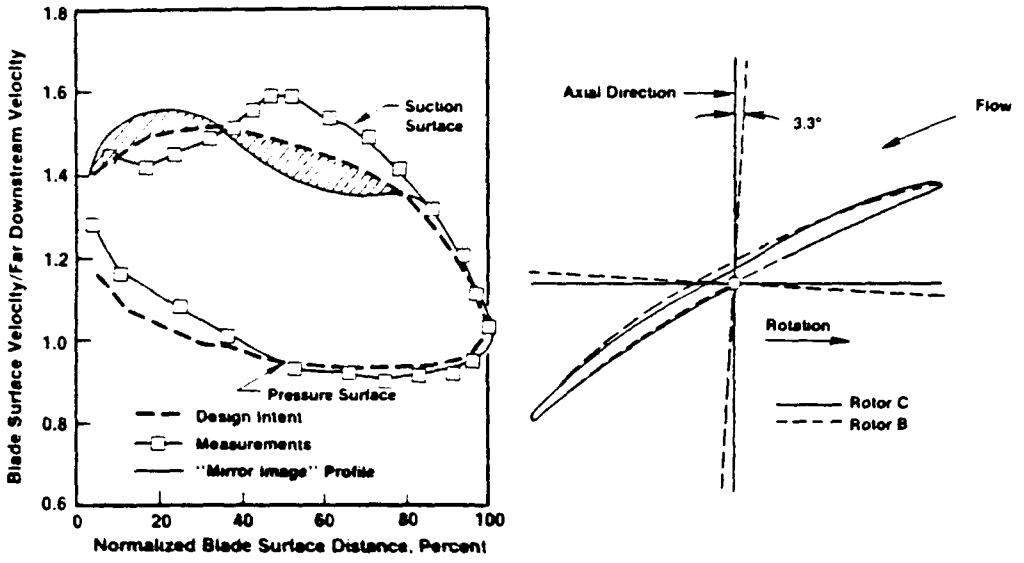

Fig. 1.3-4 Schematic of a scheme to compensate for the effects of tip leakage in the tip section profile (from Wisler,1985, Fig. 43 and 44). The method varied incidence and the tip section profile based on measured surface pressures from a baseline rotor.

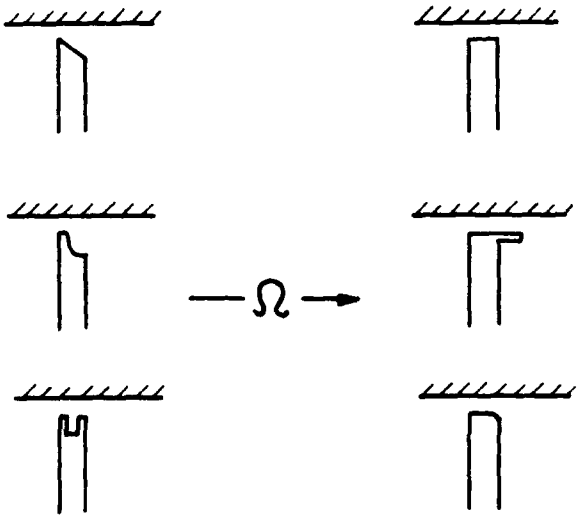

Fig. 1.3-5 Schematics of design variations of the rotor tip intended to improve tip local flow and reduce losses associated with the tip gap.

1.4 Models and Correlations

Efficiency change due to tip clearance variation has brought a very large number of models and correlations into the compressor literature over a period of time. Over the that period the observed changes in efficiency, for a small change in clearance gap, have typically been proportional to the normalized gap dimension. In that same period, there has not been systematic, and consistent, experimentation over the range of possible geometries which would have built up a broad validation base. These factors have contributed to a proliferation of models. Often the models are very similar in concept or type but differ, or are only distinguished, in their implementation.

Predictions of a change in efficiency due to clearance change by different models are compared in Figure 1.4-1. These predictions are for one compressor stage over a range of flow conditions. Large differences in predicted efficiency decrement are observed. Studies of the differences between models and their relative value have been made previously by Reeder (1968), Yamamoto (1982) and Robinson (1982). These model comparisons are substantial compilations of model equations, experimental data and predictions. They cover most models in the literature. Their predictions are presented in a similar format to that of Fig. 1.4-1. Neither Yamamoto or Robinson were particularly satisfied with the outcome of such an exercise and both proposed new models. Each author noted extended comparison of the models had limitations in terms of productive research of the topic. Some of the same models and their differences are also discussed in a review paper by Senoo (1987). It should be remembered, however, that the models have almost always been reconciled to some set of test data by their authors. They can reasonably be applied with confidence in situations similar to their validation (see Appendix A.1 for further discussion).

It was noted that the types of models are far less numerous, so the models are discussed by *type* then author in this section. Each type of modelling approach has advantages and disadvantages depending on the application, i.e., gas path design, performance estimation, blade profile design and so on. Often empirical constants are required to use the models. The constants are usually calibrated or fitted from changes in measured experimental stage efficiency. An experiment may be conducted for the model evaluation or the efficiency changes may be collected from other studies. The change data are most frequently generated by cropping the blade or increasing the case radius in an otherwise constant stage configuration (see Table 1.3-1).

1.4.1 Models Predicting Efficiency Decrement

The most numerous and frequently published characterizations involve describing the tip gap effect by fall-off in efficiency with increasing normalized clearance gap. The descriptions typically take the functional form

$$\Delta\eta = f(e/\{b, c, g, t, R\}, C_L^n) \qquad 1(9)$$

The term {b, c, g, t, R} in Eqn. 1(9) indicates one of the parameters from the range in the set { } is used. Some examples of the large selection of published models are set out functionally in Table 1.4-1. The functional dependence format used highlights the key parameters in the model. Each operator f(..) represents a different function. The most common approach has been to develop an expression for the efficiency decrement from a simple physical model of the tip flow and blade geometry. The investigator then empirically correlates certain parameters in the expression with test data.

Of this selection, Senoo's model is by far the most complex formulation. It requires conditions at zero clearance (Π_0, X_0, η_0) and also $\Delta\Pi_h$, *the pressure loss coefficient due to causes other than tip clearance*, to be known. In addition four coefficients (c_1-c_4) which account for contraction factor in the gap, pressure recovery of the gap, blockage factor of the passage and a *blockage multiplier due to clearance* are required to be known or estimated beforehand in order to predict the effect of a gap change on efficiency. The resulting curves are typically linear with e/b, so the model is primarily correlating the sensitivity $\Delta\eta/\Delta(e/b)$.

Table 1.4-1

Models of Efficiency Decrement with Tip Clearance Parameters for Axial Compressors.

Fickert (1946)	$\Delta\eta = f(e/R_t, \Phi, X, HR)$
Rains (1954)	$\Delta\eta = f(e/R_t, \Phi, X, \cos\beta, \sigma, e/\delta^*)$
Vavra (1960)	$\Delta\eta = f(e/b, \Phi, X, \cos\beta, \sigma, b/s)$
Lakshminarayana (1970)	$\Delta\eta = f(e/b, \Phi, X, \cos\beta, AR)$
Senoo (1986)	$\Delta\eta = f(e/b, \Phi, X, \cos\beta, \cot\beta, \sigma, HR, [\Pi_0, X_0, \eta_0, c_1\text{-}c_4, \Delta\Pi_h])$

The functional dependence of the models are seen to be similar, however, the functions vary substantially in algebraic form and interpretation of the same flow physics. The models are all of the inherent loss type discussed in Sec A.1. Their dependencies typically differ in the geometric parameters that are considered to be significant {e/δ^*, b/s, *AR*, etc.}. The major physical modelling differences are due to the authors respective treatment of lift coefficient near the tip, which usually introduces the Φ, X, $\cos\beta$, and σ terms and the exponent (n) of Eqn. 1(9), ($C_L = X\cos\beta/\Phi\sigma$ for moderately staggered rows). The constants [Π_0, X_0, η_0, c_1-c_4, $\Delta\Pi_h$] in Senoo's model require detailed knowledge of the blading, otherwise the equations are straightforward to use.

The models typically indicate the efficiency falls uniformly (linearly to slightly parabolically) over the clearance range (e/b = 0.005 - 0.05) for a constant flow coefficient (Φ). The rate of efficiency decrease predicted at a given Φ can vary substantially (150%) from one compressor to another depending on the {*AR*, *HR*, b/s etc.} for the compressors.

The impact of the typical one to two percent per percent spread in sensitivity observed in the stage data of Fig. 1.3-1 has been shown previously in Fig. 1.1-2 for a multistage compression over a range of pressure ratios. One percent per percent difference in sensitivity for a particular stage is roughly equivalent to a four percent change in overall compressor efficiency at 20:1 pressure ratio. It can be seen that 150% change in sensitivity, from one design to another is worthy of attention.

The models of Table 1.4-1 have been developed by modelling different proposed flow patterns at the tip. The sections which follow loosely group the models by the primary mechanism the investigator has emphasized. In order to give the reader some feeling for the models, the results of their predictions are compared in Figure 1.4-1. In this figure the first four models of Table 1.4-1 have been applied to the experimental compressor and blading flow conditions, at design, that is investigated in Part 3. A prediction based on Senoo's model was not made because too many factors had to be arbitrarily estimated. The comparison within Figure 1.4-1 clearly shows little agreement exists between the models for the same situation *and also with the trend of the experimental results* of Part 3.[13]

The model descriptions which follow outline *key features* of each investigators approach and observations by the present author. The discussion has not attempted to be exhaustive due to the large number of models which could have been considered.

1.4.1.1 Lost-Work Models

Fickert's (1946) model is the archetype of the lost work approach. The basis of his argument accounts for the reduction of working annular area as a proportion of total passage annular area as the clearance gap varies. The proportion of the flow unable[14] to be worked on is assumed to lose its share of the power input. The model predicts a larger efficiency fall off at lower flow coefficients.

A more leakage oriented lost work model is developed by Rains (1954) in which the total power loss is assumed equal to the flux of kinetic energy associated with flow normal to the blade in the tip gap. Rains' model considers both viscous and inviscid influences and primarily is based on estimating the reduction in work coefficient as tip gap is enlarged. The model estimates the decrease in tip pressure loading due to flow acceleration into the gap, reduction in effective area of the blading and the reduced influence of the case wall scraping as the gap is enlarged. This final term is calibrated in terms of case wall boundary layer displacement thickness and its scaling in the model can have a strong effect on the predicted efficiency decrements. The decline in strength of pressure side flow scraping with increasing gap causes the strong decrease in sensitivity, at large clearances, observed in the model prediction shown in Fig. 1.4-1. This is seen in the change from a strong fall off at small clearances to a gradual decline at larger values. Based on experimental observations Rains argues that the leakage flow rolls up into a tip vortex and that the energy is then dissipated without recovery in the downstream flow. The predicted efficiency fall-off is essentially insensitive to flow coefficient changes.

A very similar approach to that of Fickert is advanced by Senoo (1986) and is developed into an elaborate model. The underlying argument is explained in Senoo (1987). Essentially the pressure loss (in axial machines) is equated to the pressure rise across the rotor multiplied by the clearances' proportion of the annular area. Changes in work coefficient are neglected. Application of the model requires a significant number of correction coefficients related to the tip local flow to be known or estimated. The form of the predicted decrement is similar to Fickert. It is worthwhile noting that Senoo's model produces a prediction that is proportional to C_L while Rains' model goes as $C_L^{1.5}$.

---

[13] A similar comparison was made by Yamamoto et al. (1982, Fig. 19) for a turbine stage. The predicted efficiency change range was comparable (~0.08 if scaled over the e/b range 0.003 to 0.04). The turbine relations were more consistent in curvature from one-to-another, however.

[14] Note that Fickert's approach also involves the notion of blockage discussed in Sec. A.1.2.5.

1.4.1.2 Induced Drag Models

Induced drag models are derived from the dependence of the section profile's force balance on the drag-to-lift ratio at the tip. The profile drag component of the ratio is usually augmented to account for the induced drag due to lift. The typical model involves correcting the induced drag of the profile with an additional adjustment for tip leakage. The induced drag models develop expressions that are primarily proportional to C_L^2. Vavra's (1960, Eqn. 13(76)) model based on Betz (1926) is typical of such an approach yielding

$$C_{D_i} = 0.04\, C_L^{\,2}\sigma(s/b) + 0.25\, C_L^{\,2}\sigma(e/b)(1/\cos\beta_2)$$

A similar method, based on Betz (1926), is pursued by Lakshminarayana (1970), however, the induced drag term is derived from considerations of the lift shed or retained at the tip. The spanwise flow in the blade boundary layers is also included as an additional loss in determining the total loss, as the clearance varies. This approach was strongly influenced by experimental and visualization studies in a cascade. The induced drag part of the model is formulated as

$$C_{D_i} = 0.7\, C_L^{\,2}(c/b)(e/s) = 0.7\, C_L^{\,2}\sigma(e/b)$$

Note that Vavra's expression, if $\beta_2 = 45$ deg, becomes

$$C_{D_i} = 0.04\, C_L^{\,2}\sigma(s/b) + 0.35\, C_L^{\,2}\sigma(e/b)$$

and it can be seen that the estimates for the component of induced drag at the tip due to clearance differ by about 100% between the two models. This is a rather large discrepancy, however, if s/b is assumed to be a nominal 0.5, the relative magnitude of $C_D/C_L^2\sigma$ can be seen to be within 20% at e/b = 0.01. For practical purposes this is not a very great disagreement in estimation.

In order to arrive at an efficiency decrement the induced drag must be introduced into an efficiency expression. It is of interest to note that Lakshminarayana defines efficiency decrement as

$$\Delta\eta = d\Pi/X$$

Considering the derivative of $\eta = \Pi/X$ it can be seen that

$$d\eta = d\Pi/X - (1/X^2).dX$$

which is the same as using Eqn. 1(2) and substituting $X = P/\Phi$ into the expression. Assuming the work coefficient (X) is not affected by a change in clearance requires that either $d\Phi/d(e/b) = dP/d(e/b) = 0$ or Eqn. 1(6) to hold, as discussed previously.

It is therefore of some interest that Lakshminarayana's final expression for $\Delta\eta$ has been fitted to the compressor data in his paper without consideration of work coefficient changes with clearance. He argues work changes are negligible.[15]

[15] Peacock (1983, p. 11 col. 2 para. 2) comments more comprehensively on this discrepancy in the context of other literature and the relationship between pressure coefficient, work coefficient and efficiency.

However, it should be noted that $d\Pi/d(e/b)$ and $dX/d(e/b)$ are usually negative. Rains (1954, Fig. 26), for example, measured a slope of $dX/d(e/b) = -1.3$.[16] If both pressure and work coefficients typically decrease with increasing clearance, then Lakshminarayana's efficiency definition will overestimate his fitted constants (i.e., the C2[17] constant). This may explain why Lakshminarayana's model tends to overestimate efficiency decrement when compared to experiments.[18] Based on this observation, it would appear possible to recalibrate Lakshminarayana's model for the induced drag term within a more comprehensive definition of compressor efficiency. An attempt to do this seems to have been made by Schmidt et al. (1988) who present a "modified Lakshminarayana model" for calculation of the efficiency decrement.

Vavra's (1960, Eqn. 13(26)) defines efficiency as

$$\eta = \Phi.[(r^{\#} - \Phi.\varepsilon_R)/(\Phi + \varepsilon_R.r^{\#}) + (1 - r^{\#} - \Phi.\varepsilon_S)/(\Phi + \varepsilon_S(1 - r^{\#}))] \qquad 1(10)$$

where $r^{\#}$ is the "theoretical degree of reaction" and ε is the drag to lift ratio C_D/C_L. This expression captures more of the factors affecting the stage efficiency. The most troublesome aspect of using this efficiency definition lies in determining the "theoretical degree of reaction". In the case of an isolated rotor, however, $r^{\#} = 1$, $\varepsilon s = 0$ and the efficiency becomes

$$\eta = \Phi.(1 - \Phi.\varepsilon_R)/(\Phi + \varepsilon_R)$$

and the simplified case of an isolated rotor eliminates the reaction problem. By rearranging

$$\varepsilon_R = (\Phi - \Phi.\eta)/(\eta - \Phi^2)$$

one can see that the ε_R term can be generated from experimental stage data relatively easily. The ε_R term can then be correlated with gap (e) changes. The effect of Φ variation is not strong when compared to that of η over a small range of Φ, however, correlating isolated rotor data from different tests (with different Φ's) would include the influence of Φ using this type of efficiency definition. It can be seen clearly from 1(10) that *if* the stator ε_S is affected by a clearance change at *the rotor tip*, the stage efficiency change will reflect both ε_R and ε_S influences, i.e., matching effects.

Another general feature of the lost work or induced drag models, or modelling in general, is the *implicit assumption* that *only* the modelled physics occur in the flow when the clearance is changed. When an experimental compressor flow is changed it is by no means certain that *only* the modelled events occurred[19] and are reflected in the

---

[16] Note that Rains data were measured from $0.003 < e/b < 0.01$. This is a relatively narrow band of e/b.

[17] There are two constants in the model which seem to be fitted from experimental data. The retained lift at the tip factor ($K = 0.67 - 7.45e/s$) should not be affected if an allowance were to be made for work coefficient changes due to its origin in cascade data. The "C" constants, however, seem to be empirically fitted from compressor data.

[18] See Yamamoto et al. (1982, Fig. 19) for turbines and Fig. 1.4-1 for a comparison to other models.

[19] Most models absorb control volume inconsistencies and any lack of comprehensive physical modelling in the empirically determined constants of the model, see discussion in Sec. A.1.2.4.

measured efficiency. None of the modelers seem to have examined this aspect of their model validation too deeply. Correlative methods (to be discussed below) do not involve such an assumption. One can appreciate from this discussion that the *definition of efficiency* and how the flow physical modelling is reconciled with measurements can be *as important* as the tip local flow's particular physical description.

1.4.1.3 Other Models and Observations

Many more models have been proposed than those described above. Those presented are essentially a representative sample. The reader should note that the efficiency decrement models generally reduce the whole passage flow to a very simple physical level. For example, Senoo and Ishida (1986) treat the blade tip loading as uniform from leading to trailing edge.

Attempts at comprehensive analytical solutions of the flow in the tip gap (Wu and Wu, 1954) have not been very productive. The analytical schemes end up depending entirely on the boundary conditions which, for practical purposes, are unknown. Analytical approaches have effectively been replaced by computational methods in recent years, however, the analytical methods are helpful in constructing correlations.

The models proposed, to date, do not include any blade profile (thickness distribution or camber) parameters in the physical descriptions developed. These parameters are related to end-bends[20] in the context of the database of experiments and range or geometries explored to date. It is clear this aspect of the tip flow modelling could be expanded.

1.4.2 Correlation of Efficiency Decrement

A number of correlations have also been published that perform a similar function to that of Eqn. 1(9) but do not assume a flow model. These approaches organize the data in some logical form based on physical observation or a cross correlation of selected parameters. Correlations avoid specific assumptions about the physical origins of the observations and the problems of properly calibrating any model constants. Correlations also provide correspondingly less insight into how to design improvements. The correlations, set out functionally as F(..), include those of Smith (1970)

$$\Delta\eta = F(e/g,\ \Pi/\Pi_{max},\ g/b)$$

$$\delta^{*} = F(e/g,\ \Pi/\Pi_{max}) \qquad 1(11)$$

Smith's correlation form is shown in Figure 1.4-2. The figure shows that the correlation predicts higher sensitivity ($\Delta\eta/\Delta(e/b)$ at lower flow coefficients, i.e., at higher percentages of maximum pressure rise. The major strength of this correlation as a predictor is its ability to determine a level or ratio of decrement at zero clearance relative to a *design* efficiency level. This design level would presumably include blade element profile losses derived from a strip theory method.

---

[20] Beknev's (1961) stage showed an unusually high overall efficiency considering its arbitrary tip design. It is not clear that the tip performance of Beknev's blading was superior to other designs, but the tip is essentially an end-bent winglet. Discussion of the design rationale is elaborated in Beknev (1968).

Robinson (1982, p. 45) proposes a form of the simpler "subtractive" correlation. Subtractive correlations provide relative decrement magnitudes from an unknown or undefined level. His expression, which is also presented in Freeman (1985, pp. 5, 20), is

$$\Delta\eta = F(e/R, HR)$$

$$\delta^{\#} = c.e/g \qquad 1(12)$$

Moyle (1988, p. 6) derived an expression by a different subtractive method, which is described further in Part 2, yielding

$$\Delta\eta = F_{\text{const power}}(e/b) \qquad 1(13)$$

F(..), in each case, implies a different collection of graphical and algebraic information for each correlation. The present author's correlation indicates the efficiency falls rapidly for small clearance changes close to the wall ($e/b < 0.01$) and levels off to a linear fall-off for small increments at larger clearance levels ($e/b > 0.02$). The correlation is for a *constant power* condition. The form of the constant power curve is very similar to the correlation of Mahler (1972, Fig. 4), shown in Fig. 1.3-2. Smith's and Robinson's correlations show linear fall-offs in $\Delta\eta$ with normalized gap (e).

1.4.3 Correlation of Spanwise Loss Distribution

Another form of tip clearance loss description is formulated in terms of blade profile loss coefficient (ω). The general functional form of the loss coefficient formulation is structured to account for two-dimensional blade element losses (ω_{2D}) and an additive term (ω_{3D}) which accounts for three dimensional losses due to clearance or near wall influences. In this type of formulation

$$\omega = \omega_{2D} + \omega_{3D} \qquad 1(14)$$

and it is assumed ω_{2D} is known. For example, ω_{2D} may be defined by a design incidence diffusion factor correlation of the type (Lieblein, 1957)

$$\omega_{2D} = F(D_{eq}).2\sigma(\cos\beta_1)^2/(\cos\beta_2)^3$$

The problem then becomes one of finding a ω_{3D} correlation with varying tip local parameters.

Functional Analysis In this type of (ω) formulation it is simpler to examine the ideas functionally than deal with the detailed expressions. The idea is to set out a comprehensive loss description for a rotor at an arbitrary radius (r) and compare the parameters of the strip theory passage design process with those that have been examined to date with regard to tip clearance. The general description may be written functionally, at radius (r), as follows

$$\omega_r = \omega_{2D,r} + \omega_{3D,r}$$

where

$$\omega_{2D,r} = F(\varphi_r, R, [HR, AR, \sigma_r, \gamma_r], [\xi_r, t/c_r]) \qquad 1(15)$$

In this arrangement of parameters, the general form of the passage shape can be defined by

$$R, [HR, AR, \sigma_r, \gamma_r]$$

and the blade element profile by

$$[\xi_r, t/c_r]$$

The design point nominal loading (diffusion) for the blade element can then be defined by

$$\varphi_{r(des)}, \sigma_r, \gamma_r, [\xi_r, t/c_r]$$

and for off-design conditions the loading can be defined in terms of

$$\beta_{1r}, \beta_{2r} = F(\varphi_r, \gamma_r, [\xi_r, t/c_r])$$

The three dimensional losses near the wall (where $r \rightarrow R$) might reasonably be assumed to be characterized by additional tip local conditions, for example

$$\omega_{3D,r} = F([\xi_r, t/c_r]_t, e/\{b, c, g, R\}, \delta^*, G_w) \qquad 1(16)$$

where G_w represents wall geometry conditions such as casing treatment including roughness. The term $[\xi_r, t/c_r]_t$ implies tip local blade profile geometry changes such as squealer tips or increased camber or thickness distribution variations (Wisler, 1977).

A large number of correlations for ω or ω_{3D} based on cascade test data are available in the literature. The (ω_{3D}) term has been also correlated by Roberts et al. (1988), who proposed $\omega_{3D(max)} = F(e,\delta^*) \propto \tanh \sqrt{(e\ \delta^*)}$[21] based on analysis of a large sample of compressor rotor test data. Their data are of particular interest due to the use of only rotating tests rather than cascade tests to develop the correlation.

Functional expressions of this type have an ability to demonstrate the dependence of the losses on the different blading design parameters without becoming entangled in the detailed equations. These expressions can also be used to indicate the degree of interdependence in the problem.

---

[21] Curiously, Dring (1983; Fig. 7), presents data showing an opposite trend in a comparison of normalized pressure losses for thick and thin boundary layers in an isolated rotor. The maximum total pressure loss near the rotor tip was larger for the thin boundary layer.

Eliminating Boundary Layer Thickness $\delta^{\#}$ For example, the boundary layer thickness, $\delta^{\#}$ of Eqn. 1(16), is proposed in Smith's (1970) correlation to be dependent on the passage geometry and passage loading (Eqn. 1(11))

$$\delta^{\#} = F(e/g_t, \Pi/\Pi_{max})$$

As g_t can be defined by

$$g_t = 2\cos\gamma_t R(1-HR)/(AR\ (1+HR)\ \sigma_m)$$

then the $\delta^{\#}$ expression becomes

$$\delta^{\#} = F(e, R, [HR, AR, \sigma_m, \gamma_t], \Pi/\Pi_{max}) \qquad 1(17)$$

From this expression it is evident the three dimensional ω_{3D} term (Eqn. 1(16)) is also dependent on the passage configuration. This can be seen if Eqn. 1(17) is substituted in 1(16) and 1(16) compared with 1(15), i.e.,

$$\omega_{3D,r} = F([\xi_r, t/c_r]_t, e/\{b\}, R, [HR, AR, \sigma_m, \gamma_t], \Pi/\Pi_{max}, G_w) \qquad 1(18)$$

The same parameters can be seen to reappear. Similar problems occur when other substitutions are examined. For example Roberts et al. (1988) proposed $\omega_{3D(max)} = f(e,\delta^{\#})$ which implies by substituting 1(17) into 1(16)

$$\omega_{3D(max)} = F(e, R, [HR, AR, \sigma_m, \gamma_t], \Pi/\Pi_{max}) \qquad 1(19)$$

The two relationships above also imply the problem is recursive due to Π/Π_{max} depending on ω_r. It is clear from such manipulations that the three dimensional blade end and tip clearance losses are not easily handled separately or with analytical ease in scaling the whole passage of a particular design.

The nature of these expressions also implies the models or correlations are not able to distinguish whether the tip local clearance flow influences or is influenced by the passage secondary flow. This is a point of some concern when the physics of a tip local flow are to be examined at a level of detail below that of efficiency decrement correlation. The point was addressed in Moyle (1989) and is discussed further in Part 2. Modelling at the equation of motion level is necessary to address such issues.

1.4.4 Optimal Tip Design Based on the Models

From this review of the models and the preceding discussion of the flow field and experimental database, one can see that a large number of parameters are involved in formulating a general functional description of the tip clearance losses. Considering the expression (1(18))

$$\omega_{3D,r} = F([\xi_r, t/c_r]_t, e/\{b,\}, R, [HR, AR, \sigma_m, \gamma_t], \Pi/\Pi_{max}, G_w)$$

If we assume Π/Π_{max} is fixed by the throughflow independently of the tip conditions and argue that R, *HR*, *AA*, σ_m and $\Delta\beta$ are fixed by overall machine flow path design requirements and further argue that an optimization is required at the design flow coefficient, then many parameters still remain to be considered in a purely aerodynamic optimization process at the tip section. These parameters also all have an influence on the overall stage efficiency and it is obvious that the parameters that produce optimum overall stage efficiency need not be consistent with optimum tip local conditions.

Usually the minimum running clearance level at the design condition is fixed by mechanical and thermal requirements. Assuming e/b is fixed, then the information of most utility in the design process is a model for the change in efficiency or ω_{3D} with the remaining flexible design parameters (γ_t, *AR*, [ξ_r, t/c_r], G_w). The *AR* variation defines γ_t and reduces to a variation of chord for the constraints described so the variables are (c, [ξ_r, t/c_r], G_w). The types of variations possible for the distributions are shown schematically in Figure 1.4-3.

If the models of Table 1.4-1 are examined for their ability to predict the effect of changes in these variables, each suggests the same parametric change expression, i.e., a change in σ or *AR*. In this situation, this results in a prediction for an optimum chord. The functional forms are retabulated in Table 1.4-2 with the only variable terms indicated in braces { }.

Table 1.4-2

Optimization Form of Models of Efficiency Change with a Fixed Operating Point and Tip Clearance (see Table 1.4-1).

Fickert (1946)	$\Delta\eta = f\{-\}$
Rains (1954)	$\Delta\eta = f\{\sigma\}$
Vavra (1960)	$\Delta\eta = f\{\sigma\}$
Lakshminarayana(1970)	$\Delta\eta = f\{AR\}$
Senoo (1986)	$\Delta\eta = f\{\sigma\}$

The limitations of the models are underlined in this table. These models really only address chord through C_L. Correlative approaches have the potential to be more useful, particularly if they can be developed from extensive test experience and include parameters for camber, profile thickness distribution [ξ_r, t/c_r] and treatment conditions (G_w) as well as chord.

A final point to note in a discussion of optimal tip design is the desirability of being able to minimize the *rate of change* of efficiency decrease with clearance increase. The fall-off rate in efficiency may in some cases be as important to the designer as the efficiency magnitude. Fan stages, for example, typically have low e/b values and lower hub-to-tip ratios (or larger b for a given R) and would be expected to show larger e/b changes with thermal variations. In this situation efficiency sensitivity to e/b

changes, rather than the peak efficiency, may have a large enough impact to dominate design considerations. This would have the consequence of changing the criterion for optimization rather than the variables.

It is relevant to compare the similarity of the parameters that this functional analysis suggests influence the optimization with Wisler's (1985) discussion of research trends. There has clearly been an effort to examine the $[\xi_r, t/c_r]_t$, G_w set of variables in recent tip clearance research (Wisler, 1977 and Wisler and Beacher, 1986). From the analysis presented it is apparent that the conclusion that these variables are significant can be derived from the functional relationships. However, the reader should note this outcome is mainly a consequence of how the relationships were posed initially, i.e., 1(16).

1.4.5 Models and Correlations Summarized

Modelling and correlating flow behavior or efficiency or loss with tip clearance changes have been continuing activities in the literature. It can be seen from the model descriptions that the tendency of previous investigators to select a particular aspect of the flow pattern, formulate a model and evaluate has led to a large number of tip loss models and algorithms. These many models are based, however, on a relatively small number of flow mechanisms acting in or around the tip gap (Sec. 1.2). In this section the discussion has addressed:

(1) Models predicting efficiency decrement (Sec. 1.4.1) which covered lost work and induced drag approaches. These models typically reflect pressure driven leakage and shed circulation mechanisms.

(2) Correlations of efficiency decrement (Sec. 1.4.2) which are primarily used to account for mechanisms based on the case wall boundary layer's behavior.

(3) Correlations of spanwise loss distribution (Sec. 1.4.3). Correlations of this type typically treat case wall boundary layers and gap flow as if they were a blade surface boundary layer which has been greatly thickened at the tip.

(4) The potential for minimizing inefficiency or losses by optimizing the geometry at the blade tip using the existing models (Sec. 1.4.4). It was shown that the present models have very limited potential (relative to the geometric parameters of a blade tip section) to influence the design.

The varied models and correlations that are in the literature can be analyzed, compared and evaluated endlessly without making much headway with the basic "what is and what causes the tip effect" problem. The reason for this lies with the fact that the models are essentially *derived from* plausible *assumptions* about the flow mechanisms and then validated against the observed data. The correlative methods also place the observed data in a framework that has, to some extent, been defined by plausible assumptions, but usually without particularly detailed physical behavior in mind. In either case, as understanding of the flow mechanisms at the tip increases the models and correlations should become more consistent and productive. Identifying, understanding and comprehensively validating the mechanisms is where the basic tip clearance problem is seen to lie.

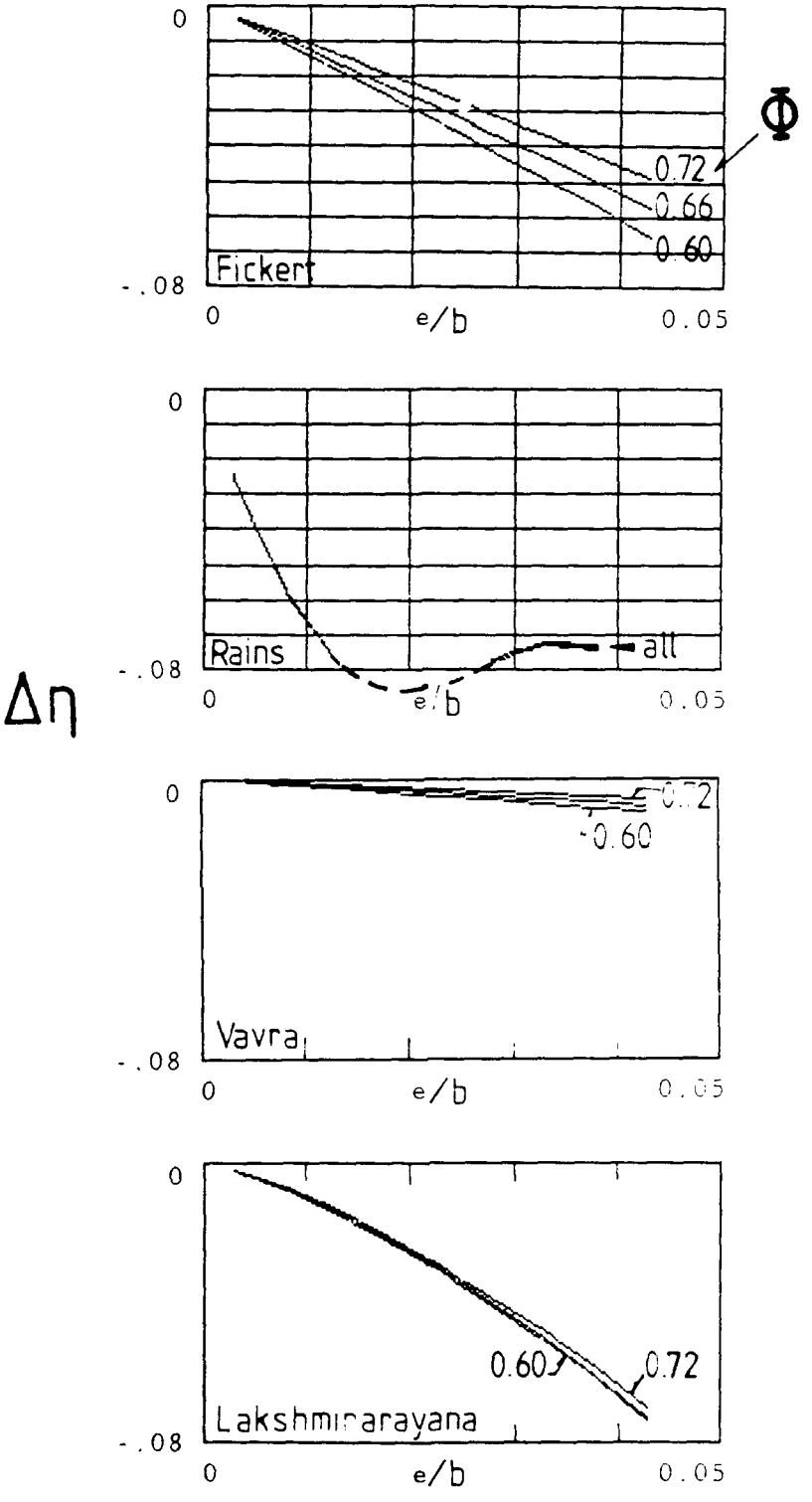

Fig. 1.4-1 Predictions of efficiency decrement using the models of various investigator for a common stage. The stage used as a comparison baseline is experimentally investigated in Part 3 of the present study.

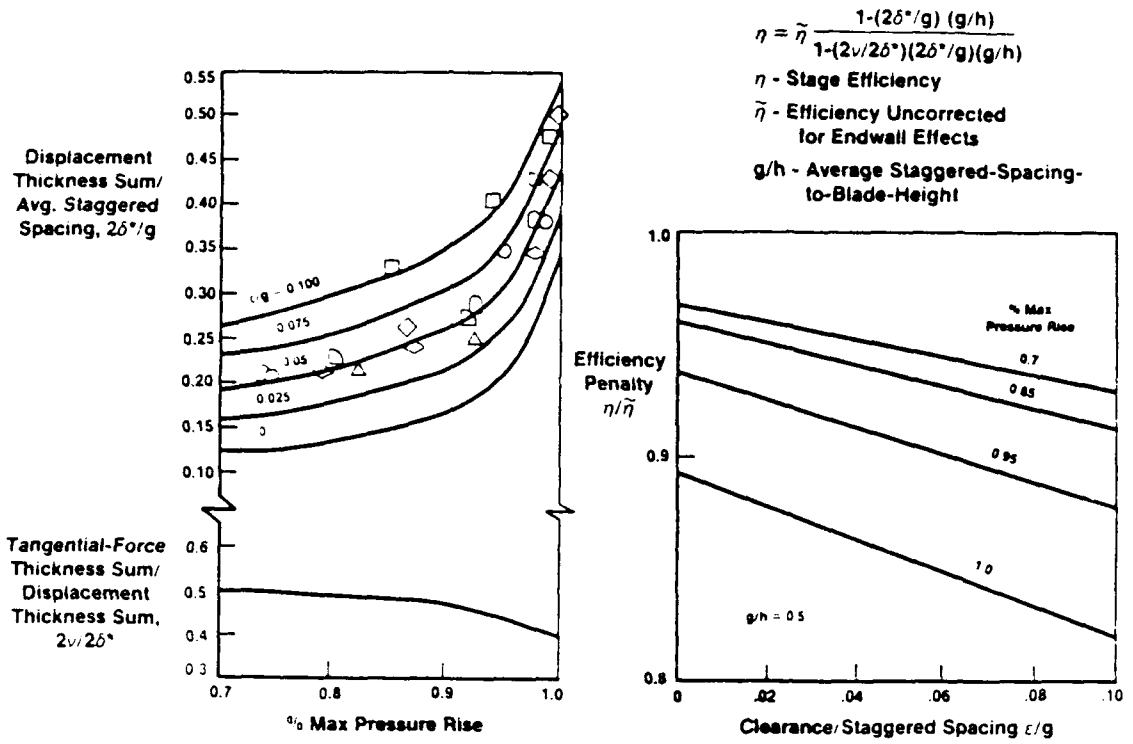

Fig. 1.4-2 Effect of tip clearance on end wall boundary layer loss based on Smith's (1970) correlation. Reproduced from Wisler (1985, Fig. 94b).

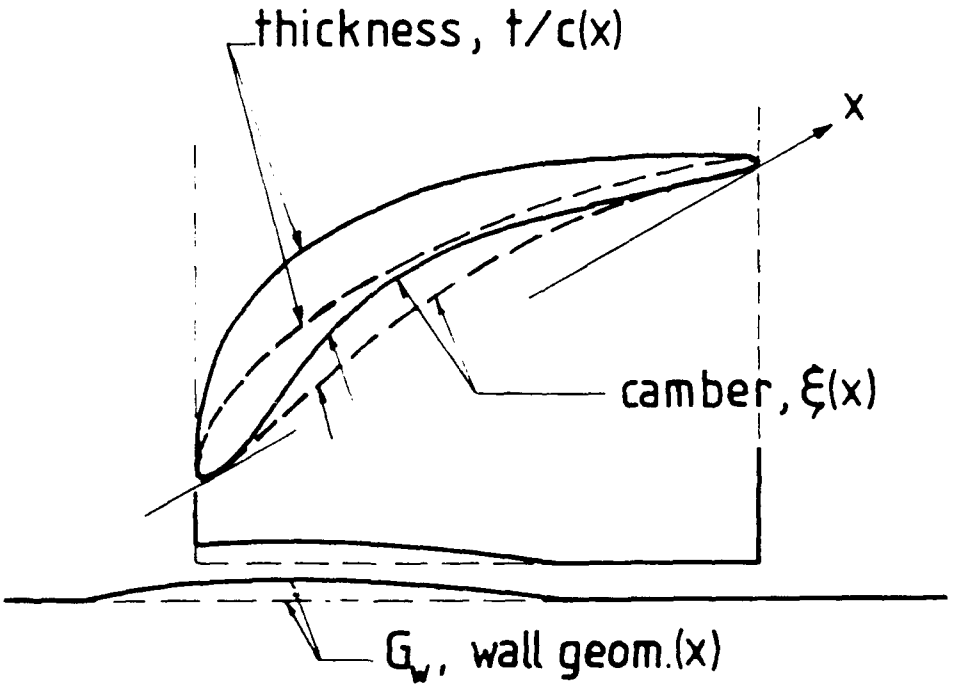

Fig. 1.4-3 Schematic of the tip local design options suggested by the parametric analysis of Sec. 1.4.4.

1.5 Summary and Directions for Further Research

From this overview of the literature it can be seen that a significant amount of experimental and analytical work on the tip clearance flow, its consequences in terms of the stage flow and attendant losses has preceded this study. The accumulation of prior work has developed into a data base of empirical test results, a large number of models for efficiency changes based on a variety of assumed flow mechanisms and some insight into the detailed flow pattern from a very small selection of experiments.

1.5.1 Observations

Some of the observations, that can be made about the prior work, have already been outlined in a previous literature survey, Moyle (1981). In that survey a number of general qualitative statements were made about the earlier literature, principally:

(1) the absence of a unambiguous demonstration of *any* proposed mechanism for the losses attributed to clearance in axial flow compressors. In fact the loss attribution is, itself, often ambiguous due to (4) below.

(2) the apparent correlation of proposed clearance loss mechanisms with the dominant pressure gradients of the experimental device(s) used. As many of the test devices were only approximations to a complete compressor, there is an experimental device bias in most proposed flow structures and mechanisms.

(3) the similarity in the order of magnitude of the effects of clearance, average boundary layer thickness and casing treatment on the flow and the similarity of their basic length scales.

It was also noted that a substantial amount of the quantitative experimental information on this subject has been published by industry. Frequently the test geometry descriptions were not disclosed. Certain correlative information or trends could be derived from this type of data but the data were not complete enough to be well suited for analysis in this study.

In the present, more extensive, review additional observations were made. These were principally:

(4) much of the experimental data has been produced by blade cropping, which reduces the working surface of the blading in the passage, as well as increasing the clearance. (Table 1.3-1)

(5) the effect of passage whirl distribution on tip flow has not been evaluated in a consistent experiment and whirl influences do not seem to have been considered in the model validations. This is particularly so for leakage models where the pressure differential across the gap is the dominant consideration in the approach. (App. A.1.2)

(6) the range of geometric parameter variation in published tests was very limited compared with the number of geometry parameters typically included in the models. (App. A.1.1)

(7) the extent of applicability of a particular model to widely varying geometry (Sec. 1.3.3) or flow conditions (Fig. 1.1-5 and Fig. 1.4-1) is essentially unknown.

(8) there are hardly any detailed surveys of changes in passage secondary flows in conjunction with changes in overall stage performance (with changes in clearance) which might provide solid experimental evidence to support, or eliminate models proposed. (Sec. 1.3.2)

(9) the inconsistency of predictions from model to model when applied to the same stage geometry and the large number of models presented in the literature. (Fig. 1.4-1)

(10) the limited capacity of the flow models to contribute to blade tip design optimization at a fixed level of clearance. For practical purposes the only variable whose change can be modelled in a design is tip local chord. (Sec. 1.4.4)

(11) the difficulty of attributing the performance changes of experimentally evaluated stage modifications to particular local aspects of the flow (modelled) (Sec. 1.3.4.2) and the highly interdependent nature of the problem in terms of passage parameters. (Sec 1.4.3)

Several areas in the literature where previous investigations have been minimal or further exploration would seem worthwhile were also noted. These were particularly;

(12) the favorable conditions for separation or recirculation in the leading edge corner of the suction side. (App. A.1.3)

(13) the limited understanding of the action of the case wall as an aerodynamic surface and the influences of its curvature on the scaling of the tip flow mechanisms and flow on the suction side of the tip gap. (App. A.1.3) It was also noted that consideration of the effects of camber, thickness distribution and wall treatments on the tip local flow have only recently been addressed. (Sec. 1.4.4)

(14) the lack of procedures for satisfactorily isolating a tip flow dependence in the experimental data when the machine and its characteristic performance are also being altered by its own flow and a duct system of unknown distortion sensitivity (a relative of (4) above). (App. A.1.2.4 and 1.3.4.1)

(15) the unknown influences of upstream blade wakes, distortions and separations on the overall tip flow pattern. The influences of the unsteady aspects of the flow field on *tip losses* have not been examined in detail. (App. A.1.2.1 and A.1.3)

1.5.2 Conclusions and Overview

In compiling the compressor tip clearance literature a number of conclusions can be reached rather quickly. These are essentially that

(a) the component of the total inefficiency of an axial compressor associated with the typical tip seal clearance gap dimension used in practice (0.01-0.02 e/b) is significant.

(b) a relatively large number of different experimental compressors (about 15) have been tested in detail with definition of clearance related phenomena in mind. The results of the testing have been similar in terms of some of the effects observed, namely roughly linear efficiency decrement increases with increasing normalized clearance and growth of a near wall loss core region in the passage. On the other hand the results have differed in the slope or sensitivity of the decrement curve observed and in the nature of the secondary flow pattern (vortex or no vortex) present with the loss core. The magnitude of the inefficiencies observed in the experiments have also been significant and consistent with the practical experience.

(c) there have been three dissimilar physical mechanisms proposed to account for this significant tip gap related inefficiency. The three mechanisms have become "established" in the literature and have been embroidered and refined over a period of time.

(d) from the three basic mechanisms about 10 to 20 analytical models or correlations have been derived and proposed to quantitatively characterize the experimental data available at the time.

These conclusions more or less fall out of the compilation process. If the compiled literature is then studied to see what is *known* about the nature of tip clearance loss mechanisms the state of knowledge boils down to (b) above. Note that (b) is a concise statement of a relatively straightforward situation.

If the compiled literature is studied to see what has been *derived* with this knowledge you end up at (d) above via (c). If what has been derived (d) is studied as a body of knowledge one ends up with a reconciliation nightmare.[22] Reeder (1968) became particularly disheartened with the contradictions, fragmentation and multiple modelling viewpoints as he compiled his 1968 review. Since that time the literature has expanded considerably and today producing a reconciled picture of the models and correlations is even more difficult. One eventually concludes that one can conclude very little from such an approach.

If the literature is studied to see what *needs to be known* that has not been resolved already, a few simple conclusions are reached. These are

(e) The primary knowledge problem lies at the mechanism(s) level, (c) above. An improved resolution of whether (one of) gap leakage, tip local vorticity generation or boundary layer growth dominate the entropy production is required. Alternatively, the means by which they interact or combine to produce the inefficiency is required.

(f) To be useful for blade design or machinery optimization, models based on better understood and defined mechanisms need to be additive to two dimensional strip theory design (section profile loss) estimation procedures for any blading. Smith's (1970) correlation is the only method in the literature that presently approaches this ideal.

In summary, the tip clearance literature can be very complicated if you approach it from a model viewpoint expecting to see different facets of the same phenomenon. Rather,

---

[22] A very cumbersome feature of the literature is the number of competing physical descriptions and, consequently, the excessive (in the author's opinion) number of analytical models put forward to explain or predict the same phenomenon. In reviewing the literature one cannot fail to notice how many similar models have been proposed and the relative lack of weeding out or consolidation of these propositions over a forty year period of active research on the subject. A compilation of models and methods which consolidates the literature and is *widely accepted* would be valuable.

the literature consists of a great deal of independently derived material based on a variety of mechanisms of similar strength deduced from almost independent sets of experimental results. Finding such a situation in the literature, the "what is known" and "what needs to be known" influenced the present research much more than the derived (d) information in the literature.

1.5.3 Research Directions Selected for the Present Study

In formulating the present program to make a further contribution to the tip flow literature, it was clear that all of the observations above could not be addressed. The approach chosen (Sec. 1.1.3) emphasizes evaluating the flow pattern and loss production mechanisms over a wide range of geometric and operating parameters. The reason for this choice was the need to know what is, in fact, generally applicable as a tip clearance related phenomenon, before considering plausible mechanisms and how they might be modelled or controlled in a design sense. Considering the conclusions above and such a theme, the observations of interest from the literature worth *analyzing* more thoroughly were particularly:

(2), (7) and (14) The question of whether improved tip effect isolation methods might provide a better understanding of, or insight into, the entropy producing mechanisms at the tip. There appeared to be need to organize and analyze the prior experiments and existing database more systematically with a view to identifying the key phenomena in the flow mechanics.

(12) The question of whether the conditions near the case wall in the tip leading edge corner favored separation and whether this was a general condition in all machines and a strong influence on losses.

(4) and (13) The effects of case wall curvature seemed to be largely unknown. The geometric relationships, the extent of wetted wall area and preliminary analysis (Taylor Number magnitudes near the stability limit) suggested case wall curvature influences and flow transition or stability should be examined in more detail.

An experimental study over a wide range of geometries could not be attempted in this program (experiments are discussed in Part 3). The compressor available for experiments was not well suited to hub-tip ratio or solidity variations. Blade spacing and number of stages could be varied, however. Considering the experimental equipment available, the other facility resources and the unresolved issues the following items were selected for *experimental* emphasis in the present study:

(8) and (14) Obtaining more intersections of performance data and detailed measurements to contribute to the data base.

(7) The test compressor facility was able to operate with small clearance gaps, $(e/b)_{min} = 0.002$, so an effort was made to acquire small clearance data.

(15) Exploration of consequences of stator proximity (wakes) on the blade-to-blade rotor tip flow near the case wall.

In addition an attempt was made in the program to make skin friction or wall shear measurements on the case wall. Such measurements were not available in the literature and might aid in experimentally identifying loss mechanisms near the tip.

Part 2

Analysis of the Tip Gap Flow Effects

While the literature contains much derived material (i.e., hypotheses, models etc.), the observable effects of tip gap changes in compressors can be counted on one hand. The reason for this precipitous decrease in information can be explained by inspecting Eqn. 2(1) which functionally relates the typical variables an experiment (see App. A.1.2.5).

$$\{\Pi', P'\} = F_{A'}(\{\Omega,\Phi\},(e'/b),\{Z,\ R,\ AR,\ HR,\ \sigma,\ AA,\text{tip geom.}\}_{A'}) \qquad 2(1)$$

The literature is largely preoccupied with accounting or modelling for the independent quantities on the right of the equation. The consequences of tip gap changes, however, manifest themselves on the left side of the expression. The present author, in retrospect, attempted to study the accounting for independent quantities on the right by studying and analyzing the nature of the changes on the left of the expression. Because this approach has no precedent in the prior clearance literature, the rationale is outlined below.

The outcome of experimenting with a compressor of a fixed geometry is a set of pressure rise and power curves $\{\Pi', P'\}$ that depend on speed and throughflow settings $\{\Omega,\Phi\}$. If one recalls that efficiency changes are the most widely available measure of the effect of a clearance change in a compressor and efficiency can be defined as $\eta = \Pi\Phi/P$, it can be seen that the left side of the expression above can be replaced by $\{\eta', P'\}$ if a control volume is defined. By examining the changes in $\{\eta', P'\}$ for a wide range of geometries, the influences of $\{Z,R,AR,HR,\sigma,AA,$tip geom.$\}$ in conjunction with (e'/b) can be explored. This is the basic rationale behind the work of Sec. 2.1.

Section 2.2 focuses on the Π' of $\{\Pi', P'\}$. While the power quantity P' can only be defined in terms of a control volume, the Π' quantity can be described in terms of the equation of motion governing the flow field without regard to control volume. For an incompressible flow in the relative frame the gradient of relative total pressure can be expressed as (Vavra, 1960 Eqn. 7(39))

$$\nabla(P_R/\rho) = -\partial_R(\underline{W})/\partial t + \underline{W} \times (\nabla \times \underline{W} + 2\,\underline{\Omega}) + \underline{f} \qquad 2(2)$$

The expression shows that a total pressure defect may be the consequence of several factors. As change in the near wall total pressure defect core is the primary outcome of changing the tip clearance gap, then the equilibration of the accelerations in the equation indicates that unsteady velocity conditions, finite vorticity not aligned with the velocity or friction could produce such a core. In the analysis of Sec. 2.2, a steady inviscid situation near the wall is examined. The analysis shows that the gradient of total pressure in the radial direction can be very different from machine to machine if a velocity gradient, typical of a shear layer, is present near the wall. Unsteady and frictional forces near the wall are addressed experimentally in Parts 3 and 4. The results of the Part 2 present an alternative picture, of the right side of Eqn. 2(1), to what one might arrive at from a reading of the prior literature.

2.1 Efficiency Sensitivity to Clearance at Constant Power

The fact that the ratio of change of efficiency to change of clearance gap varies significantly for different compressors in the published data has been mentioned previously. An analysis of this sensitivity range in terms of the blade and stage design parameters is described below.

The clearance effect is generally understood to mean the change in the compressor characteristic as the tip clearance gap is varied over a small range of the gap dimension. Typically, but not universally, the overall pressure rise and efficiency substantially decrease for a multistage compressor with increasing levels of clearance. Stage test data, however, always seem to show a fall in efficiency with clearance across the stage flow rate range.

2.1.1 Sensitivity Data

Clearance sensitivity data are developed experimentally by measuring compressor or stage performance for a range of clearance dimensions or parameter increments and establishing the difference in efficiency between each dimension or parameter level. Direct methods of effecting the clearance change in terms of dimension have included cropping the blades (Ruden, 1937 and Williams, 1960), enlarging the case wall diameter (Inoue et al., 1986), recessing the clearance (Wisler and Beacher, 1986) and varying the blade root depth (Schmidt et al., 1987). Parametric changes in terms of a clearance gap (e) normalized in terms of some other dimension or feature of the flow have also been addressed by considering the boundary layer (Smith, 1970), its thickness (Hunter and Cumpsty, 1982) or case wall roughness (Bettner and Elrod, 1982). In all these experiments the compressor (or stage) configuration was not significantly altered; that is, the change could be considered a small perturbation of the configuration primarily related to the clearance parameter or local roughness.

The results generated were frequently correlated in terms of the efficiency change of the stage ($\Delta\eta$) as a function of the normalized clearance gap. The normalizing dimension most commonly used is the blade height (b), however staggered spacing, tip section chord and blade thickness have also been used (App. A.1.1). Data plotted by Lakshminarayana (1970) and subsequently by Senoo and Ishida (1986) and Schmidt et al. (1987) are shown in Figure 1.3-1. These are typical examples of the data generated. The sensitivity (slope) has been shown previously to vary from 0.75 to 2.25 percent per percent around the one percent level in (e/b) for near design flow.

The data suggest certain bladings have lower sensitivity than others. From a design perspective it would be desirable to know how to produce the lowest sensitivity for any stage configuration. Reducing end wall losses associated with the clearance is discussed by Wisler (1977) in terms of the tip loading of several test rotors and was discussed in Sec. 1.4.4.

2.1.2 Interpretation Of The Sensitivity Data

The initial intent of the analysis was to address the extended set of geometric parameters (discussed above) and attempt to correlate the sensitivity spread observed in the literature with design variables that might be optimized. The first task was to gather the details of known test stages and their tip geometry. In so doing, it was noted that the sensitivity varied with flow rate or stage flow coefficient, Φ. It was also noted that certain sensitivities were defined in terms of decrease in peak efficiency

while others were derived at constant flow rate. A more general definition of the sensitivity was then sought to apply to all the data available.

2.1.2.1 Definition based on Losses

The primary outcome of a clearance variation is a change in stage pressure rise at any flow rate. As this process can be thermodynamically characterized in terms of the shaft power converted into flow work per unit time and the power lost to inefficiencies, a general definition of the losses is given by

$$L = P - \Phi\Pi \qquad 2(3)$$

Where the lost work rate (L) plus the flow work rate ($\Phi\Pi$) equals the power input (P). The aggregate lost work rate can be related to the integral spanwise passage average loss coefficient and in turn to the blade element loss coefficients by appropriate manipulation. For any change of compressor geometry from one configuration to another, for example from clearance 1 to clearance 2, the change in losses can be expressed as

$$L_1 - L_2 = P_1 - P_2 - \Phi\Pi_1 + \Phi\Pi_2$$

and if the efficiency is introduced as

$$\eta = \Phi\Pi/P$$

Then the efficiency to loss correlation is

$$L_1 - L_2 = P_1.(1 - P_2/P_1 + \eta_1 - \eta_2.(P_2/P_1)) \qquad 2(4)$$

It is apparent from this formulation that the change in efficiency is not generally equivalent to the lost work rate change between two configurations. Alternatively, *a change in efficiency only directly reflects a change in losses between two configurations if the efficiency change is determined at the same input power level*, i.e., if $P_1 = P_2 = P$ then

$$(L_1 - L_2)/P = \eta_1 - \eta_2$$

This expression indicates that *if* the efficiency decrement at a constant flow coefficient is used to determine the clearance sensitivity of a stage, it does not solely reflect the change in losses over the blading but also includes any shift in the stage power characteristic that may occur, see Eqn. 2(1) where both η and P change with e for a constant Φ. This point is significant if the flow mechanisms creating the loss are of primary interest or are being modelled.

2.1.2.2 Efficiency Change with Shaft Power

The composite effects are shown schematically in Figure 2.1-1 where flow work ($\Phi\Pi$) is plotted versus power input (P). A straight line passing through the origin in this plane is a line of constant efficiency. By plotting the compressor characteristic on this coordinate plane, at two different clearance levels, and linking points of constant flow coefficient, the distinction between the increase in losses and efficiency change at

constant flow rate and at constant power is clearly demonstrated. The lost work rate differs substantially between the two clearance levels as the power increases over the range shown.

However, the change in efficiency at constant flow, spanning the two power levels, is seen to be relatively small. The efficiency correlations with gap/blade height of Fig. 1.3-1 have been established by this method of subtraction of efficiency levels at constant flow over a range of clearance increments. This mode of derivation of an efficiency to clearance correlation will inherently produce a linear expression with a low slope, as shown in Fig. 1.3-1. As flow rate is reduced, the slope of the constant flow efficiency curve will tend to increase then flatten out. This trend has been detected in the data by Schmidt et al. (1987), however, the reason for the trend was not discussed.

It should also be noted that changes in peak efficiency more closely relate to constant power efficiency decrements (and hence losses) than decrements at constant flow. In order to standardize the reported sensitivity data, several sets of experimental data were plotted in this graphical format and the clearance sensitivities determined at constant power.

Low Speed Cropped and Recessed Data As the flow work vs. power characteristic was entirely general in terms of the losses indicated, comparisons could be made between the effects of clearance changes by cropping the blades, increasing the case wall diameter, increasing hub diameter and recessing the clearance. Provided input shaft power had been measured in the experiment, data from different tip and wall perturbation experiments could be compared. Data from four low speed compressor experimental programs are shown plotted on Figures 2.1-2 and 2.1-3. The data are all for air compressors except Williams' stage, which was for water.

The figures show, respectively, the data of Ruden (1937) for a cropped blading in an isolated stage without guide vanes and Williams' (1960) cropped data for a stage with inlet vanes. The data are carpet plotted on Figure 2.1-2. The incremental change in loss with gap increments can be clearly seen. There is a trend towards larger efficiency improvements as the clearance is decreased. Ruden's data shows the strongest improvement as the clearance is reduced. This trend is generally consistent with peak pressure rise data shown schematically by Koch (1981) and is *not* consistent with the trends shown in Fig. 1.3-1.

Inoue's (1986) data for an essentially isolated rotor with no preswirl vanes and Wisler and Beacher's (1986) data for a four stage (averaged) compressor at two clearance levels with different degrees of recessing of the clearance are shown on Figure 2.1-3. The data from Wisler and Beacher show the losses to be largely insensitive to the gap location (i.e., either in or out of the wall) but strongly dependent on the gap dimension. In terms of effecting changes in performance with local profile variations, their data were not encouraging.

This situation notwithstanding, the striking feature of the sample data is the almost identical effect of the clearance change on the characteristics and the *decrease* of the constant power sensitivity with increasing clearance. The trend is consistent for three of the four substantially different configurations, bladings and power levels, as well as, two fluids. Wisler and Beacher's data did not provide a trend.

The *decrease* in constant power sensitivity with increasing clearance is the opposite of the constant flow sensitivity *increase* shown by Lakshminarayana (1970). Although the sensitivities were different in terms of derivation a similar trend was expected to be

discernable. Lakshminarayana's (1970) correlation seemed to provide an excellent fit to Williams' (1960) data, so the data were verified by the present author. Williams' Φ = 0.343, e/b = 0.0129 point, as plotted by Lakshminarayana, is in error by about 0.7 percent (low). In addition, Ruden's Φ = 0.388, e/b = 0.032, 0.040, 0.048 points were positioned one percent low. When positioned correctly, the constant flow data are consistent with the decreasing sensitivity trend of the constant power plots, as the clearance is increased. The corrected data points are plotted in Fig. 1.3-1, which is a composite of (essentially the same) data plotted by Lakshminarayana, Senoo and Schmidt. It should be noted that the data of Schmidt et al. (1987) also follow the trend discussed quite clearly, more so than other tests. Schmidt et al. noted the disagreement with Lakshminarayana's model and developed a modified "Lakshminarayana model" to reflect the curvature trend observed in their data.

High Speed Cropped and Recessed Data As the clearance effect in terms of losses seemed to be consistent between low speed stages, high speed data were also correlated on a flow work vs. power characteristic. Data on high speed stages are not as abundant as at the low speed and fewer test conditions are reported. Testing by Holman and Kidwell (1975), Moore and Osborne (1977) and Moore (1982) have included clearance variations and efficiency measurements.

The data of Moore (1982) included rotor efficiency variation with clearance and has been plotted in Figure 2.1-4. Although the data are sparse, the general trend of the low speed data is evident and sensitivity to clearance could be generated. The 100% and 70% speed conditions had sufficient test points and these data have been included on the figure. The 70% speed case showed lower sensitivity overall. This was consistent with less blade growth at the lower speed and, hence, a larger clearance level. Both of Moore's experiments employed case wall inserts of increasing radius to alter the clearance. Holman and Kidwell cropped the rotor tips.

Low vs. High Speed Sensitivity Because the test points were sparse and power was not extractable from some of the high speed test data, changes in peak efficiency were used as a substitute for determining constant power sensitivity. In comparing the low and high speed data, the sensitivity derived from Figures 2.1-2 to 2.1-4 and Table 2.1-1 were set out on Figure 2.1-5 in a log-log plot of sensitivity ($\Delta\eta/\Delta e/b$) vs. gap/blade height (e/b). It is apparent from this figure that the high and low speed data are consistent. The high speed showing much larger sensitivity at clearances less than one percent. The log sensitivity can be *roughly* correlated with log (e/b) by a linear relationship. The sensitivity for each set of stage data also maintain the nominal slope indicated by the whole sample. Ruden's data appear to show a distinct transition about the 2.5% (e/b) level. The data are not detailed enough to isolate a change of flow character which might be suspected if the gap dimension exceeds the passage boundary layer momentum thickness.

Table 2.1-1

Characteristics of the Stages and Experimental Compressor Test Data used to develop the Efficiency Sensitivity.

($\Delta\eta$ = Stage Peak Efficiency Change, ?=data value could not be established)

	R_t (m)	U_t (m/s)	RPM (%)	e/b_{min}	$\Delta(e/b)$	$\Delta\eta$	$\Delta\eta/\Delta(e/b)$
Low Speed Stages							
Ruden (1937)	.250	?	100	.008	.040	.010	2.5
Williams (1960)	.178	3.7	100	.0025	.023	.045	2.0
Inoue et al (1985)	.225	?	100	.006	.050	.055	1.1
Wisler & Beacher (1986)	.762	70.8	100	.014	.014	.015	1.09
Schmidt et al. (1987)	.254	39.4	100	.003	.022	.075	3.33
High Speed Stages							
Holman & Kidwell (1975)	.059	474	100	.008	.014	.060	4.41
		427	90	.010	.014	.045	3.31
Moore & Osborne (1977)	.250	423	100	.002	.009	.071	7.55
		296	70	.004	.009	.027	2.87
Moore (1982)	.250	423	100	.002	.009	.054	5.74
		296	70	.004	.009	.027	2.02

In addition to the graphically derived constant power sensitivities, the average stage peak efficiency sensitivities tabulated were log-log plotted on Fig. 2.1-5 at the lower clearance of the increment. An approximated functional dependence is sketched on the plot.

2.1.2.3 Correlation of the Sensitivity at Constant Power

The approximate dependence of the sensitivity shown on Fig. 2.1-5 can be integrated to yield the constant power variation of efficiency decrement with clearance. By selecting a constant of integration to normalize the function at the 1% $\Delta\eta$ and the 1% e/b point the curve of Figure 2.1-6 can be obtained. The curve shows an initially rapid increase in the efficiency decrement associated with the clearance very close to the wall and a gradual tapering-off of the decrement toward the limit of a 1% efficiency decrease for a 1% clearance increase at clearances greater than one percent. This constant power efficiency curve strictly represents the lost work rate associated with a clearance perturbation and is roughly representative of the peak efficiency variation with clearance change. The expression for the approximate curve shown in Fig. 2.1-6 is

$$\Delta\eta = 0.214\ (e/b)^{.227} - 0.065$$

It should be stressed that this correlation is an approximation to the data sample addressed in the discussion and it is expected it could be refined with more data over a wider range. The form of the efficiency curve derived in this manner contrasts with

the linear to slightly parabolic (increasing) correlations proposed by recent[23] studies for axial[24] machines.

2.1.3 Consequences of the Constant Power Correlation Form

It can be seen that the results of this analysis (i.e., the general form of the constant power sensitivity correlation with gap/blade height) strongly suggest that the passage geometry or flow variables do not affect the loss character greatly. An alternative inference in the data is that the only significant correlating parameter is the gap/blade height. The conclusions were summarized as follows:

(1) The efficiency change due to clearance, formulated in terms of sensitivities derived at constant power, showed a well defined decreasing trend in efficiency change with increasing clearance gap. This is a trend that is contrary to some earlier published data and correlations.

(2) The use of linear extrapolations of efficiency changes at constant flow to zero clearance does not reflect the non-linear character of the loss development, especially for small clearances. Also, the relatively complex parametric models developed from loss considerations in the tip region might be simplified by use of constant power rather than constant flow efficiency sensitivities in analyzing test data.

(3) The slope on the log-log efficiency sensitivity vs. gap/blade height plot is similar for the stages where constant power sensitivity was calculated. Normalization of the clearance gap by any other characteristic dimension of the blade passage will not alter the slope presented or the exponent derived.

The final observation (3) indicates there is an underlying consistency in the loss generation mechanism in the data examined that is independent of normalizing dimension but dependent on gap. This point is worthy of further exploration as it may provide the basis for an improved analytical description of the tip clearance mechanisms or better approximation of empirically derived model constants.

---

[23] Curiously, one of the earliest experimental (single stage axial) studies found, in all the literature, (Sedille, 1939) shows the strongest non-linear efficiency correlation of the form derived above. At constant flow, the clearance level of e/b = .0083 showed a sensitivity of 5 for smaller gaps and roughly 2.5 for larger values with a trend to 1 percent per percent.

[24] Similar trends have been observed in recent centrifugal compressor testing with clearance changes. Studies by Engeda et al. (1988, Fig. 7) and Brasz (1988, Fig. 12) show significantly greater efficiency improvements as clearances decrease, i.e. sensitivities become large at small clearances.

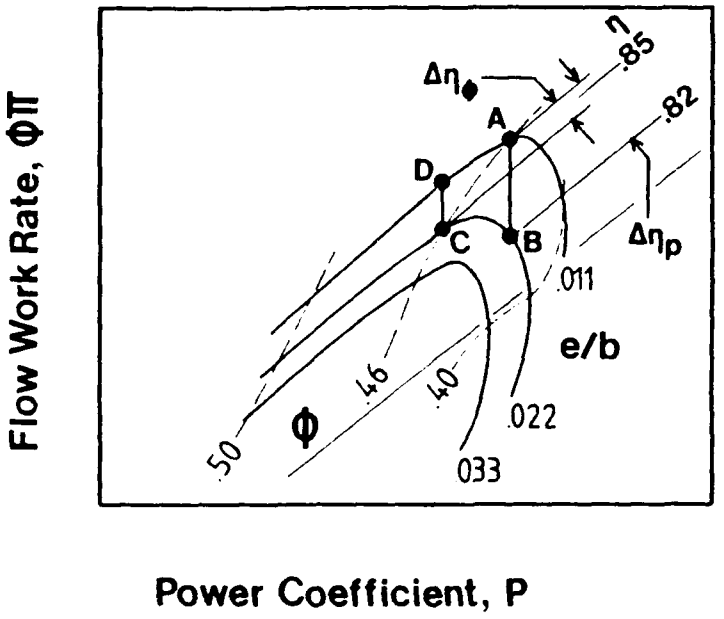

Fig. 2.1-1 Schematic flow work vs. power input characteristic illustrating methods of efficiency decrement determination based on data from Inoue et al. (1986).

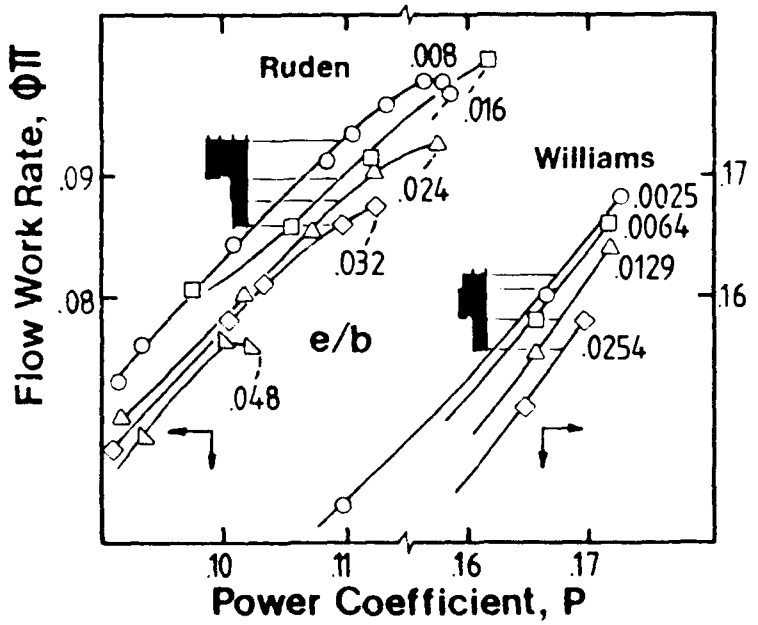

Fig. 2.1-2 Flow work vs. power input characteristic for cropped blades tested by Ruden (1937) and Williams (1960). The solid bars projected away from the e/b curves indicate the corresponding change in efficiency between curves.

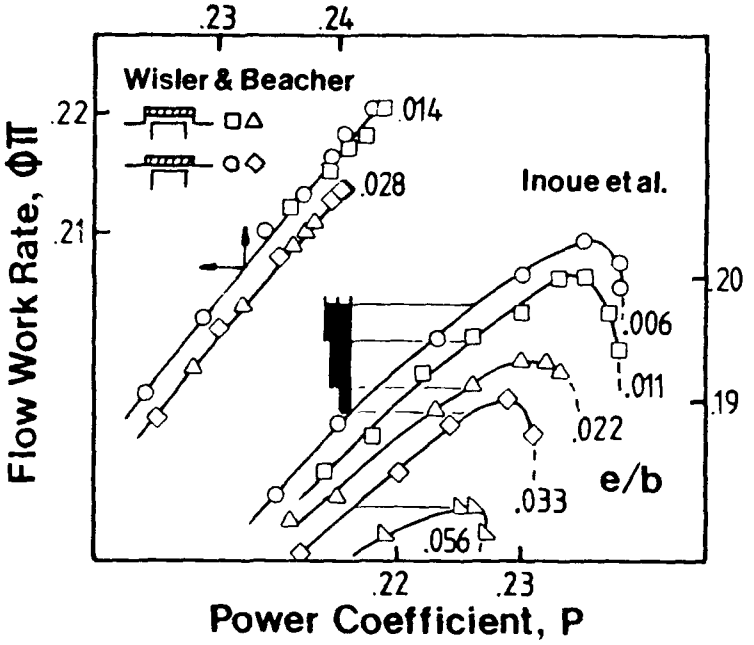

Fig. 2.1-3 Flow work vs. power input characteristic for case wall diameter changes by Inoue (1985) and recessing by Wisler and Beacher (1986). The solid bars projected away from the e/b curves indicate the corresponding change in efficiency between curves.

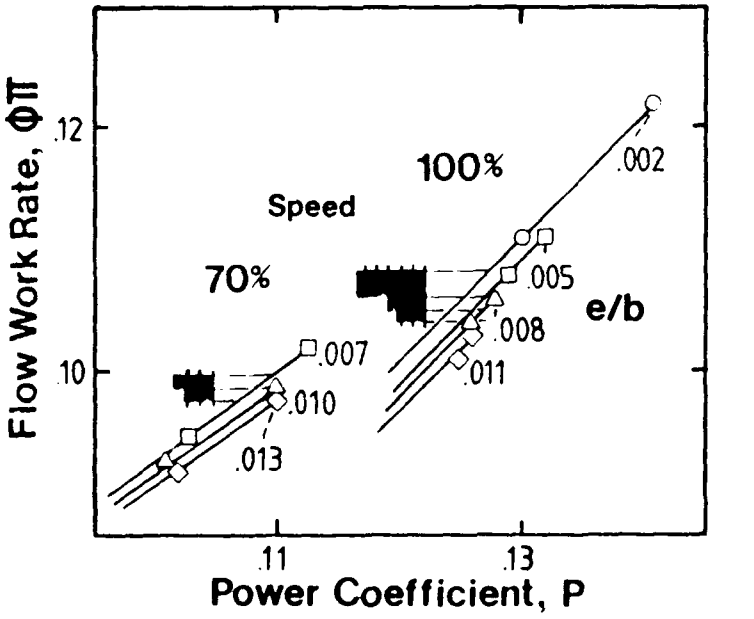

Fig. 2.1-4 Flow work vs. power input characteristic for a transonic rotor at two speeds tested by Moore (1982) with wall diameter variations. The solid bars projected away from the e/b curves indicate the corresponding change in efficiency between curves.

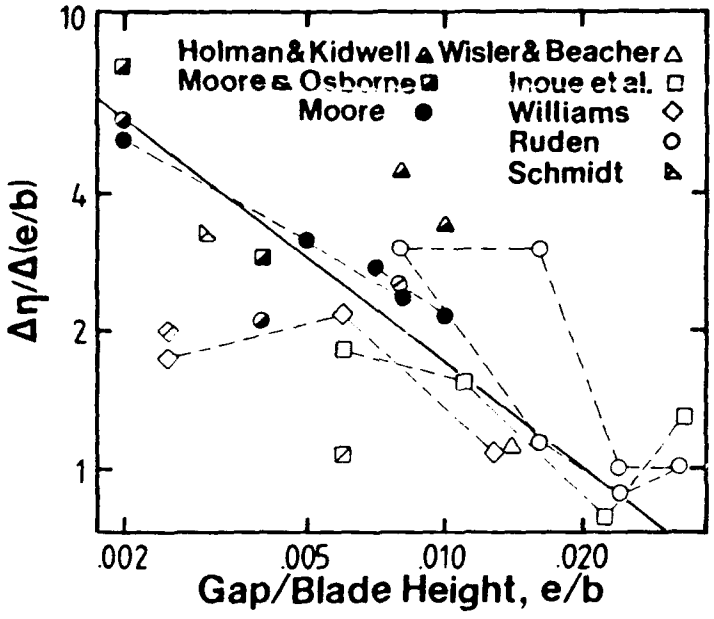

Fig. 2.1-5 Log-log correlation of constant power and peak average efficiency sensitivity to gap/blade height for high and low speed stages.

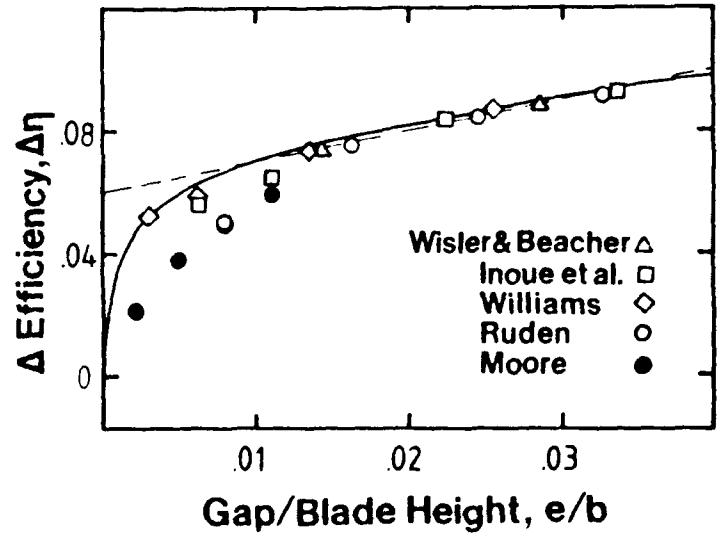

Fig. 2.1-6 Efficiency decrement correlation with gap/blade height developed by integration of the approximation to the data of Fig. 2.1-5.

2.2 Flow near the Wall

A major question, which developed from the conclusions reached in the analysis of the efficiency sensitivity, concerned the form of the interaction between the secondary flow field and the tip gap local flow. Prior to the analysis above, arguments that a tip clearance vortex formation description of the flow (suitably calibrated for some degree of retained lift in the clearance gap) had seemed (to the present author) to be a plausible model for the observed clearance effects. However, the empirical curve which was the primary result of Sec. 2.1 resembles the curve of the retained lift factor (K) which determines the strength of the tip vortex. The similarity of the curves suggested that a vortex is not needed to explain the efficiency trends. This observation focused attention on conditions where a vortex had been measured in the secondary velocity field and how these conditions might be characterized.

2.2.1 Radial Forces and Wall Shear

A relatively simple method of analyzing the dependence on geometry and speed of the rotor relative secondary flow near the case wall is to examine the nature of the component terms of the gradient of total pressure in the relative frame as the case wall is approached. In the relative frame, the region of the passage at the rotor case wall bounded by a finite clearance height forms a thin flow layer, extending from blade-to-blade. The flow is required to meet boundary conditions of zero axial and circumferential velocity (assuming no slip) and zero radial velocity (no mass flow through the wall) at the wall. On the passage side of the wall layer throughflow conditions form the other boundary condition. If the flow is considered to be inviscid, steady and is described in a relative frame with gravitational effects neglected, the equation of motion in the radial direction is given by, (Vavra, 1960 p. 123)

$$\underline{\mathbf{i}}_r \cdot \nabla(P'_r/\rho) = \underline{\mathbf{i}}_r \cdot (\underline{\mathbf{W}} \times (\nabla \times \underline{\mathbf{W}} + 2\,\underline{\Omega})) + \underline{\mathbf{i}}_r \cdot \nabla(1/2\Omega^2 r^2) \qquad 2(5)$$

Where P'_r, the total pressure at some radius in the relative frame can be expressed as

$$P'_r = p + 1/2\,\rho W^2$$

Expression 2(5) can be expanded by evaluating the curl in cylindrical coordinates and if axial and tangential gradients of the radial velocity are considered small, or $W_r = 0$, everywhere near the wall, it reduces to

$$\underline{\mathbf{i}}_r \cdot \nabla(P'_r/\rho) = W_u^{\,2}/(R-y) - 1/2\,\partial(W^2)/\partial y + 2\,\Omega\,W_u - \Omega^2(R-y) \qquad 2(6)$$

The distance (y) is measured positive, radially inward from the wall, consistent with a boundary layer convention.

While the equation of motion defines the equilibrium required between the velocity and pressure fields, the relative total pressure gradient term is also a component of the resultant acceleration on the fluid and its magnitude and sense give an indication of the forces being cancelled or balanced in the flow. The ability of the flow to follow, separate (detach) from or circulate near the case wall, in terms of net relative acceleration, results from summation of this term with other accelerations. Due to the need to introduce the actual blade pressure forces into equation 2(5) to define the

velocity field near the blade or wall, the nature and magnitude of the $\underline{i}_r.\nabla(P'_r/\rho)$ term is of interest near the case wall and the tip clearance.

2.2.1.1 Pressure Gradient Term in the Passage near the Wall

The magnitude of the radial component of the total pressure gradient in the passage near the tip wall can be quantified by expanding the expression for $\underline{i}_r.\nabla(P'_r/\rho)$ above. A diagram of the coordinate system and notation is shown in Figure 2.2-1. The gradient term is given by

$$\underline{i}_r.\nabla(P'_r/\rho) = (V \sin\alpha - U)^2/(R-y)$$

$$- 1/2\partial(U^2 - 2\,U\,V \sin\alpha + V^2)/\partial y + 2U_t/R\,(V \sin\alpha - U)$$

$$- (U_t/R)^2(R-y)$$

when the velocities are defined as

$$W_u = V \sin\alpha - U\ ;\ W^2 = U^2 - 2\,U\,V \sin\alpha + V^2$$

$$\text{and } U = U_t\,(1 - y/R)$$

If the gradient term is normalized by the centripetal acceleration at the rotor tip (U_t^2/R) to allow for speed and radius variations, any residual dependence should reflect passage geometry or flow direction influences. Evaluating the derivatives and normalizing by U_t^2/R yields the expression

$$\underline{i}_r.\nabla(P'_r/\rho)/(U_t^2/R) = (\sin\alpha\ V/U_t - (1 - y/R))^2/(1 - y/R)$$

$$+ (1 - y/R) + (1 - y/R)\,RV/U_t \cos\alpha\,\partial\alpha/\partial y$$

$$+ (1 - y/R)\,R/U_t\,\partial V/\partial y \sin\alpha - \sin\alpha\ V/U_t$$

$$+ RV/U_t^2\,\partial V/\partial y - 2((1 - y/R) - V/U_t \sin\alpha) - (1 - y/R)$$

If boundary conditions $V \rightarrow 0$ and $\partial V/\partial y \rightarrow \tau_w/\mu$ as $y \rightarrow 0$ are assumed[25], near the wall, as limiting conditions and terms that are small are neglected, then

$$\underline{i}_r.\nabla(P'_w/\rho)/(U_t^2/R) = -1 + (R\,\tau_w)/(\mu\,U_t)\sin\alpha_w \qquad 2(7)$$

For the simple case of axial throughflow ($\alpha_w = 0$), or a skewed flow on a frictionless wall (i.e., $|\alpha_w| > 0$ and $\tau_w = 0$) then

[25] The limiting velocity gradient (derived in an inviscid context) is approximated by a gradient typical of a shear or boundary layer flow (i.e., a viscous flow). Such an approximation is often used to model a near wall flow condition or to introduce losses into inviscid analyses (e.g., Rains, 1954 p. 34, assumes this approximation to model scraping flow near the clearance)

$$\mathbf{i}_r.\nabla(P'_w/\rho)/(U_t^2/R) = -1$$

However, for a skewed flow on a frictional wall the pressure gradient term has a magnitude which depends on the tip speed, skew, radius and the shear near the wall. The sense of the pressure gradient term depends on the direction of the skew or the shear. It can be shown by straightforward manipulation that the non-dimensional term in 2(7) is equivalent to

$$(R\,\tau_w)/(\mu\,U_t) = [\,1/2\,\Phi^2\,C_f\,Ru\,AR/(1 - HR)](\tau_w/\tau_{wa})$$

$$= [WS]\,(\tau_w/\tau_{wa}) \qquad 2(8)$$

In this form of the term, a chord Reynolds Number $Ru = \rho U_t c/\mu$ and a wall friction coefficient for an annulus flow, given by $C_f = \tau_{wa}/1/2\rho(\Phi U_t)^2$, were chosen to adapt the term to usually available, or familiar, compressor and stage parameters. The factor (τ_w/τ_{wa}) is the ratio of the passage wall local shear (τ_w) to that of the nominal pipe flow value for the passage annulus (τ_{wa}) based on the throughflow, Φ. Defining WS as

$$WS = 1/2\,\Phi^2\,C_f\,Ru\,AR/(1 - HR) \qquad 2(9)$$

It can be seen that (3) becomes

$$\mathbf{i}_r.\nabla(P'_w/\rho)/(U_t^2/R) = -1 + [WS]\,(\tau_w/\tau_{wa})\,\sin\alpha_w \qquad 2(10)$$

and that the gradient term depends on the WS factor, the ratio of the local shear near the wall to the reference annulus value and the near wall skew.

The WS factor might be considered a non-dimensional property of rotating passage. The term depends on (non-dimensional) throughflow, wheel speed, wall friction and geometry parameters. It basically gives a non-dimensional measure of conditions near the wall. WS is not influenced by tip clearance. It may also be interpreted as the non-dimensional (apparent) wall shear stress in the relative frame. The term resembles a commonly used non-dimensional wall shear expression in boundary layer analyses.

The magnitude of WS provides an indication of the strength of the pressure gradient's radial component in the passage near the case wall. If the near wall shear is typical of pipe or annular flow and skew angles are not zero then the factor multiplies the shear and angle terms. For the case of smooth walls at a typical chord Reynolds Number of 0.5×10^6 for compressors, the factor is then dependent on the passage geometry (AR, HR) and throughflow (Φ). If the passage geometry is fixed by (AR, HR) then the factor only changes with throughflow. In typical clearance experiments on a constant speed throttle line for a stage, throughflow (Φ) is held constant and clearance gap is varied. In this particular case the factor (WS), is a constant for the experiment.

In the context of tip clearance phenomena and losses, a stage property that is flow or geometry dependent near the wall is of some interest. Cumpsty (1982), for example, conducted an experiment specifically to examine the influence of staggered spacing normalization for tip flow effects.

The change in magnitude of the *WS* factor from one experimental machine to another was discussed in Moyle (1989). Selected material from that discussion showing the range of the *WS* factor in the compressor test literature are covered below. The paper (Moyle, 1989) primarily explored correlation of the secondary flow velocity fields and case wall flow angles measured by other investigators by using the *WS* factor. A principal conclusion of the paper was that the secondary flow velocity field tended to exhibit a well defined tip clearance vortex if the *WS* number was small (order 200). This tendency decreased, however, as the *WS* factor increased and for numbers (*WS* > 1000) typical of the larger (1 m) diameter low speed compressors, evidence of a well defined vortex at the rotor exit had disappeared.

2.2.1.2 Non-dimensional Wall Shear Magnitudes in the Test Literature

Using equation, 2(9), it relatively straightforward to determine the magnitude of the *WS* factor for each compressor used in a tip clearance or secondary flow experiment, (see Table 1.3-1). Assuming a constant C_f typical of a smooth wall and using the described geometry and operating point, the experimental stages can be ranked by the magnitude of this factor. Based on a nominal C_f value of 0.003, for all the machines, the ranking is shown in Table 2.2-1.

Table 2.2-1

Case Wall Pressure Gradient Factor and Ranking for Experimental Compressors used for Flow Studies with Tip Clearance or Case Wall Boundary Layer Parameter Variation. (Z=No. Stages, Z=0 indicates an isolated rotor, G = AR/(1-HR), WS = Ranking Pressure Gradient Factor).

Investigator(s)	Z	R (m)	*HR*	*AR*	Ut (m/s)	*G*	Φ	*Ru* x10^{-6}	*WS*
Williams (1960)	1	0.178	0.60	2.00	3.7	5.0	0.41	0.13	165
Inoue et al.(1986,F 1(a))	0	0.225	0.60	0.76	35.3	1.9	0.50	0.28	200
Schmidt et al. (1987)	0	0.254	0.50	2.63	39.0	5.3	0.53	0.13	275
Cumpsty (1982)	4	0.185	0.78	2.00	58.3	9.1	0.55	0.08	329
Ruden (1937)	1	0.250	0.50	1.27	75.0	2.5	0.45	0.50	383
Holman&Kidwell(1975)	1	0.059	0.39	1.11	474.0	1.8	0.44	1.03	556
Fabri & Reboux (1975)	0	0.233	0.96	0.16	182.6	3.7	0.37	0.78	587
Laksh. et al(85,Fig 1(b))	1	0.469	0.50	1.52	51.6	3.0	0.50	0.54	610
Bettner & Elrod (1982)	1	0.610	0.80	1.05	56.0	5.2	0.47	0.44	760
Hunter (82,F 2a)	0	0.762	0.40	3.00	41.9	5.0	0.49	0.43	773
Dring (1983)	2	0.762	0.80	1.50	51.9	7.5	0.46	0.35	840
Dring (1980, Fig 2(b))	0	0.762	0.80	1.00	40.7	5.0	0.59	0.42	1070
Wisler& Beacher (1986)	4	0.762	0.70	1.90	71.0	6.3	0.49	0.57	1289
Moyle (1986)	1	0.457	0.60	2.25	76.8	5.6	0.64	0.42	1450
Dring (1980, Fig 2(b))	0	0.762	0.80	1.00	40.7	5.0	0.77	0.42	1830
Moore (1982)	1	0.250	0.50	2.40	423.0	4.8	0.47	1.48	2396

Note that the *WS* value above is not the gradient term, Eqn. 2(7). It is a constant for the stage and throughflow that is multiplied by (τ_w/τ_{wa}) and $\sin\alpha$ to give the gradient, Eqn. 2(10). The factor clearly has significance if the skew (α) distribution on the passage case wall is the same (nominally) in all stages and wall shear levels are also similar. In such a case, the wall pressure gradient component in each experiment only

depends on the stage configuration's *WS*. Alternatively, if tip leakage (changing with gap dimension) *modifies* the skew and shear distributions at a fixed operating point in a machine with a low *WS*, the same (or similar) skew or shear *modifications* in a machine with a high *WS* would have a different effect.

It is also noteworthy that the lowest ranked machine (Williams, 1960) has given extremely clear photographs of a secondary flow tip clearance vortex. These photographs are shown in Rains (1954), Figs. 29-33, and were discussed in later analyses by Vavra (1960, p. 380), and Lakshminarayana (1970). It is also relevant that the extensive series of detailed measurements in Lakshminarayana's compressor (*WS* = 610) between 1980 and 1987 using hot-wires, rotating probes and laser doppler velocimetry have not been able to clearly exhibit the vortical flow in the velocity field shown by Inoue et al. The vortex's presence is *inferred* from the total pressure defect rather than observed directly (Lakshminarayana and Murthy, 1987; Conclusion 8).[26]

The *WS* factor can be considered a scale factor in the gradient term. Its magnitude varies substantially (an order of magnitude) for the compressors of the table above. Correlation of the form of the secondary flows from the experiments with the *WS* factor suggests that compressors with low *WS* should have well ordered vortices near the rotor tip. This observation is expanded in Sec. 2.2.2.

2.2.1.3 Non-Dimensional Wall Shear as a Similarity Parameter

If the *WS* term discussed above is considered to be a scaling factor in the non-dimensional equation of motion near the tip, it is clear the term can be used as a measure of flow similarity in the case wall-tip clearance corner. Examining this factor as a similarity parameter shows how well the data from a model compressor would represent the full scale machine. Using the non-dimensional term of 2(7) and equating the *WS* magnitude for two different devices, then

$$(R\,\tau_w)/(\mu\,U_t)_{model} = (R\,\tau_w)/(\mu\,U_t)_{full\text{-}scale}$$

This may be reduced to

$$(\tau_w/(\mu\,\Omega))_{model} = (\tau_w/(\mu\,\Omega))_{full\text{-}scale}$$

and substituting $\tau_w = 1/2\rho(\Phi R\Omega)^2 C_f$ yields

$$1/2\rho(\Phi R\Omega)^2 C_f/(\mu\,\Omega))_{model} = 1/2\rho(\Phi R\Omega)^2 C_f/(\mu\,\Omega))_{full\text{-}scale}$$

Using F for full-scale and M for model, the terms can be arranged

$$(\nu_F/\nu_M)(\Phi_M/\Phi_F)^2(R_M/R_F)^2(\Omega_M/\Omega_F)(C_{fM}/C_{fF}) = 1$$

Model testing is usually conducted with model flow coefficients the same as those of the full scale machine, i.e., $(\Phi_M/\Phi_F = 1)$. However, Mach Number equivalence $((R_M/R_F)(\Omega_M/\Omega_F)(c_F/c_M) = 1)$ is rarely preserved, so the general scaling relation can be expressed as

---

[26] Eqn. 2(2), however, indicates that other causes, unsteady flow or friction could produce the same total pressure defect.

$$(\nu_F/\nu_M)(R_M/R_F)^2(\Omega_M/\Omega_F)(C_{fM}/C_{fF}) = 1$$

If we roughly approximate the ratios for air, some insight into the scaling required to model end wall phenomena can be obtained. For example, assuming a 10,000 RPM full-scale core compressor and a 1000 RPM model with a kinematic viscosity ratio representative of a 100-200 degrees Centigrade higher temperature in the full-scale machine, then $(\nu_F/\nu_M) = 2$ and $(\Omega_M/\Omega_F) = 0.1$. If we assume the surface roughness scale is preserved $((C_{fM}/C_{fF}) = 1)$ between the full-scale and model then (R_M/R_F) needs to be about five or R_M about 2.23 times R_F. This simple result clearly indicates that models need to have very large diameters to get the end wall effects scaled correctly in an air-to-air simulation of aerocompressor flows. A corollary of this observation is that data and interpretations of end wall phenomena developed from measurements taken in model compressors with diameters less than the full-scale machine are unlikely to be applicable to the full-scale machine unless the model was spun at very high speed. The radius scaling is given by

$$(R_M/R_F) = ((C_{fF}/C_{fM})(\Omega_F/\Omega_M)(\nu_M/\nu_F)) \qquad 2(11)$$

Note that increasing the wall roughness of the model relative to the full-scale reduces the model diameter required to achieve similitude. This implies it is experimentally beneficial to roughen up the wall when down scaling the angular velocity.

The similarity implications of this wall shear parameter are obviously relevant to the evaluation of models and analytical predictions of case wall or tip clearance effects. Particularly those that are derived from interpretation of low speed experimental measurements. The equations are useful in practice when low speed end wall performance data is intentionally acquired for scaling to a high speed application. The high speed conditions that would be similar are easily established.

In a more general sense, however, it is important to note that end wall flows with different *WS* values would be expected to be different in the analysis presented. This is the equivalent of saying no two end wall flows are the same unless they have the same *WS* factor. The overall point is that most investigations and studies to date have assumed that the flow in the machine being examined is representative of a, more or less, universal case wall flow structure or pattern in all machines. The analysis presented indicates this is probably not the case and that any generalized tip gap-wall flow model will need to account in some way for the wall relative motion and shear magnitude in addition to the tip gap or leakage flow.

2.2.2 Vorticity Production in Leading Tip-Wall Corner

In the discussion, so far, the *WS* factor has been physically interpreted as a non-dimensional wall shear. It is relevant to note that the *WS* factor can also be related to the Ekman Number ($Ek = \mu/(\rho R^2\Omega)$ which is used to characterize the ratio of viscous to inertial forces (due to rotation, i.e., $R\Omega$) in the surface layers of rotating disks. If

$$WS = (R\ \tau_w)/(\mu\ U_t)$$

and using friction velocity given by $c^{*2} = \tau_w/\rho$, then $\tau_w = \rho c^{*2}$, and as $U_t = R\Omega$ and $Ek = \mu/(\rho R^2\Omega)$ then

$$WS = (R\,\rho/\mu)(c^{\#2}/U_t)(R\Omega/U_t) = (1/Ek)(c^{\#}/U_t)^2$$

thus, if to a first approximation $\tau_w = C_f \rho U_t^2$, then $WS = C_f/Ek$.

Chen et al. (1988, p. 12) note the resemblance of the flow in the corner of a tank of rigidly rotating fluid, having a lid, to that of *the leading edge zone of a rotor*. They make an analogy between the production of vorticity in the leading edge tip corner and the vorticity production in the Stewartson layers on the tank wall and lid. A toriodal ring vortex is shown to concentrate in the tank-lid corner as *Ek* decreases in their Fig. 27. By extrapolating flow patterns observed in tanks at $Ek = 0.01$ and $Ek = 0.001$ to values typical of air compressors (10^{-6}) they are able to support arguments for a variety[27] of vortex filament phenomena observed in radial compressors near stall.

As the WS factor combines the wall friction coefficient and the Ekman Number, it can be seen that the trends developed for increasing *WS* in Moyle (1989) at constant C_f can be interpreted in a similar manner to Chen et al.'s discussion of flow effects that occur with decreasing *Ek*. Chen et al. were primarily concerned with the vortex filament nature of the flow on the case wall and argued that the filament tended to cross the passage and swing forward with decreasing *Ek* (increasing *WS*). This behavior is consistent with the disappearance of a well ordered vortex exiting from the passage noted in Moyle (1989) for increasing *WS*. The similarity of these results (considering $WS = C_f/Ek$) suggest that tip clearance vortex production is related to the ratio of inertial forces (due to rotation) to viscous forces in the passage, rather than to fluid passing through the gap (leakage) or retained lift. Considering the wide range of *WS* magnitudes for compressors in the literature in conjunction with their relatively consistent efficiency fall-offs, these observations also suggest that the losses may not be strongly coupled to the presence of a vortex formation.

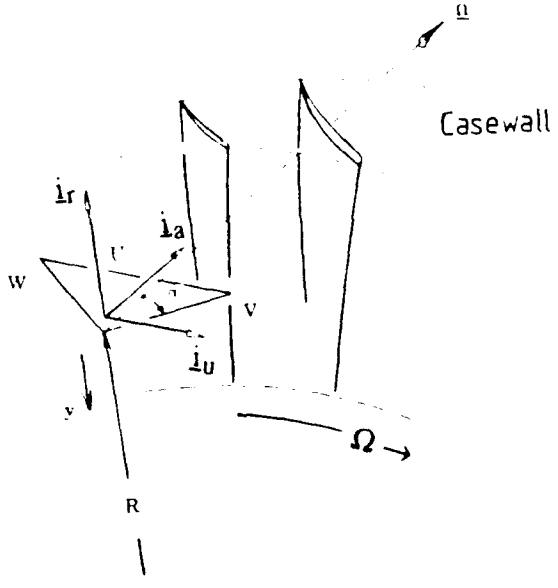

Fig. 2.2-1 Schematic diagram of rotating coordinate system showing notation and directions.

[27] One pre-condition for flow reversal is the existence of a "nose bubble" or leading edge tip separation.

2.3 Experimental Plan Formulation Based On Analysis

The analyses set out above provided some new insights regarding the nature of the flow at the case wall near the tip. The main points may be summarized as follows:

(1) The efficiency change due to clearance at constant power (Sec. 2.1), showed a well defined decreasing trend in efficiency change with increasing clearance gap. This implied a non-linear character of the loss development, especially for small clearances.

(2) Normalization of the clearance gap by any other characteristic dimension of the blade passage did not alter the slope presented or the exponent derived for the constant power efficiency sensitivity. This implied there is an *underlying consistency in the loss generation mechanism in the data examined which is (cascade) passage parameter independent.* The strong correlation with gap size suggested the loss production is a gap local phenomenon (Sec. 2.1).

(3) A non-dimensional term (WS) was shown to persist in expressions for the near wall total pressure gradient if there was finite wall friction and some skew in the flow. From examining the published data on secondary flow patterns it appeared that the secondary flow velocity field tended to exhibit a well defined tip clearance vortex if the WS number was small (order 200) (Sec. 2.2). This tendency decreased, however, as the WS factor increased and for numbers ($WS > 1000$) typical of the larger (1 m) diameter low speed compressors, evidence of the vortex had disappeared.

These observations suggested that the tip flow mechanisms which strongly affect losses may occur much closer to the blade tip and wall than previously suspected. On the other hand, the passage secondary flow (vortex) which has been considered a major contributor to the overall loss may be more of a reflection of both the tip local leading edge flow and the overall passage throughflow situation. It was also clear that passage secondary flow patterns may differ from machine to machine and have quite a range of structures. This is consistent with the WS magnitudes observed in the data.

The conclusions drawn from the analysis suggested measurements to be made in an experimental study should resolve the tip local flow in some detail and be made close to the blade and in the tip gap.

Part 3

Clearance Variation Experiments in an Axial Compressor

The experimental study, which is described in the following Part 3, developed as the analysis work of Part 2 was completed. The experiments therefore changed their emphasis as the project unfolded. Initial instrumentation development focussed on passage average spanwise flow distributions. The emphasis then shifted to blade-to-blade secondary flow patterns and finally to blade-to-blade pressure and wall shear measurements based on the analyses of Part 2.

The flow measurements were conducted in a low speed multistage axial compressor (LSMSC) at the Naval Postgraduate School (NPS), Turbopropulsion Laboratory in Monterey, California. The LSMSC had a test section radius of 457 mm (18 in) with a hub-to-tip ratio of 0.6. The test section could be fitted with up to three stages of blading with as many as 30 rotor blades and 32 stators per stage. The casing had provision for one pre-swirl inlet guide vane row upstream of the first rotor and two exit guide vane rows after the last stator.

For this program, the blade whirl distribution was of the solid body type and the velocity diagram was symmetric. A summary description of the blading design is provided in Appendix C.1. The test facility is described in Yavra et al. (1973). Test work on the blading was not initiated until 1979 when it was decided to pursue this study of tip clearance effects in a multistage machine. Initial work on developing the compressor, blading and test facility was started by Zebner (Moyle and Zebner, 1980), and was continued by the author.

Blade-to-blade measurements of the case wall pressure in the passage became of particular interest in the experimental study, as it proceeded, due to the pressure field's pronounced dependence on stator relative position of the rotor. It was clear from the measurements that the flow field was unsteady in the relative frame and that pressure field changes were large with respect to the passage average dynamic pressure. The significance of these changes, in the context of the analysis of Part 2 and tip losses in general, is discussed in Part 4.

3.1 Scope of the Experimental Program

The overall experimental program was conducted in several phases. The preliminary work was concerned with the differences in the baseline flow field in the compressor for single and multistage arrangements of the blading. The flow baselines were measured with minimal clearances (e/b = 0.0025 to 0.0035) *near design conditions on constant speed throttle lines*. The results of the baseline surveys on a single stage of the blading are presented in Moyle (1986). Subsequent instrumentation development and the flow baseline results for the two stage build have been consolidated in this document. More recent throughflow computations for the two stage build are described by Yeo (1989). Results relevant to changes in the flow field due to tip clearance variation have been selected from the various phases of the test program for presentation in Part 3.

3.1.1 Experimental Objectives

The experimental work had a number of objectives. Initial flow measurements were intended to establish baseline flow fields for the symmetric blading in single and multistage configurations. The effect of tip clearance gap on the flow field for the two stage build was then to be examined by successively increasing the clearance and remeasuring the field. The same measurements were not necessarily to be repeated at all clearance levels.

Baseline Flow Measurements The stage flow field, itself, was of some interest because the blading was symmetric and had a relatively low rotor entry velocity at the tip compared to other whirl distributions, see Figure A.1-3. Schlachter (1981) had examined a variety of whirl and energy addition distributions in the context of their probable tip loss characteristics at NPS prior to this experimental study. Consequently, it was thought desirable to carefully measure the flow distribution in the symmetric blading to provide a reference for comparison with other whirl distribution test data and throughflow computations. The baseline measurements were also important to satisfactory instrumentation development for the clearance variation work.

A secondary motivation for the single to multistage comparison related to the observations of Hunter and Cumpsty (1982) concerning the tip wall passage average velocity distributions. They had argued that the fundamental wall boundary flow character in an isolated rotor was the same as, or very similar to that of an embedded stage. As *multistage* testing of stages to determine embedded stage performance was emphasized by Smith (1970), it was of interest to examine both single and multistage data to see the consequences of stage addition on the passage average flow field.

Tip Clearance Variation Measurements A minimum objective of the program was to generate pressure rise and efficiency data in a multistage machine similar to those of Smith (1958) and Wisler and Beacher (1986) over a range of clearance gaps. Acquiring blade-to-blade rotor exit velocity field measurements comparable with those of Dring (1981) and Inoue (1985), (in isolated rotors), for a documented multistage blading was a further goal of the program.[28] A final objective (developed later in the program) was to acquire blade-to-blade case wall static pressure and wall shear stress distributions over selected parts of the tip gap variation range.

---

[28] Within these objectives an effort was made to generate flow field data which would permit data comparison with the predictions of computational methods in a manner similar to Hah (1985) and Dring (1985). Computational comparisons were made in this study, however, these comparisons were not at a code verification level.

3.2 Experimental Constraints and Limitations

The principal mode of investigation reflected in the tests conducted was to compare the stage performance, blade-to-blade survey or similar measurement pattern with a repetition of the measurement pattern at a different clearance level. Clearly, the success of this approach would depend on the selected measurement patterns and their *sensitivity* to the clearance changes at the compressor flow condition.

As much of this necessary clearance sensitivity information was *unknown for this compressor beforehand*, a very important constraint in this program was the inability to restore a small clearance level once the clearance had been enlarged.[29] The method of enlarging the clearance was to grind down the blade tips. This "no going back" constraint forced an ambitious program of instrumentation development early in the program. In order to be able to fully explore the flow, a wide range of measurement techniques were required. The techniques all had to be mature before changing the tip clearance in the compressor. Not all measurement approaches were found to be satisfactory after some development and, although they are all reported in this thesis, the survey techniques applied narrowed as the program proceeded.

A significant limit on the experimental options, as the program was formulated, was the very restricted access to make complete circumferential surveys in the test section of the LSMSC. In a two stage configuration circumferential surveys were only possible upstream of the first rotor and downstream of the last stator. The compressor casing was made of cast iron and was over 25 mm (1 in) thick, 914 mm (36 in) in diameter and over 1000 mm (40 in) long. It was not casually moved or machined and had not been originally fabricated with a large selection of circumferential survey slots or holes. This constraint was largely circumvented in the program, however it did limit the quality of passage average data.

The compressor was also of a relatively large scale and representative of a full scale machine with a design point wall shear factor (WS) of 1450. For the clearance variation testing it was bladed with two complete stages having a realistic tip solidity of 1.0. It also had small interblade spacings, fore and aft of the survey rotor, typical of operational machines. As only limited detailed test data on clearance flow phenomena are available from multistage compressors, the ability to make some types of detailed surveys in a multistage configuration was a useful contribution to this subject.

3.2.1 Experimental Strengths of the Equipment

One strength of the equipment was the heavy casing just described. The rigidity of the casing and bearing support allowed it to remain concentric and round to a high tolerance relative to the clearance changes considered in the tests. The casing was out-of-round by less than 5 parts in 100,000 (0.00005 of the radius) making it an excellent vehicle for clearance testing in terms of tip gap uniformity. Tip gaps were expected to be varied over a range of 0.001 to 0.008 of radius which implied respective circumferential clearance gap uniformities of 5% to 0.5% for the experiments.

[29] This constraint was a consequence of the need for low cost blades. Due to the large number needed to blade a multistage machine a method of restoring the clearance would have been very expensive to implement. A number of options, including sleeves and linings, were determined to be unworkable.

3.2.2 Operational Limits

Measurements of the flow field and the experiment were limited by certain characteristics of the test facility, the compressor test section arrangement and the type of survey access in and around the blading. The major operational limits are summarized as follows:

(1) The compressor shaft turned at a constant mechanical speed of 1610 RPM for Build III (1620 for Builds I and II).

(2) The throttle flow resistance, and hence flow coefficient, was fixed while the compressor was operating.

(3) Ports for radial access of survey probes were only available between the blade rows.

(4) Circumferential surveys could only be made in a vacant blade row position or after the third stator position.

By arranging test section builds in a suitable sequence, a variety of circumferential surveys could be conducted. However, it should be noted that the experimental plan was tailored to conform to the equipment's capabilities. The facility and instrumentation are described in the following section.

3.3 Experimental Facility and Instrumentation

The compressor test facility was an open loop 914 mm (36 in) diameter tunnel mounted horizontally in the Laboratory. Ambient air was drawn from outside the building through an inlet nozzle, passed through the test section annulus and discharged into the building. A drawing of the tunnel arrangement is shown in Figure 3.3-1. The inflow leg to the test section consisted of a mesh enclosure surrounding an inlet bellmouth nozzle on a solid backplane, a duct length of four diameters and then a throttle plate (or screen) housing. This section was followed by another duct length of two diameters connecting to the annular test section bullet and compressor face. The outflow leg consisted of a short annular diffuser opening to the Laboratory work space. The compressor drive shaft passed through the diffuser centerbody and connected to a belt drive downstream of the diffuser section. The belt drive connected to a 112 KW (150 HP) synchronous motor. The nominal compressor rotational speed was 1610 RPM with a tip speed of 77.08 m/s (252.9 ft/s) in this program (Build III). Due to stress limits this speed was a maximum.[30]

Flow rate variation was achieved by inserting screens or plates of different flow resistance into the throttle housing. Combinations of screens increased the range of flow conditions possible, however, only discrete resistances and hence flow rates could be achieved over a range. The compressor rotational speed could be changed by assembling different belt drive elements on the drive shaft. Neither flow nor speed could be varied continuously or while the compressor was operating. This arrangement was simple to operate, however, the lack of continuous throttling was sometimes cumbersome. The leading characteristics of the facility are set out in Table 3.3-1.

Table 3.3-1

Low Speed Compressor Test Facility Dimensions and Leading Characteristics.

Overall Length	16.46 m (54.0 ft)
Duct and Tip Diameter	914.4 mm (3.0 ft)
Test Section Length	1066.8 mm (3.5 ft)
Test Sect. Inner Diam.	548.6 mm (1.8 ft)
Low Rotation Speed	1200 RPM
Med. Rotation Speed	1620 RPM
High Rotation Speed	2290 RPM
Maximum no. of Stages	3

3.3.1 Compressor Test Section

The compressor test section consisted of two cast iron case halves, approximately 25 mm (1 in) thick, enclosing two steel end-rings which supported the rotor bearing housings centrally in the case using six struts. The end rings fitted into deep recesses in the case and their inside diameters were concentric with the machined bore in the

[30] This wheel speed gave a nominal single stage static-to-static pressure rise of 250 mm (10 in) of water. The small pressure rise made measurements of pressure exacting in terms of sensor accuracy and also led to some flow stability problems. Small end-to-end changes in static pressure between the inside and outside of the building, 2.5 mm (0.1 in) of water, could produce significant velocity changes (6.7%) in the test section for single stage Builds (I and II). Fluctuations were lower for the two stage configuration (Build III). A substantial effort went into minimizing small leakage flows, determining the optimum building door and window configuration and tripping boundary layers to achieve consistent, repeatable data.

case halves. The rotor shaft had provision for three rotor rows to be mounted on steel drums which were keyed to the shaft. The arrangement of the test section is shown in Figure 3.3-1. The hub to tip diameter ratio for the section was 0.6. The inlet contraction was accomplished with a curved bullet fairing and the outlet expansion with a conical annular diffuser.

The test section was extremely rigid due to such construction and clearances could be maintained to the extent the bearings permitted. The bearings arrangement required a thrust bearing in the downstream ring and movement in this bearing was the principal limit to the clearances that could be tested. Without special restraint of the rotor axial motion, clearance gap-to-blade height (e/b) levels of 0.003 (fwd. stage) to 0.004 (aft stage) could be safely permitted as minimum clearances. The test section was bladed in the second and third stage positions for the clearance work reported.

Probes were inserted into the flow through ports machined in the casing for a standard plug fitting. Although there were many locations of the ports in each blade row position, the number of relative positions to the stator blade stacking centers was limited to two. Larger probe access plugs, spanning two blade passages (circumferentially) were available over each blade row, however these slots did not permit inter-row surveys and were only utilized over a vacant blade row position for extensive circumferential surveys.

3.3.2 Blading

The blading used for the tip clearance study was designed at NPS and is fully described in Vavra (1970). The blade whirl distribution was of the solid body type and the velocity diagram was symmetric. The blading design is summarized in Appendix C.1.

3.3.3 Low and High Response Instrumentation and Data System

Low response instrumentation was used to measure overall flow conditions in the test section (the operating point) and radial distributions of the passage average flow between the blade rows. The probes and sensors were primarily pneumatic due to the, effectively, incompressible and isothermal nature of the test section flow. Reference measurements of inflow temperature and dew point were used to determine compressor face density. Shaft torque and angular velocity were to used to define power input and wheel speed. Otherwise, pneumatic measurements could be used to establish the aerodynamic quantities of interest. A schematic diagram of the low response instrumentation configuration is shown in Figure 3.3-2. The instrumentation was conventional and is described further in Appendix B.2. The pneumatic probe measurement accuracy and the techniques developed for velocity, yaw and pitch calibration are discussed in Appendix B.3.

Variation of tip clearance provided an opportunity to survey the consequences of clearance changes on the blade-to-blade time-average flow field of the embedded (second) stage rotor relative to the stator. By using high response sensor elements and a timing signal from the rotor, the sensor output could be correlated relative to stator blade position. By moving the position of the sensors relative to the nominal position of the wakes of the upstream blade row, it was possible to detect the wake convection in the blade-to-blade data. It was also possible to form rotor average blade-to-blade quantity distributions by averaging the data from many stator relative positions. A plate arrangement was developed for the circumferential survey slots which would permit this type of survey and averaging. The plate is shown in Figure 3.3-3. The high response instrumentation and its calibration is discussed generally in B.2 and

details of hot wire sensor utilization are discussed in Appendix B.4. The case wall pressure and shear measurement calibrations are described in Appendix B.5.

3.3.4 Instrumentation and Measurement Uncertainty

Pressure difference was the principal measurement in the program and was used extensively to establish or derive other quantities. These were primarily velocity and loss quantities in the flow field. By using Scanivalves, the same pressure transducer was used for the majority of the low response measurements and bias error was not a significant component of uncertainty. The precision of the primary measurements is shown in Table 3.3-2.

Table 3.3-2

Precision of Primary Measurements from Calibration.

Measurement/Quantity	Sensor/Calibration	Prec.(±%pt.)
Pressure Difference	Scanivalve/Micromanometer	0.1
Absolute Pressure	Barometer	0.015
Absolute Temperature	J/T Thermocouples/NBS#561	0.05
Wheel (Shaft) Speed	1/Blade pulse/Oscilloscope	0.006
Shaft Torque	Torquemeter/Static Moment	0.4
Dew Point Temp	EG&G Humidity Analyzer	0.03
Probe Radial Posn.	Vernier Scale	0.15
Probe Angular Posn.	Digital Level/Vernier Scale	0.66

Overall, the measurements were of high accuracy and repeatability for the experiments and were typically of the order of one to five parts in one thousand. The analysis of the experimental uncertainty is summarized in Appendix B.2.4.

3.3.4.1 Measurement Uncertainty

Small changes in tip clearance gap produced changes in the overall performance of the LSMSC that were close to the order of the uncertainty in the low response pneumatic instrumentation measurements. Taking measurements in such a regime was imposed on the program by stress limits constraining rotational speed. This, in turn, limited the maximum stage pressure rise that could be achieved. Higher speed would have greatly improved signal to uncertainty levels.

Due to the low pressure level constraint, it was therefore desirable that the data be highly averaged to minimize data noise levels due to random flow disturbances. Appendix B.1 discusses in detail the peculiarities of the LSMSC test rig that led to the selecting the Build III configuration as the best arrangement for clearance variation work. The overall data acquisition process for the low response instrumentation was developed, *after considerable effort*, to a satisfactory level of signal-to-noise and signal-to-uncertainty discrimination.[31]

[31] The measurement averaging scheme for the test data was based on repeated reading of each data channel as it was opened (usually 5 to 10 timed interval readings per point) with subsequent ensemble averaging of the collected data points from 3 to 5 sweeps of all the channels. The ensemble average and standard deviation of the ensemble data were stored on the magnetic medium as a record of the test point. The standard deviation permitted later evaluation of the noise level in the ensemble average data. These levels were generally considered acceptable below the one percent-of-point threshold for differential pressure data. The ensemble average data derived by this procedure showed very good repeatability over 4 to 5 hour periods and over time intervals of months between the same test.

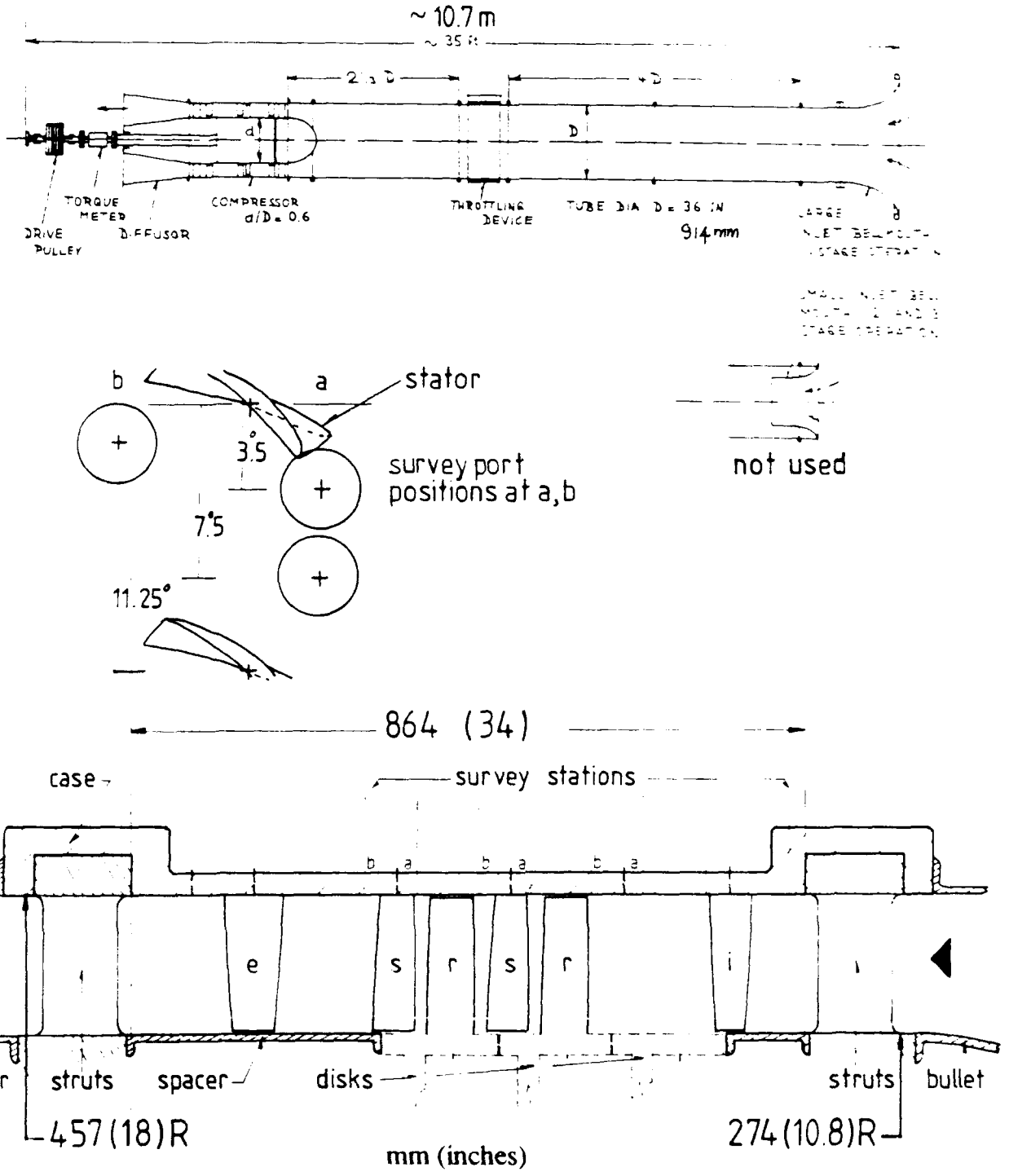

Fig. 3.3-1 Low speed compressor test facility and test section detail, showing the two stage configuration of Build III used for tip clearance testing.

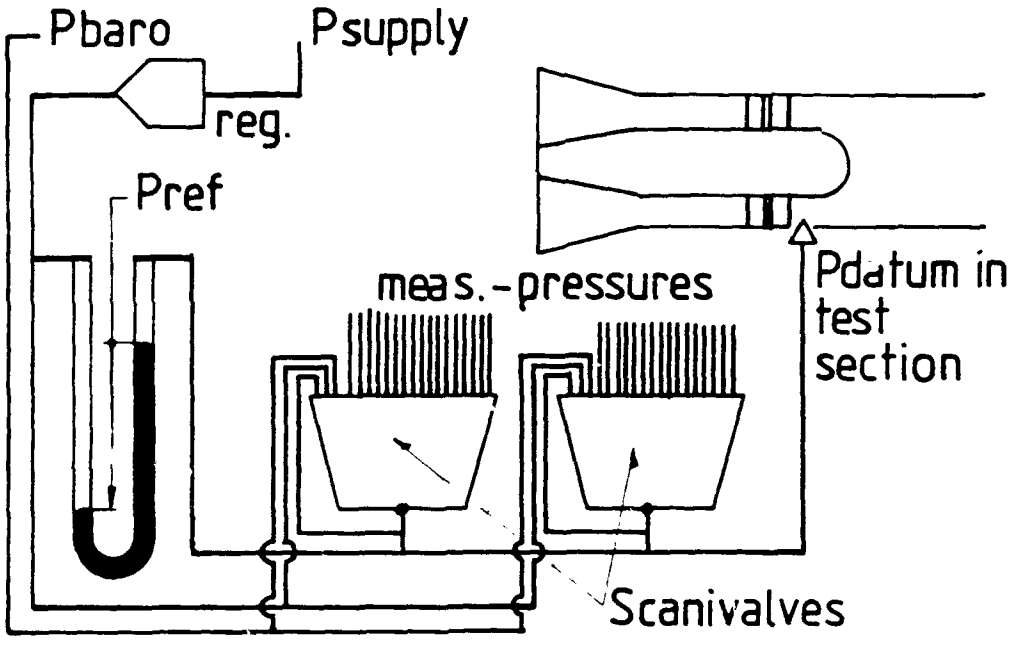

Fig. 3.3-2 Pneumatic measurement system schematic diagram showing the arrangement of Scanivalve reference pressures used to minimize uncertainty due to pressure fluctuations in the system.

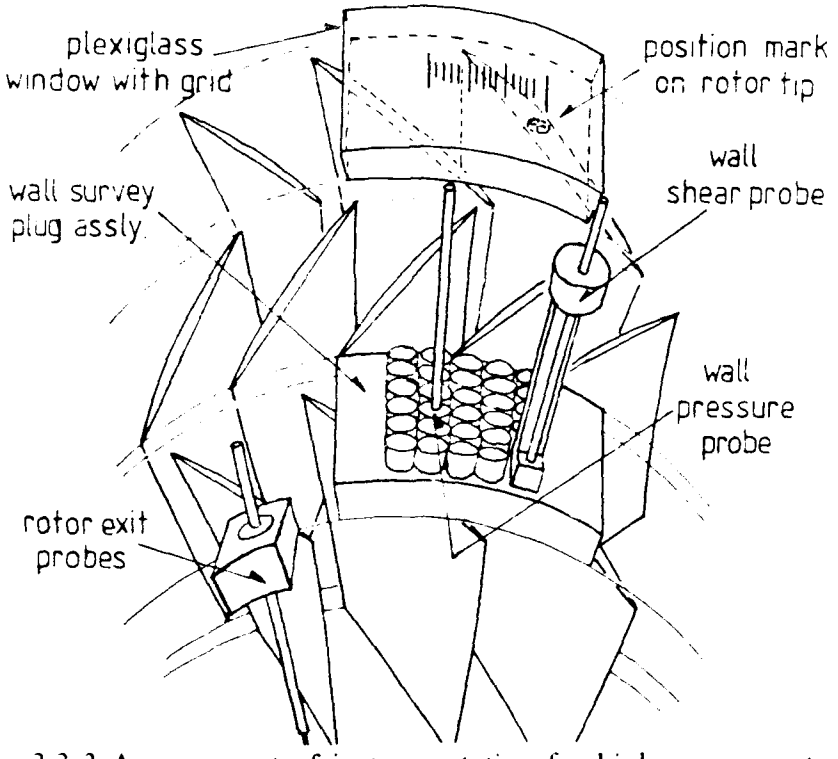

Fig. 3.3-3 Arrangement of instrumentation for high response stage flow measurements showing the position of the wall pressure survey plate relative to the stage.

3.4 Experimental Program Description

The measurement program to meet the experimental objectives of Sec. 3.3.1 was developed by sequential evaluations of the flow field in the machine. Blading arrangements for the different builds of the compressor test section are shown in Table B.1-1. Each build is assigned a roman numeral and the builds are referred to throughout the report by these designations. Builds I and II were single stage arrangements with the rotor positioned immediately behind the inlet guide vane. In Build III a two stage configuration was built with the first rotor positioned one stage spacing behind the guide vane. The blade rows then had minimal interblade spacings until the spacing between the last stator and the exit guide vane.

The flow rate, or flow coefficient, range was selected to span the design point flow coefficient (0.64) of the stage. Because it was undesirable to fully stall the blades due to uncertainties about their ultimate mechanical strength, a flow rate approximating the peak power coefficient (0.60) was selected as the low flow coefficient and roughly 1.15 times design flow coefficient as the maximum flow (0.72). The test speed was nominally 1610 RPM (1620 for Builds I and II). Analysis of the minimum safe clearance and mechanical ability to crop the blades provided the target clearances for the program. The clearance range selected is shown in Figure 3.4-1. Tip clearance uniformity was within ±0.038 mm (±0.0015 in) of the nominal gap dimension. The grinding arrangement and fixtures used to change the clearance are shown in Figure 3.4-2.

3.4.1 Program of Measurement

The following section briefly summarizes the *type of testing* that occurred.

3.4.1.1 Single Stage Baseline Testing

Measurements for Builds I and II consisted of characteristic determination over a range of flows (on a constant speed throttle line) and radial surveys upstream and downstream of the blade rows. The radial surveys were made near the design flow (Φ = 0.64) condition. In addition, boundary layer surveys were made at the compressor face. A limited survey was made with an uncalibrated hotwire in the tip region downstream of the rotor in order to establish the form of the flow in that region of the passage. The clearances were at minimal (e/b = 0.0025) levels.

3.4.1.2 Two Stage Baseline Testing

A more comprehensive testing pattern than that of the single stage was completed on Build III-A prior to commencing the clearance variation testing. The Build III-A baseline was also the minimum clearance of the tip clearance variation range. This clearance was at e/b = 0.0035. Additional work on the baseline included a more comprehensive survey of the compressor face case wall boundary layer and radial distributions of compressor face pressure.[32]

3.4.1.3 Tip Clearance Variation Testing

Tip clearance testing for four clearance levels was planned in a matrix fashion in the program. The dimensions of the matrix were the clearance levels (4), the surveys

[32] A slight static pressure gradient was detected at the survey plane upstream of the IGV's and downstream of the struts. Pressure distributions at this plane were of some concern due to their importance as an initial condition in computations of the compressor flow field. This gradient was not of major significance in the tip clearance study.

possible (5)[33] and the flow coefficients (3).[34] The approach was similar to that followed by Inoue et al. (1986). Results[35] of the first (e/b = 0.0035) measurements altered the plan. The throttle settings for the measurements acquired are shown below in Table 3.4-1. The <> signifies a range of throttles, $\Phi = 0.64$ is the design flow throttle, $\Phi = 0.60$ is slightly below max power, $\Phi = 0.68$ is an open throttle condition.

Table 3.4-1

Throttle Settings (Φ) Measured in Detailed Surveys for the Build III Configuration. Surveys are described in Sec. 3.4.2.

Survey Type Clearance	CC	RS	WP	HW	WS
e/b=0.0035	<>		0.60		
(-A)		0.64	0.64		0.64
			0.68		
e/b=0.0060	<>		0.60		
(-B)			0.64		
			0.68		

Clearance Varied in Both Stages The concept of "repeated stage" testing was discussed in Sec. 1.1.1. In a repeating stage arrangement, the performance of the tip section profile (that is of interest) is also a function of the inflow that the profile has itself generated in prior row. The advantages of making detailed surveys at different clearance gaps, in one rotor, with a non-varying stage upstream were weighed against the need to generate representative stage average performance data, for analysis, over two stages. The former had advantages in terms of computations. It was concluded, however, that the detailed data would be more valuable if acquired under realistic clearance conditions. *The clearance was therefore cut to the same gap in both rotor blade rows for the e/b levels tested.*

---

[33] Surveys possible included CC (compressor characteristic), RS (radial passage average velocity field surveys), WP (wall static pressure surveys, blade-to-blade), HW (hot wire exit velocity field, blade-to-blade) and WS (wall shear, blade-to-blade).

[34] Nearly all published studies can be defined in the context of this matrix. Schmidt et al. (1987), for example, chose a simple measurement (one survey) and varied clearance and flow enough to develop efficiency vs. clearance for a range of flows. Considering the extent of previous work using this approach, their main contribution was to the experimental understanding was to increase the clearance by lowering the blade into the hub wall shroud. Lakshminarayana et al. (1970-1989) have approached the matrix by keeping clearance and throttle constant and have tried many variations of surveys. The picture that has emerged from their work is not at all clear in a comprehensive sense. However, a considerable body of detailed data has been developed on a particular flow. Inoue (1986) made notable progress by using a range of surveys and clearance while keeping flow varaition minimal in order to conduct blade-to-blade surveys.

[35] Initial measurements of the case wall static pressure distributions showed the minimum suction pressure in the blade passage to lie a significant distance (approx. 10% of blade spacing) away from the blade suction surface. Because this appeared to be an anomalous result (at the time), a preliminary wall shear survey was made and an extra throttle setting (0.68) was surveyed. A significant verification effort was also mounted to ensure the position measurements were correct. Midway through the (0.68) survey the compressor bearings failed. Considering the downtime involved in installing new bearings it was decided to grind the (-B) clearance in concert with the bearing teardown and rebuild.

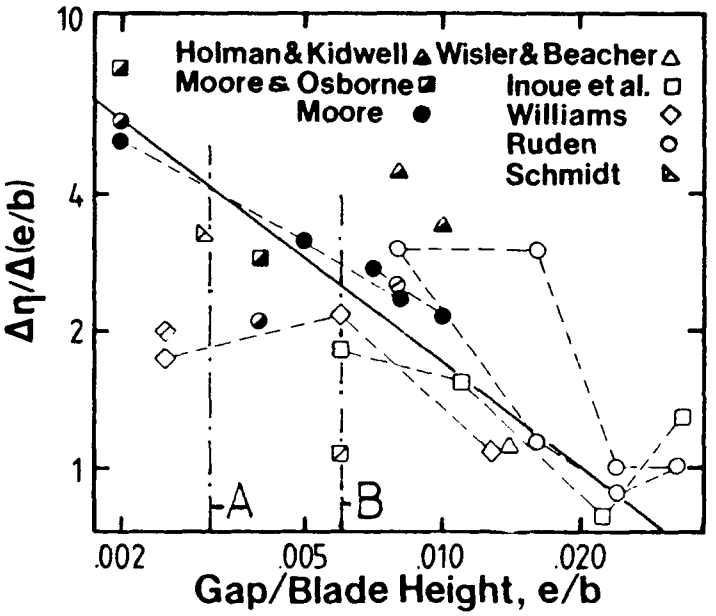

Fig. 3.4-1 Clearances selected for testing in the present study compared to the variation range of other experiments.

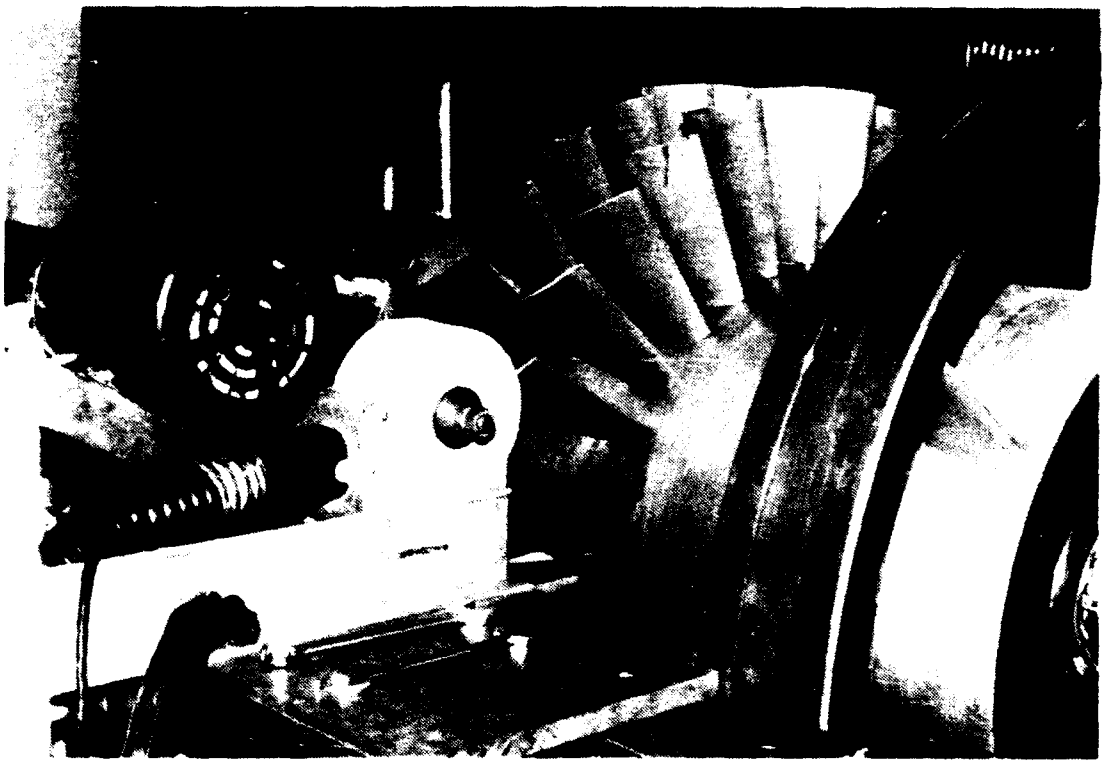

Fig. 3.4-2 Tip grinding fixture arrangement showing the first stage of the two stage rotor being ground by turning the rotor under the grinding disk.

3.4.2 Description of the Survey Configurations

The survey (or probe) configurations defined to address the matrix, discussed above, are described in the following section. Details of the sensor development and calibration of the probes have been appended or are covered in other reports.

3.4.2.1 Operating Line (CC)

The compressor performance on a constant speed throttle line was determined from sensors which were not altered through the course of the clearance variation program. The upstream configuration consisted of the (inlet) nozzle which was used to determine flow rate and a probe station ahead of the throttle housing which served as the dew point and inflow temperature measurement station. Combined with local total and static pressure, the temperature and dew point measurements were used to fix a reference density. Compressor face conditions were established upstream of the inlet guide vane using a Pitot static probe on the mean line, a radial total pressure rake (P) and static pressures on the hub and case wall. This probe arrangement allowed a local flow rate to be determined by integration of the velocity distribution derived from the rake and the hub, mean line and case wall static pressures. Nozzle flow rate was checked against this calculation periodically and was found to be consistent to within the uncertainty of a typical blockage correction (1%).

Compressor pressure rise was determined using averaged circumferential wall static tappings upstream and downstream of the stages. Exit flow conditions were established downstream of the exit guide vane where the flow was nominally axial and another total pressure rake (Q) was installed. Shaft torque and speed were derived from a torquemeter on the drive shaft and a "one-per-revolution" timing pulse from the shaft. Temperature rise was also used to verify the torque meter and was routinely recorded. The temperature rise measurement was not sufficiently well averaged, in terms of spatial distribution of probes in the flow, and the thermocouples uncertainty was too large to use the temperature rise for efficiency calculations. However, it was a useful check on the *static* torquemeter calibration and confirmed the torquemeter readings acquired under *dynamic* conditions. Averaged and corrected data from this arrangement of probes was used to define the flow, pressure rise and work coefficients and the efficiency.

3.4.2.2 Radial (Passage Average) (RS) Surveys

The probe arrangement for Build III is shown in Figure 3.4-3. Radial surveys could be completed upstream of the rotor, Station 1, between the rotor and stator (rotor exit, Station 2) and downstream of stator (stator exit, Station 3) in either stage. Five hole pneumatic probes (designated X, Y and Z) could be traversed at these stations and the circumferential rake (R) could also be traversed at the upstream rotor inlet and the downstream stator exit. The circumferential rake spanned two passage widths with eleven Kiel tips and the passage average total pressure could be obtained by direct or weighted averaging of the rake data. The rotor inlet condition could be obtained by surveying on multiple radial lines, at different circumferential locations, and averaging, whenever a full circumferential survey was not possible. Traverses mounted with cobra probes (S, U and V) could also be positioned at the rotor inlet and outlet to survey the near (case) wall velocity and angle.[36] The S cobra probe could be traversed

[36] The velocity field at the rotor exit was peripherally averaged by the rotor motion and was usually measured at a single peripheral position. Circumferential variations (stator-to-stator), which were present, due to stator wake transmission through the rotor were not readily averaged by this arrangement due to the extremely limited peripheral access at the rotor exit.

from hub to tip and was usually positioned at the upstream rotor inlet. The U and V probe's radial motion was limited to a 50 mm (2 in) extension from the case wall. To the extent possible with this instrumentation and survey access, the data were passage averaged.

3.4.2.3 Case Wall Static Pressure (WP, B-B) Surveys

The static pressure distributions at the case wall, blade-to-blade, were acquired by moving a plug, fitted with a centrally located, flush mounted Kulite XCS-093-1D high response pressure transducer, to various hole locations on the wall. A curved plate positioned flush with the wall above the second rotor carried a matrix of five rows of six holes spanning the axial chord. At each axial station there were five holes spanning one stator pitch in the circumferential direction. The plate's spatial position relative to the blade rows is shown in Figure 3.4-4. The arrangement has been previously shown isometrically in Fig. 3.3-3. Only one transducer was used for all the wall pressure data acquired. Systematic error in the data was minimized by having the same calibration and sensor characteristics for all the readings. As the measured flow was unsteady in the absolute frame, the unsteady response of the mount, protective screen, cavity and transducing sensor combined as a system had to be examined thoroughly. A variety of tests were made to verify that the pressure response of this transducer arrangement was, in fact, tracking the unsteady wall pressure under the rotor path. These calibration, response and verification tests are described in Appendix B.5.1. The phase lock procedure, described in Appendix B.2.2, was used to define the blade edge locations. The rotor blade pitch was divided into 100 time increments for measurement and acquisition and two passages were routinely surveyed and stored.[37,38]

Acquisition of blade-to-blade information results in voluminous quantities of data. Each of the six axial stations on the wall survey plate contained five circumferential holes for a total of (6 x 5 x 200 = 6000) wall pressure readings per survey and a matching 6000 standard deviation records. Linear data interpolation in the axial direction between holes enhanced the data visualization and the interpolated data (from a row of axial holes) were stored in (60 x 1 x 200) matrices for plotting and reduction. Readings from each of the axial holes at one circumferential location, or the average of all circumferential holes for each axial position were stored in these 60 by 200 matrices. Data matrices of this type size were interpreted by using contour plots and three dimensional surface representations of the data set. *It should be noted that the interpolation fills in a large amount of data in the axial direction.* When surfaces or contours are examined in terms of local flow features smaller than one sixth of axial chord, it advisable to recall the picture is based on a 6 x 1 x 200 data point set. The filling in of detail by the interpolation is demonstrated in Figure 3.4-5.

Data Reduction and Analysis The reduction methods applied to the data involved interpolation of the pressure magnitudes between the axial stations surveyed and a

---

[37] More passages were surveyed initially, however, the ensemble average traces for many passages were essentially indistinguishable from one to another for the (-A) clearance. In terms of the major flow features observed in the data, recording two passages appeared to be sufficient to verify the features were repeating in each passage. Over a period of time a coarse, grimy build-up developed on the pressure side of the blade's tip section and slight differences in signature of each blade could be detected. These discrepancies were negligible compared to the major flow features and the grime build up was useful for visualization purposes. It was removed periodically.

[38] Larger changes in passage-to-passage wall pressure signatures were detected for the (-B) clearance (with clean blades). It was not clear whether increased variations in tip geometry for the (-B) grind or the higher flow sensitivity to small changes in geometry were responsible for these observations. The variations were at a nominal 5% of signal level.

modest amount of smoothing of data to form continuous surfaces. The data were not overly smoothed due to the presence of occasional "bad" points resulting from electronic system errors in the data acquisition[39]. Surface views and contour plots of the resulting pressure distribution, or differences between two distributions are used extensively in the following discussion to demonstrate the features of the flow structure.[40] By searching the smoothed data matrices, minima, maxima and pressure magnitudes near the blade edges were readily established for any axial location. Pressure differences, blade loadings and average loadings could also be compared, plotted and analyzed as a function of axial chord.

Pressure Coefficient Definition A conventional pressure coefficient (C_P) not used for data presentation in the thesis due to the problem of identifying a unique and physically meaningful reference *flow* dynamic pressure ($q_t = 0.5\rho W_t^2$) near the wall. The relative velocity (W_t) of the flow is unknown *near* the blade tip or wall. A pressure coefficient, C_{Pu}, defined by dividing the pressure difference by the dynamic pressure of the wheel velocity at the tip ($0.5\rho U_t^2$) has been used in this thesis. The reference pressure ($0.5\rho U_t^2$ = 368.3 mm (14.5 inw)) was also constant to within one percent for all the data acquired. The reader should note from consideration of the velocity diagram near the tip that the value of W_t approaches U_t at the wall *in a viscous flow*. Consequently there was some physical basis for adopting this approach to the data presentation prior to further analysis[41] of the nature of the wall flow. A contour interval of 0.04 or 4% of C_{Pu} was used for analysis of the data. This interval is equivalent to 6% of a C_P based on the velocity diagram's calculated tip relative velocity (W_t) at design conditions.

3.4.2.4 Rotor-Exit Hot Wire Velocity (HW, B-B) Surveys

Rotor exit flow conditions from the case wall to 80% of span could be surveyed by traversing a 30 deg slant hot wire, or film, radially inward from the wall. The procedures and methods for conducting these surveys were developed in the program but complete surveys were not initiated. This technique was dropped from the two stage measurement plan because it became clear from the single stage results that this survey technique was showing unacceptable wall effects on stem type probes at near clearance immersion levels. It was only marginally viable in a near wall boundary layer flow with commercially available probes and specially made probes were required. It also presented circumferential survey difficulties in the two-stage compressor build with either stem or forward facing probes. Due to the expensive

---

[39] Each wall pressure data matrix represents a nominal 5,000 relay closure and 50,000 timed trigger, read and store operations by the data acquisition system. Acquisition errors from the system were experienced at a nominal rate of 1 per 300,000. Consequently there are occasional notches in the pressure data distributions due to system errors. Extensive data smoothing would blend these errors into the results so a light smoothing method was used. The smoothing mainly removed jagged and rippled edges from interpolated contours presented. Measured data were not altered by the smoothing process so some jagged edges and notches may be observed near the axial locations in the matrix where the probes were positioned.

[40] Seven data matrices were formed for each flow condition tested. The five stator-to-stator axial hole sets were averaged to form a sixth matrix which represented the stator-average or passage-average wall pressure distribution for the passage. A seventh matrix was formed by subtracting the average distribution from each of the stator-to-stator distributions and storing the sum of the square of the differences. This resulted in a distribution of wall pressure fluctuation intensity, i.e. large magnitudes of the matrix value indicated large pressure deviations from the stator or passage average value.

[41] From inspection of the raw data it was clear that the pressure distributions from blade to blade were substantially different depending on the rotor position relative to the stator. This indicated the flow pressure distributions near blade tip could not be collapsed in terms of passage average flow quantities (i.e. a pressure coefficient based on throughflow conditions). To determine whether the passage averaged distributions could be collapsed was left for later analysis.

implementation expected in this compressor and the new information that the wall pressure measurements were providing, the technique was not pursued. Single stage results are described briefly in Sec. 3.5.4.3. A description of the procedures are appended in B.4.

3.4.2.5 Case Wall Skin Friction (WS, B-B) Surveys

A skin friction sensor based on the principle of a pneumatic fence gauge was developed by capping a high response pressure transducer (Kulite XCS-093-1D) with an abrupt step fixed on a screen over the sensing element, Figure 3.4-6. The sensor and its development and calibration are described in Appendix B.5. Additional data traces, at up to six probe yaw angles for each hole in the wall plate, were used to resolve the direction and magnitude of the wall shear vector. Wall pressure (from WS) was used as the case wall static pressure datum needed to determine the shear. A 60 x 200 data matrix was created from the measurements and could be processed and presented in a similar manner to the wall pressure data. Only preliminary measurements using prototype hardware were made with this system in this program, however, these measurements were particularly valuable in interpreting the flow near the tip gap. The utility of the preliminary results suggested that a more durable shear measurement system should be developed. Consequently, a survey traverse unit, calibration test section and more durable sensors were developed. This work is described in Appendix B.5.

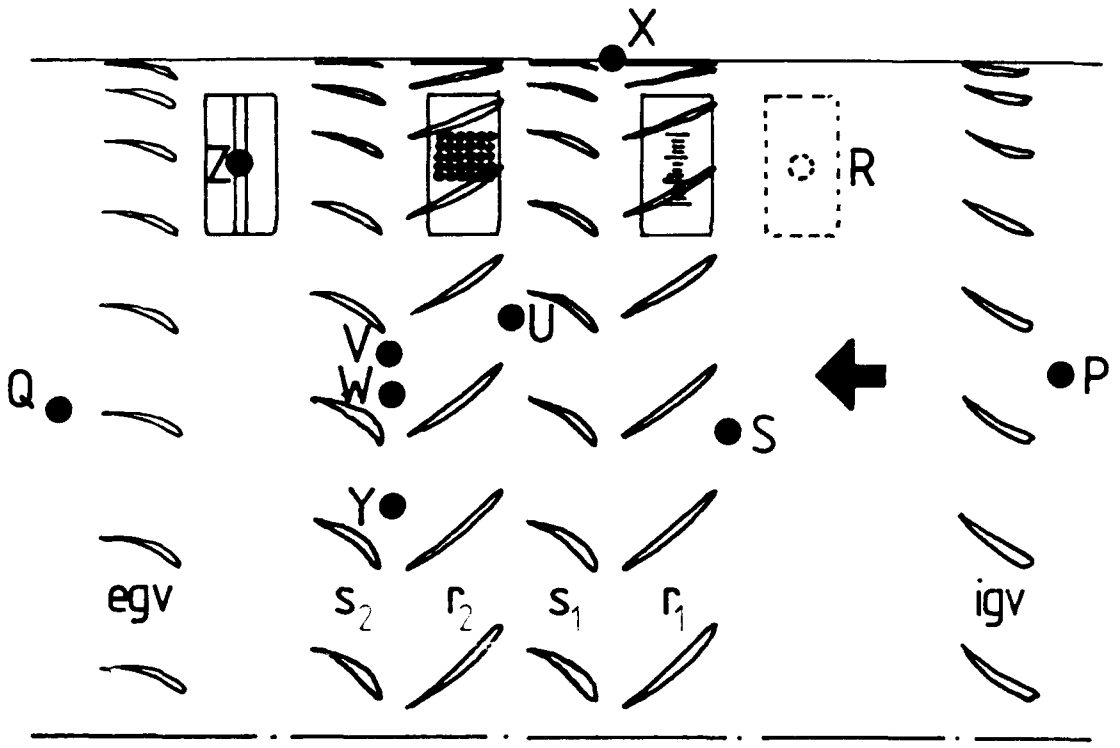

Fig. 3.4-3 Probe configuration for low response passage average pressure surveys (RS).

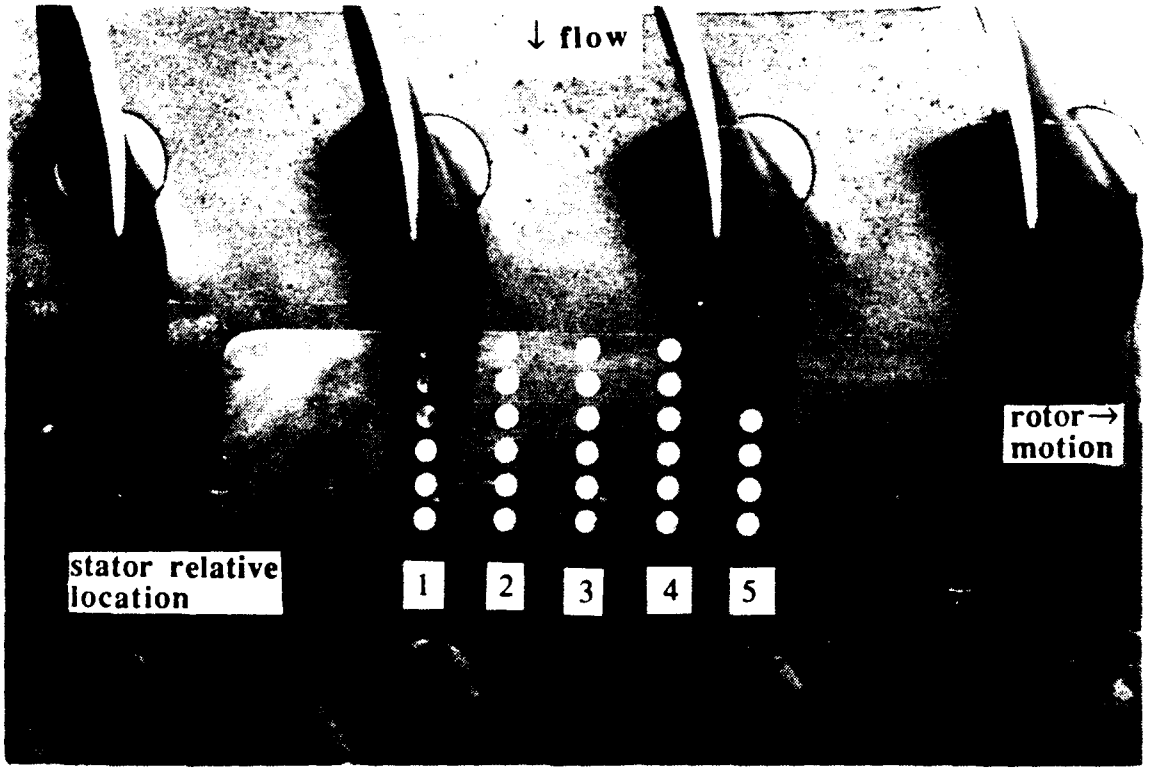

Fig. 3.4-4 Wall survey plug and spatial position of survey holes relative to the blading (WP and WS).

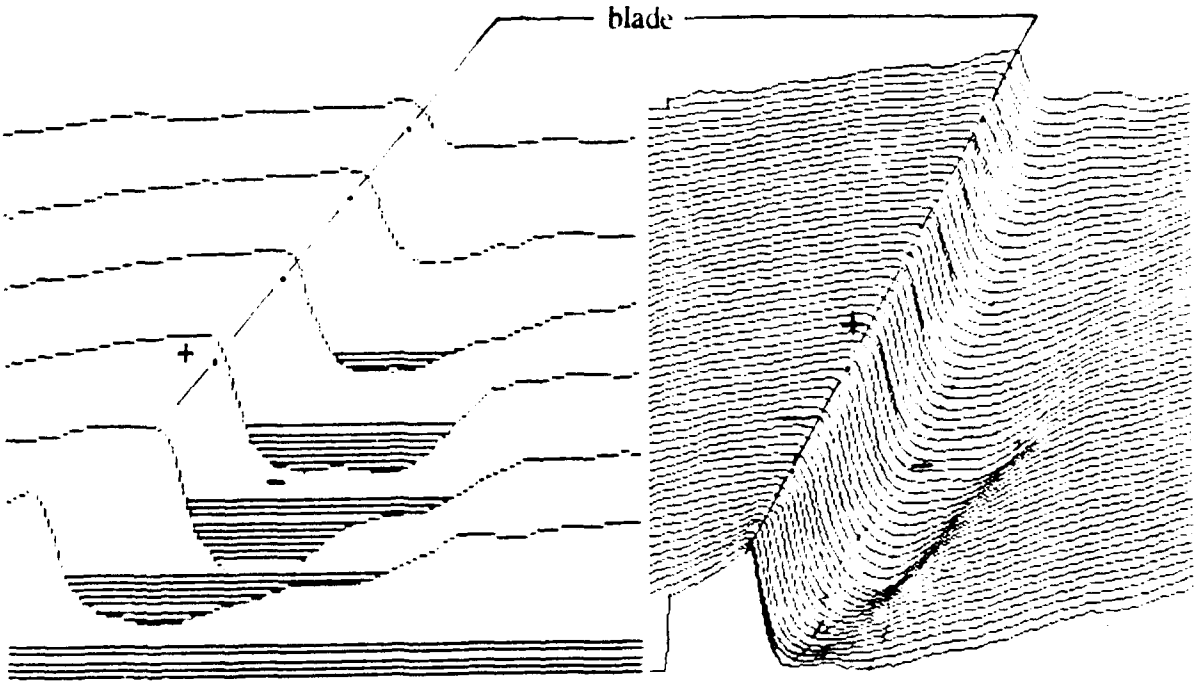

Fig. 3.4-5 Comparison of measured and interpolated wall pressure distribution data showing the degree of enhancement of the distribution (WP).

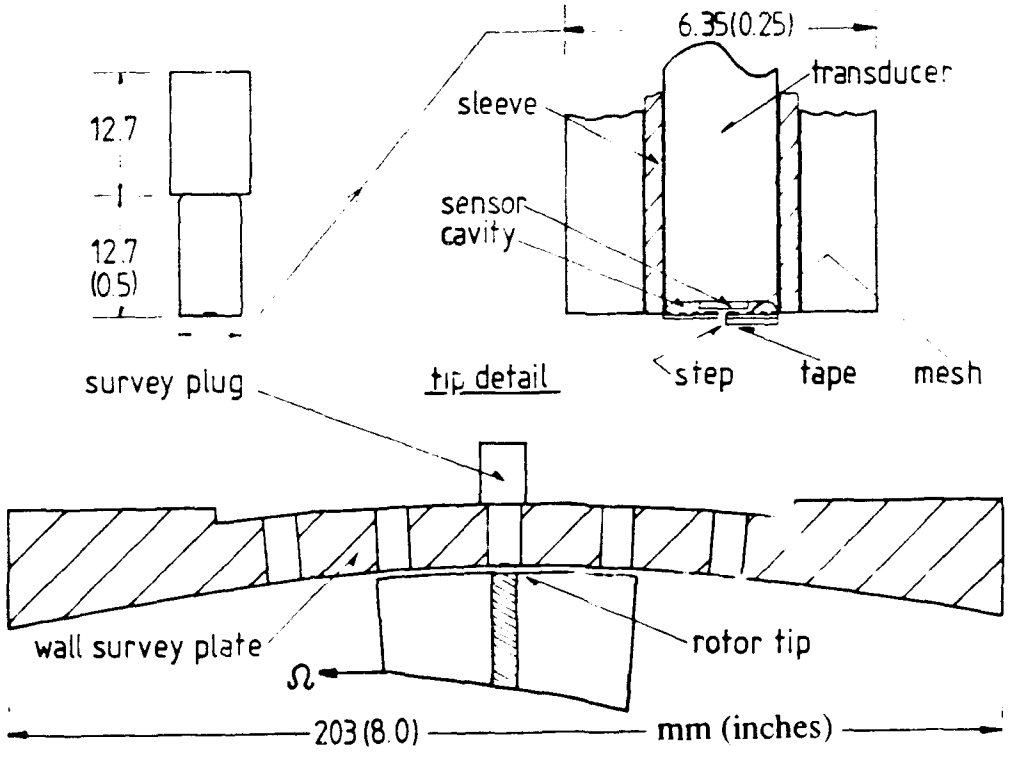

Fig. 3.4-6 Case wall skin friction sensor detail and survey configuration (WS).

3.5 Results - Flow in the Stage

Understanding of the stage flow was developed from a series of experiments. Details of these testing activities are reported in Moyle (1980-81), Waddell (1982), Moyle (1986) and Tarigan (1988). The overall interpretation of the stage flow measurements which developed in the prior work has been drawn upon in this discussion.

3.5.1 Test Section Inlet Average Flow

The flow conditions at inlet to the compressor test section define an initial condition of the flow which is modified by the succession of downstream blade rows. The typical test section inlet conditions are shown in Figure 3.5-1 at near design flow. The inlet section flow was slightly non uniform between the hub and case wall boundary layers favoring a higher velocity on the hub wall side. The case wall layer could be detected in the velocity profile as far as 38 mm (1.5 in) or 20% of span from the wall. This was consistent with the very long development length of the upstream duct. The displacement thickness was nominally 2.5 mm (0.1 in) or 0.013 of span. The profile shape reflected the rapid area reduction from the duct into the test section at the inlet bullet. The profile was bulked toward the wall.

3.5.2 Compressor Characteristic and Overall Performance (CC)

The two stage compressor pressure rise coefficient and efficiency are plotted versus flow coefficient in Figure 3.5-2 for the range of clearances tested. The same information is also plotted in a flow work versus power coefficient format in Figure 3.5-3. The single stage characteristic is also shown for the e/b = 0.0025 clearance level.

The measured characteristic curves were consistent with the design characteristic in terms of slope but showed a higher pressure rise for both the single and two stage configurations. These increases in pressure rise relative to the design projection were reconciled with the inlet guide vane underturning in Moyle (1986). There seemed to be a slight fall-off in pressure rise at higher throughflow for the two stage build. The efficiency curves had a similar form for the two builds but in the two stage configuration the inlet guide vane underturning did not boost the second stage pressure rise, which appeared to perform near design. The efficiency of the two stage configuration (maximum 82%) was consistent with the single stage (maximum 92%), however, the single stage was substantially lower than design expectations[42] (expected maximum 95%).

A clearance change from e/b = 0.0035 to e/b = 0.006 is shown to have a very small impact on the two stage performance (Fig. 3.5-2 and 3). This outcome was not anticipated based on the analysis of Sec. 2.1. Considering the analysis of Lakshminarayana (1970), this result might be thought of as an indication of a clearance optimum, i.e., performance improvement at larger than minimum clearance. However, there are a number of other factors which were described in Part 1 to be considered. This outcome, from a clearance change, was found to be consistent with the detailed measurements to be discussed in following sections and is discussed further in Sec. 4.2.2 after all the measurements have been presented.

---

[42] The efficiency in the present compressor was comparable but slightly lower than other low speed test compressors surveyed in a similar manner in the literature. While it may be useful to have high baseline efficiencies in university test machines for comparison with industry, lower efficiency in laboratory machines does not invalidate them as vehicles for legitimate flow field study. It should also be noted that representative but lower efficiency may assist in delineation of the basic physics of loss production by having stronger mechanisms present than is typically the case.

3.5.3 Inter-Row Passage Average Flow (RS)

The main features of the *inter-row hub-to-tip passage average* flows are summarized and discussed in the following section. A few comparisons are also made of the single stage results (Build I/II) and the two stage (Build III-A,-B) results. Evidence of interactions by the multiple blade rows are also discussed.

3.5.3.1 Velocity and Angle Distributions

Data representative of the velocity and angle distributions acquired from the radial (RS) surveys are shown in Figure 3.5-4 for the single stage and the two stage configurations, at design flow conditions. The single and two stage velocity and angle survey results were similar in overall form and were consistent with the overall performance observed. The velocity diagrams were in reasonable agreement with the design diagrams, except in the first rotor inlet region. The velocity diagram data was typically more free-vortex than the design intent, i.e., the axial velocity near the case wall was larger than design. As wheel speed was a constant, the velocity diagram was therefore distorted and the flow directions tended toward design (minimum) incidence in all cases.

3.5.3.2 Spanwise Energy Addition and Efficiency

Single Stage Figure 3.5-5(a) shows the energy addition and pressure rise coefficients (measured) compared to the design values. The spanwise efficiency is shown in Fig. 3.5-5(b). A pronounced underturning from the inlet guide vane, near the case wall, had the effect of substantially reducing circumferential velocity (V_{u1}) upstream of the rotor. As the rotor exit angle is largely independent of incidence angle, a substantially larger work input occurs over the whole blade span.[43]

Two Stage Comprehensive surveys of the two stage Build III configuration were not completed due to the bearing failure of the III-A test series. Preliminary surveys were conducted, however, and showed the flow conditions in the two stage machine to be very similar at both rotor exits. The compressor map indicated the first rotor continued to perform in a similar manner to the single stage, while the second rotor pumped more like the design intent.

3.5.3.3 Rotor and Stator Incidence and Deviation

Single Stage While the pressure rise decreases noticeably relative to the work input in the single stage, it was apparent that the incidence at the rotor face was uniformly consistent with the design (minimum) incidence. This is shown clearly in Fig 3.5-5(c). The data suggested the rotor adjusted the axial throughflow to meet its incidence requirement rather than tolerate the increased blade-to-blade pressure gradient that a

---

[43] The measured velocity diagram at 85% span, Fig. 3.5-5(c) shows the substantial work input increase, however, the significant reduction in axial velocity across the rotor also suggests a very strong diffusion. The calculated diffusion factor is 0.49 for this diagram (Deq = 1.838). As the radial velocity is also significant, there is clearly an adjustment of the flow and probably a separation in the outer section of the span. This would be consistent with the substantial fall in efficiency toward the tip and the increased loss coefficients for both the rotor and stator. The stator losses are particularly large considering the apparent forcing of the flow in the rotor to near design conditions. The growth of the stator loss coefficient commences at 75% span and rapidly rises to 0.1 at 90% and continues to grow towards the case wall. The rotor however shows a uniform 0.1 loss factor from about 70% span to the wall. The combination of these losses is to strongly reduce the pressure rise in the outer part of the span relative to the increasing work input. The evident decline of spanwise efficiency can clearly be traced to the divergence of the intended pressure rise from the work input rather than a larger work input than anticipated.

larger incidence would require.[44] The stator conversely, stalled near the tip, toward the leading edge, and showed a strong radial outflow as the flow turned to the axial. Evidence of this stator tip corner stall also appears in the flow field computations, Appendix B.7. The low stator tip solidity noted in Section 3.2 should also be recalled. The flow in this region was substantially worse than intended.[45] The rotor's ability to induce flow was relevant to the tip clearance observations and is discussed further in Part 4, Sec. 4.1.1. The degree to which the apparent stator tip stall would be reduced by a following rotor row was unclear until examined in the two stage configuration.

Two Stage The rotor exit conditions in the two stage build also agreed with the single stage rotor exit profiles (i.e., the design intent). The mean line values of rotor exit angle (β_2) were 21 deg for rotor 1 and 20.2 deg for rotor 2 compared to the design value of 19.7 deg. The single stage surveys showed that the major angle discrepancy occurred at the rotor inlet, however. This station could not be fully surveyed circumferentially in the two stage build and oil streaks were used to further understand the flow in this region. Figure 3.5-6 shows the difference in streak patterns observed on the first and second stator suction surfaces for the e/b = 0.0035 clearance. While a large case wall separation is visible on the second stage stator, the same region of the first stage stator shows a very small separation zone. This was consistent with the first rotor's exit angles being close to design and the second rotor tending to flow at design incidence. This first stator immediately precedes the region where the case wall measurements were made and the state of the flow was of concern in this region. The overall conclusion from these indications was that the flow leaving the first stator was close to design angles over the flow coefficient range.

3.5.3.4 Stage-Exit/ Average Flow Comments

Spanwise dynamic pressure normalized by average dynamic pressure ($q(r)/q_{av}$) showed a strongly parabolic form about the compressor mean line with span at the stage exit, Fig. 3.5-5 (d). The form of the profile at this station indicated much higher losses in the case wall regions than would be anticipated from the design profile losses. These results were qualitatively[46] consistent with the inter-row measurements.

From comparison of the single stage with the two stage build results, it was clear that single stage test results (or last stator measurements) were not representative of the stage flow. The extent to which the flow in the second rotor was disrupted by the second stator corner stall was not totally clear, however, it was apparent that the two stage flow more closely matched the design intent for the repeating symmetric stage. The improvement was attributed to the presence of at least one rotor discharge flow passing into an unstalled stator for deceleration. This stator then set-up the flow for the following rotor which was measured in detail in the tip clearance study.

---

[44] This was a surprising phenomenon, and it is a substantial variance, in a design sense, from what is supposed to occur. In general, the overall whirl distribution and axial velocity field is presumed to define what will happen on a stream surface. Had this been the case in this blading, the axial velocity would have been lower and the incidence much higher. However, the indications from the data are that the rotor induced flow at a much higher velocity and lower incidence and deflected (inward) flow that could not be accepted by the stator.

[45] A general analysis of the streamline shift in a symmetric blading is given in Vavra (1974, p. 462). However, the shifts observed were much stronger, albeit following the general pattern, than those discussed. For the velocity diagram of 3.5-2(c), the axial velocity reduction across the rotor was 13% for the cylindrical surface shown.

[46] Quantitative comparison required peripheral surveys in the interblade row spaces. Surveys of this nature were not possible for the Build III blading arrangement.

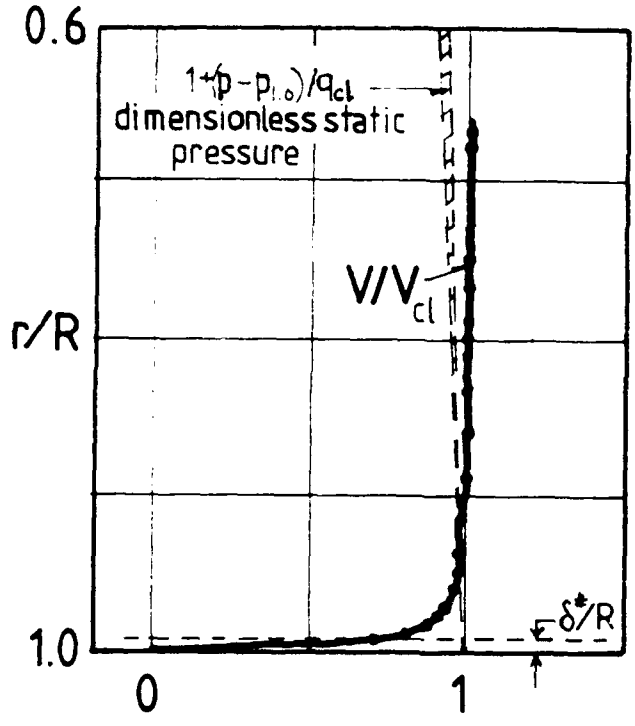

Fig. 3.5-1 Compressor face inflow conditions; static pressure and boundary layer profiles referenced to center line (cl) conditions.

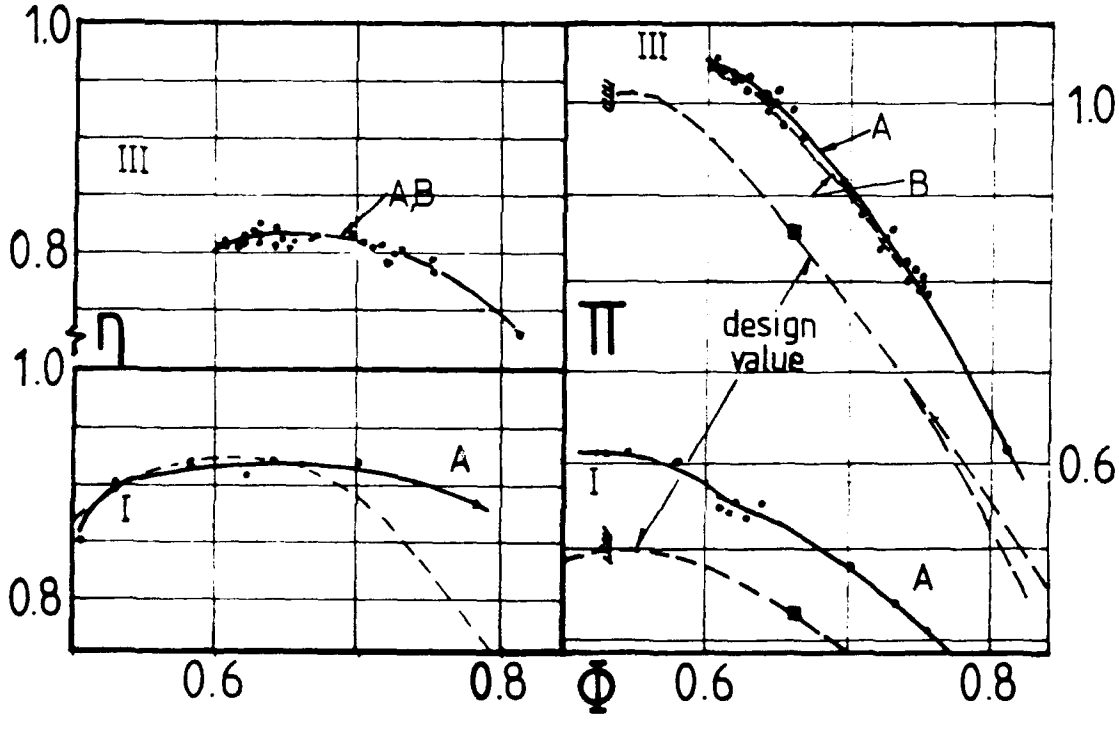

Fig. 3.5-2 Pressure rise and efficiency as a function of flow coefficient for the clearance ranges tested and single stage (I) and two stage build (III).

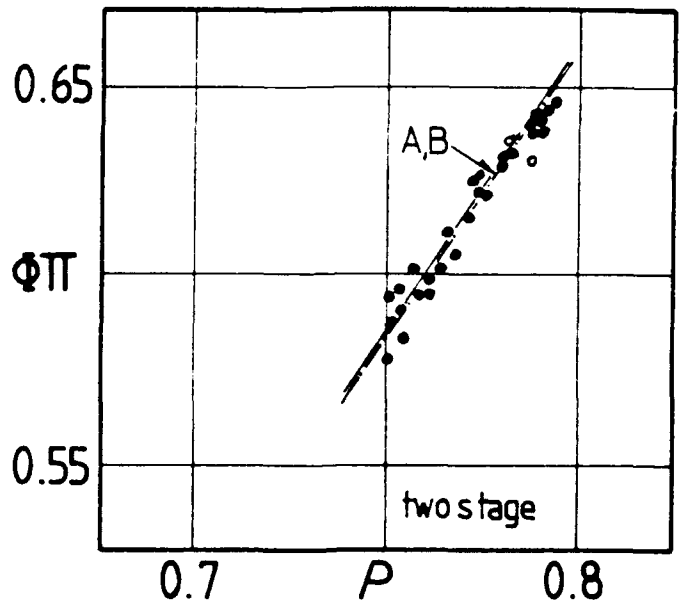

Fig. 3.5-3 Dimensionless flow work versus power coefficient for the range of flow coefficient and clearances tested.

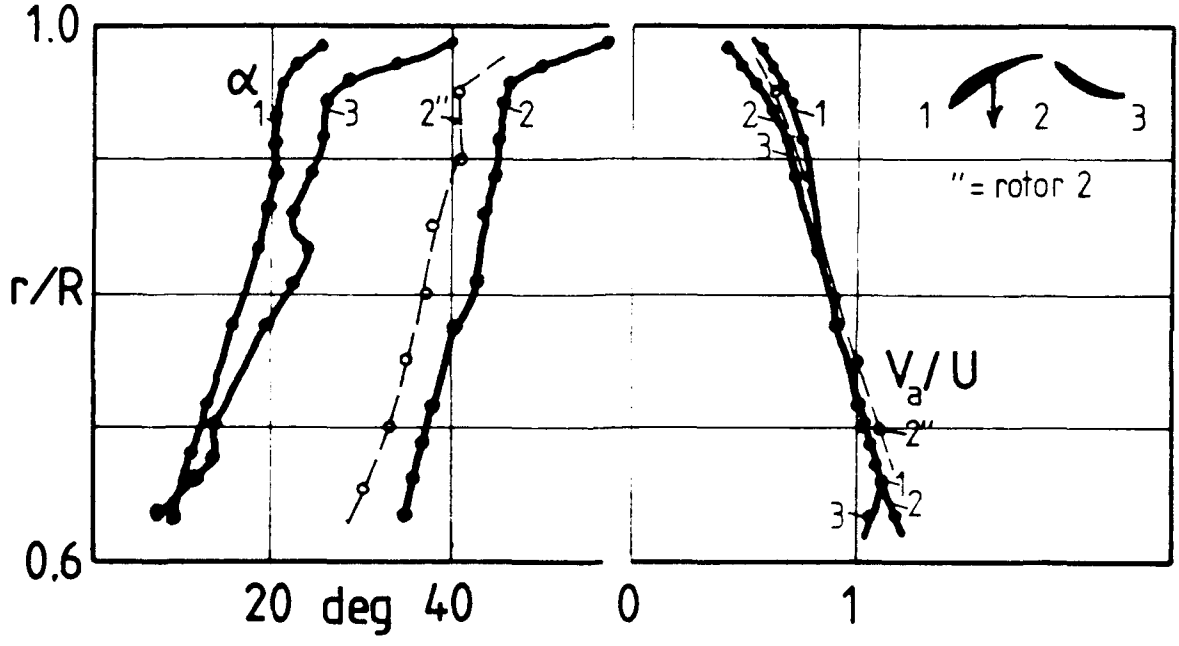

Fig. 3.5-4 Flow angle and velocity distribution comparisons for the single and two stage configurations.

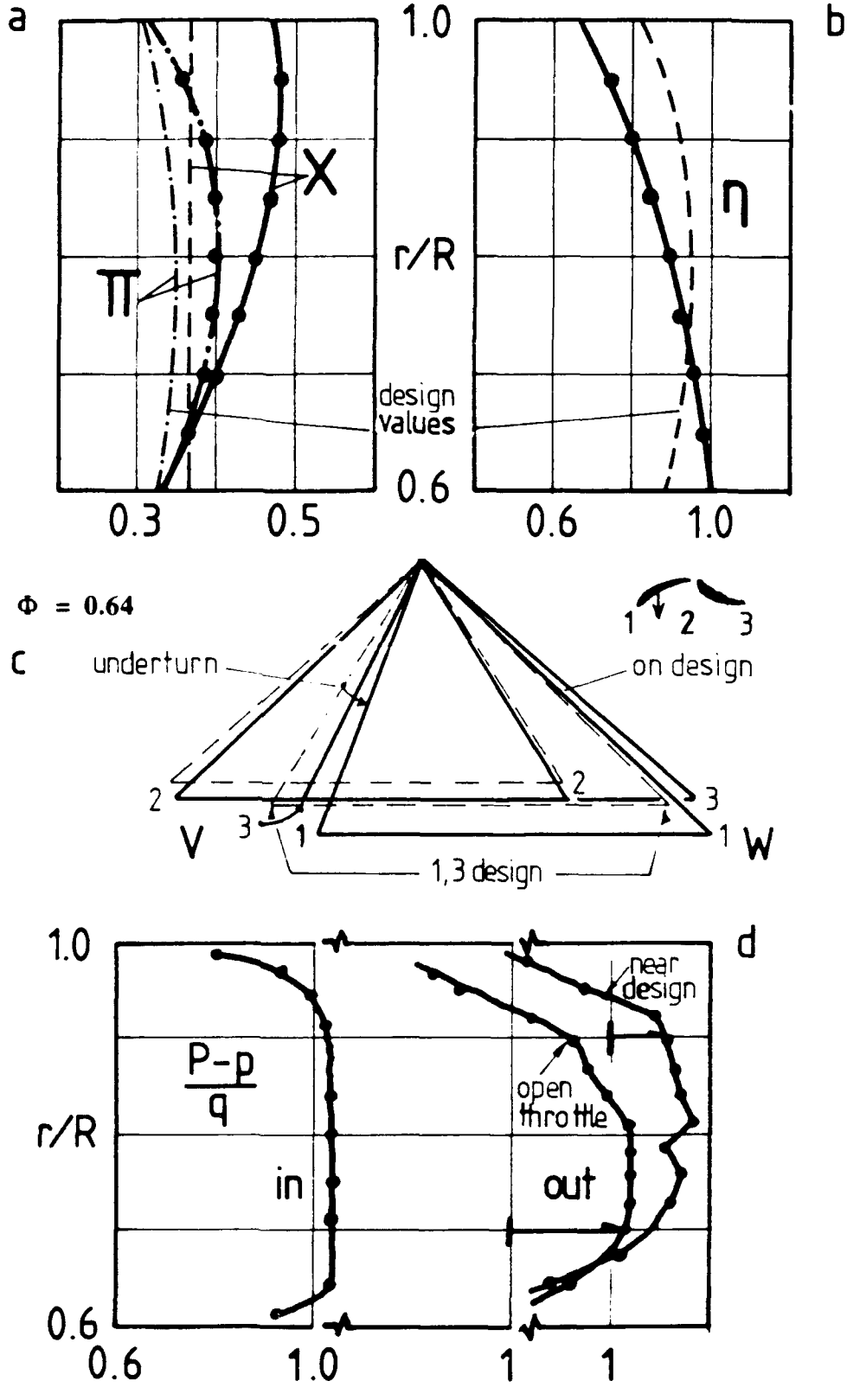

Fig. 3.5-5 (a) Spanwise energy addition and pressure coefficients for the stage. (b) Spanwise efficiency distribution. (c) Measured velocity diagram at 85% span for the single stage (Build II). (d) Spanwise stage exit total pressure distribution.

3.5.4 Stage Blade-to-Blade Flow (WP,HW,WS)

An overview of the stage blade-to-blade flow measurements on or near the case wall and exiting from the second rotor are presented in the following section.

3.5.4.1 Flow Visualization Observations

Over a period of time a coarse, grimy build-up developed on the pressure side of the rotor blade at the tip section. Very slight differences in the signature of each blade could also be detected in the high response data. Although it was removed periodically, the build-up was useful for general visualization purposes The build-up for the e/b = 0.0035 clearance clearly indicated the scraping of case wall fluid up the pressure side, Fig. 3.5-6 and Figure 3.5-7(a). There was not a similar build-up of grime on the suction side. The suction side was notably free of fouling at the tip. *Oil streaklines* on the blade sweep toward the tip, as shown in Figure 3.5-7(b). The sweeping pattern shown was consistent with a combination of the centrifugal force acting on the *oil* in the blade boundary layer and the shear of the throughflow fluid moving through the passage. As the density of oil is much higher relative to air, the curvature of the oil streaks indicated there was no strong centrifugation of the air flow radially outward on the suction side.

Oil streak lines were also visible on the case wall under the rotor path and on the hub drum wall. The wall streak patterns are shown in Figure 3.5-7(c). The oil paths on the wall in this (e/b = 0.0035 clearance) case are more representative of net airflow direction[47]. From the velocity diagram, a circumferential shift of roughly two stator passages is consistent with flow entering the rotor on the pressure side and leaving on the pressure side. This is approximately what is observed under the rotor tip. A similar situation was observed in the single stage (e/b = 0.0025) wall streak pattern (Moyle (1986, Sec. 5.2)). These results were consistent with little or no leakage flow in the tip gap.

3.5.4.2 Case Wall Pressure Distribution (WP)

Case wall static pressure time traces were collected in sets of six axial stations for five stator-to-stator circumferential locations, as described in Sec. 3.4.2.3. The time varying wall pressure measurement is, in itself, a relatively simple diagnostic. However, due to the phase-locked acquisition of the signal, the ability to position the blade edges precisely in the data matrix and the repetitive measurement of the same axial station at different stator relative positions; a relatively powerful flow field diagnostic capacity was developed from a single sensor.[48] With the exception of one data set,[49] complete sets of case wall pressure distribution matrices were generated for the throttle conditions set out in Table 3.4-1. In these tests the tip gaps were the same over the entire axial chord of both rotor rows.

A single trace of the wall static pressure for one axial and circumferential case wall location is shown in Figure 3.5-8. The trace is shown as it appeared on the oscilloscope and after capture by the data acquisition system. Figure 3.5-9 shows wall

---

[47] Oil streak traces are widely used in industry as a crude form of flow diagnostic to detect flow separations and changes in flow character, e.g., discussion of Benser (1974) by Koch.

[48] In Moyle (1989) the present author noted that analysis of the prior experimental data suggested measurements close to the tip would be required to explore and identify the entropy production mechanisms associated with tip clearance changes. The case wall pressure distributions generated by the technique described above met this objective.

[49] Wall pressure distributions for this throttle condition were only half mapped due to a bearing failure while testing, (data set WP-A53)

pressure traces from one axial station spanning one stator pitch. The variation in the trace with stator relative position is apparent. A low pressure trough outboard of the suction side can be seen to vary in shape with stator relative position. The trough also extends a considerable distance into the passage. The nature of the case wall pressure distribution and it's relationship to the tip clearance flow will be expanded upon substantially in Sec. 3.6 and 3.7.

3.5.4.3 Rotor Exit Velocity Field (HW)

Single Stage Due to the difficulties with development of this instrumentation, only cursory surveys of the rotor exit blade-to-blade flow were made with hot-wires in the single stage build. Either an oscilloscope or the System Voltmeter acting as a digital oscilloscope was used to record the signal. The data was qualitative due to the use of an uncalibrated wire. The dominant pattern observed at the rotor exit in the single stage was a loss core positioned nominally at mid passage. This core was situated away from but close to the wall at 90-95% span. The average velocity defect magnitude was significant, however, the individual readings indicated the excursions about the average were large. The data resembled a blade wake but broader in spanwise extent.

3.5.4.4 Case Wall Shear Distribution (WS)

Two Stage Initial wall shear measurements using a prototype probe tip were able to resolve the direction and approximate magnitude of the shear. The measurements were only qualitative indications of the shear because the probe was not calibrated over its entire operating range. A null output, however, was was known to be a zero shear condition due to the design and operation of the probe. When the flow was measured, the probe output was null in the region preceding the blade pressure-side, under the blade tip, and for some distance from the suction-side. This indicated that there was no shear (or no absolute flow) near the wall in this region. This zone of stagnant flow occured close to the suction side and is interpreted in greater detail in the context of the the tip wall corner flow in Sec. 3.6.3. Levels of shear elsewhere across the blade-to blade spacing were constant and indicated the absolute flow was drawn across the passage in the direction of motion of the rotor.

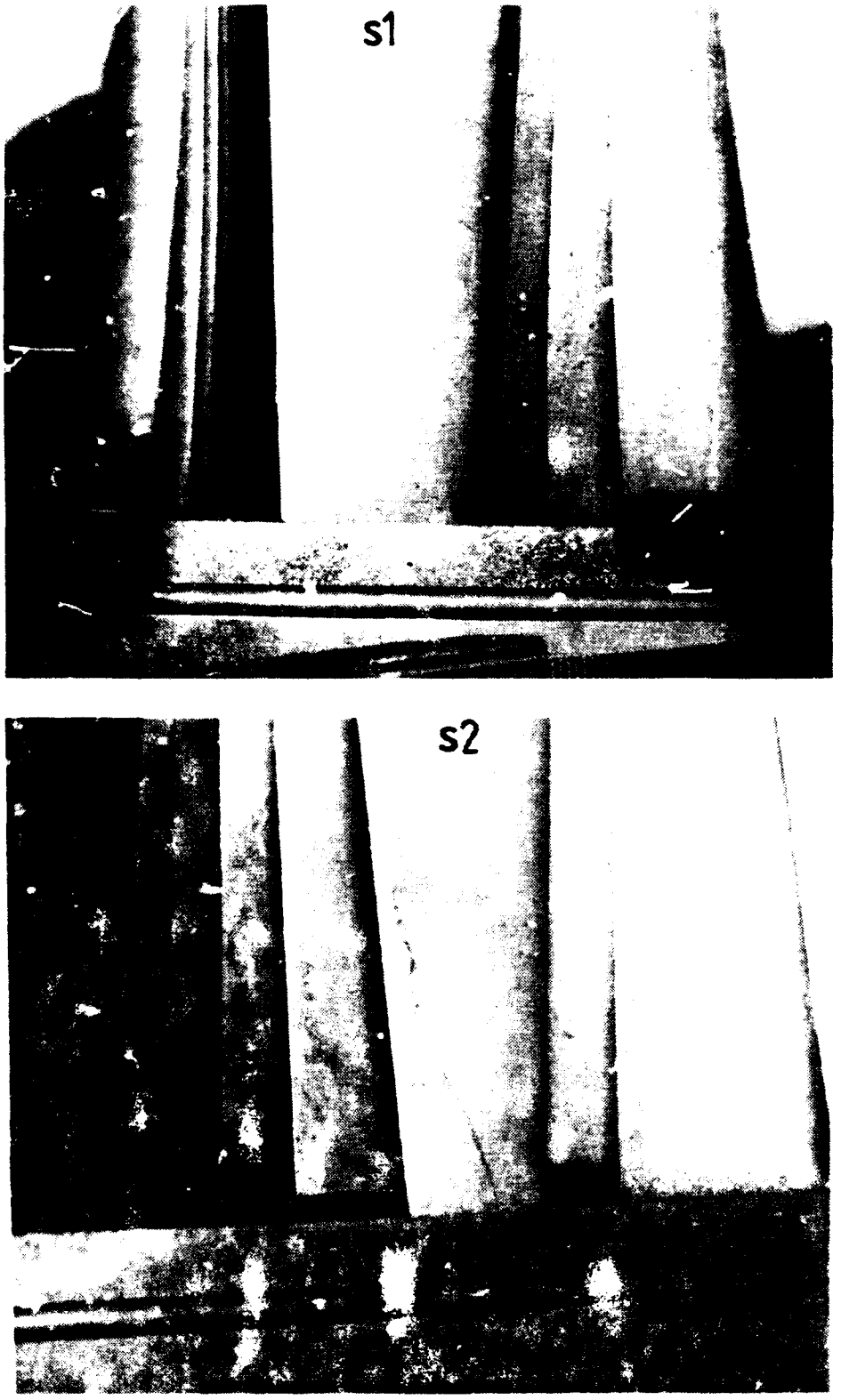

Fig. 3.5-6 Comparison of trailing edge conditions on the first (S1) and second (S2) stators in the two stage configuration. S2 shows a separated region extending from the case wall while S1 shows a well attached flow.

Fig. 3.5-7 (a) Grime build up on rotor pressure side. (b) Oil streaklines on rotor suction side curving toward tip but not straight outward. (c) Oil streakline pattern on compressor casing under rotor path consistent with flow entering and exiting the passage on the same side of the blade.

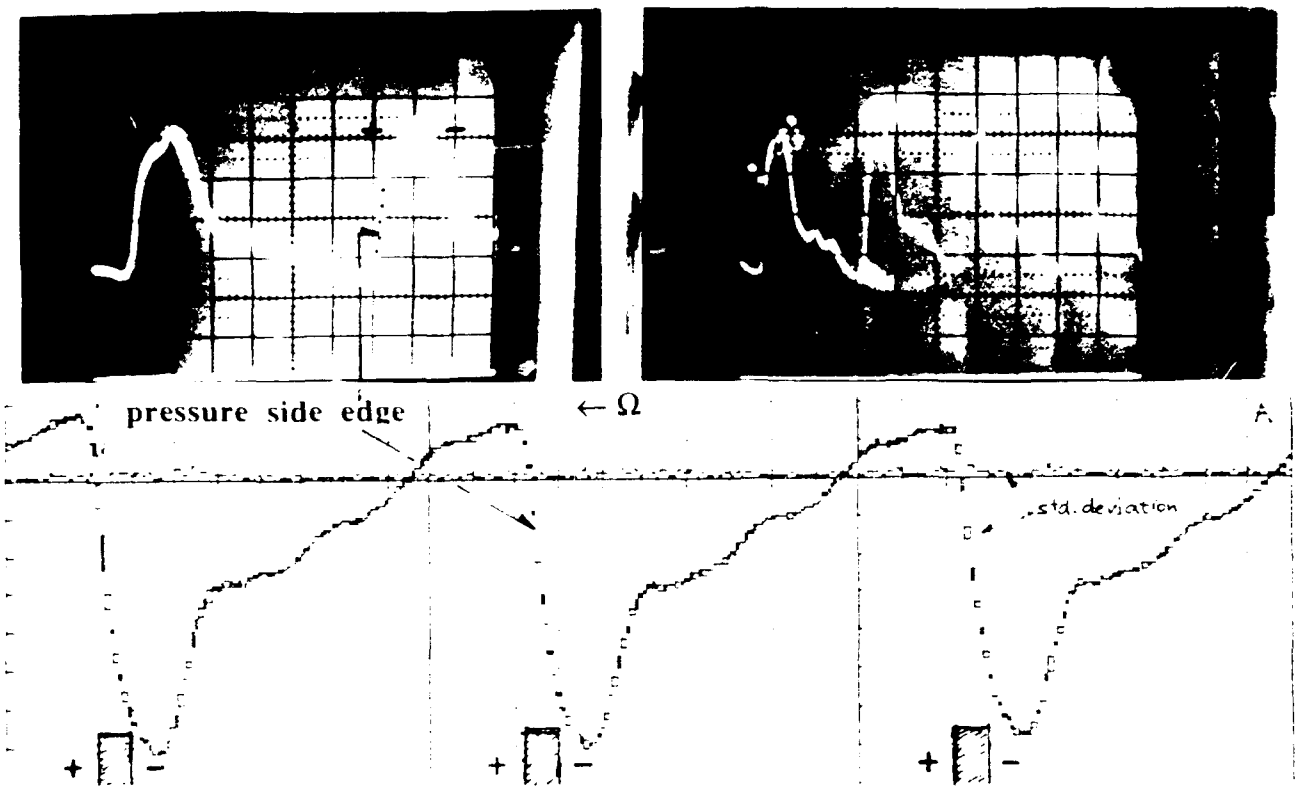

Fig. 3.5-8 Comparison of wall pressure traces recorded on an oscilloscope and plotted by the data acquisition system. Values are plotted as rectangles with a width of the sample interval and a height of the standard deviation of the ensemble. It can be seen that the pressure varies most outboard of the suction side.

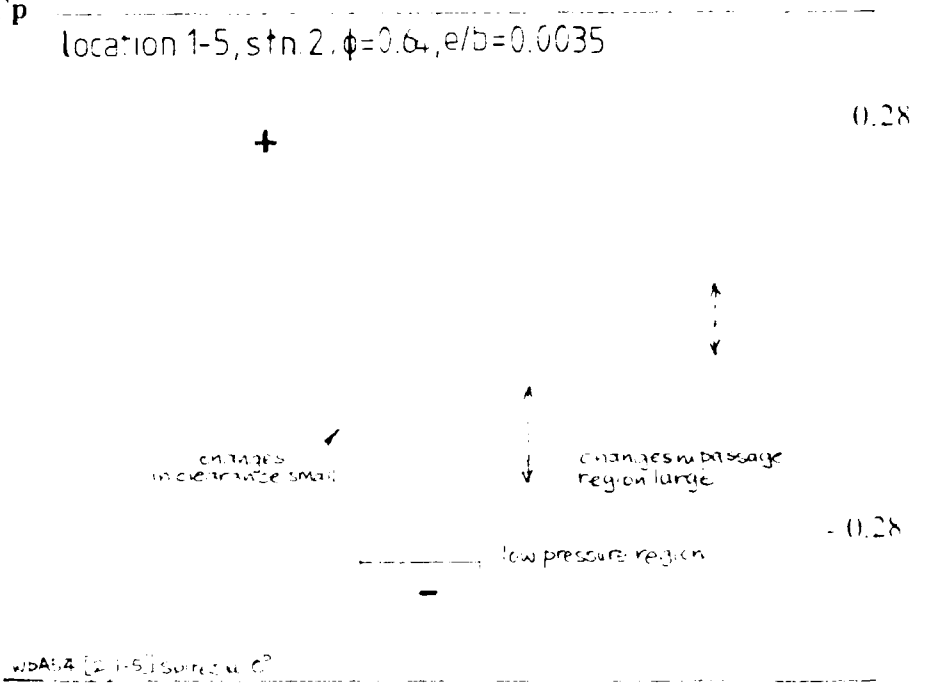

Fig. 3.5-9 Wall pressure traces from one axial station at five circumferential positions relative to the stator showing the large variation in the trace with stator relative position and the extent of the low pressure outboard of the blade suction side.

3.6 Results - Flow Structure in the Tip/Wall Corner

The flow structure near the blade tip and case wall corner can be explored by analyzing the distribution of pressure contours *at one clearance level* over a range of flow conditions. A pressure coefficient (C_{pu}), defined as the difference in wall pressure from a pressure datum divided by the wheel dynamic pressure at the tip ($0.5\rho U_t^2$), was used to normalize the data. Use of C_{pu} is discussed in Sec. 3.4.2.3. A contour interval of 0.04 or 4% of C_{pu} was used for analysis of the data. This interval is equivalent to 6% of a C_p based on the velocity diagram's tip relative velocity (W_t) at design conditions. The uncertainty in C_{pu} was less than 0.4% or 0.004. Contours of pressure coefficient were found to exhibit distinct and consistent flow features over a wide range of conditions. These features manifest different behavior with changing stator relative position of the rotor and, to a lesser extent, flow coefficient.

The results are discussed in three sections. The average flow pattern is presented first (Sec. 3.6.1), then the flow pattern is examined relative to the stators (Sec. 3.6.2). Finally the wall pressure and wall shear results are examined together (Sec. 3.6.3).

3.6.1 Stator Averaged Pressure Pattern

A passage average condition can be obtained by *averaging* the pressure patterns at the *same clearance level* for all stator relative axial hole rows. The distribution which results shows the *passage or stator average blade-to-blade flow* from leading edge to trailing edge of the rotor.

This pattern is described first to familiarize the reader with the main features of the wall flow pattern. Figure 3.6-1(a) shows a surface view of the wall pressure distribution looking from the aft of the rotor forward towards the leading edge for the design flow (Φ = 0.64), e/b = 0.0035 clearance case. The radial direction of the view is from outside the case wall looking into the passage. The high pressure ridges running from top left to bottom right across the distribution coincide with the pressure sides of rotor blades, 2 (leftmost) and 3. The throughflow is down the page and the rotor motion is from right to left. The surface shown is created by carpet plotting of the ensemble average wall pressure traces recorded by the acquisition procedure. These data were then passage averaged and then interpolated. The step values in each corner of the plot have been artificially inserted to permit the pressure magnitudes to be scaled. The step values are always drawn in the same locations on the figures. Sixty traces are carpet plotted on each figure and each trace can be scaled from the visible corner step values.

Figure 3.6-1(b) shows the *same data viewed from the leading edge* of the rotor looking aft. The rotor motion is still from right to left however the throughflow direction is now up the page. This view of the surface shows the main features of the flow. The (leftmost) high pressure ridge running from bottom left to top right corresponds to the position of the rotor 2 pressure side. The pressure pattern can be seen to be very repeatable from passage 1-2 to 2-3 to 3-4 consistent with the expected periodicity of the flow.

The main features of the flow are marked on the figure. A pressure depression or basin (A) is clearly visible in the (b) view sitting roughly 15% of chord aft of the leading edge and about 20% of spacing from the blade suction side. The central region of this depression invariably includes the lowest pressure in the whole passage distribution. Two pressure gullies are also persistent features of the flow. The gully marked (C) is also evident in all the patterns and runs diagonally across the passage from the blade suction-side leading edge toward the pressure side trailing edge. The

trailing-edge end of this gully is slightly more visible in the (a) view, while its origin in the basin is more visible in the (b) view.

Perhaps the most interesting feature of the wall pressure distributions is the *location* of the blade-to-blade pressure minimum at all axial stations in the pattern. This minimum condition corresponds to the gully marked (B) on the (b) view. It is not visible in most of the (a) view. This blade-to-blade pressure minimum at any axial station is found to lie approximately *two blade thicknesses away from the suction side*.[50] The diagonal (C) gully is a *local* minimum in the distribution in the otherwise monotonic pressure rise towards the pressure side. The pressure magnitude is typically uniform from leading to trailing edge on the pressure side of the passage and forms a broad, gradually rising plateau of high pressure advancing in front of the blade pressure side.

The measured pressure pattern differs most noticeably *near the suction side* of a two-dimensional computational solution for the flow at the tip, as shown in Figure 3.6-2. This computed blade-to-blade pattern was generated from a meridional throughflow solution for the flow in the second rotor which is discussed in Appendix B.7. The main differences are seen to be the low pressure basin formation and its position well aft of the leading edge, the low pressure gullies which show as local bulges in the measured data pattern and the minimum pressure location lying in the basin rather than very close to the suction side on the leading edge. Apart from the suction side corner local detail, there is clearly a correspondence in the patterns.

3.6.1.1 Maximum Depression (Basin) Displaced from Suction Side

In conjunction with the path of the pressure minimum in the passage, lying roughly two blade thicknesses from blade suction side at tip, the low pressure basin further extends the region of low pressure into the passage. An abrupt rise to a plateau of higher pressure precedes the pressure side of the blade. This basin of low pressure is clearly visible in the pressure contours of Figure 3.6-3(a) as an oval trough lying off the blade suction side. The axis of the oval is turned slightly away from the direction of the suction side. Its upstream end is closer to the blade suction side and its downstream end is nearer the pressure side.

Pressure Basin Change with Flow Coefficient Variation This low pressure basin changes its shape with flow coefficient variation as shown in Fig. 3.6-3(a) but always includes the 25% axial chord station in terms of position. It elongates, extending toward the leading edge at low flow coefficient and extends aft, further away from the blade and becomes shallower as flow coefficient is increased.

3.6.1.2 Behavior of the Pressure Minimum (Gullies) In Pattern

The two elongated low pressure depressions (or gullies) which were noted in the pressure pattern behave differently with changing flow conditions. Figure 3.6-3(b) shows the behavior. The minimum depression gully (B) which stands off the blade suction side and runs the length of the blade, roughly parallel to the chord, does not change its position with flow coefficient variation. The other low pressure gully, running diagonally from the leading edge of the blade on the suction side toward the pressure side region of the passage (C), tends to move closer to and swing toward the blade suction side as flow coefficient increases. The trailing edge end of this low pressure path tends to swing the most with flow coefficient and has a tendency to split, fork or fan out toward the trailing edge as shown in Fig. 3.6-3(b).

---

[50] Similar observations seem to have been made by L. H. Smith in cascade calculations. Smith (1955) shows pressure lows near the cascade wall (of up to 6% of freestream dynamic pressure) can be analytically related to case wall boundary layer thickness.

It should be noted that the region between the two paths of low pressure is consequently a slightly higher pressure region with a wedge like shape extending from a broad base near the trailing edge to a point immediately downstream of the low pressure basin. This wedge is frequently visible as a distinct saddle (low-high-low) at the downstream end of the wall pressure basin when viewed on an oscilloscope.

3.6.1.3 Blade loading Distributions

Figure 3.6-3(c) shows the *passage average* pressure loading, based on the maximum to minimum pressure in the passage and pressures at the blade edges, as a function of axial position (axial chord) for the flow coefficients shown in Figs. 3.6-3(a) and (b). A graph of pressure distribution is shown in the upper part of the panel and the tangential loading is placed in the lower part of the panel. The pressure distributions show the *passage* minimum pressure level to decline only slightly over the flow coefficient variation range. The maximum pressure level *in the passage* corresponds closely to the level of the pressure-side blade *edge* at all throughflows and the trend shows the main change in pressure level occurs on the pressure side of the blade as flow rate varies. The pressure levels on the suction side blade *edge* are significantly higher than the *passage* minimum value for all the flow cases. The *passage* minimum pressure is found to lie out in the passage. The shape of the suction side blade edge pressure distribution is remarkably similar for the two higher flow coefficients.

The tangential loading clearly shows the difference in level between the *passage* loading and the *blade edge* loading. The peak tangential loading occurs at about 20% of axial chord. The horizontal slashes marked on the tangential loading plot correspond to the arithmetic averages of the loading distributions shown. The leftmost slash is the average of the passage loading. The rightmost slash is the average of the blade edge loading and the centered slash is the difference between these two average loadings. *The passage loading average is seen to remain almost constant over the variation in throughflow.* The blade edge loading average is substantially lower than the passage average value and is lowest at the design flow condition.

Figure 3.6-3(d) shows the circumferential position of the pressure minimum and maximum, relative to the blade edges. The circumferential spacing between the minimum and maximum pressures is also shown as a function of axial position (axial chord) and can be compared to the blade tip tangential thickness (also plotted in the figure).

The same *passage average* data that was shown in Figs. 3.6-3(a), (b) and (c) is plotted on Fig. 3.6-3(d). The position of the pressure maximum in the passage and the blade pressure side edge can be seen to correlate closely. The minimum pressure is seen to lie well away from the suction side blade edge. The tangential distance from maximum to minimum is seen to be much larger than the corresponding tangential distance between blade edges. The point of maximum tangential spacing moves aft on the blade with increasing throughflow. The maximum tangential spacing can be seen at 20% of axial chord when $\Phi = 0.60$ and is at 60% of axial chord when $\Phi = 0.68$.

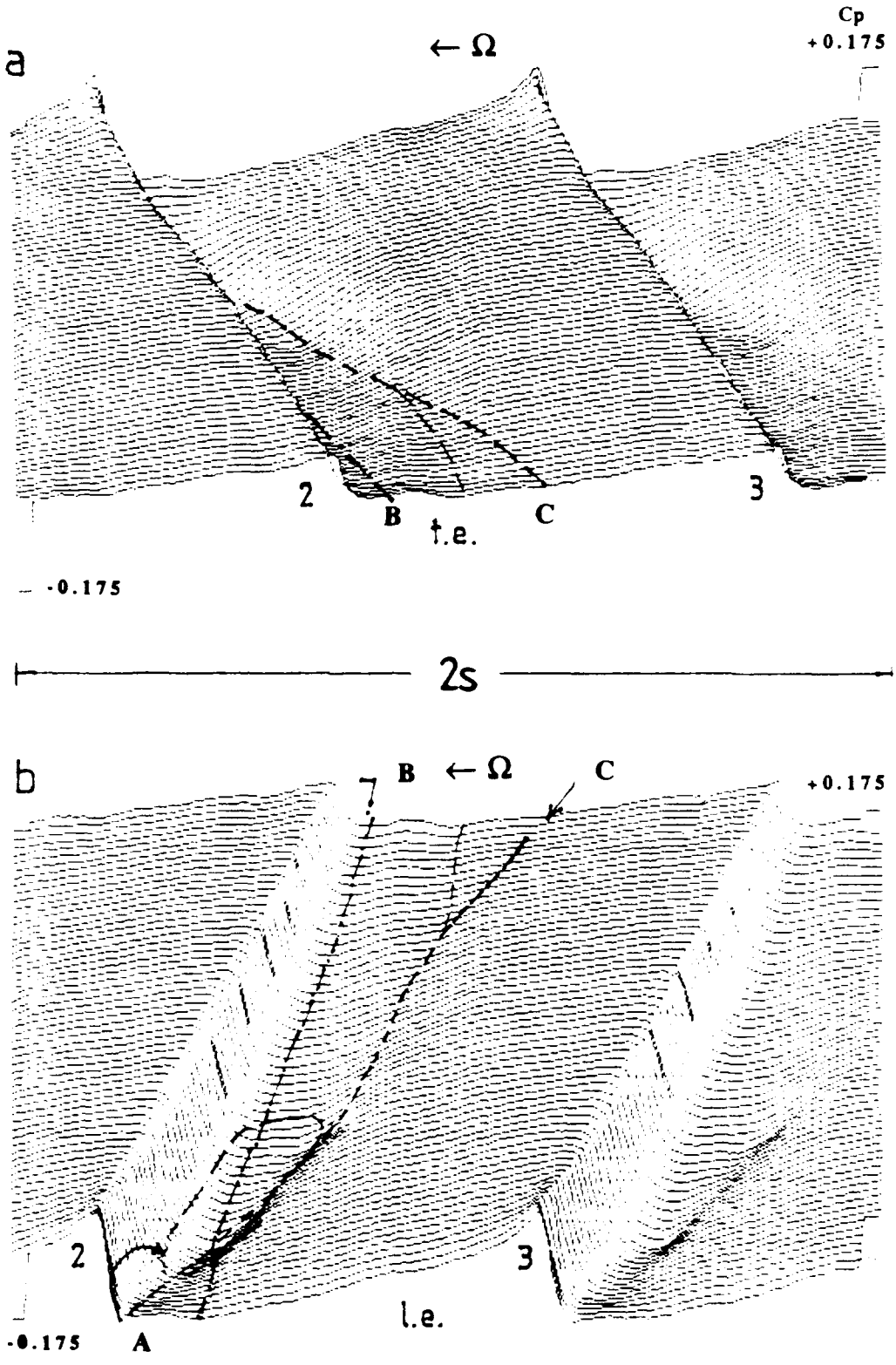

Fig. 3.6-1 (a) Surface view and key features of wall pressure distribution looking upstream from aft of rotor passage (e/b = 0.0035 clearance, *stator average*, design (Φ = 0.64) flow). (b) The same surface viewed from leading edge looking aft. Blade 2 is on left hand side in both views.

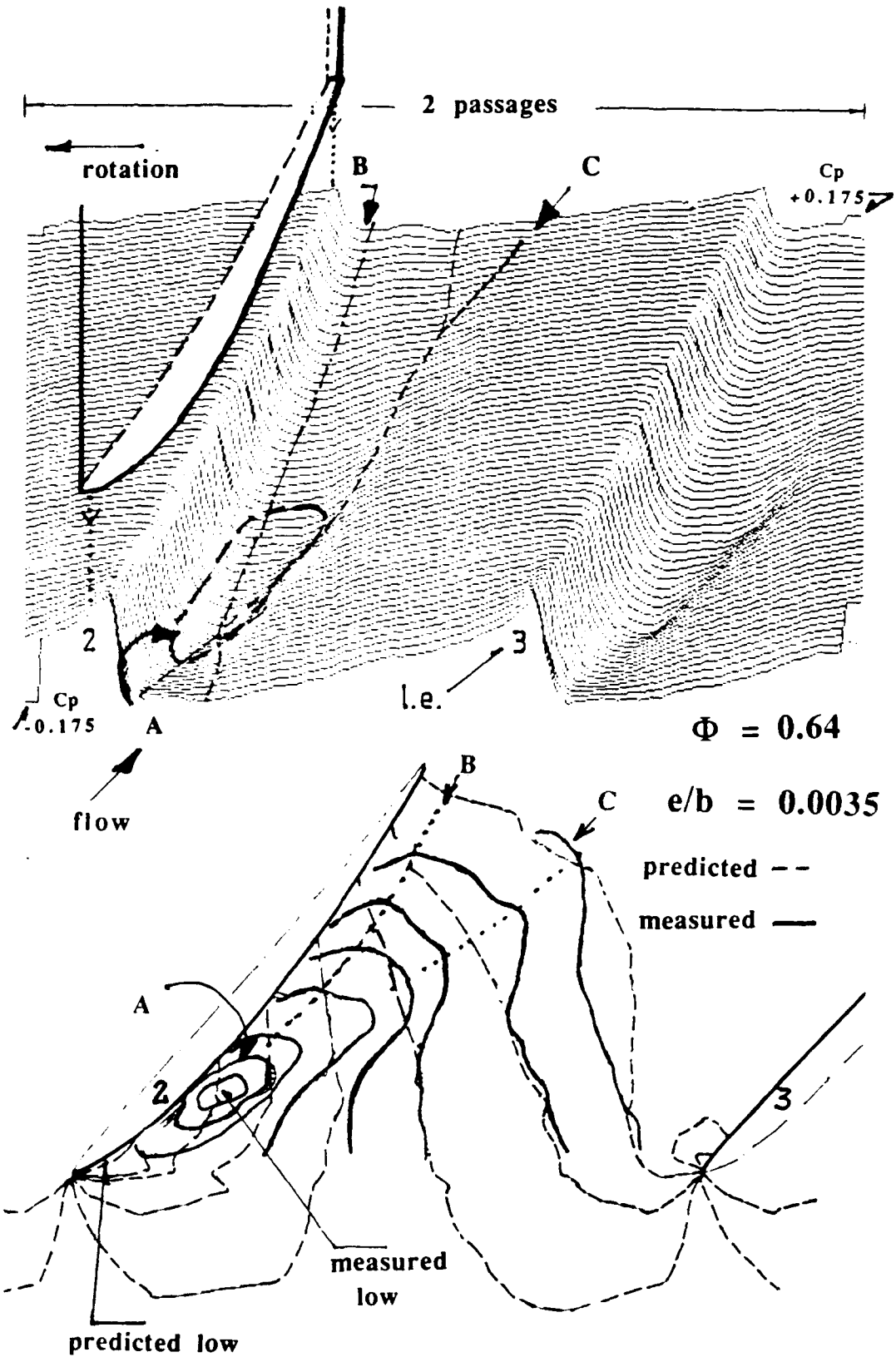

Fig. 3.6-2 Comparison of a quasi-three dimensional throughflow code prediction of the blade-to-blade design flow static pressure pattern (Φ = 0.64) with the measured flow and with the corresponding view of the pressure surface.

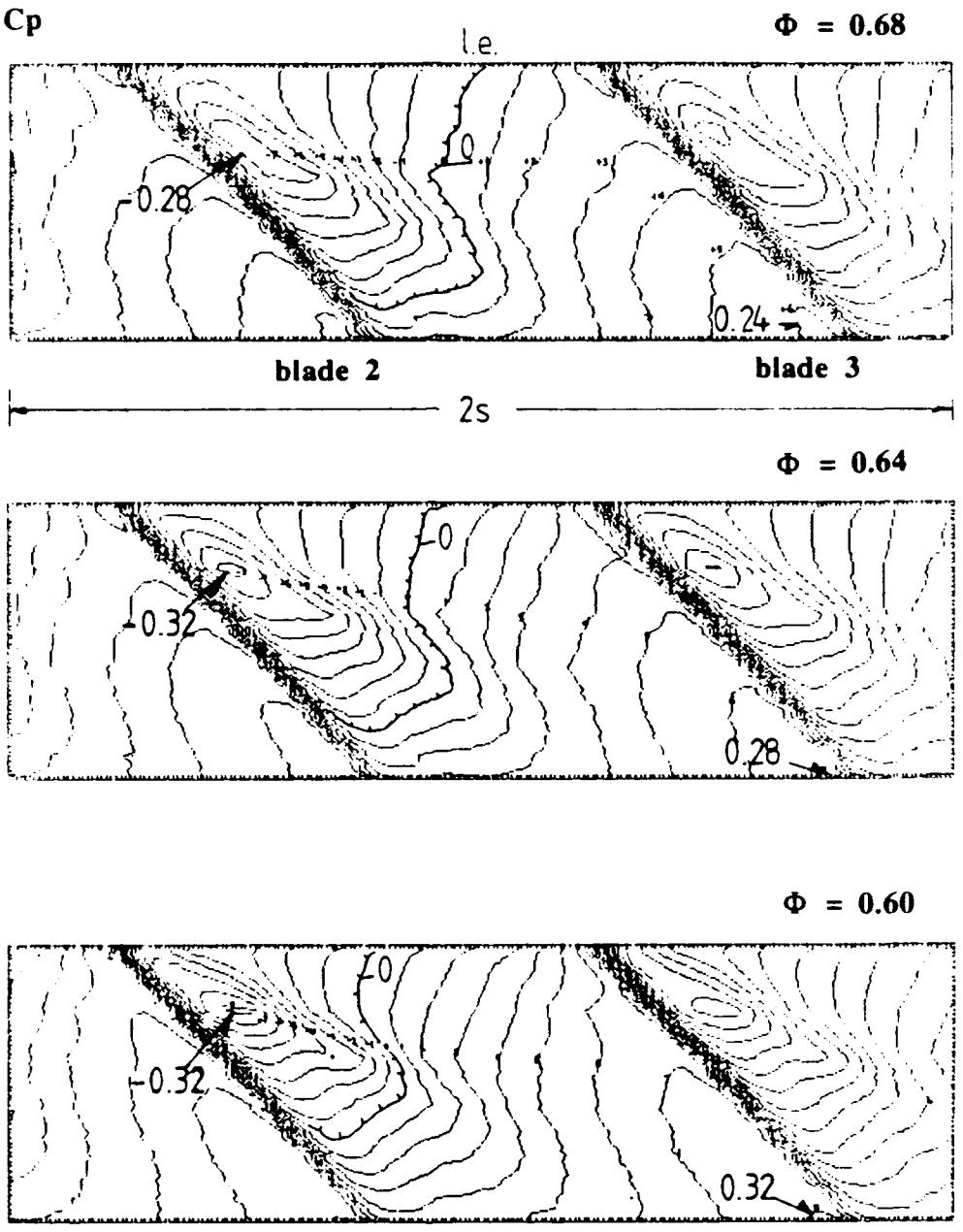

Fig. 3.6-3 (a) Wall pressure contours (e/b = 0.006 clearance, *stator average*) for three flow conditions, (top) open throttle (Φ = 0.68), (mid) design flow (Φ = 0.64) and (bot) near peak power (Φ = 0.60).

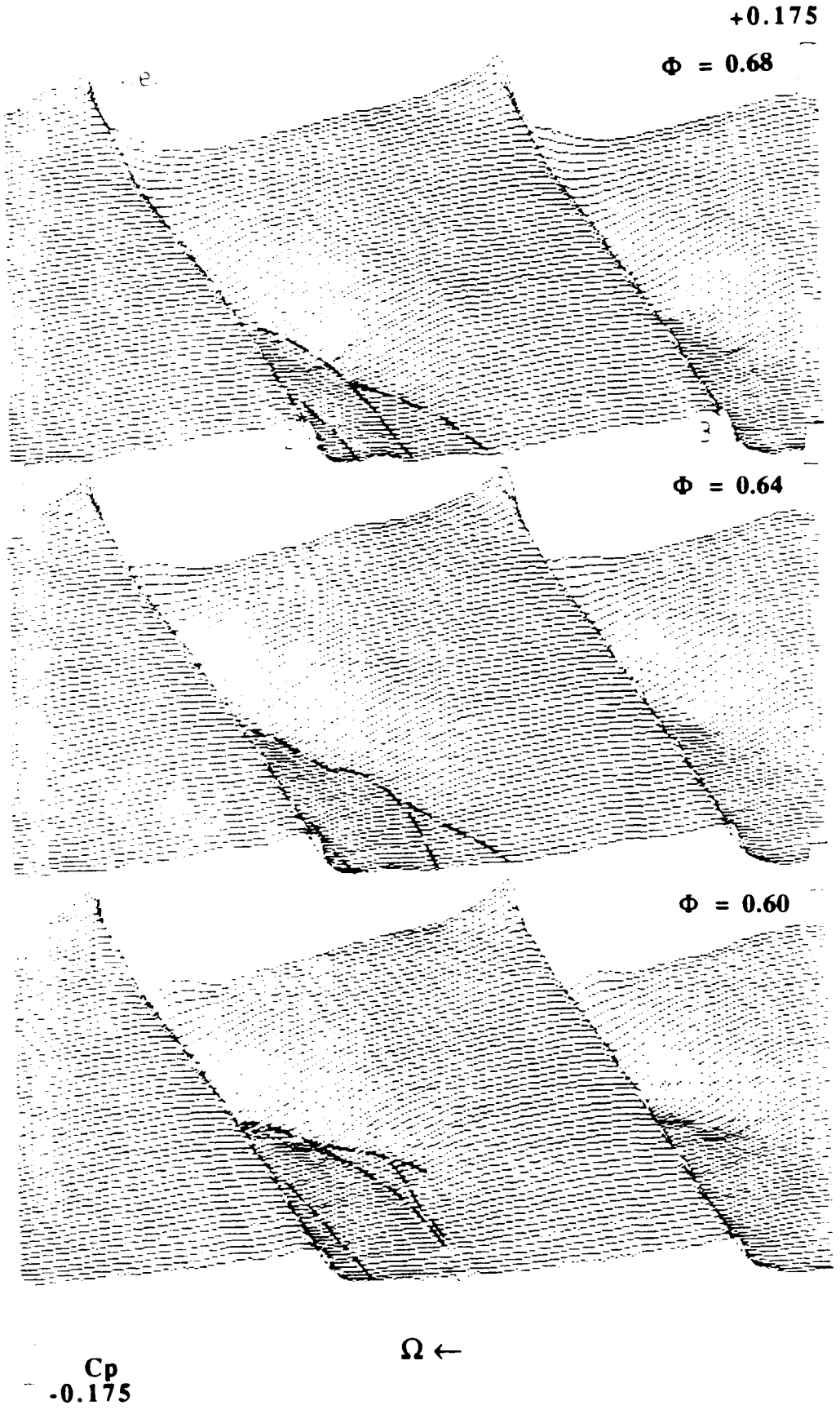

Fig. 3.6-3 (b) Surface views of wall pressure distribution (e/h = 0.006 clearance, *stator average*) for three flow conditions, (top) open throttle (Φ = 0.68), (mid) design flow (Φ = 0.64) and (bot) near peak power (Φ = 0.60).

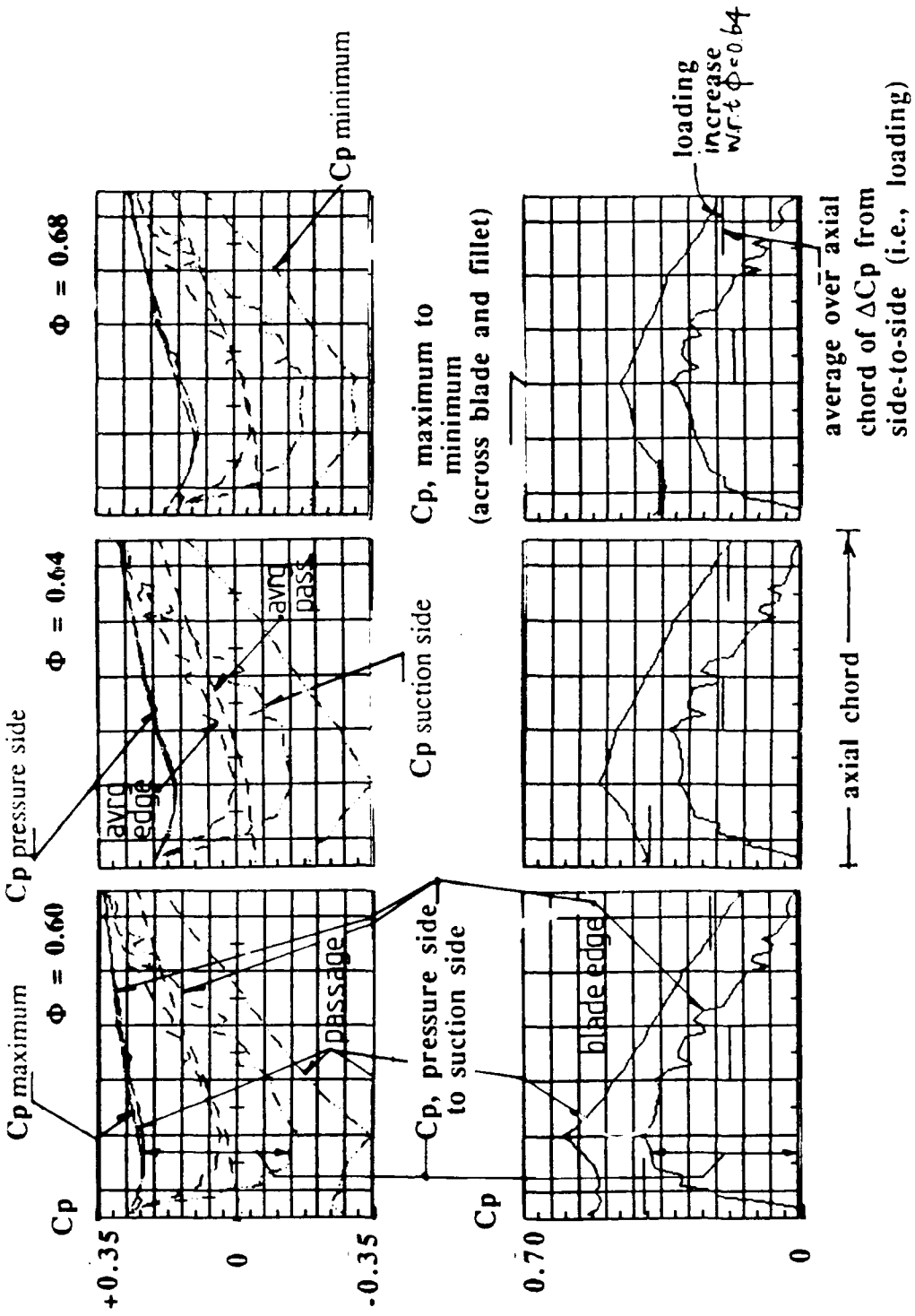

Fig. 3.6-3 (c) Pressure distribution and tangential loading as function of axial position (e/b = 0.006 clearance, *stator average*) for three flow conditions, (right) open throttle (Φ = 0.68), (mid) design flow (Φ = 0.64) and (left) near peak power (Φ = 0.60).

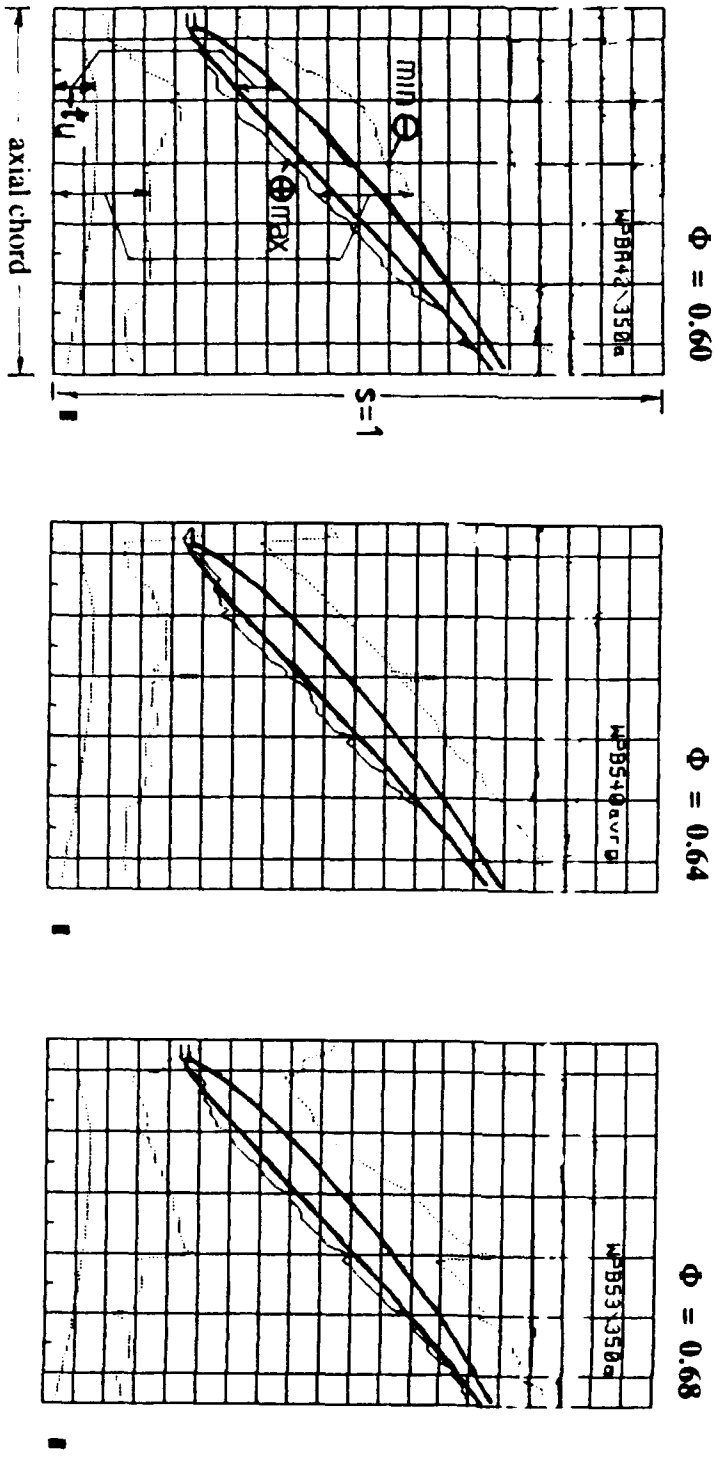

Fig. 3.6-3 (d) Circumferential positions and separations of pressure maximum, minimum and the blade edges as function of axial position (e/b = 0.006 clearance, *stator average*) for three flow conditions, (right) open throttle (Φ = 0.68), (mid) design flow (Φ = 0.64) and (left) near peak power (Φ = 0.60).

3.6.2 Stator Relative Pressure Patterns

The data examined so far have been passage or stator averaged. As the wall pressure measurements were acquired from a matrix of holes relative to the stator, it was possible to examine the rotor flow along different lines relative to the stator. Figure 3.6-4, for example, shows the same situation as Fig. 3.6-3(b) but only along the second axial hole row relative (circumferentially) to the stator. The surface is clearly more rippled and shows larger pressure amplitude changes in the passage than the average of all the axial hole rows. For example, at low flow the cross passage gulley is more pronounced near mid chord. By definition, the stator relative data should show more varied pressure amplitudes than the average, however, for these flow data the variations are mainly identified along the passage side of the low pressure basin. Toward the pressure side of the passage, the stator relative pressure data are similar.

3.6.2.1 Cross-Passage Pressure Minimum (Gully) Extension

Figure 3.6-5(a) and (b) show contour plots for the five stator relative positions for two flow conditions at the e/b = 0.0035 clearance.[51] From inspection of the patterns for all relative locations, the immediate observation is the noticeable extension of the cross passage low pressure gully at stator relative location 2. The rotation and bulged extension of the low pressure region towards the pressure side appears to be incidence related. Location 2 correlates well with the expected convection of the suction side corner defect of the upstream stator into the rotor. The apparent necking of the low pressure extension in the passage (marked by arrows in location 2) can be seen to be due to an advance of a higher pressure forward along the suction side. At this location the whole pressure pattern tends to swing forward to reflect a higher incidence. Correspondingly the fourth circumferential location, shows the pressure basin axis much more closely aligned with the curvature of the suction side. This location correlates with presumed lower incidence associated with the freestream section of the upstream stator passage flow passing into the rotor.

Gully Change With Flow Coefficient Variation The results are very similar in pattern at both flow rates (compare 3.6-5(a) to (b)). With variation of flow coefficient, the length of the low pressure extension in location 2 remains similar, however the direction of the cross passage gully varies slightly. For the low flow coefficient case shown in Figure 3.6-5(b) the pressure pattern shifts upstream and the cross passage low pressure direction becomes more tangential. A series of three flow conditions for the *second hole row* are compared for the e/b = 0.006 clearance in Figure 3.6-6. The situation is similar to that of e/b = 0.0035 in terms of pattern across a wide flow variation range. The pattern or form of the contours is clearly similar for the three cases although the pressure levels change. The same general changes, i.e., higher pressure moving forward on the suction side as flow decreases, are observed in the stator average contours of Fig. 3.6-3(a)

3.6.2.2 Pressure Disturbances radiating from Leading Edge

By taking the difference between the pressure pattern of one line of axial holes and another, the stator-to-stator flow field changes can be viewed as differentials. In this mode of presentation of the data, the radiative nature of pressure disturbances from the suction side of the leading edge can be seen. Figure 3.6-7(a) shows contour plots of the *differences in pressure pattern* between the third hole row location and the other

[51] Note that the fifth hole row location is in the same stator relative position as the first. These two patterns are almost identical, demonstrating the periodicity of the flow pattern with respect to the stator

four stator relative locations, i.e., (1) minus (3), (2) minus (3), (3) minus (3) which is the null or blank panel and so on. The contours in the top panel can be seen to radiate from the leading edge at the suction side. The 2-3 and 4-3 panels show a distinct tendency for the contours to elongate in the tangential direction. The fifth panel closely resembles the first, consistent with the periodicity, and has a clear set of wavelike ridges moving away from the leading edge of the suction side. Because these contour are difficult to interpret, the first, second and fourth panels are shown as a surface views looking aft from the leading edge in Figure 3.6-7(b). This presentation assists in reading the contour patterns. In the first and fifth positions shown in the top panel, the undulating, interference nature of the pattern is consistent with the relative spacing of the sensor locations with respect to the stator.[52] A distinct ridge of high pressure near the suction side is visible in the surface view towards the rotor exit. The lower panel of the surface view corresponding to (4) minus (3) shows a wave like fold in the pattern running tangentially across the passage.

Disturbance Radiation with Flow Rate Variation Figure 3.6-7(c) shows a surface view of the same rows of holes differenced at a higher flow ($\Phi = 0.64$), lower incidence condition. The pattern has a similar form but greater initial perturbation in the leading edge corner and a more extended pressure pulsation in the passage. This is consistent with more of an incidence change as the rotor passes into the stator shadow at a higher flow coefficient. The lower panel of the surface view corresponding to (4) minus (3) does not show a wave like fold running tangentially in the pattern and it was concluded this tangential swing of the low pressure is peculiar to low throughflow conditions.

3.6.2.3 Pressure-Rise Fluctuation on Far Side of Basin

By plotting the sum of the square of the difference of the pressure pattern of each of the axial hole rows from the passage average, the degree of pressure variability in the passage can be shown. Contour plots of this quantity are shown for three flow coefficients in Figure 3.6-8. Pressure fluctuations are largest on the pressure side of the low pressure basin. This region of the wall pressure distribution makes an abrupt pressure rise to the pressure side plateau from the low pressure basin. The strength of the intensity contour in this region is to be expected as small circumferential changes in the rise position will cause large pressure excursions from the average. Lakshminarayana et al. (1982, Part II, Fig. 8) placed an intense zone of turbulence in this same region and in more recent work (Lakshminarayana, Zaccaria and Marathe, 1991) show large losses in this region. The square of the difference plots are noteworthy for other reasons, however. It is apparent that there are no *other* significant fluctuating pressure regions on the passage wall.

Change With Flowrate Variation Sum of the square of the difference pressure patterns under the blade, where the most rapid change in pressure occurs, show no change over the flow range (see Fig. 3.6-8). This indicates changes in *spanwise* incidence do not affect the tip local conditions. The changes in the plots with flow coefficient variation are similar to those of the incidence waves mentioned above. As the flow coefficient increases the pressure fluctuation intensity decreases on the pressure rise side of the basin. This is consistent with lower loading. A more diffuse pattern of less intense fluctuation nodes also appears to radiate further into the passage (see the top right corner of the top panel of Fig.3.6-8).

[52] Pressure disturbances due to wakes from blade rows further upstream than the preceding stator seemed to be negligible in these data compared to the impact of the stator immediately upstream. This conclusion was deduced from the observation that the changes in the overall pattern of the rotor flow wall pressures showed consistent graduation (relative to the upstream stator) over the range of flow coefficients and range of circumferential locations surveyed.

fluctuation nodes also appears to radiate further into the passage (see the top right corner of the top panel of Fig.3.6-8).

By examining pressure patterns at the *same clearance level* but comparing patterns from different stator relative locations over a range of flow coefficients, the influence of the stator on the rotor flow field near the wall can be seen. It was observed that;

(1) the pressure levels along the suction side of the rotor blade vary as the blade passes passes across the stator passage, however the changes relative to the spatial average level are small. Pressure changes with stator relative position on the pressure side of the passage were negligible.

(2) Much larger changes occur relative to the average pressure some distance out in the passage at a position which corresponds to the abrupt pressure transition from the low pressure basin to the high pressure plateau.

(3) At low flow conditions, the orientation of the pressure patterns began to turn to the tangential direction at particular stator relative locations. The locations correlated well with high incidence conditions locally at the blade.

(4) The general form and pattern of the low pressure basin and gulleys persist in the stator relative flow (Fig. 3.6-5(a) and (b) and also maintain a relatively stable pattern with changes in flow coefficient. Spanwise incidence appeared to have little influence on the near wall conditions.

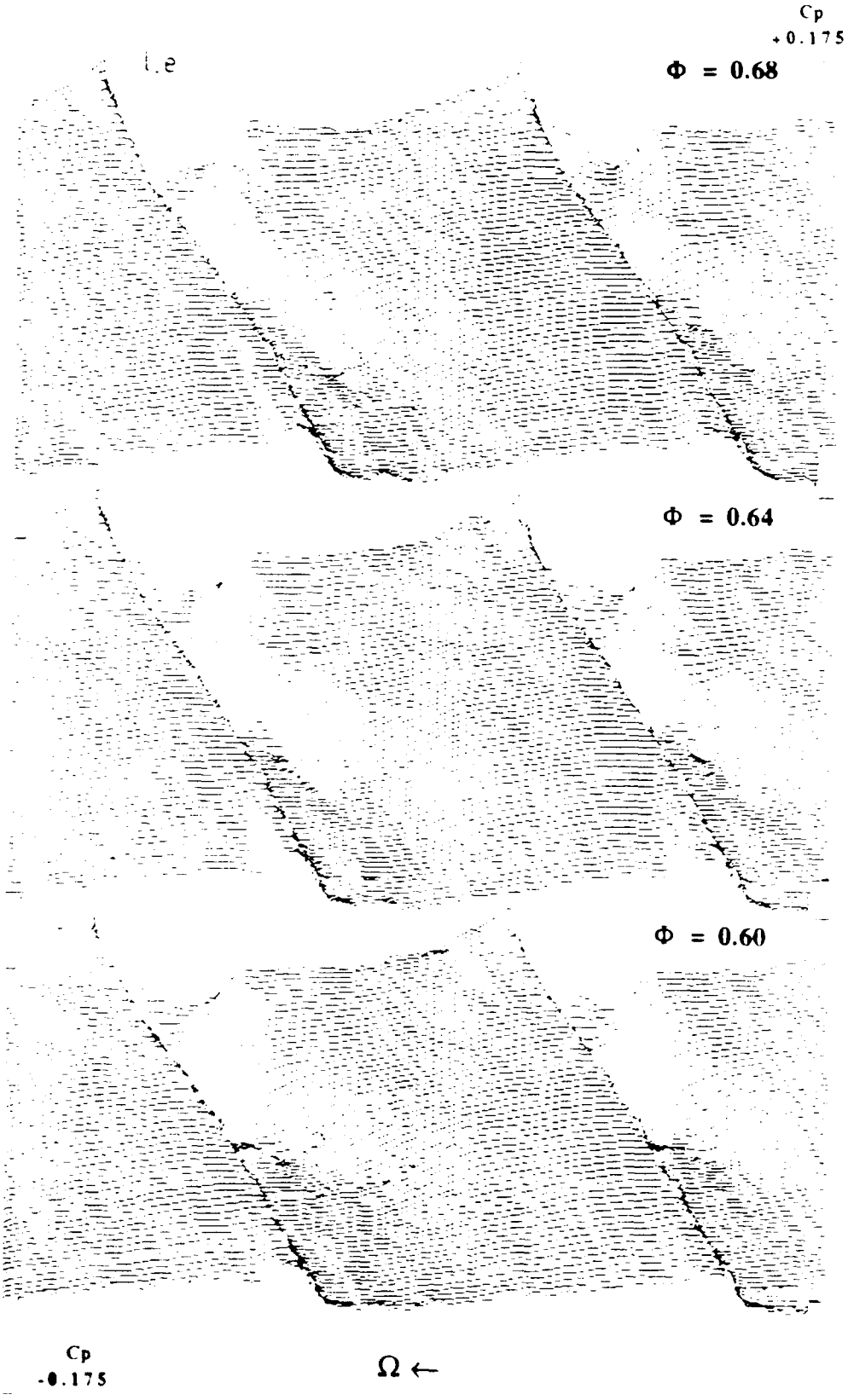

Fig. 3.6-4 Surface views of wall pressure distribution (e/h = 0.006 clearance, *stator relative location* 2) for three flow conditions, (top) open throttle (Φ = 0.68), (mid) design flow (Φ = 0.64) and (bot) near peak power (Φ = 0.60). Compare *with stator average* in Fig. 3.6-3(b).

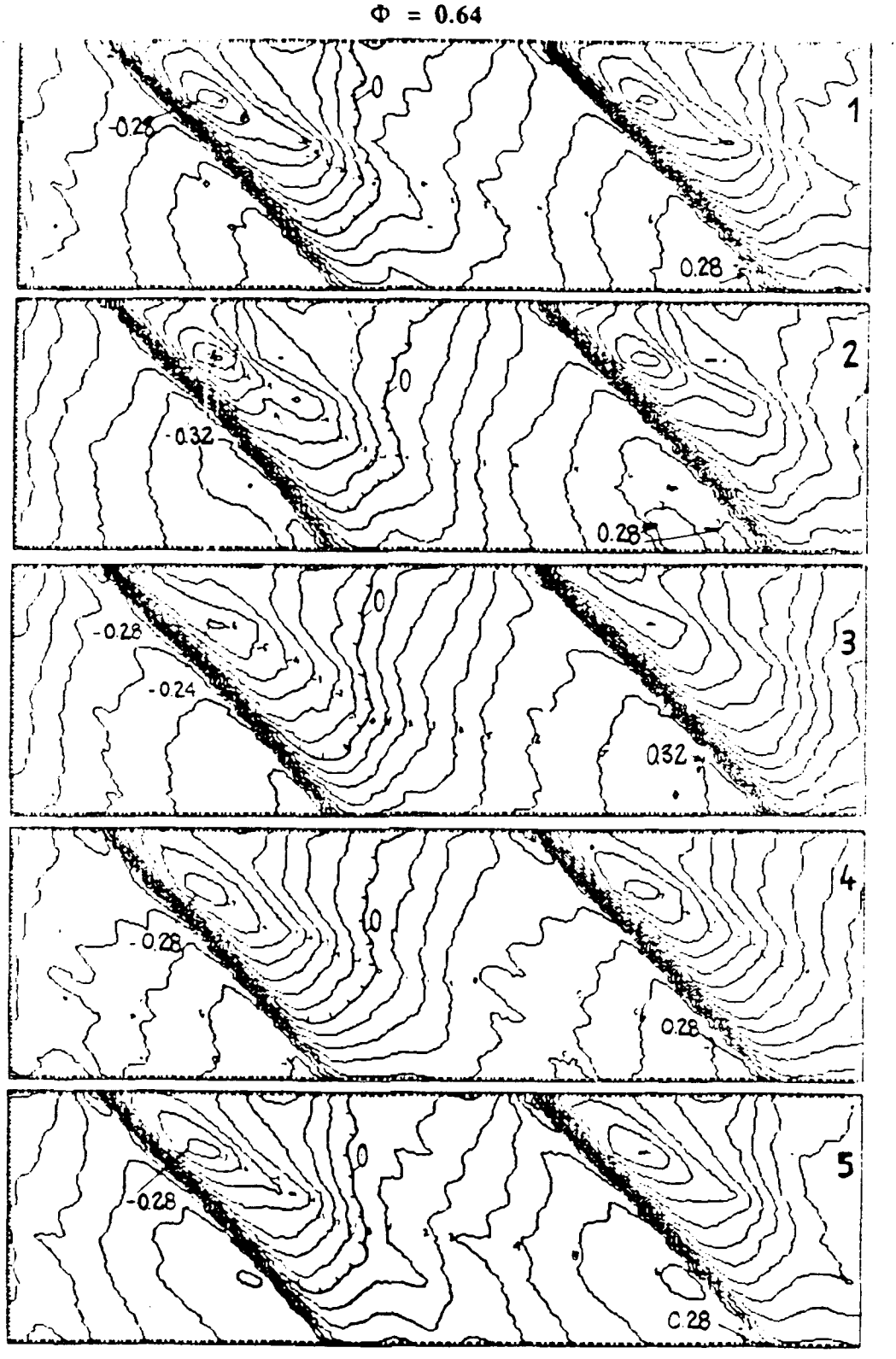

Fig. 3.6-5 (a) Wall pressure contours in rotor measured at five stator relative locations (e/b = 0.0035 clearance, design flow (Φ = 0.64)).

Φ = 0.60

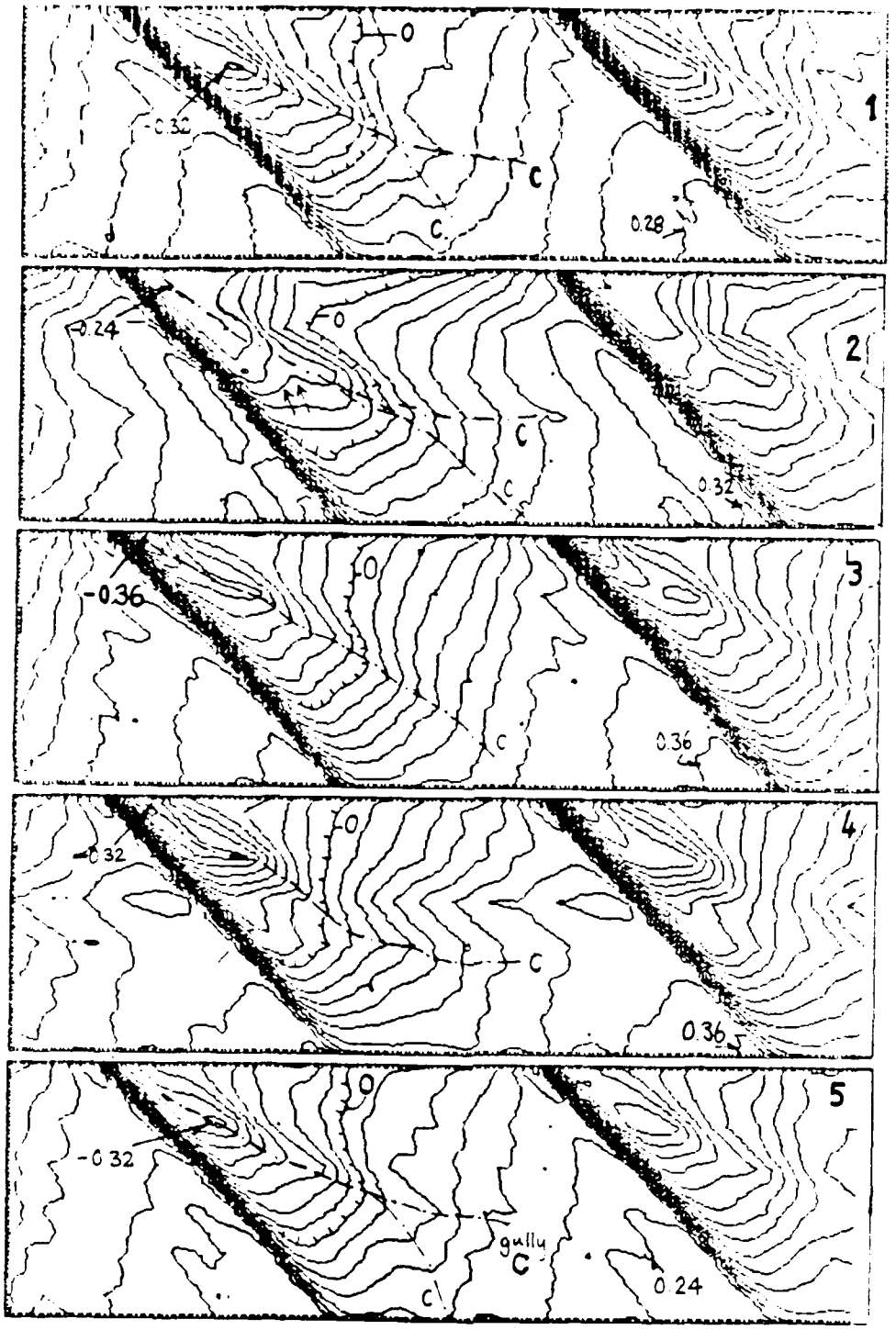

interval of Cp contour = 0.04

Fig. 3.6-5 (b) Wall pressure contours in rotor measured at five stator relative locations (e/b = 0.0035 clearance, near peak power (Φ = 0.60)).

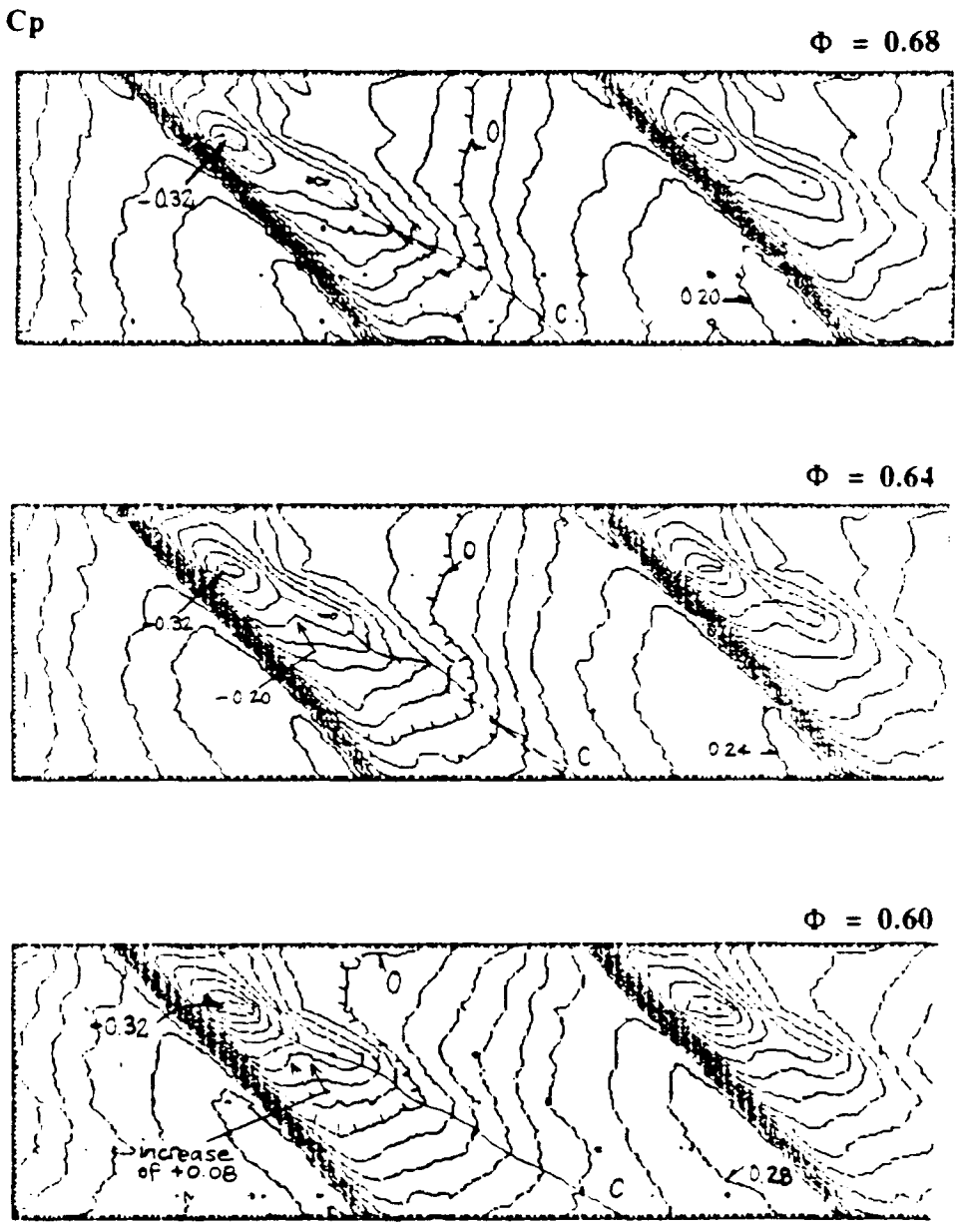

Fig. 3.6-6 Wall pressure contours (e/b = 0.006 clearance, *stator relative location 2*) for three flow conditions, (top) open throttle (Φ = 0.68), (mid) design flow (Φ = 0.64) and (bot) near peak power (Φ = 0.60).

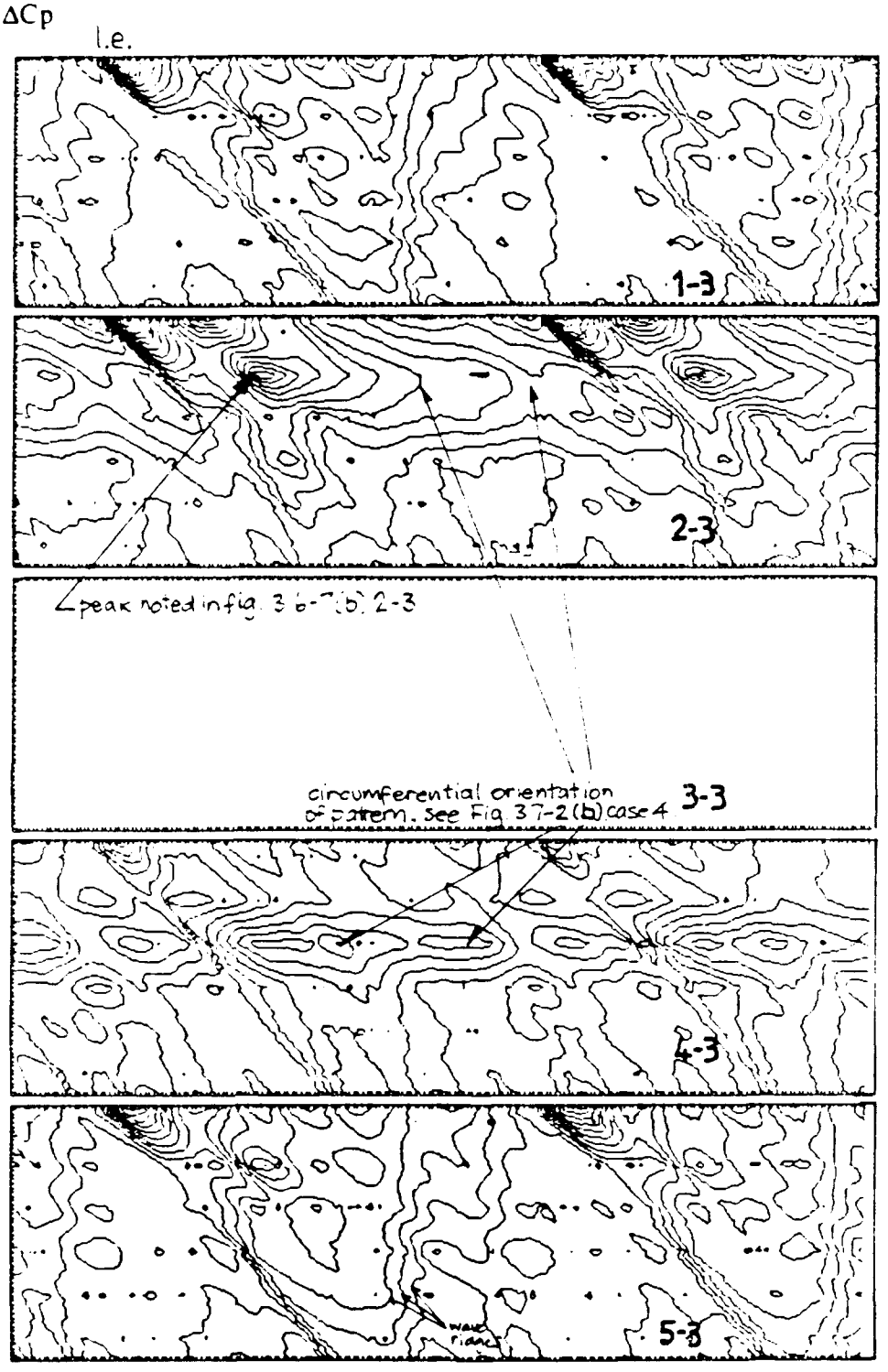

interval of ΔCp contour = 0.02

contours unmarked, data used for pattern comparison only

Fig. 3.6-7 (a) *Contours of the differences* between wall pressure in the rotor at five stator relative locations (e/b = 0.0035 clearance, near peak power (Φ = 0.60)) with respect to stator relative location 3.

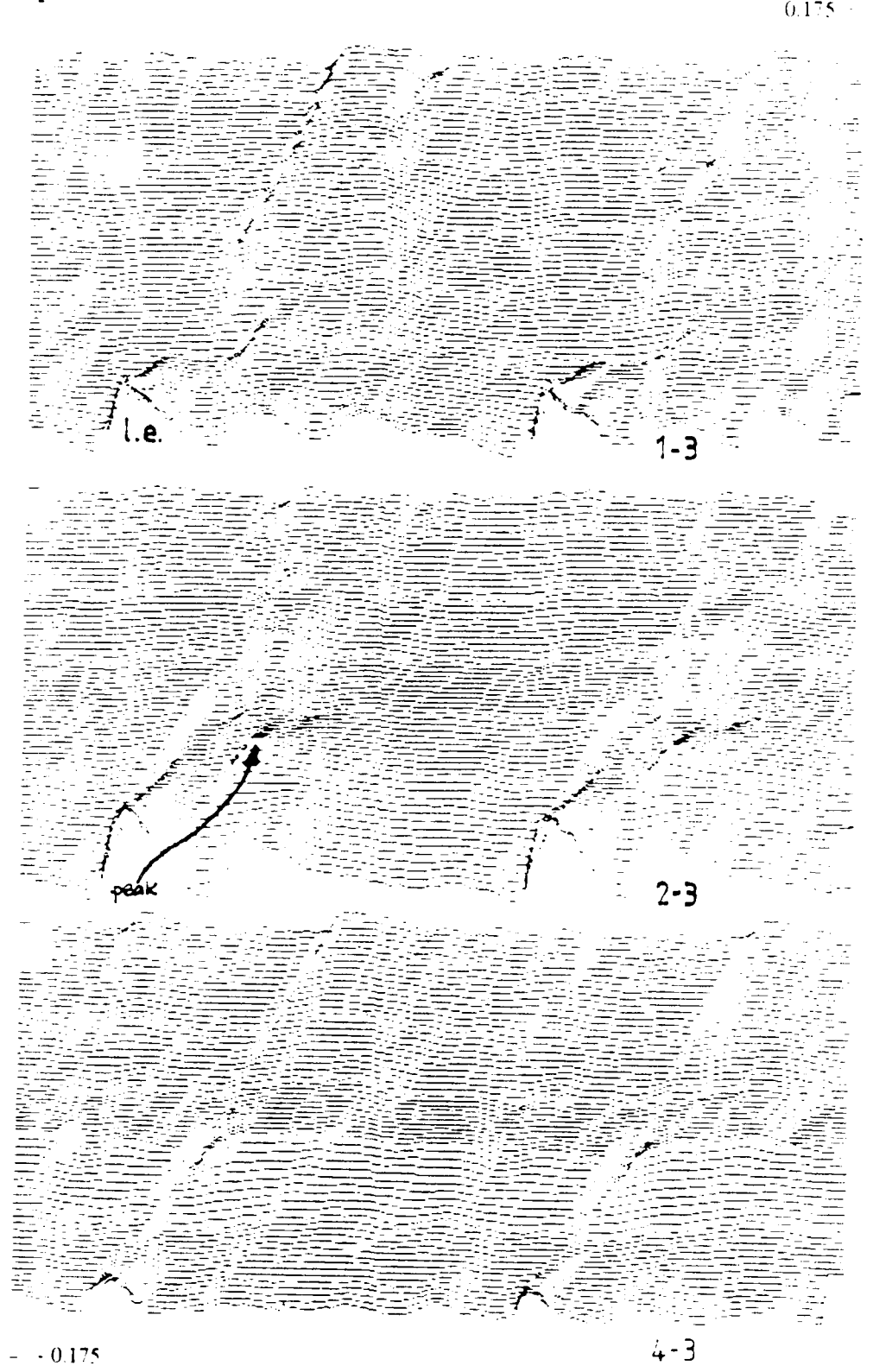

Fig. 3.6-7 (b) *Surface view of the differences* between wall pressure in the rotor at locations 1,2 and 4 of the five stator relative locations (e/b = 0.0035 clearance, near peak power ($\Phi = 0.60$)) with respect to stator relative location 3.

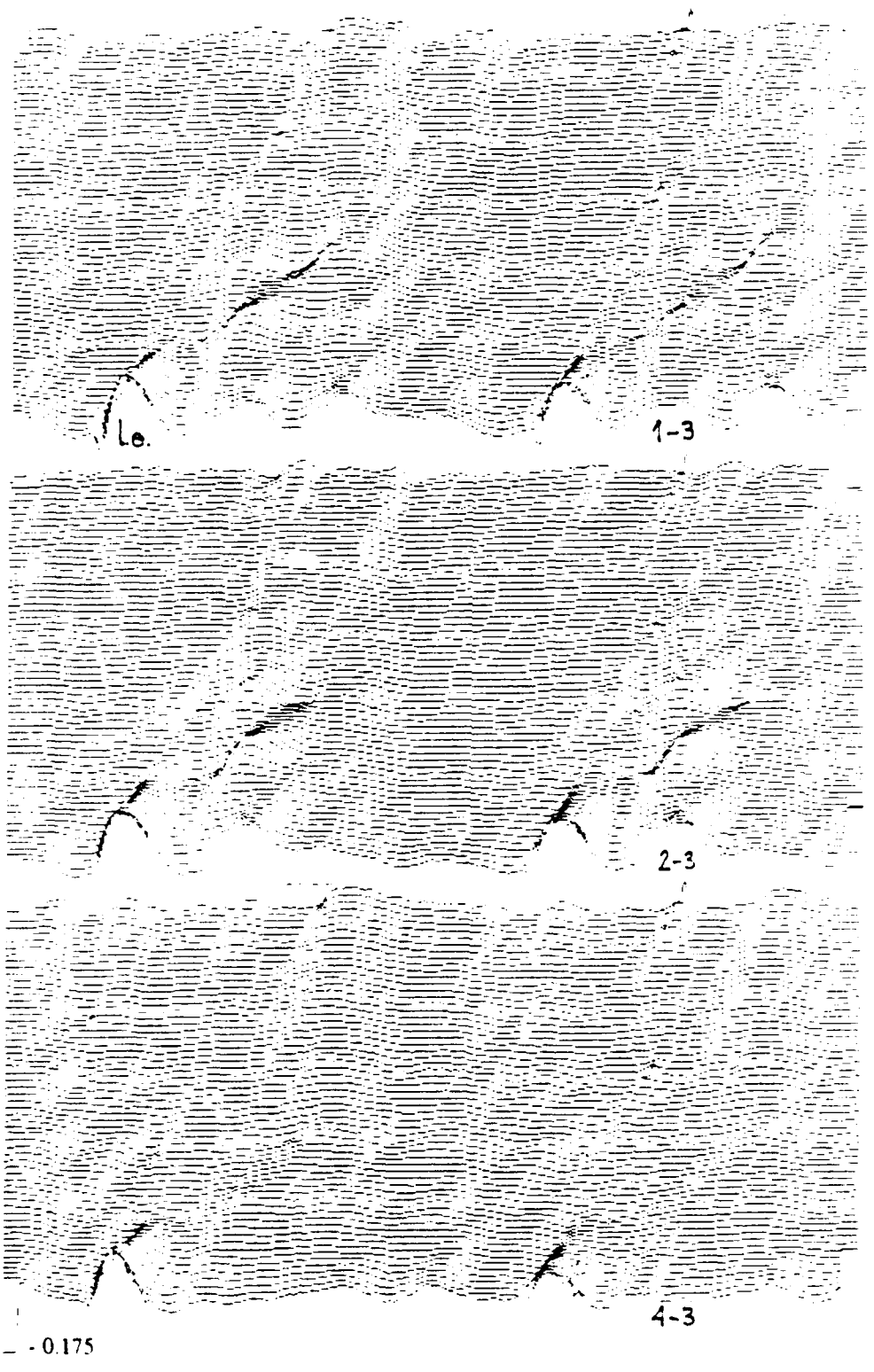

Fig. 3.6-7 (c) *Surface view of the differences* between wall pressure in the rotor at locations 1,2 and 4 of the five stator relative locations (e/b = 0.0035 clearance, at design (Φ = 0.64)) with respect to stator relative location 3.

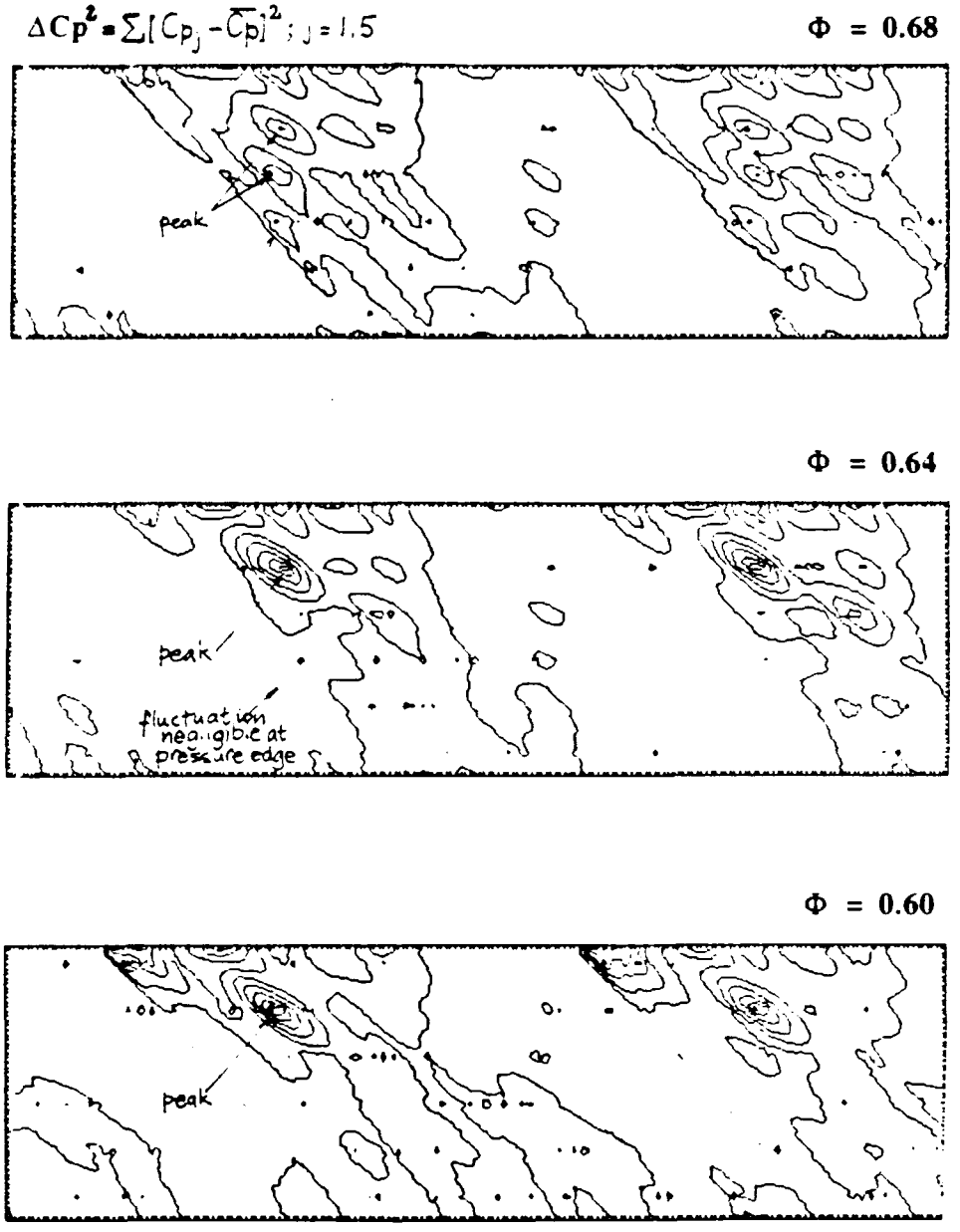

Fig. 3.6-8 *Contours of the sum of the square of the difference* in wall pressure between the stator average condition and all five stator relative locations (e/b = 0.006 clearance) for three flow conditions, (top) open throttle (Φ = 0.68), (mid) design flow (Φ = 0.64) and (bot) near peak power (Φ = 0.60).

3.6.3 Wall Shear Correlation with Wall Pressure

A qualitative picture of the flow structure near the wall and tip gap can be developed from the wall pressure distribution. To develop a quantitative description of the velocity field requires the (relative) total pressure near the wall in conjunction with the wall static pressure. Such measurements require rotating probe or laser doppler surveys. These are complex techniques. However, shear measurements can be made near the wall in a similar manner to wall pressures and by assuming a relationship between the wall shear, pressure gradient and velocity; *estimates* of the near wall velocity can be made.

The survey method to establish wall shear in this study is described in Sec. 3.4.2.5 and the overall shear distribution found in the passage is briefly described in Sec. 3.5.4.4. Wall shear magnitudes shown in Figure 3.6-9(a) were collected from a low response, pneumatic version of the probe which provided *rotor average* data relative to the stator. These data were used to gain some understanding of the wall shear pattern on average under the rotor from stator-to-stator. Non-uniformity of the shear due to the stator blade outflow can be detected in the data. In the zone labelled as stator shadow (shaded), the average shear direction was erratic. This zone can be seen to lie in the stator wake and direction fluctuations (which could be detected with a low response probe) were consistent with the wake occasionally changing its position in the passage. The shear levels (indicated by the length of the vector arrows) were roughly constant in this zone but lower than elsewhere in the stator exit region.

Blade-to-blade wall shear measurements in the relative frame for two survey plate holes (labelled 5,3 and 2,3 in Fig. 3-6-9(a) or Stations 5 and 2 on axial hole row 3) are shown in Figure 3.6-9(b). Note that these survey locations were not in the stator shadow zone. Regions of zero shear can be seen in the blade-to-blade traces for both Station 2 and Station 5. The zero shear regions lay under and slightly outboard of the rotor suction side at the tip and correspond to stagnant flow in the absolute frame. Figure 3.6-10(a) shows the pressure output traces recorded from six orientations of the probe at Station 5. In order to determine the shear level, the case wall static pressure trace for the same flow condition was subtracted from the output trace of the shear probe. The wall pressure recorded for the flow condition was indistinguishable from the pressure output of the probe in the orientation with the lowest pressure output (i.e., consistent with no impact on the raised face of the probe). In the region of stagnant flow, the probe had negligible response in any orientation. This is demonstrated in Figure 3.6-10(b) which shows the difference between the pressure output of the probe (at the lowest output orientation) and the other (5) orientations.

This behavior (stagnation at the wall) correlated strongly with the prominent features of the wall pressure data. The correlation is shown in Figure 3.6-11 and is discussed as follows:

(1) The wall shear levels at the second axial station in the wall survey plate coincide with the axial position of the low pressure basin on the blade suction side. The preliminary measurements at the wall indicated that the flow is stagnant (in the absolute frame) in the interval between the blade suction side and the minimum pressure line running outboard of the suction side. In the relative frame this is equivalent to f. w passing under the blade at wall speed and in the secondary flow frame (where a tangential component of velocity is subtracted from the relative flow) is equivalent to a *zero or low velocity* outward flow from the suction side toward the minimum pressure line. In other words there was *not evidence of significant pressure driven leakage flow*[53] in the basin region of the pattern. The low pressure basin would appear to be mainly due to the wall (relatively) dragging low energy fluid away from the blade at wall speed or conversely the absence of passage flow fluid penetrating into the tip wall corner aft of the peak suction location higher up on the blade. The general impression these measurements gave is that the stagnant fluid region is moving with the blade. However this aspect of the interpretation requires further measurement to confirm the flow stagnation is not a stator relative phenomenon.[54]

(2) Wall shear measurements further aft in the passage at the fifth axial position on the survey plate have a similar form, however the shear level begins to increase closer to the blade suction side after a short interval of stagnant flow near the suction side.

(3) Both blade-to-blade shear trace locations show a ramp like transition from a region of stagnant flow up to a uniform level of wall shear. The uniform region is spatially correlated with the high pressure plateau leading the pressure side of the blade. The level dips back to a low or near zero shear level immediately in front of the blade pressure side and remains at that level under the blade and then gradually ramps upward moving away from the suction side.

(4) Time averaged shear levels measured over the wall survey plate are consistent with the situation described above. They additionally indicate the shear level has a wave like form which matches the periodicity of the stator spacing. Some stator relative holes behave somewhat erratically in terms of shear magnitude and direction for average readings. These holes correspond well, spatially, with the stator suction side corner flow shadow where the shear sensor sensitivity is expected to be low.

The picture of the flow structure at the tip that develops from consideration of both the wall pressure and the shear data, for a small clearance condition, appears to consist of only two main mechanisms:

---

[53] This observation is significant (relative to the mechanism proposals of Part 1) as it suggests the tip "leakage" flow is dominated by the relative flow at a small clearance for at least this part of the axial chord. The measurements support, to some extent, an argument put forward by Chen et al (1988) that at some (small) level of clearance the tip effectively becomes closed (sealed) with respect to the passage flow conditions.

[54] Measurements by Inoue et al (1988, Figs 3,4) show a similar velocity stagnation just above the wall in an isolated rotor secondary flow plot. Their measurements lend support to the impression that the stagnation moves with the rotor. In their case there were no upstream stator wakes or corner shadow regions to consider in the sensor readings. The velocity stagnation region in their data was situated further aft and did not extend as far from the suction side.

(1) The first can be argued to be a cross passage low pressure (higher velocity) region originating at the blade leading edge corner, or in a separation lying in the corner, whose direction is largely independent of *spanwise* incidence[55] in the forward part of the passage. With downstream convection the direction and strength of this cross passage formation fluctuates with incidence.

(2) The second strong mechanism is a fillet-like region of relatively low energy fluid located in the pressure-side-to-wall and suction-side-to-wall corners. This fillet-like region of the flow has a larger footprint on the suction side wall and extends from the blade surface on the suction side to a line of minimum pressure some distance off the blade.

The two regions of distinct flow motion coalesce or converge at the low pressure basin, which stands off the suction surface downstream of the leading edge. Upstream of the basin they appear to be overlaid (when it is positioned further aft at higher throughflow). It is relevant that the basin feature was invariant in this testing and appears where the two coalesce.

3.6.4 Circulation at the Wall

The observation that the passage pressure minimum regularly lies some distance off the suction side of the blade and the behavior correlates with a stagnant flow region at the tip presents new information about the tip and wall flow structure. The pressure maximum lies slightly ahead of the blade pressure side as expected, however the position of the minimum away from the blade implies *the relative motion of the wall, in conjunction with the pressure disturbances radiating from the leading edge corner, is modifying the two-dimensional blade circulation near the tip*. If considered in a two dimensional flow sense, the flow behaves as if the blade section is effectively increased by the fillet near the wall in terms of its circulative ability. This pressure offset behavior on the suction side occurs independently of spanwise incidence (and also independently of the clearance level). This aspect of the observations will be discussed further in Part 4.

---

[55] The insensitivity to direction is relevant to the comments on curvature (Sec. 1.2.2.3) and the considerations of Ekman Number in Sec. 2.2.3. These influences are likely to be flow angle or incidence independent in terms of vorticity production on the passage wall.

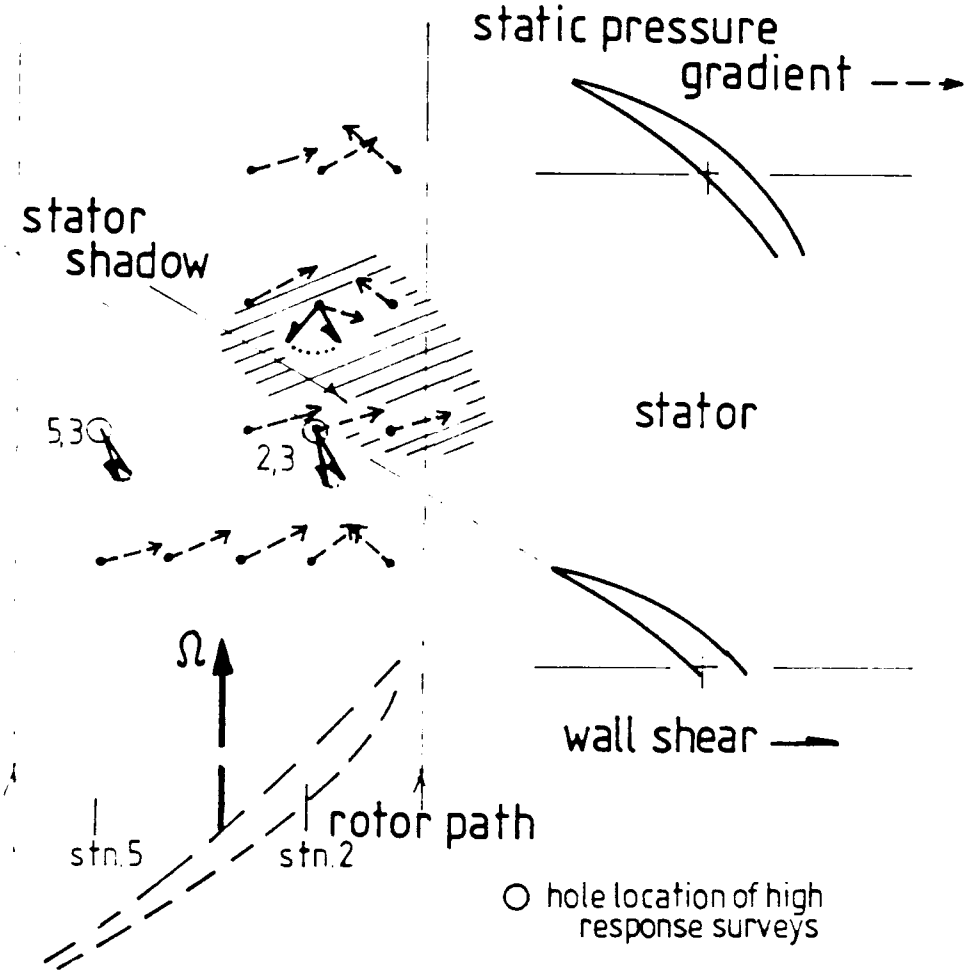

Fig. 3.6-9(a) *Rotor average* wall shear pattern on the case wall at Φ = 0.64 and e/b = 0.0035 clearance showing the changes in shear level (or direction) with stator relative position. A zone of erratic direction was detected in the stator (wake) shadow.

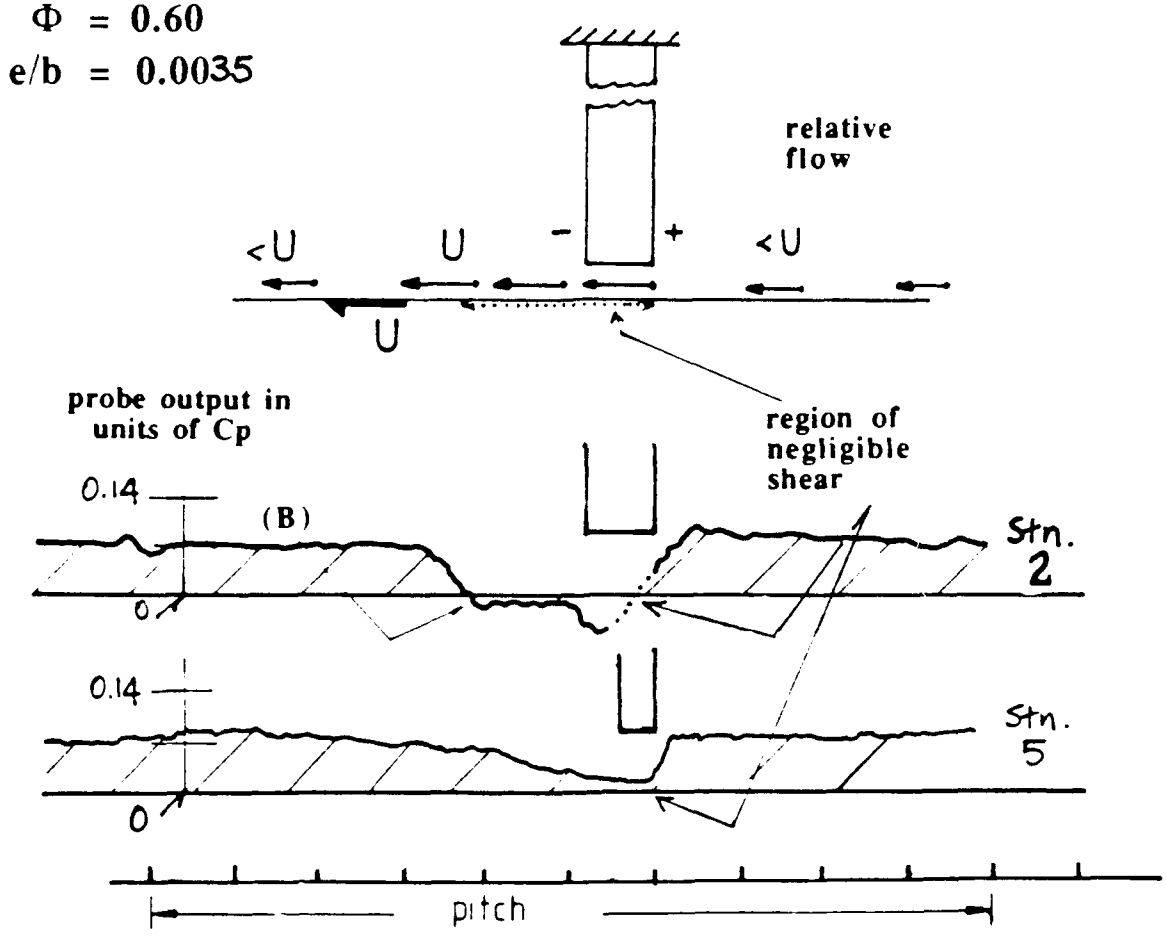

Fig. 3.6-9(b) Blade-to-blade wall shear pattern measured on the case wall at axial Stn. 2 (near maximum blade thickness) and Stn. 5 (toward the trailing edge) showing regions of zero shear corresponding to stagnant flow in the absolute frame.

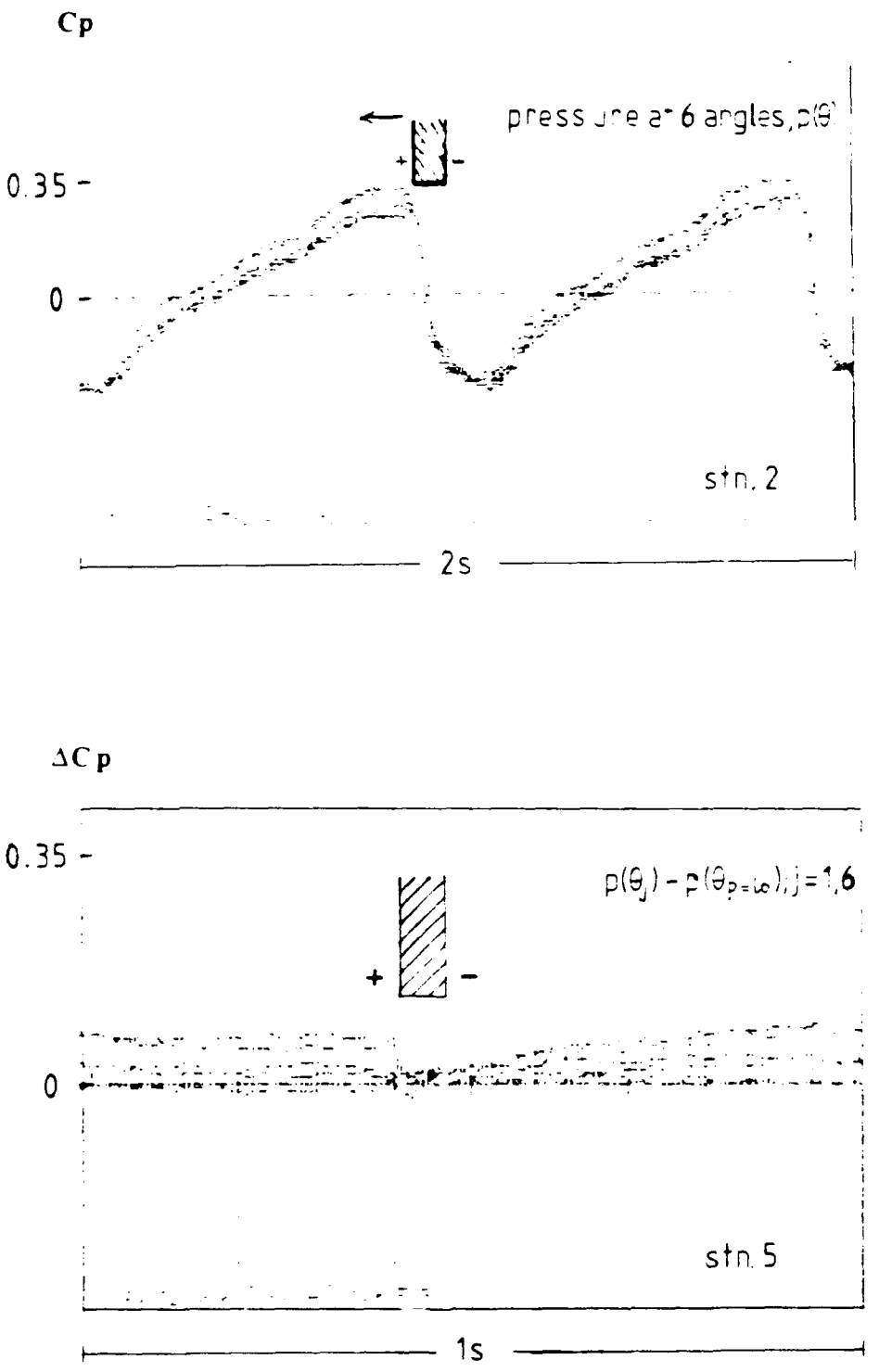

Fig. 3.6-10 (a) Pressure output of the shear probe, blade-to-blade wall for six orientations. (b) Shear on the case wall showing the *difference* between the pressure output of the probe (at the lowest output pressure orientation) and the other (5) orientations. The region of zero shear is seen to be independent of probe orientation and lies under the blade.

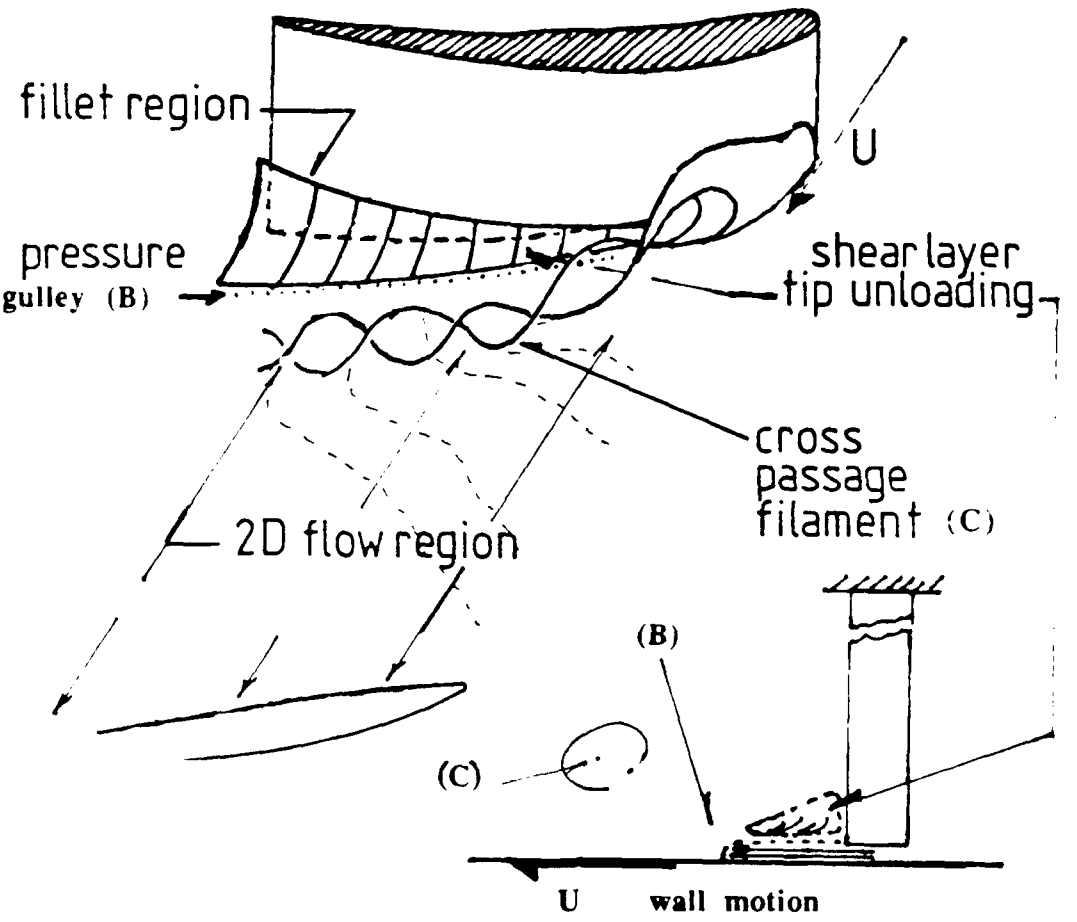

Fig. 3.6-11 Correlation of flow blade-to-blade wall shear pattern measured on case wall with the wall static pressure.

3.7 Results - Flow Structure with Clearance Variation

Having examined the structure of the flow at the tip, the consequences of changing the tip clearance were explored by observing changes in pressure pattern, at the same flow or stator relative location of the rotor, at different clearance levels. In the test summary of Table 3.4-1 only two clearances were surveyed comprehensively over a wide range of conditions. However additional clearance variation could be realized by sealing the tip gap. These data are compared in Sec. 3.7.2 at one stator relative location. How the passage average structure changed with clearance variation is discussed below.

3.7.1 Change in Stator Averaged Pressure Pattern

The contour patterns of Figure 3.7-1(a) result when the *difference* in the pressure patterns due to a clearance level change, averaged over all stator relative locations, are plotted. These data are contours of the *pressure differential between the two clearance conditions*. The same *difference* data are shown as surface views in Figure 3.7-1(b). The results are seen to be very similar for two throughflow conditions. That is, an unloading right at the gap and a slight depression ripple extending diagonally across the passage. The lower flow case shows a stronger region of unloading developing near the leading edge. These results show distinctly that the only significant effect of changing the clearance is to change the flow conditions under and very close to the blade tip on the suction side. There is no evidence of any change on the pressure side of the blade.

3.7.1.1 Pressure and Position Distributions

The changes in pressure distribution, loading, circumferential positions and the spacing of pressure maximum, minimum and the blade edges are shown for the lowest (Φ = 0.60) flow case at two clearances e/b = 0.0035 and e/b = 0.006 in Figure 3.7-1(c) as a function of axial position. As the clearance is enlarged from e/b = 0.0035 to e/b = 0.006, the following are noted:

(1) The pressure-side edge and maximum pressure levels do not change significantly while the suction-side edge pressure increases noticeably. Note, however, that the passage minimum pressure trace remains almost constant.

(2) The circumferential spacing between the maximum and minimum pressure remains unchanged but the minimum pressure trace location of the larger clearance moves slightly further outboard from the suction side.

Blade Surface Unloading With Flow Coefficient Variation Comparison of Fig. 3.7-1(c) and the design flow case Figure 3.7-1(d) shows that the *changes* in pressure distribution and loading that occur *with clearance change* at another flow coefficient are essentially the same.

Pressure-Rise Bluff on Far Side of Basin Unchanged The average pressure patterns show that certain features identified previously are consistent or invariant with changes in clearance. The pressure basin location and general shape and orientation in the passage showed minimal change. Similarly the position and abrupt pressure rise on the pressure side of the basin showed minimal change at the small clearances tested.

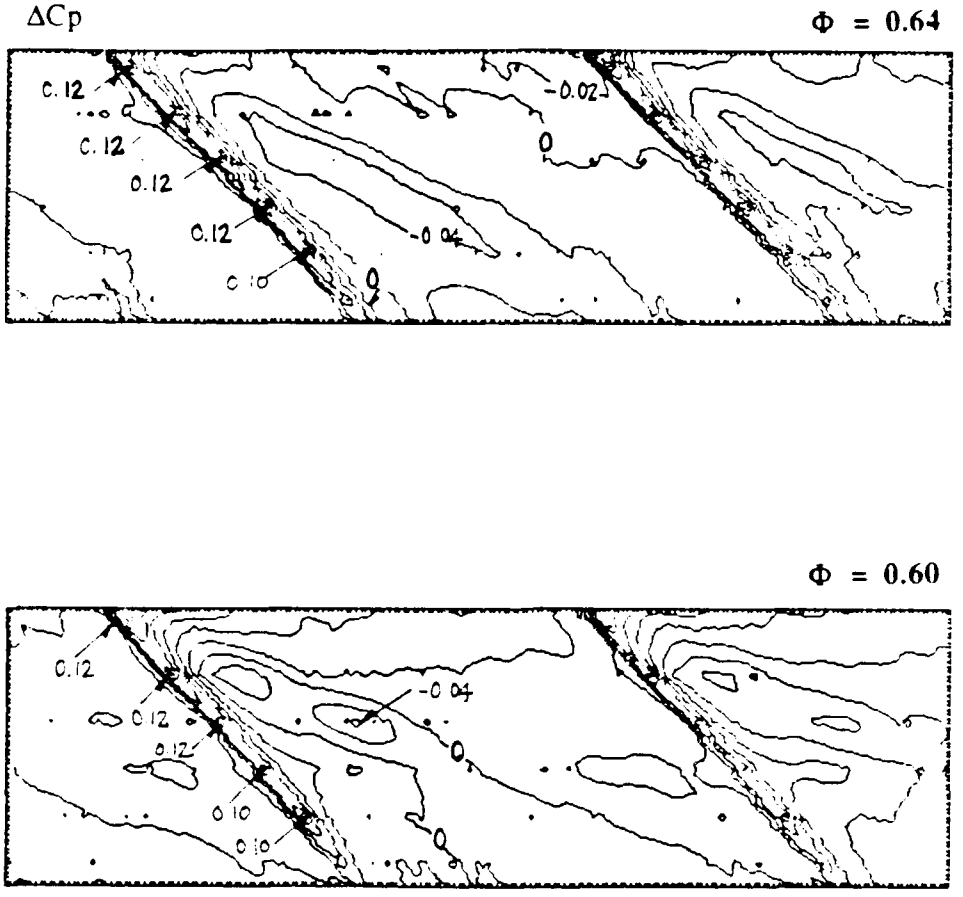

Fig. 3.7-1 (a) *Contours of the differences* in *stator average* wall pressure *due to a change of clearance* in the rotor (pressures of e/b = 0.006 clearance minus e/b = 0.0035 clearance, (upper) design flow ($\Phi = 0.64$), (lower) near peak power ($\Phi = 0.60$)).

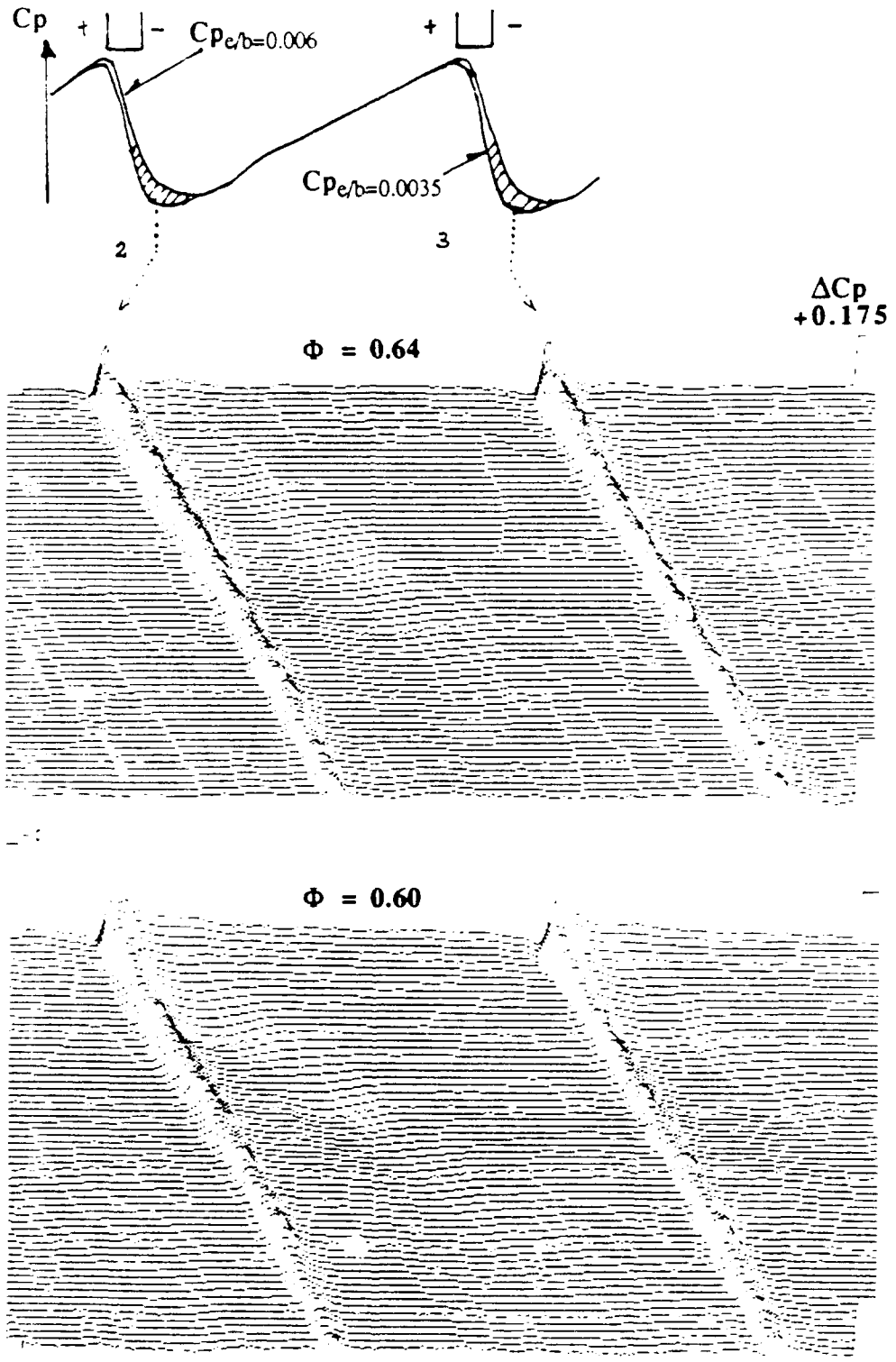

Fig. 3.7-1 (b) *Surface views of the differences* in *stator average* wall pressure *due to a change of clearance* in the rotor (pressures of e/b = 0.006 clearance minus e/b = 0.0035 clearance, (upper) design flow (Φ = 0.64), (lower) near peak power (Φ = 0.60)).

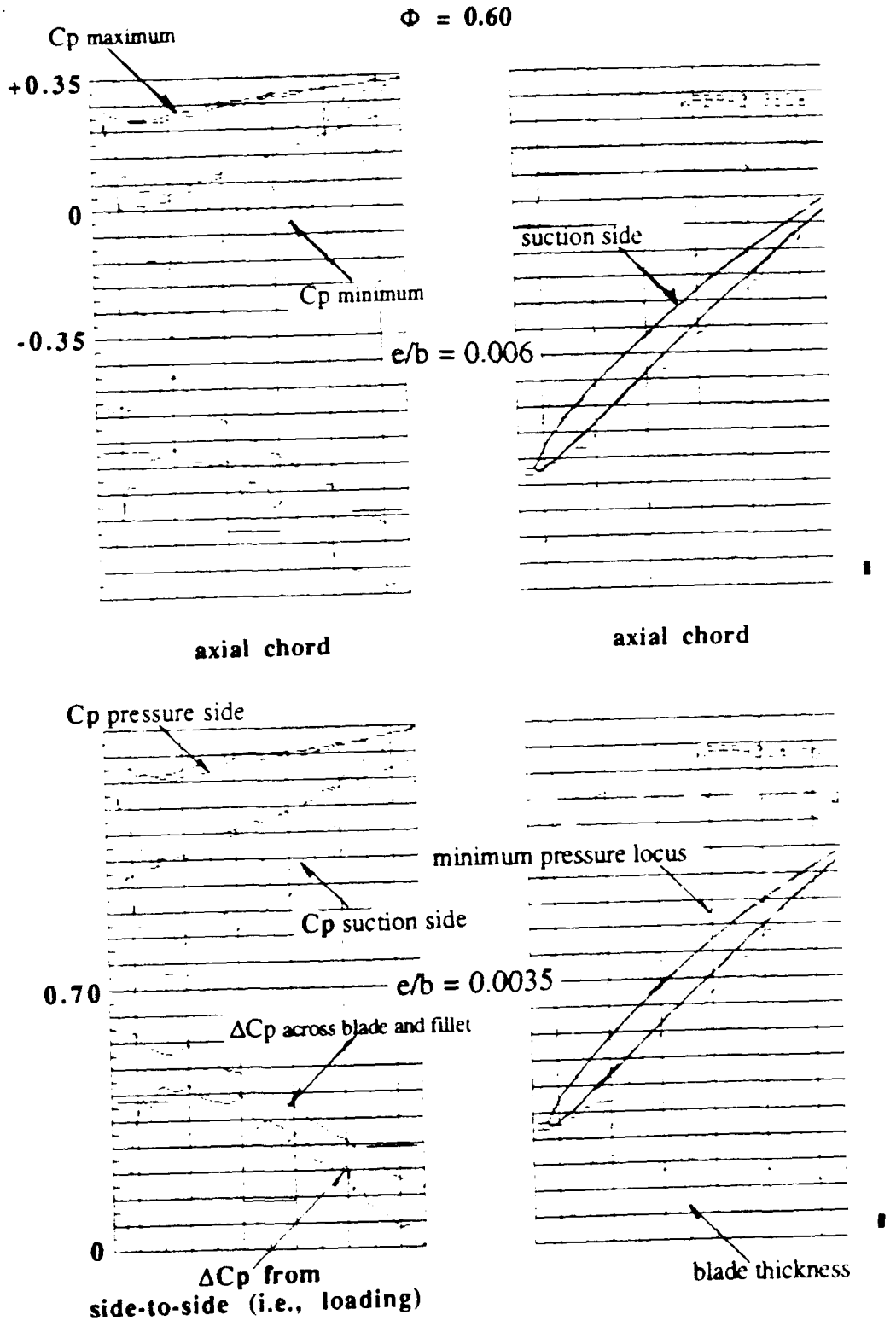

Fig. 3.7-1 (c) Wall pressure distribution and loading: circumferential positions and separations of pressure maximum, minimum and the blade edges as function of axial position (upper e/b = 0.006 clearance, lower e/b = 0.0035 clearance, *stator average*) for near peak power (Φ = 0.60) flow.

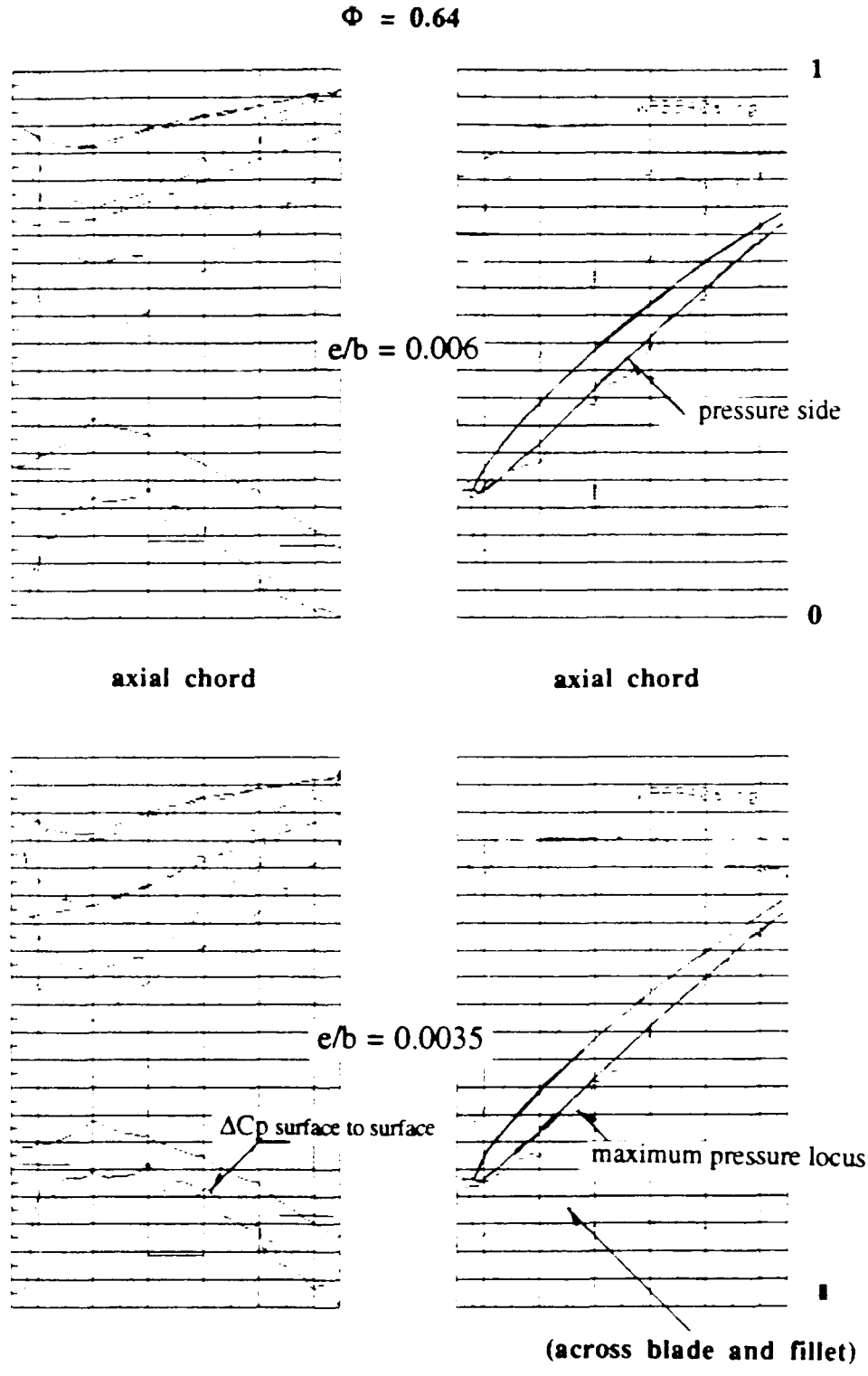

Fig. 3.7-1 (d) Wall pressure distribution and loading; circumferential positions and separations of pressure maximum, minimum and the blade edges as function of axial position (upper e/b = 0.006 clearance, lower e/b = 0.0035 clearance, *stator average*) for design (Φ = 0.64) flow.

3.7.2 Change in Stator Relative Pressure Pattern

Figure 3.7-2(a) shows the change in pressure contour pattern that occurs at one stator relative location for three clearance levels.

Sealed Tip Measurements By sacrificing circumferential uniformity of the flow, it was possible to alter the tip of one blade (or series of blades) in the rotor row and measure a local wall pressure distribution. This was done for the e/b = 0.0035 clearance level by placing a strip of cellulose tape on the pressure side of blade number 2 of the second rotor to form a squealer tip with a rubbing (approaching zero clearance) contact with the wall. The distribution which resulted permitted a flow condition approximating a sealed tip gap to be created in blade passage 2-3. This passage could then be compared to a e/b = 0.0035 flow condition in passage 3-4. Consequently, case wall pressure distributions for *three clearance levels* were available for analysis, i.e., a sealed tip, e/b = 0.0035 and e/b = 0.006.

It can be seen that the general form of the pressure pattern is not dependent upon whether a finite clearance gap is present (i.e., the overall pressure pattern appears to be generated by wall relative motion). The pressure level in the trough (or basin) in the passage is seen to decrease as tip gap increases. It should be noted that the pressure near the blade edges increases in this figure as clearance increases, however, this is difficult to see from the contour plot and is better seen in the pressure distributions of Figure 3.7-4(b).

Figure 3.7-2(b) and (c) show the *difference* in pressure patterns for two clearances at the five stator relative locations for (b) the low, near peak power (Φ = 0.60), flow condition and (c) at design flow (Φ = 0.64). Comparisons of these patterns show the differences for the low flow coefficient case have a similar form in locations (1), (3) and (5) and two dissimilar patterns in locations (2) and (4). These two patterns appear to be peculiar to the high incidence, small clearance case. The design flow case shows a much more consistent pattern in all stator relative locations. The pattern observed consists of a uniform and very abrupt unloading of the blade tip with a much more diffuse lowering of the wall pressure in the passage. This occurred on the diagonal line from suction-side leading to pressure-side trailing edge which corresponds to the cross passage low pressure gully.

Figure 3.7-3(a) shows both the pattern at three clearance levels and the *difference in pressure* between them on the same figure. The data are from the *second* stator relative location at design (Φ = 0.64) flow. The upper panel shows a test case where the (leftmost) blade (2) gap was closed with a strip of tape on the pressure side to approximate a sealed tip. The position of the tape is clearly visible in the panel (second from the top) which shows the difference between the upper and the middle panel. A very rapid change in pressure can be detected on the pressure side of the left blade when compared to the right blade. The right blade had the same clearance in both the upper and middle panels. It is interesting to note the blade on the right is visible in the difference plot and indicates the pressure field around the blade is not identical with the field in the middle panel. This is consistent with the loss of circumferential uniformity but also indicates geometric non-uniformities may propagate pressure disturbances

considerable distances in the case wall pressure field.[56] Enlarging the clearance to e/b = 0.006 does not radically alter the pattern. The differential in pressure pattern between each clearance level is also similar in nature.

Change With Stator Relative Position The change in the pattern is seen by inspection in Figure 3.7-4(a) which is an identical figure to 3.7-3(a) and presents data for the *third* stator relative location. These data are the same as those of Fig. 3.7-2(a). In this location the tip local incidence is higher (than location 2) and the tape on the sealed blade is more visible. A distinct jog in the pressure contours can be seen developing along the location of the cross passage gully as the clearance is increased.

3.7.2.1 Pressure and Position Distributions

Figure 3.7-3(b) and (c) show the changes in pressure distribution, loading, circumferential positions and separations of pressure maximum, minimum and the blade edges as function of axial position for the design ($\Phi = 0.64$) flow case at the three clearances for the second stator relative location. As clearance changes the pressure at the blade edge on the suction side is the only pressure that changes at all. Note that it approaches the passage suction side value for the sealed case. The *passage* minimum pressure is stable in shape and magnitude for the three clearance conditions. The blade edge tangential loading falls appreciably with clearance increase.

The minimum/maximum position plots show a number of phenomena in Figure 3.7-3(c). Sealing the gap brings the pressure minimum much closer to the blade. However, the pressure basin is not displaced correspondingly so the shaded region shown on the panel of the sealed blade is a local pressure dip closer to the blade. It was clear from this result that the clearance changes mainly affect the pressure pattern between the blade suction surface and the offset minimum gully. Similarly the bulges outward of the minimum position are not accompanied by appreciable changes in pressure level between the suction side and the minimum line. Bulges are also apparent in the pressure maximum line.

Change With Stator Relative Position An almost identical situation to the above, in terms of changes, is seen by inspection in Figure 3.7-4(b). This figure shows the pressure loading data for the third stator relative location. The blade and *passage* loading differ, primarily on the suction side. Figure 3.7-4(c) shows the minimum/maximum position plots for the third stator relative position. Once again the results are qualitatively similar to the second hole location but differ quantitatively. Distinct bulging of the pressure minimum appears and increasing clearance displaces the minimum gully further from the suction side.

3.7.2.2 Radiative Pressure Wave Structure

Comparisons of pressure wave patterns at particular holes showed a less orderly fan like structure of the radiated pressure waves from the leading edge as clearance increased. The pattern became smeared and more ragged. This trend appeared to be consistent with a larger gap at the leading edge decreasing the sharpness of the cut into the stator wake formation (shadow) near the wall.

---

[56] This observation is relevant to the wave like ripples riding or pendent (Heinemann (1985) refers to the ripples as a "pending") on the pressure waveform that can be seen when a trace covering many blade passages is displayed on an oscilloscope. The ripples seem to be periodic and of appreciable amplitude, however, spectral analysis of the signal indicates peaks at exact multiples of blade passing frequency. Minor geometric differences in the blading's peripheral uniformity coupled with random flow fluctuations may be responsible for the pending as a relatively small geometry change, in this case, seems to have propagated an average pressure disturbance some distance.

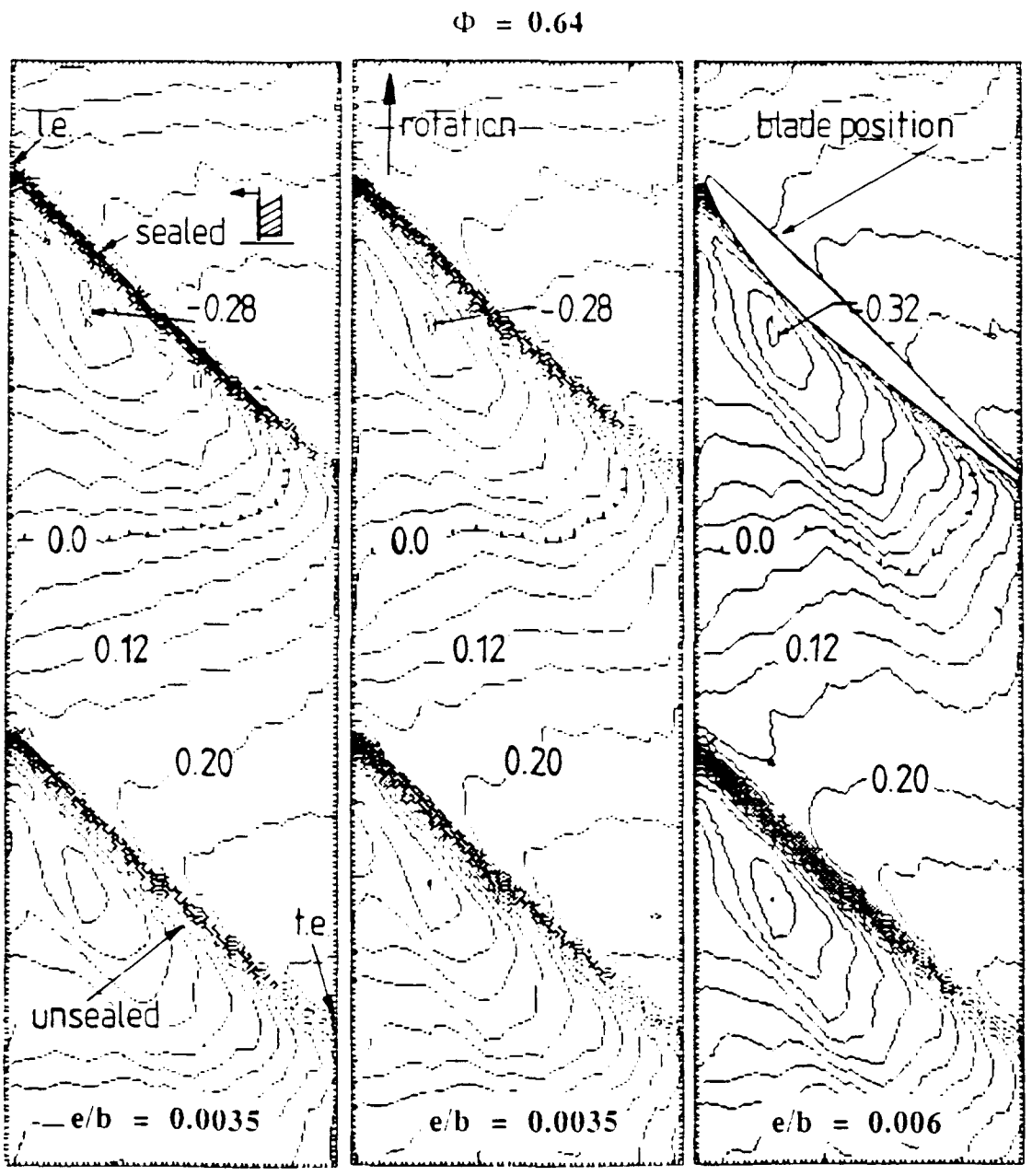

Fig. 3.7-2 (a) Wall pressure contours *at stator relative location 3* for three clearances, (left top) sealed tip on blade 2, (mid) e/b = 0.0035 clearance and (right) e/b = 0.006 clearance for design flow (Φ = 0.64). The pressure trough outboard of the suction side becomes deeper as clearance increases. The trough is also present in the sealed case where no leakage is possible.

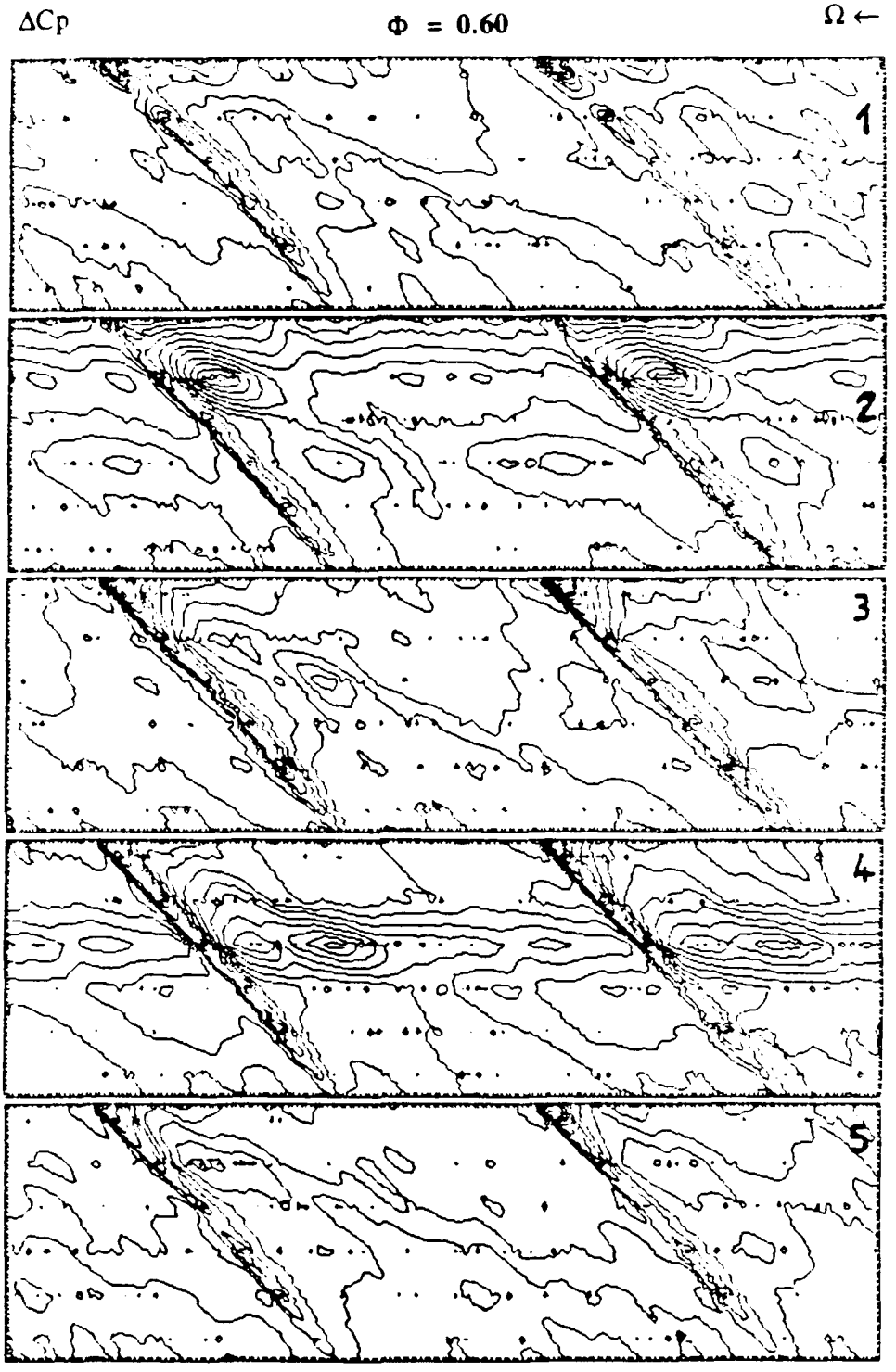

Fig. 3.7-2 (b) *Contours of the differences* in wall pressure *due to a change of clearance* in the rotor at five stator relative locations (pressures of e/b = 0.006 clearance minus e/b = 0.0035 clearance, near peak power ($\Phi = 0.60$)).

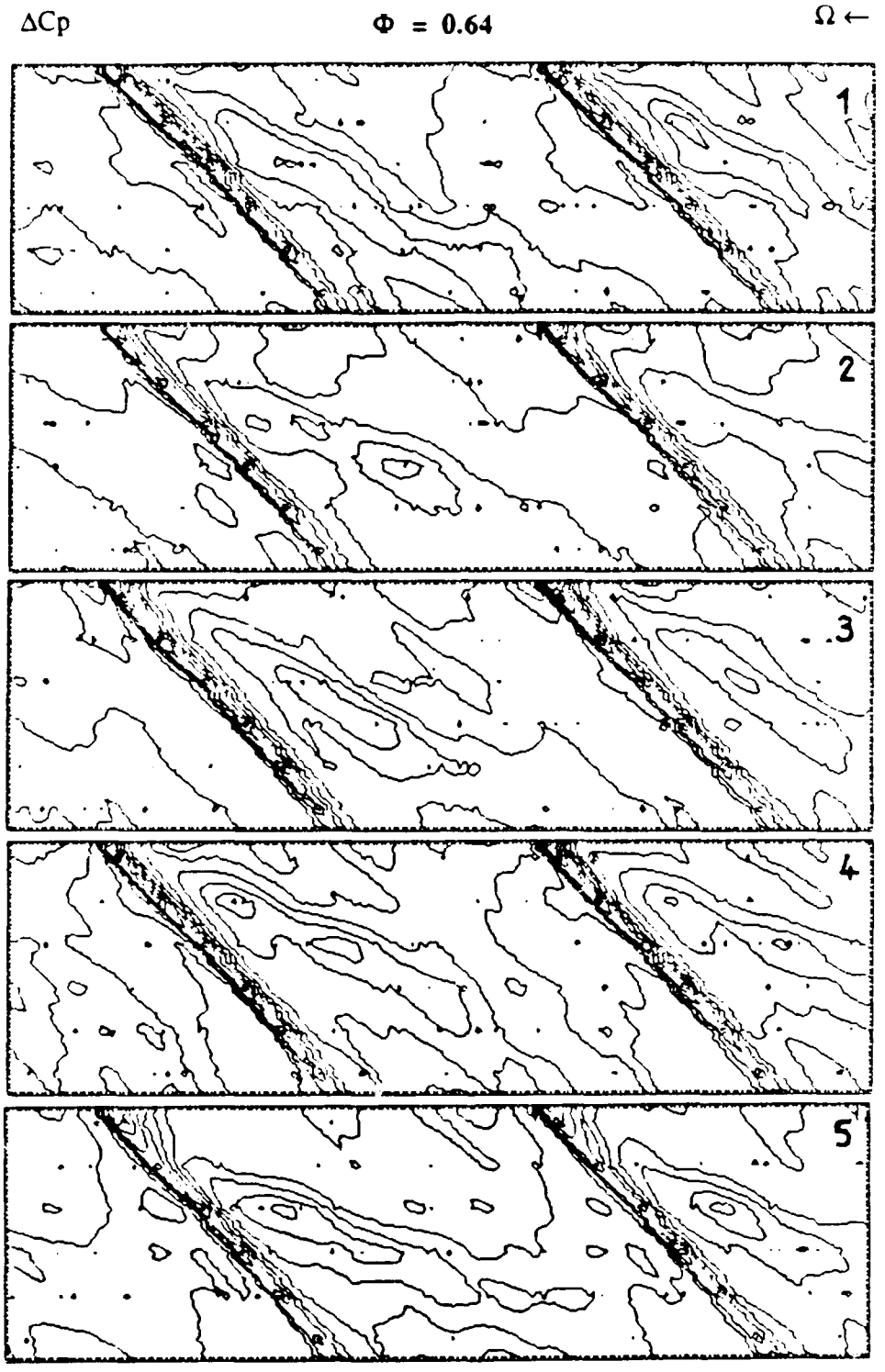

Fig. 3.7-2 (c) *Contours of the differences* in wall pressure *due to a change of clearance* in the rotor at five stator relative locations (pressures of e/b = 0.006 clearance minus e/b = 0.0035 clearance, design flow ($\Phi = 0.64$)).

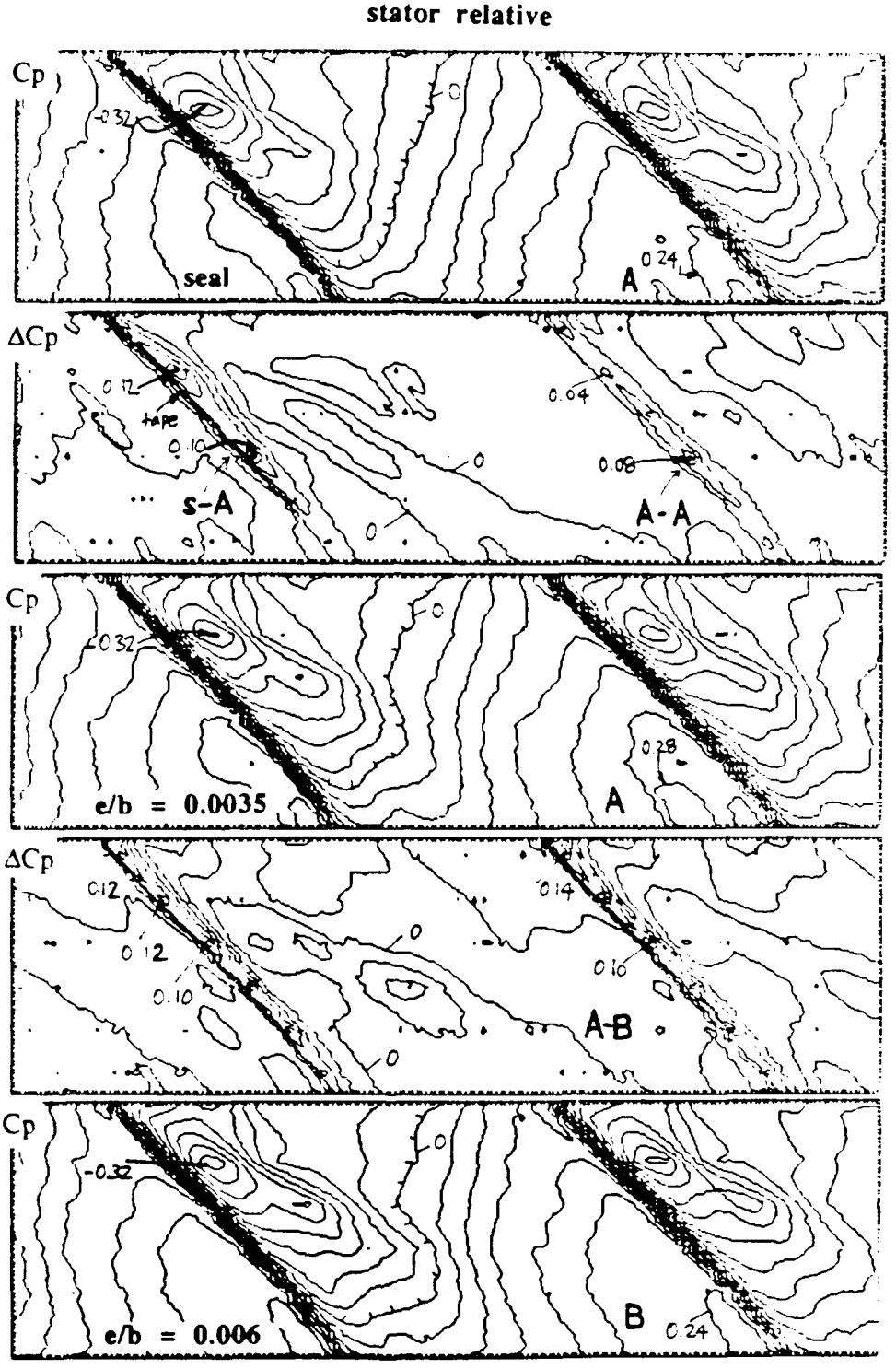

Fig. 3.7-3 (a) Wall pressure contours separated by contours of differences between them *at stator relative location 2* for three clearances, (upper) sealed tip on blade 2, (mid) e/b = 0.0035 clearance and (lower) e/b = 0.006 clearance for design flow (Φ = 0.64).

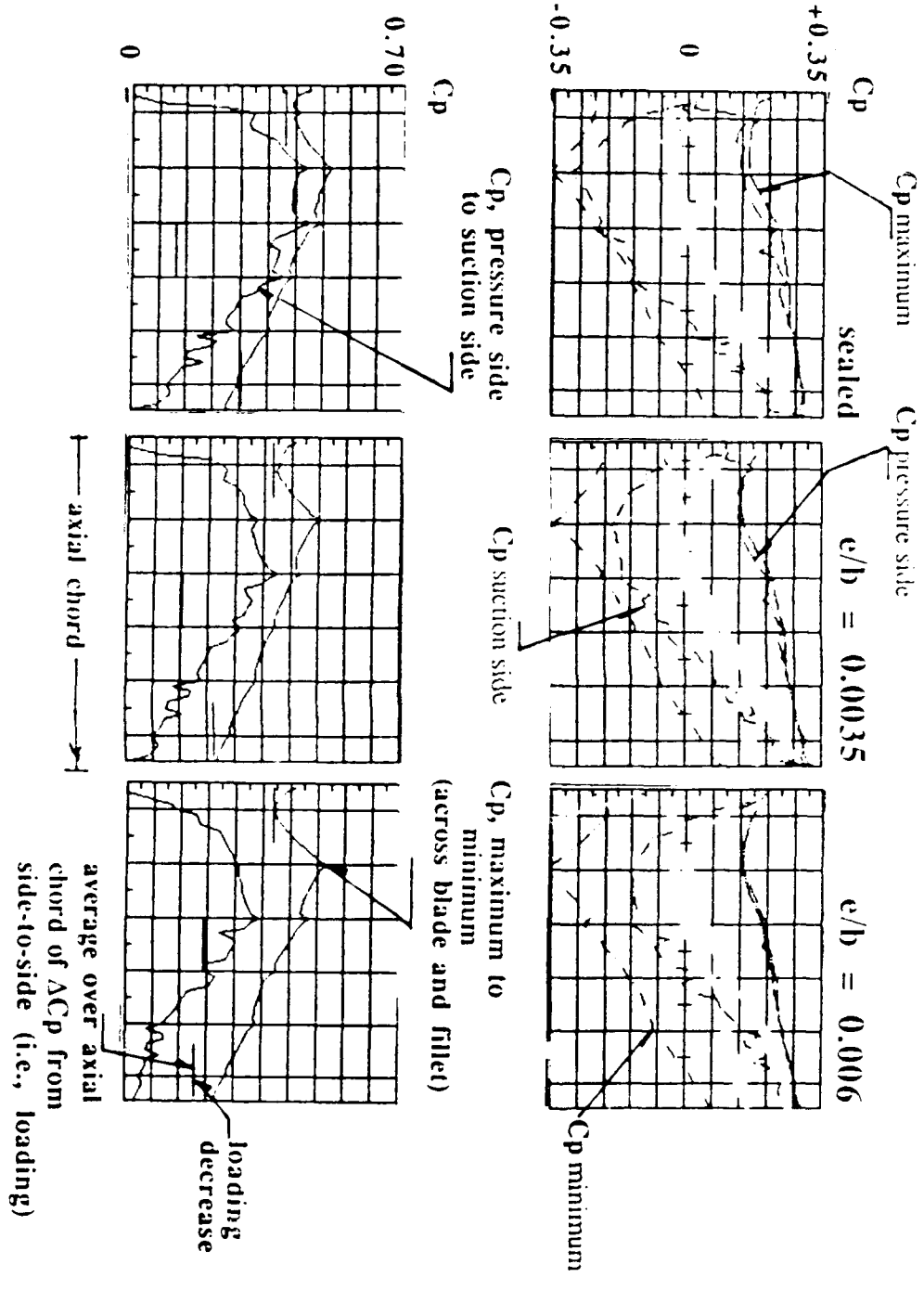

Fig. 3.7-3 (b) Wall pressure distribution and loading as function of axial position *at stator relative location 2* for three clearances, (left) sealed tip on blade 2, (mid) e/b = 0.0035 clearance and (right) e/b = 0.006 clearance for design flow ($\Phi = 0.64$).

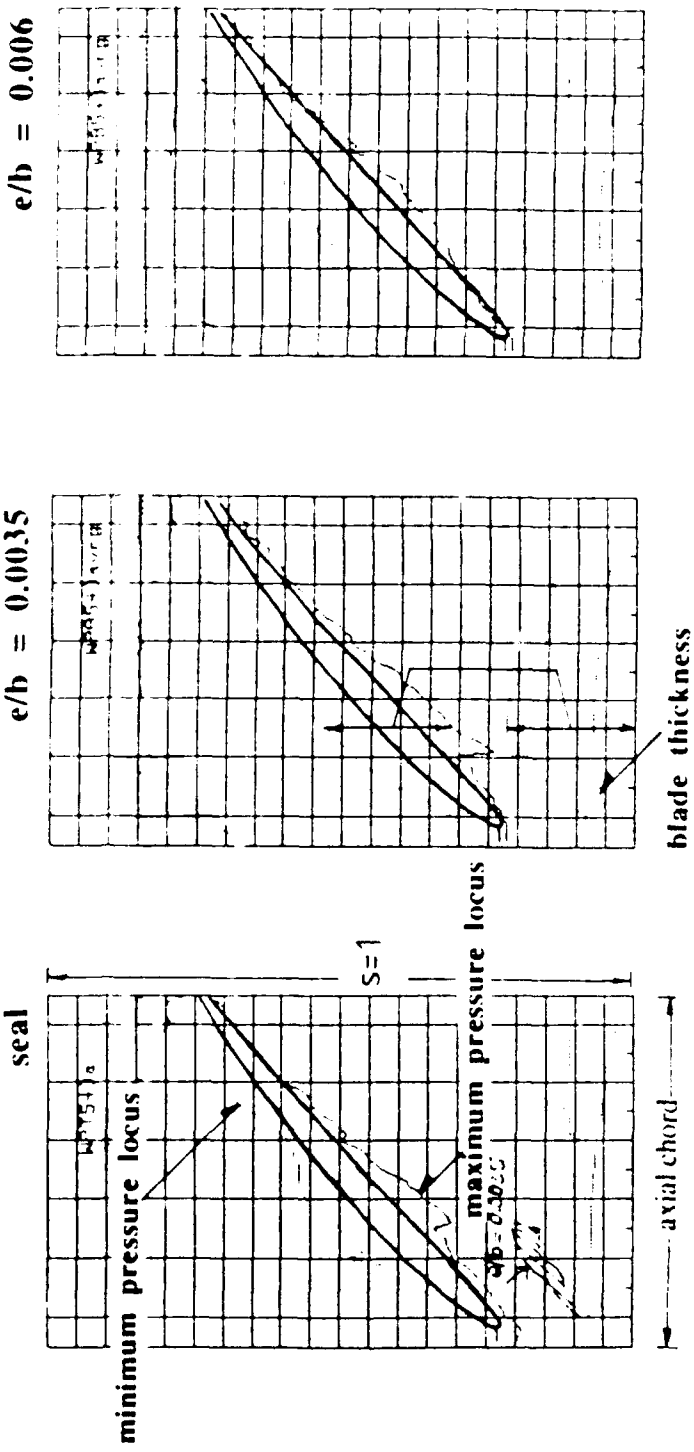

Fig. 3.7-3 (c) Circumferential positions and separations of pressure maximum, minimum and the blade edges as function of axial position *at stator relative location 2* for three clearances, (left) sealed tip on blade 2, (mid) e/b = 0.0035 clearance and (right) e/b = 0.006 clearance for design flow ($\Phi = 0.64$).

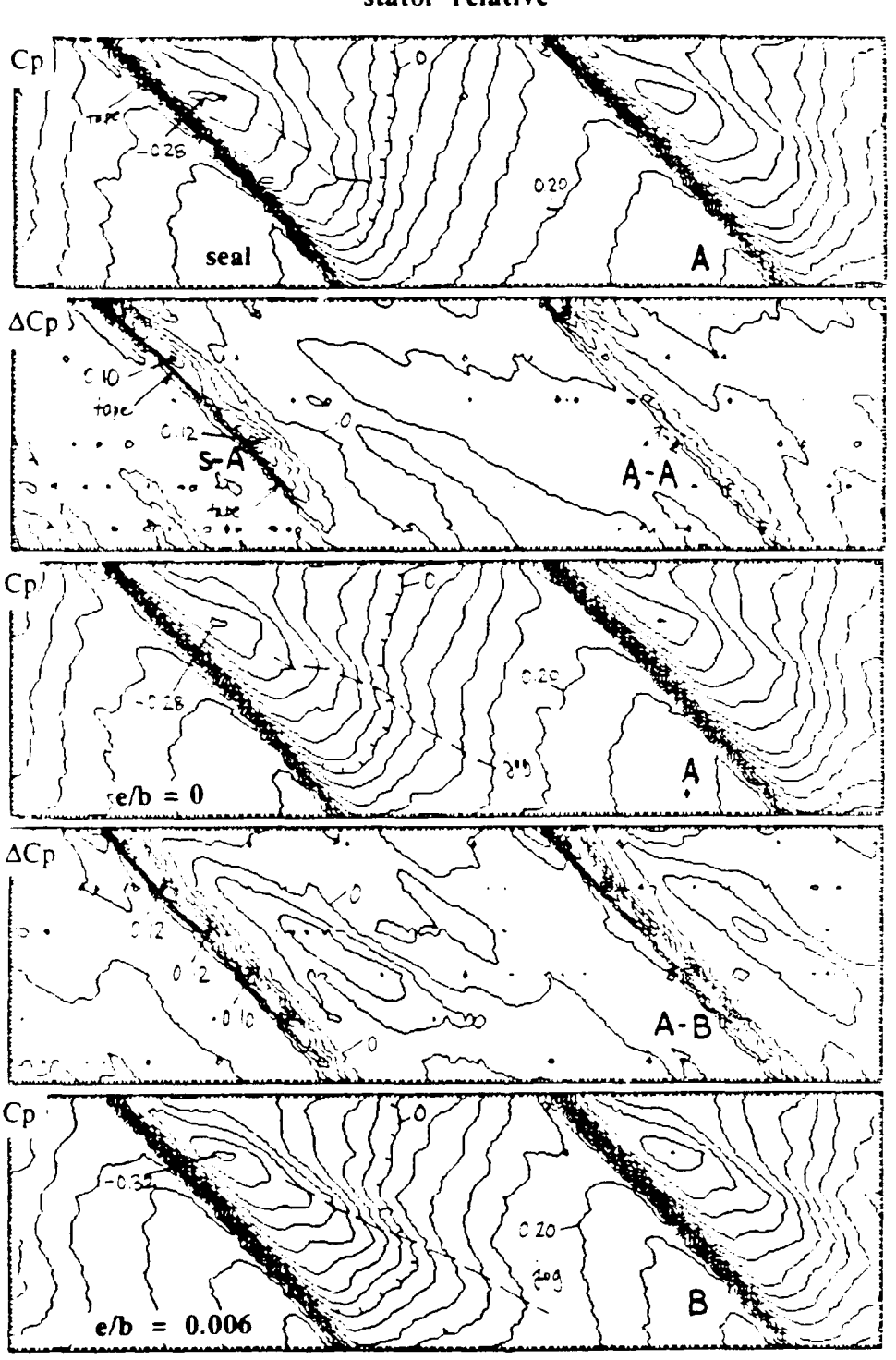

Fig. 3.7-4 (a) Wall pressure contours separated by contours of differences between them *at stator relative location 3* for three clearances, (upper) sealed tip on blade 2, (mid) e/b = 0.0035 clearance and (lower) e/b = 0.006 clearance for design flow (Φ = 0.64). (see also Fig. 3.7-2 for the same data)

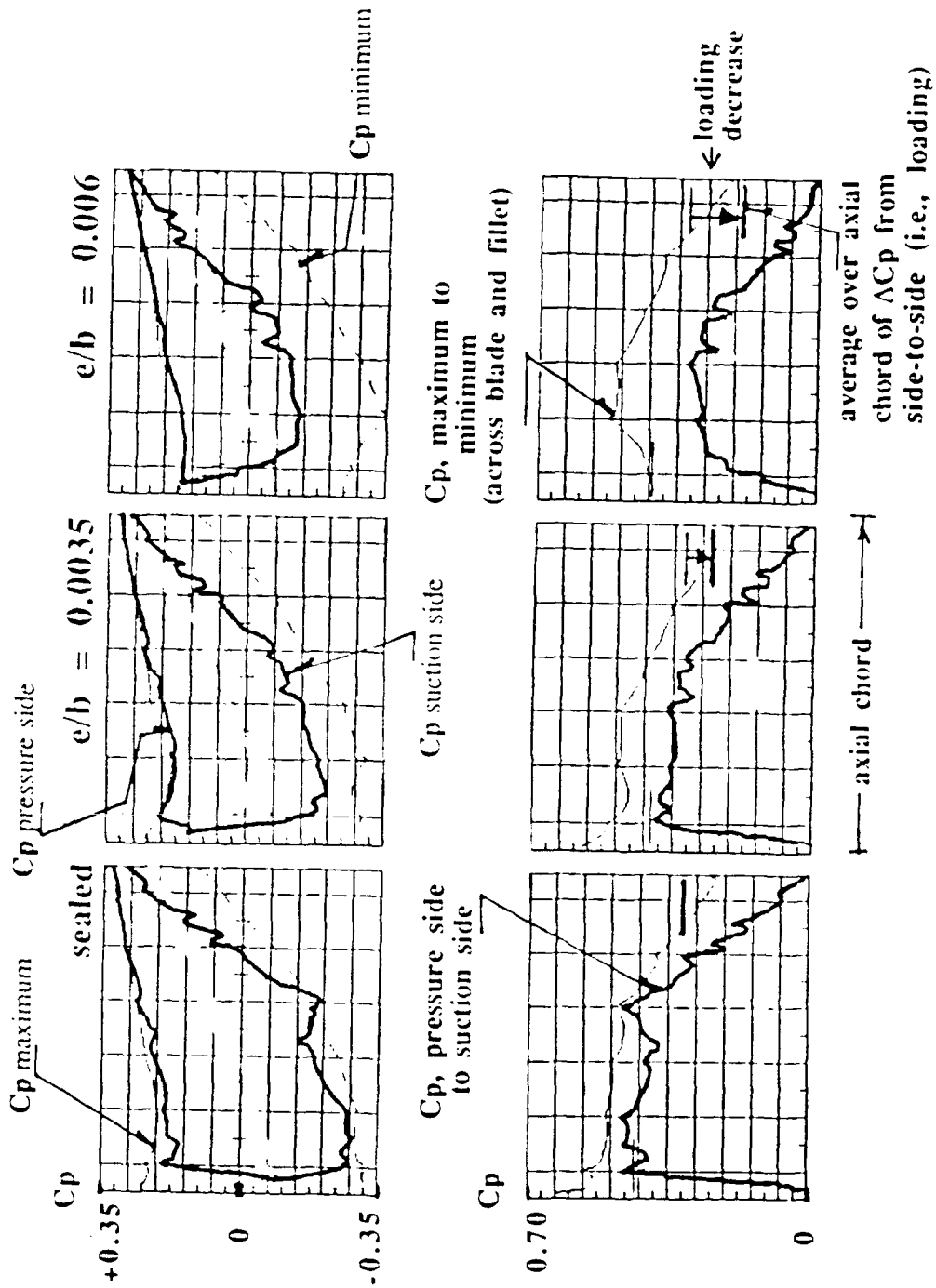

Fig. 3.7-4 (b) Wall pressure distribution and loading as function of axial position *at stator relative location 3* for three clearances, (left) sealed tip on blade 2, (mid) e/b = 0.0035 clearance and (right) e/b = 0.006 clearance for design flow (Φ = 0.64).

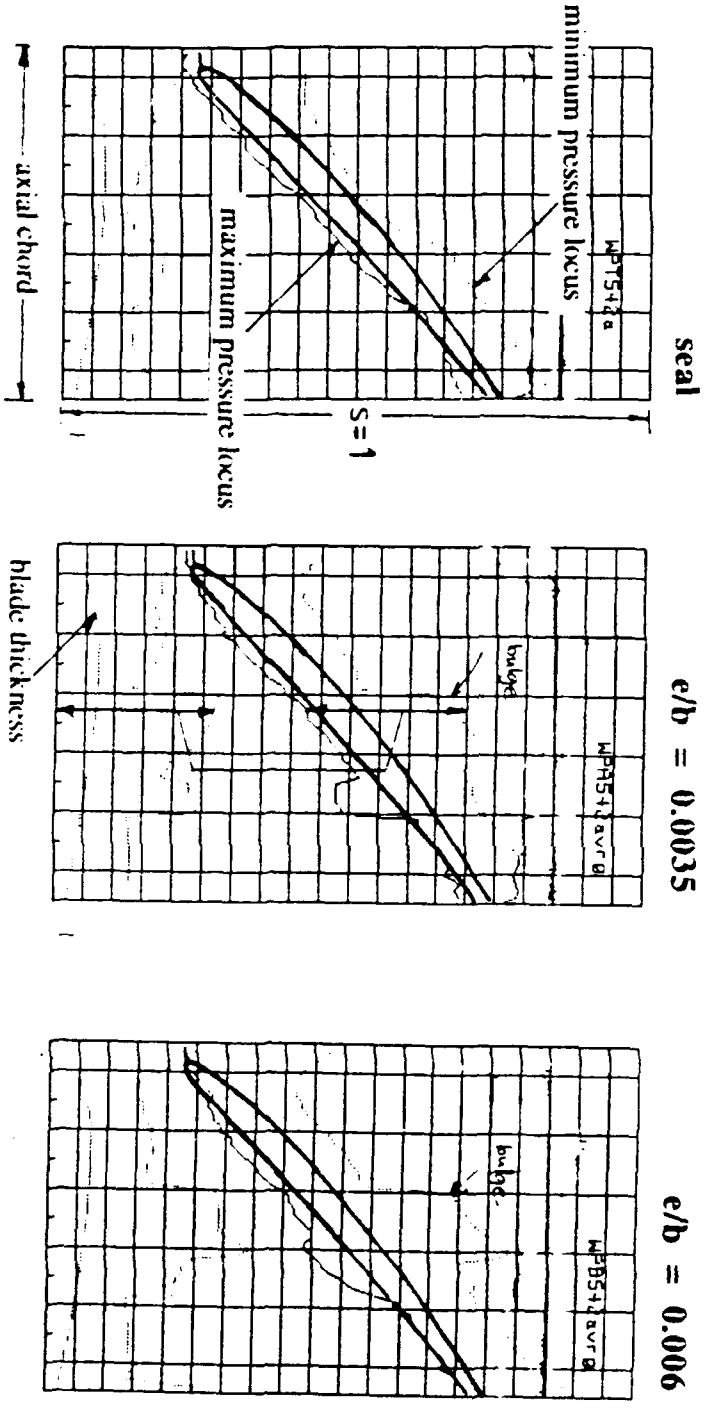

Fig. 3.7-4 (c) Circumferential positions and separations of pressure maximum, minimum and the blade edges as function of axial position *at stator relative location 3* for three clearances, (left) sealed tip on blade 2, (mid) e/b = 0.0035 clearance and (right) e/b = 0.006 clearance for design flow ($\Phi = 0.64$).

3.8 Summary of Flow and Clearance Variation Testing

The results derived from the program of measurements amounted to a significant body of experimental information to interpret. The major observations and results of the flow measurements and clearance variation testing are summarized below:

(1) The flow field of the two stage blading configuration differed in character from the single stage arrangement, particularly in terms of spanwise rotor incidence and overall throughflow distribution. The presence of a second stage constrained the flow in both stages to a condition that was more representative of the design intent for the stage. It did not appear likely that the wall boundary layer character was similar in the two configurations based on the changes in the flow separations observed in the stators.

(2) The flow structure near the case wall at the rotor tip had distinct features. The most remarkable feature of the flow structure was the minimum suction pressure position in the passage. At all axial stations the pressure minimum was displaced approximately two blade thicknesses away from the blade suction surface rather than coinciding with the suction surface. Several other features of the structure persisted for the conditions tested (small clearances). These comprised;

(a) a cross passage low pressure gully in the pressure distribution which traversed the passage from the suction side leading edge toward the pressure side trailing edge and varied in position slightly with flow coefficient

(b) a distinct and large low pressure basin positioned well aft of the leading edge of the blade but lying over the minimum pressure gully standing off the suction side and

(c) an abrupt pressure rise on the pressure side of the basin which shifted in the passage with stator relative position.

The C_p distribution around the blade and fillet region at the wall was similar to the distribution predicted around only the blade contour in an inviscid flow. This suggested the expected circulation pattern of the blade tip was present in the flow at the wall but rather than coinciding with the blade suction side at the tip, the higher velocity flow was curving around the fillet out in the passage. The resulting pattern had the nature of the circulation about the blade tip being extended to the wall out in the passage. *The peak suction level for the passage was observed to remain constant, in absolute pressure magnitude, over the range of flow coefficient tested.* In absolute terms the pressure level on the pressure side near the tip rose with decreased throughflow to produce higher blade loading. This observation strongly suggested the nature of the flow on the suction side of the blade depends on the relative motion of the blade, to the wall, rather than throughflow.

(3) The effect of changing the clearance from a sealed tip to a small gaps (-A at e/b = 0.0035 and -B at e/b = 0.006) was to unload the blade tip while maintaining an almost constant pressure difference from pressure to suction side *in the passage*. Corresponding to the tip unloading (suction side pressure increase), a diffuse (weak) decrease in pressure, aligned with the cross passage minimum pressure gully, occurred. Correlation of the two effects did not suggest that the additional circulation shed by the blade surface with tip unloading was appearing as increased vorticity in the cross passage direction.

(4) Regions of intense pressure fluctuation detected in the passage coincided with the abrupt static pressure rise on the pressure side of the low pressure basin shifting in the passage with stator relative position. This zone of pressure fluctuation extended from roughly the leading edge of the blade to the end of the pressure side of the basin at about 1/4 of blade spacing from the suction side. The wall pressure pattern showed little evidence of spatial change with stator relative position other than in this region. This phenomenon appeared to be unaffected (either spatially or in magnitude) by the clearance changes.

(5) The observed flow pattern changes with clearance were not especially influenced by flow coefficient at the small clearances tested. As changes in flow coefficient would reflect changes in spanwise incidence on the blade, the wall pattern did not appear to be affected by *spanwise* incidence (which varied from -1.25 to 3.5 degrees at mid span for the flow range examined). However, the clearance changes affected the wall flow structure in a manner which was similar to what one would expect of incidence in a two-dimensional cascade flow.

In summary, the fundamental flow structure at the wall (i.e., the two gullies and the basin) appeared to be defined by the blade motion relative to the wall. Changes in spanwise incidence, stator relative position and tip clearance gap appeared to interact with this basic structure without causing any pronounced change in its character. Changes in *spanwise* incidence had only a slight effect on the wall flow structure, although the pressure levels changed. Changes in stator relative position could be seen to result in cyclic excursions in pressure about the average pattern, particularly on the pressure side of the basin. The leading edge region of the blade was also seen to unload at certain positions. Increases in tip clearance gap, however, had the effect of unloading the blade tip *almost uniformly* from leading edge to trailing edge.

In the context of the discussion of Parts 1 and 2, these results were not totally surprising. However, the lowest pressure lying outboard of the blade in the passage was unexpected. This suggested locally viscous (high shear) behavior was a significant influence in narrow zone in the suction side corner. This shearing influence is discussed further in Part 4.

Part 4

Discussion of Results

The discussion examines the results of Part 2 and Part 3 by first addressing the local tip and wall corner flow results in Sec. 4.1. The results are then examined in the context of the stage flow in Sec. 4.2. The more general implications of the results in terms of existing models[57] and mechanisms are then discussed in Sec. 4.3.

In summarizing the experimental results it was noted that the fundamental flow structure at the wall (i.e., the two gullies and the basin) appeared to be defined by the blade motion relative to the wall. Changes in spanwise or passage average incidence, stator relative position and tip clearance gap appeared to interact with this basic structure without causing any pronounced change in its character. The information of value developed from these analytical and experimental results point to the influence of viscous forces in or very close to the tip gap on the suction side as a source of losses. This aspect of the observations is expanded and reviewed in the discussion.

---

[57] Due to the effort expended on modelling in much of the previous literature on this subject, the present study has not emphasized new modelling or extensive quantitative comparison of the many models that have been proposed. Previous quantitative studies of the differences between models have been made by Reeder (1968), Yamamoto (1982) and Robinson (1982). These studies produced mixed results. The latter authors advanced new models (see discussion in Sec. 1.5). The present study has favoured a more collective and evaluative approach to the tip local flow field and losses and has tried to identify and isolate the flow mechanisms at work by a variety of methods in Parts 2 and 3.

4.1 Tip/Wall Corner Local Flow

In this section, the flowfield has been divided into two regions and discussed separately. The dividing line was chosen along the pressure minimum path through the passage. The measurements suggest the two regions do not interact strongly and any need for one to compensate for the other is adjusted for in strength and position of the cross passage pressure gully. This gully most probably reflects a vortex filament, but as the discussion will show, the vortex is unlikely to be due to a roll-up of *pressure driven* leakage flow. The flow extending from the blade pressure side under the tip to the minimum pressure line has been called the "gap and fillet region flow" and from the minimum line across the passage to the pressure side has been called the "passage flow." The two regions are shown schematically in Figure 4.1-1(a).

4.1.1 The Gap and Fillet Region Flow

The pressures in the gap and fillet region change markedly with changes in tip clearance up to the locus of minimum pressure. The pressure gradient in the gap and subsequently the pressure loading at the blade edges are altered by a clearance change.[58]

Combined, the wall pressure (p) and preliminary wall shear measurements (τ_w) in this region indicate *the flow is stagnant in the fillet region* in the absolute frame or moving at wall speed in the relative frame. Inoue and Kuroumaru's (1988) velocity measurements also show the same magnitudes near the suction side followed by a reverse flow on the passage side of the minimum line. Their results are consistent for two survey heights in the gap (Figure 4.1-1(b)) and leads them to propose a thin vortex sheet lying or forming over the *relative* leakage flow. The most interesting information in the (present) shear and (their) velocity measurements is the consistency of the data with the form of a shear flow in a pressure gradient. This type of flow is often assumed to represent the flow in the gap, *for a wall shear boundary condition of zero*. This type of flow was examined for the present gap, to see how it reconciled with the test results.

4.1.1.1 Gap Flow and Shear Layer

The experimentally observed behavior indicates the non-dimensional pressure gradient[59] based on wall speed in the gap is about unity for the small clearances measured. From inspection of the wall pressure traces, the pressure gradient in the gap was observed to decrease as the clearance increased. The correlation of the effective gap size (e") and pressure gradient was of principal interest. An approximate and somewhat general relationship between the near wall velocity and wall shear in a pressure gradient is given by Brown (1967, Eqn. 1) from consideration of power series expansions for a boundary layer velocity profile under different conditions. His expression is

$$u(y) = (\tau_w/\mu).y - (1/2\mu)(dp/dx).y^2$$

which becomes

---

[58] Note the order or priority of the interactions. Previous work has considered the priority reversed

[59] See definition in Schlichting (1955, p. 61)

$$u'(y) = (\tau_w/\mu).y - (1/2\mu)(dp/dx').y^2 - U(y) \qquad 4(1)$$

in the relative (') frame of a rotor ("x" is distance in the circumferential direction). The boundary conditions in the neighborhood of the tip gap require that

$$u'(0) = - U_t$$

at the wall, which is directly satisfied at y = 0, and at the blade edge

$$u'(e) = 0$$

which requires

$$dp/dx' = 2\tau_w/e - 2\mu U(e)/e^2 \qquad 4(2)$$

As the experimental measurements indicate $\tau_w = 0$ in the neighborhood of the tip gap, and assuming $U(e) = U_t$, the boundary condition reduces to

$$dp/dx' = - 2\mu U_t/e^2 \qquad 4(3)$$

which defines the pressure gradient in the gap matching the boundary conditions. The pressure gradient is seen to depend only on the tip clearance dimension (e) for a fixed wheel speed (U_t) and fluid (μ). Note that the same result can be obtained by solving the derivative of the general Couette flow expression given by Schlichting (1955, p. 61), for dp/dx, and applying the condition $\tau_w = 0$ at the wall. Typical Couette velocity distributions are shown in Figure 4.1-2(a).

When equation 4(3) is compared to the experimental results it is immediately clear that the extent of the shearing region must be much smaller than the mechanical gap to produce the pressure gradients observed in the measurements. By using the measured dp/dx' it is possible to determine the effective gap dimension (e") from

$$e" = (2\mu U_t/(dp/dx'))^{0.5}$$

A comparison of e, e" and the dp'/dx data is shown in Figure 4.1-2(b). The measured gradients best match the analytical result for the condition that

$$(dp/dx')/(2\mu U_t/e"^2) = \pm 1$$

or unity[60] magnitude of the non-dimensional pressure gradient. This condition is applied with the wall side bulked in velocity as it would be found in a compressor.

Velocity Profile in the Gap The velocity profile in the gap is defined once the pressure gradient 4(3) is known from 4(1) and if $\tau = 0$ from y = 0 to (e - e") then

[60] The sense or sign depends on which frame, relative or absolute, is being considered, but in both cases the velocity is bulked near the wall side of the gap

$$u'(y) = -U_t \; ; \quad y < (e - e'')$$

$$u'(y) = U_t((((y - (e - e''))/e'')^2 - 1) \; ; \; y > (e - e'') \qquad 4(4)$$

The velocity profile in the gap, that results from this analysis, is still consistent with the Couette flow result. However, the shear layer that results is a very small proportion of the total gap height.

If the velocity profile situation in a moving wall simulation of the relative motion is compared to the result above, noting that dp/dx' is relatively *small* in most of the passage, and the same boundary conditions apply, then the velocity near the wall is given by

$$u'(y) = U_t(y/e - 1)$$

and the approaching profile would be expected to have a *near wall* shear layer form. The difference is shown schematically in Figure 4.1-2(a) and it can be seen that the flow situation approaching the gap is quite different from what appears to be present in a rotating device.[61,62,63] The differences shown in the velocity schematics of Fig. 4.1-2(a) appear, at a very detailed measurement level, to present a fundamental problem in applying observations made in moving wall cascade tests to rotating devices. But, in fact, all the turbine cascade studies may have a simulation problem in this region similar to that found in this study for compressors. For example, Heinemann's (1985) data, for a *rotating* turbine cascade, shows the pressure maximum to minimum separation to be 50 to 100% wider than the blade dimensions. That is, there is also a pressure minimum offset in turbines.

Discharge Coefficient When integrated across the gap, the velocity profile 4(4) yields a mass flow per unit length of blade of from $2/3\rho e U_t$ if $e'' = e$, to $\rho e U_t$ if $e'' = 0$. This result indicates an area discharge coefficient (C_d) of 2/3 = 0.66 to 1.0 can be applied to the inviscid tip *relative* leakage rate based on *tip speed* to estimate the leakage flow. This result spans the range of measured values of C_d (0.6-0.8) for a relatively low turning, turbine cascade tip gap by Yaras et al. (1988, Fig. 13). Their leakage is *pressure driven* (i.e., the wall is stationary) and from detailed surveys in the gap (Fig. 4) show the velocity distribution bulked on the wall side (unlike the Couette profile for

---

61 It is also relevant to note that the moving wall velocity distribution is Taylor-Goertler stable at some curvature, while the stagnant flow, wall shear = 0, case observed in the present tests is unstable (see Sec. 1.2.2.3)

62 A number of experiments have been conducted using moving walls in either linear or annular cascades to approximate conditions at the rotor tip. In such testing the relative flow would not be as bulked toward wall speed near the wall. The results from the present experiment indicate the shear in the compressor is concentrated near the blade tip end and there is little or no pressure driven leakage near the wall. Recent moving wall tests have mainly been conducted in turbine cascades and very detailed near and in-gap pressure measurements have been made. The results of Morphis and Bindon (1988) and the discussion of Bindon (1988) for example have particularly emphasized high losses associated with separation bubble formations on the blade side in the gap. These observation may be peculiar to the shear being generated by the moving wall side in their gap and pressure driven leakage

63 Morphis and Bindon (1988) did not provide information on velocity gradients, particularly in the gap entry region. This was consistent with their pressure measurement and visualization orientation at the time, however the entry conditions may be partially responsible for the discrepancies between different turbine cascade measurements. The differences are outlined in Yaras and Sjolander (1989) between their own observations, Dishart and Moore (1989), and Bindon (1988)

a turbine). Their reference velocity was based on the component of the *pressure driven* dynamic pressure normal to the chord. Due to the similarity in profile, the correspondence of C_d is not surprising. However, the similarity of the profile to that of a compressor, in terms of side of the gap where the velocity is bulked, should be troubling in terms of turbine simulation.

Shear Layer Thickness In terms of utility or prediction, the agreement of the compressor measurements with the Couette solution is valuable information and the pressure gradient expression, $dp/dx' = -2\mu U_t/e''^2$, appears to provide a way to estimate the suction edge unloading with tip clearance change when the relationship of e" to e is known. From the present measurements it was deduced that e" does not change rapidly with e and to first approximation can be considered constant. The quantitative correlation was found to be

$$e'' = 0.076 + 0.02e \text{ (mm)} \; ; \; e'' = 0.003 + 0.02e \text{ (in)}$$

This description of the gap flow as a thin shear layer is consistent with Inoue's proposal of a thin vortex sheet lying or forming over the *relative* leakage flow. It is useful to note that this flow situation and its attendant pressure change can be approximated quite well (tangentially) with a simple area reduction across the gap from e to (e - e"). The pressure change (decrease) measured at the blade edges with changing clearance (e) is in good agreement with this approximation along 70% of axial chord for both the e/b = 0.0035 and e/b = 0.006 clearances measured in this study.

4.1.1.2 Shear Layer influence on Tip Unloading/Corner Flows

Pressure Adjustment at the Suction Edge From the preceding discussion it would seem the gap flow is consistent with a Couette flow along its whole length establishing a pressure gradient that depends only on a thin shear layer near the blade end and the relative velocity in the gap. The thickness of this layer weakly depends on gap size. The experimental results suggest this regime adjusts to the blade-to-blade pressure field of the passage some distance past the suction-side edge. If the gap corner flow is thought of in this manner, it can be seen that the passage's "cascade" pressure gradient from blade-to-blade would only match the pressure condition at the exit of the gap (under the blade edge) in special circumstances, i.e., when

$$p^+ - (dp'/dx).t = p^+ - \Delta p_{b\text{-}b,cascade} \qquad 4(5)$$

An analogy to this situation would be the under or over expansion of a jet entering a region of adverse pressure gradient. From the empirical equations above, the effective clearance which corresponds to a matched condition is given by

$$e''_{match} = (2.\mu U_t.t/\Delta p_{b\text{-}b,cascade})^{0.5}$$

and the total clearance is given by

$$e = 50.(e''_{match} - 0.076) \text{ (mm)} \qquad 4(6)$$

Tip Unloading The present experimental conditions are consistent with an under expanded jet, except in the smallest (sealed) clearances case. The pressure traces suggest the blade *relative* leakage is over expanded in that case. This analogy indicates

fluid emerging under the blade in the relative frame would sense an accelerative pressure condition over much of the chord for the larger clearance cases. This supposition is supported by the data of Fig. 3.7-2(c) and (d) which show the pressure minimum moving slightly further from the suction-side edge. The respective under or over expansion at the suction side, in the situation where the pressure gradient in the gap is independent of external conditions, would vary with incidence; or more exactly with the change in $\Delta p_{\text{b-b.cascade}}$ with incidence and this may account for losses. This the difference between the blade pressure and passage is shown schematically in Figure 4.1-3(a).

Under these conditions the blade tip loading, which is most likely to reflect the gap pressure on the suction side, is defined independently of the passage flow conditions or the blade surface pressures. This is a different situation to that of a cascade, for example Storer and Cumpsty (1990, Fig. 17) show blade loading at the tip increasing with increasing clearance. The results from the present rotor and other rotors typically show tip loading falling with increasing clearance. They also clearly demonstrate a pressure driven leakage in the gap (Fig. 8). Their results are discussed further in Moyle, Walker and Shreeve (1991). The cascade results of Storer and Cumpsty also show the pressure minimum at any axial station lying at (or very close to) the suction side edge of the blade in the cascade. The results in the present study were quite different. The results of the compressor and cascade are compared in Figure 4.1-2(c).

Pressure Minimum Location - Vortical Flows in the Corner If the pressure distribution of a collateral flow in a corner is examined, it is apparent the conditions are more complex due to the presence of a clearance or a moving wall and it seems the expansion conditions may be modified by other factors. Measurements by Hararika and Raj (1987) and Bhargava and Raj (1989) on an isolated, uncambered blade positioned on a flat plate, without clearance or transverse wall motion, show a fillet region in the corner for zero incidence flow. The mean line chord Reynolds Number was 0.40 to 0.45×10^6 for the experiments. Figures 4.4 and 4.5 of Hararika and Raj (1987), particularly, show a fillet region quite clearly in a visualization of the streamlines. Figures 4.57-4.59 show their interpretation of the Bernoulli surfaces measured.

Their interpretation suggest the presence of several circulations lying between the horseshoe vortex and the corner. Distributions of C_P and wall shear for the same situation are shown by Bhargava et al. (1987, Figs. 5-10). Figure 10 shows the location of the maximum shear on the flat plate wall to be positioned in a very similar location to the minimum pressure line of the present measurements. The maximum shear location sits off the blade edge and extends for the length of the blade. The C_P results (Fig. 5) show a very slight local pressure low, corresponding to the maximum shear locus *and the maximum shear magnitude*, at the station before maximum blade thickness. This local low pressure persists as a notch in the pressure distributions along the length of the blade, although for most of the blade the pressure minimum is at the blade surface. A presumably diffusive pressure rise occurs near the blade surface at the trailing edge. Scaled, their minimum locus lies approximately 0.02 of chord from the blade edge. The present compressor data positions the minimum locus at 0.09 of chord from the suction side. The difference (0.02 to 0.09) is consistent with the wall relative motion found in the compressor.

However, choosing an appropriate scaling for position data of this type is problematic. Similar measurements by Honami et al. (1988, Fig. 6) show the horseshoe vortex core, minimum pressure locus, moving continuously away from the blade surface for a constant thickness, blunt body section; so it is clear that section thickness distribution

is a factor in minimum line position. Clearance is also likely to affect the flow. For example, measurements by Storer (1989, Fig. 4) show the situation at the suction-side exit of a cambered stator blade in a linear cascade when a clearance is opened at the blade tip. The zero clearance case shows a strong *corner vortex* formation suggested by Hararika and Raj (1987) sitting under a much weaker horseshoe displaced up the blade. Further opening of the clearance in the corner, in increments, shows a distinct upwelling of flow move away from the blade toward the passage. This re-establishes a strong horseshoe vortex rotation in the corner and apparently pushes the corner vortex out into the passage. Figure 4.1-3(b) shows a comparison of the results of Hararika and Raj (1987) and Storer (1989). This flow pattern transformation takes place in an adverse pressure gradient unlike the isolated aerofoil cases and presumably explains the displacement of the horseshoe vortex up the blade. The similarity of Storer's results to those of Schulz et al.'s (1989) steady flow case should be noted. Schulz found the large apparent separation in the corner to diminish substantially in a fluctuating flow. That fact notwithstanding, from Storer's measurements one would expect the local low of the wall pressure, associated with the re-established horseshoe vortex core, to move away from the suction side as clearance increased. This movement is observed in the present compressor.

Pressure Minimum Location- Streamwise Boundary Layers An alternative and analytical reason for the existence of a pressure minimum locus lying away from the suction corner is provided by Barclay (1982) in a solution for the flow in streamwise corners under different conditions of corner radius. In the present flow, the fillet region might be considered to be like a radius in the tip to wall corner. A schematic of the solutions for the streamwise and crossflow are shown in Figure 4.1-4(a). The crossflow *similar solution* on the plane of symmetry is shown to have a maximum velocity some distance out of the corner. The scaling applied is a Reynolds Number based on downstream distance. This result is particularly informative as it indicates a local maximum of outward velocity, some distance from the corner, is necessary to satisfy continuity and a no slip condition on the walls. Using Barclay's Reynolds Number scaling, Bhargava et al.'s (1987) minimum locus position scales to a non-dimensional value of 13.2 at the chordal distance. This seems to be in reasonable agreement with Barclay's non-dimensional value of 8, considering the differences between the analysis and the experiment. An analytical solution for the minimum line is given by

$$x = 4z(2\mu/\rho W_t)^{0.5}$$

and is compared with the present experimental data in Fig.4.1-4(b). The predicted minimum locus lies closer to the blade than the measured locus, however, once again the method does not account for wall motion.

Pressure Minimum Location - Other Experimental Data The location of the pressure minimum away from the blade surface appears to be due to pressure gradient of the gap shear layer (moving in the opposite direction to the blade motion) interacting with the blade-to-blade pressure gradient distribution. A similar trend is evident in the *low speed* measurements of Cat (1977, Figs. 30-31) where the pressure maximum to minimum spacing was substantially wider than the blade thickness 14% of chord upstream of the blade leading edge. Cat's pressure transducer and cavity seem to have exhibited severe resonance when the sensor was placed under the blade at 2, 50 and 67% of chord. If a mean line is faired through the "ringing" in Figs. 32-34, Cat's data are in reasonable agreement with the present observations. A pressure minimum and basin structure can be seen sitting off the suction side. Wall pressure data from a *high*

speed turbine and compressor are given respectively by Heinemann (1985)[64] and Reid (1987)[65]. Their data are shown in Figure 4.1-5(a). Both show the separation of the maximum to minimum pressure values in the passage substantially exceed the blade thickness.

From consideration of these results, it appears that there is both an experimental and analytical basis for a local low pressure to be present in the suction side corner, with or without a clearance leakage, and the thin layer of clearance shear flow may simply issue into this region and adjust itself to the corner condition. The blade-to-blade pressure gradient would then change accordingly. The pressure loading on the blade surface will largely reflect the tip shear layer pressure condition at the blade edge and be unresponsive to conditions in the passage.

4.1.1.3 The Interaction of Relative Leakage, Incidence and Camber

The shear layer produced by the relative flow leakage also permitted interpretation of several other observations about the data.

Camber Analysis of the present measurements in terms of mass addition to or extraction from the throughflow, on each side of the tip gap, was not consistent with the *blade edge pressure* data observed (particularly with the pressure rise on the suction side).[66] Rather, the pressure gradient in the gap, balancing the wall velocity, seems to alter when the gap size changes and this change modifies the suction side pressure. This change has a similar effect on the flow to that of blade camber. A camber correlation might provide an alternative method of incorporating the effects of gap size into a design system. However, due to the lack of a strong physical basis for such a correlation it has not been pursued in the present work.

Pressure Minimum Level Constant It was noted in the experimental results that the peak suction side minimum pressure occurred off the blade and remained almost constant for all the tests conducted. The constancy of this pressure, relative to the far field pressure (ambient) and the passage average at the same axial position is shown in Figs. 3.6-3(c) and 3.7-3(c). The measurements suggest the pressure is determined solely by passage (rather than tip local) geometry, wheel speed and far field conditions. In terms of the discussion so far, the constancy of this pressure is a most

---

[64] Heinemann's (1985) turbine speeds were not given but axial Mach Numbers were 0.5, 1.0 and 1.3. The blade edge spacing was 21.6% of pitch while the nominal spacing of pressure maximum to minimum was 29-36% pitch. Heinemann used 5 different types of probe screens and cavities over the pressure transducer in an attempt to reconcile the noted edge location or spacing problem. Measured results were roughly the same in each case. The blade edge position was not correlated with the pressure in his data so he was primarily concerned with the excessive width of the blade. Using the present arguments, the pressure gradient interaction would occur on the *pressure side* of a turbine section. In this case the pressure decreases across the passage, then decreases further in the gap due to the shear layer and then depresses the pressure side rise until some distance further into the passage. In a turbine the pressure maximum would be displaced from the pressure side. Heinemann's data are in reasonable agreement with such a hypothesis.

[65] Reid's (1987) data are for a 11,500 RPM rotor speed. The tangential spacing of pressure maximum to minimum was 19 to 21% of pitch. Tip section profile data was not available, however, this amount of the spacing requires an extremely thick tip profile (when laid out at high stagger) to match the blade edges to the pressure peaks. The data shows the pressure minimum off the blade for any reasonable section thickness.

[66] Considerations of the effect of increased leakage under the tip on the blade edge velocities suggested the leakage could be construed to point the tip profile at higher stagger into the flow and hence lower the incidence and unload the blade. This would raise suction side pressure. The main problem with this argument was reconciling the constancy of the passage pressure minimum to maximum at the wall with such a correction.

perplexing aspect of the measurements.[67] The strong similarity of the apparent dependence with the parameters of the term ($R\tau_w/\mu U_t$) which yields the *WS* factor should be noted.[68] Another consideration is the ability of the case wall boundary layer to communicate far field pressure levels. As the near wall fluid is stagnant over large surface areas in the absolute frame, back pressure can be communicated upstream on the case walls and interact with the throughflow.[69] At this time the consistency of the peak minimum value over a wide range of conditions is unresolved. It is clear, however, that interpretation of C_p distribution data could be misleading in interpreting the physical situation. For example, the C_p distributions based on an arbitrary reference value in Fig. 3.6-3(c) would suggest the peak pressure minimum on the suction side changes with incidence. In fact, the pressures redistribute relative to a minimum which seems to be fixed by the system boundary conditions rather than a throughflow pressure. The redistribution of the pressures is shown in Figure 4.1-5(b).

Spanwise (Passage Average) Incidence The peak minimum pressure's constancy seems to be a common factor in the behavior of clearance changes and tip local (rather than passage average) incidence changes at high incidence. But in general, flow pattern changes with clearance change *did not seem to be especially sensitive to* flow coefficient changes. This indicates that the tip local flow had low sensitivity to *passage average blade incidence* at the small clearances tested. Engeda et al. (1988, p. 3 and Fig. 3), commenting on results of Huerlimann suggest a high dependence on flow incidence is "hinted at" due to the drastic changes in blade loading with clearance change. The present test results would plot in a very similar manner to Huerlimann's data as presented by Engeda et al. However, in terms of a mechanism, the loading change is traced to a force equilibration in the gap shear layer rather than incidence change. Cross-correlating the data in this manner is of some utility, however, and permits one to be aware that so much clearance change has about the same effect as so much incidence change. A similar *quid pro quo* is the basis of a correlation with the camber, as was discussed above. But, neither seem to have a strong physical connection with the mechanisms of loading change.

---

[67] The measurement system behavior was scrutinized to ensure the observations were not a measurement error. The peak minimum pressure value is an ensemble average and the system tracked much lower pressure excursions with good fidelity.

[68] The term in question, however, is derived in the context of a pressure datum, i.e. it is a gradient. In this situation the datum itself is the issue and might be thought of as the constant of integration for the gradient. So while there appears to be some relationship, the information is not suited to correlation.

[69] This prospect has to be contemplated seriously due to the demonstrated ability of modifications on the exit diffuser walls to modify flow yaw angle stability in the test section inlet.

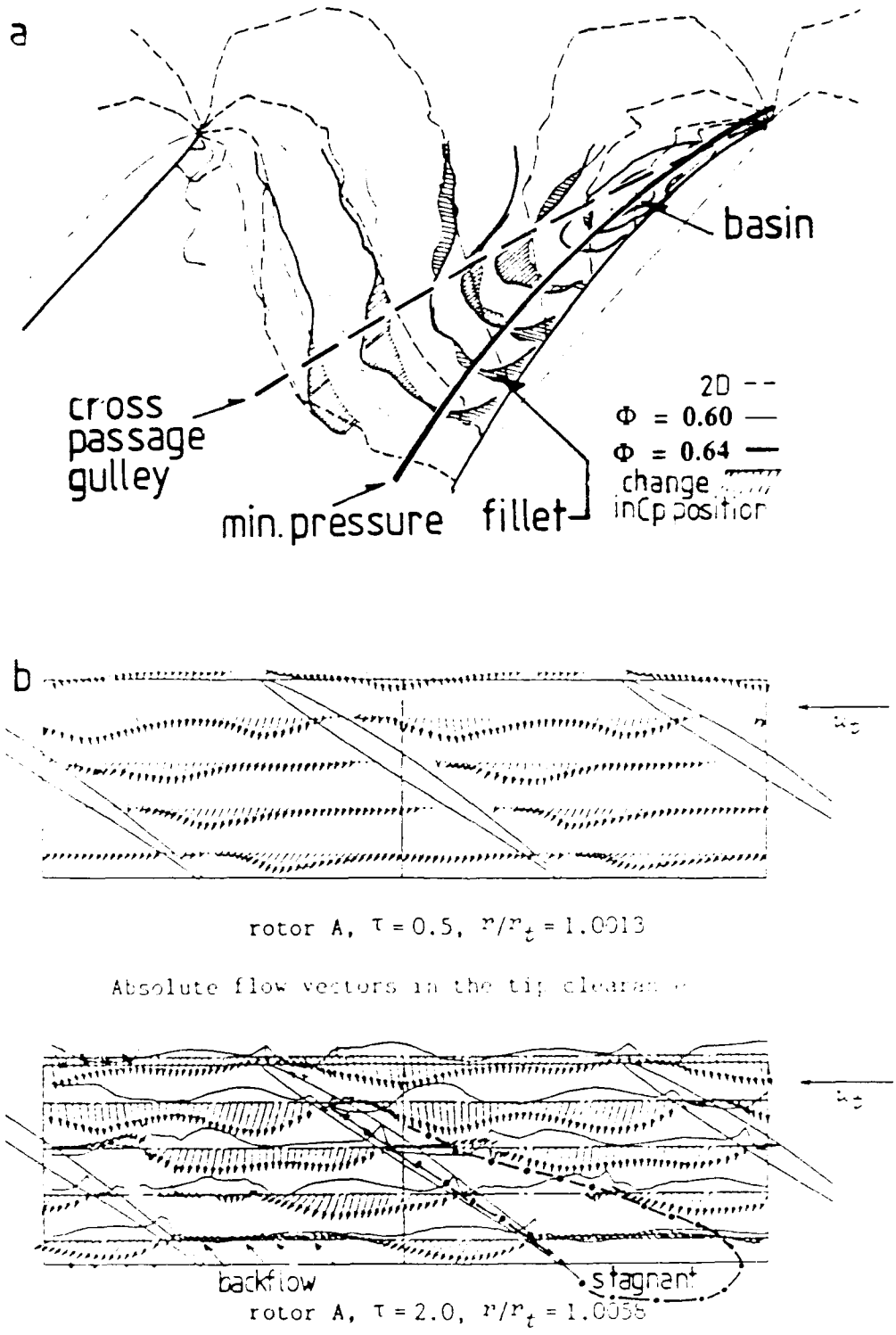

Fig. 4.1-1 (a) Schematic of the regions of flow in the passage (b) Inoue and Kuroumaru's (1988, Fig. 7) velocity survey data near the wall showing stagnant flow on suction-side.

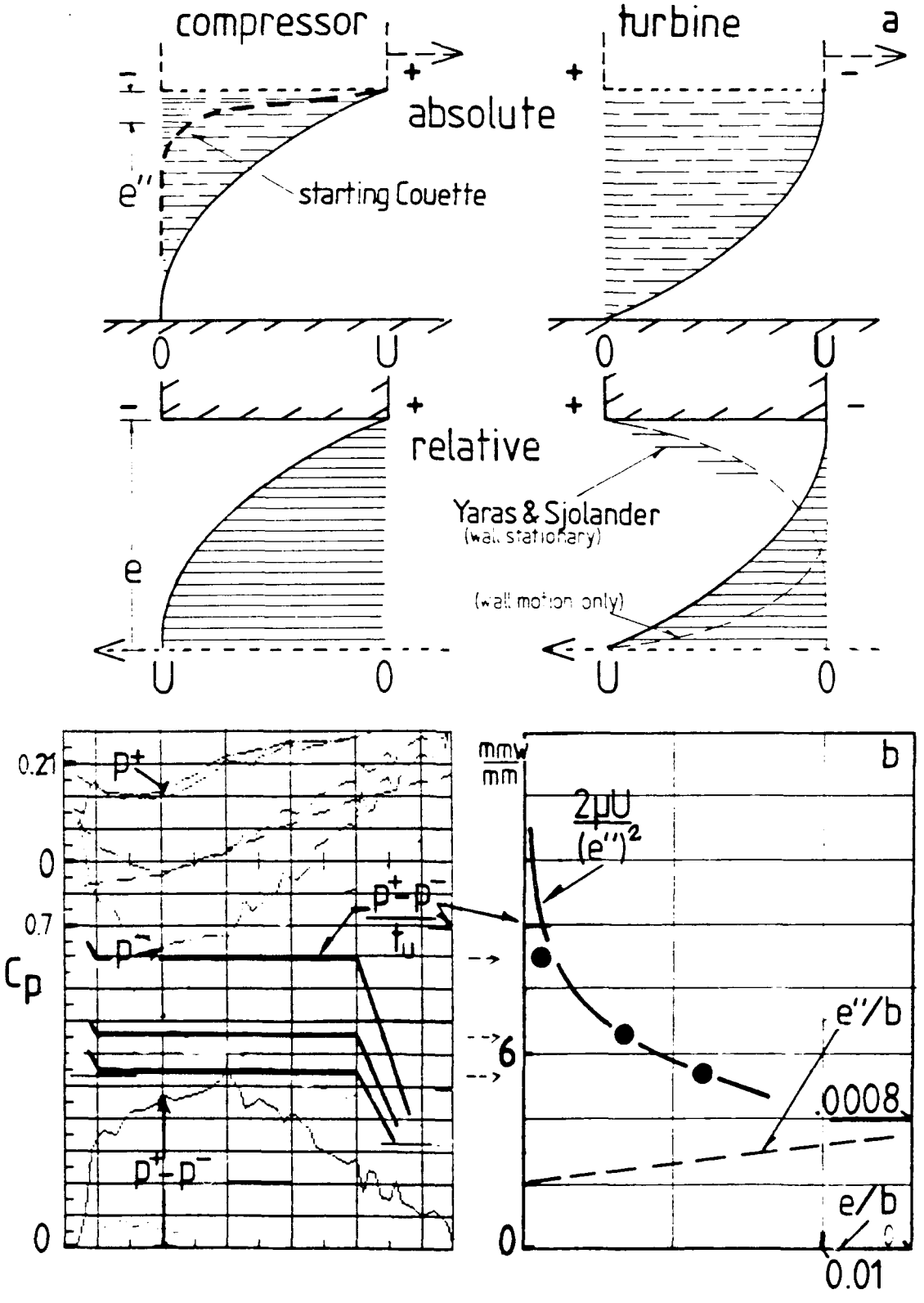

Fig. 4.1-2 (a) Couette flow solutions from Schlichting (1955, p. 61) showing the flow situation for compressors and turbines (b) Comparison of experimental pressure gradients with analytical results. *Note that the pressure difference between the blade edges divided by the tangential thickness (i.e., dp/dx') is a constant over the axial chord, but the constant value varies with clearance e.*

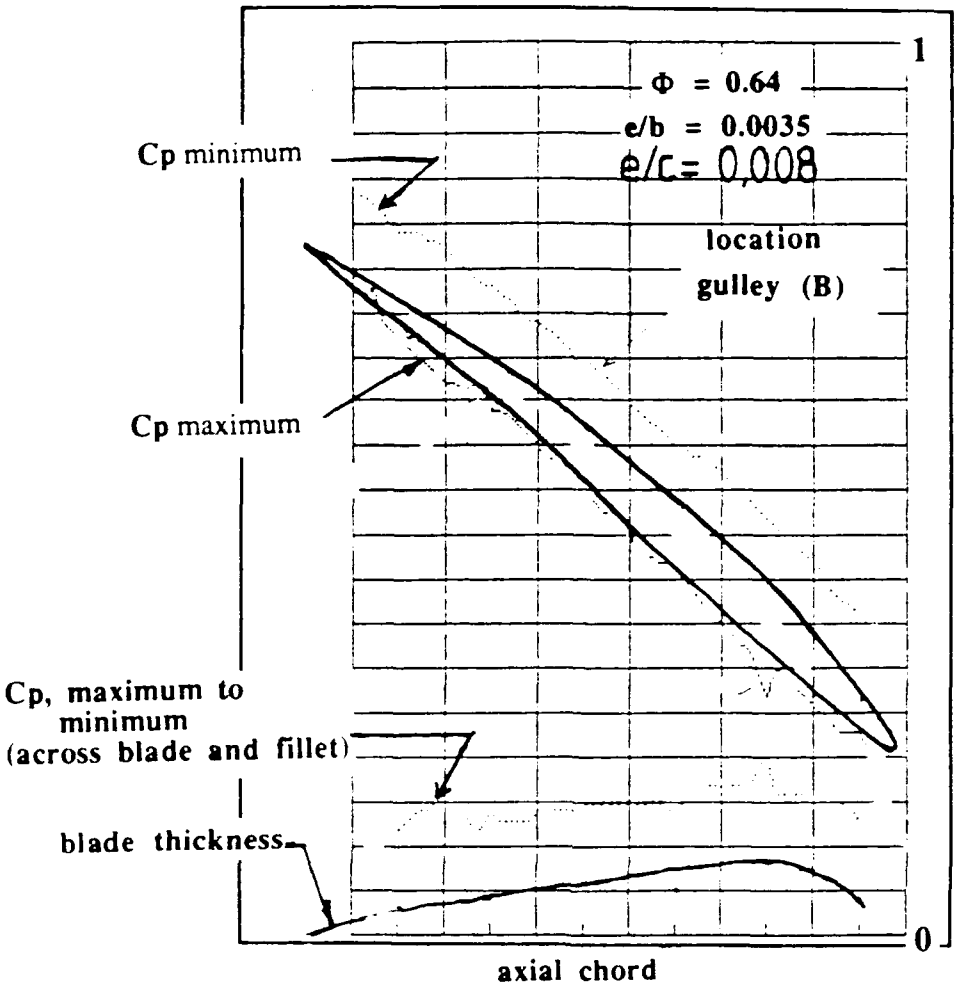

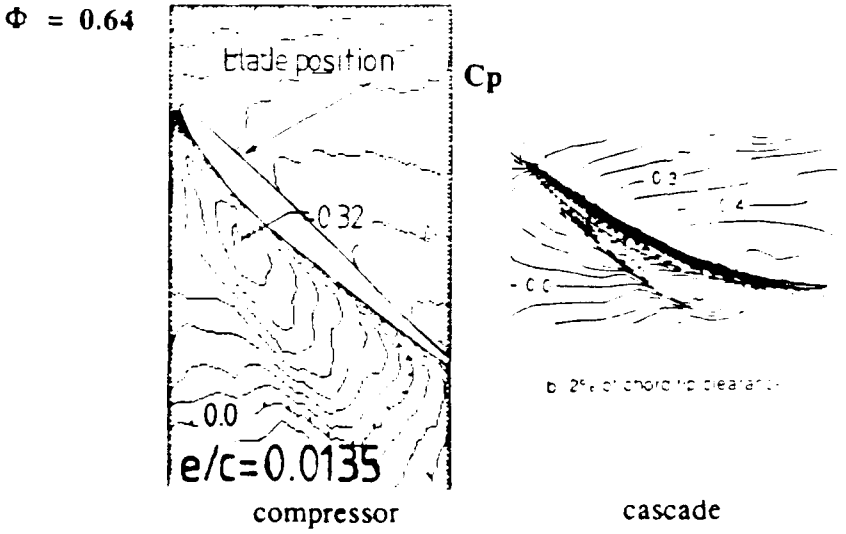

Fig. 4.1-2(c) Position of locus of minimum pressure (at any axial station) relative to the blade in the passage and comparison of the spacing between minimum and maximum pressure locii to the tangential thickness of the blade. Cascade data of Storer and Cumpsty (1991) are shown for comparison.

a

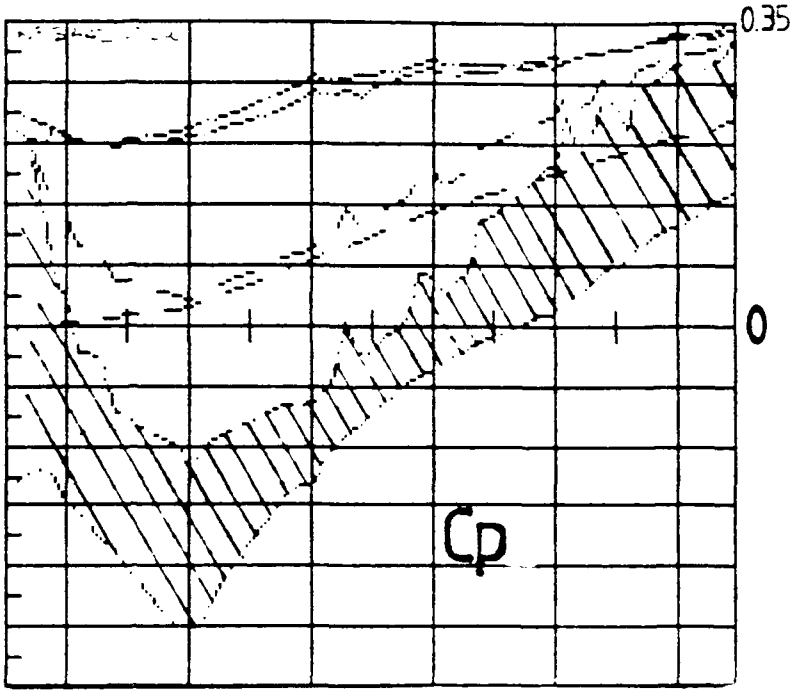

b

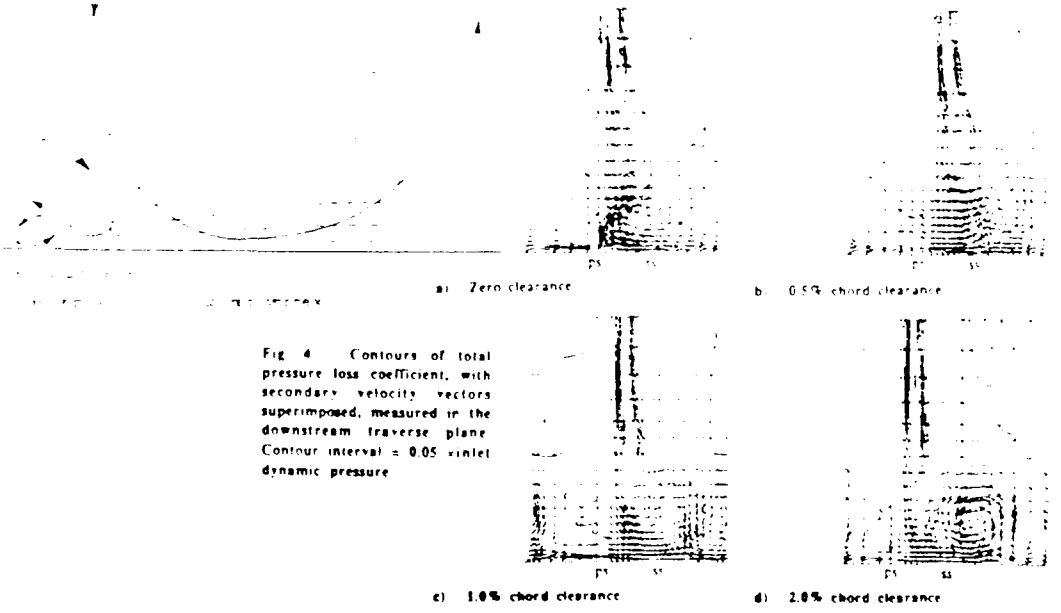

Fig. 4 Contours of total pressure loss coefficient, with secondary velocity vectors superimposed, measured in the downstream traverse plane. Contour interval = 0.05 xinlet dynamic pressure

Fig. 4.1-3 (a) Pressure mismatch between flow in gap and flow in passage. (b) Schematics of corner circulations from Hararika and Raj (1987) and Storer (1989, Fig. 4).

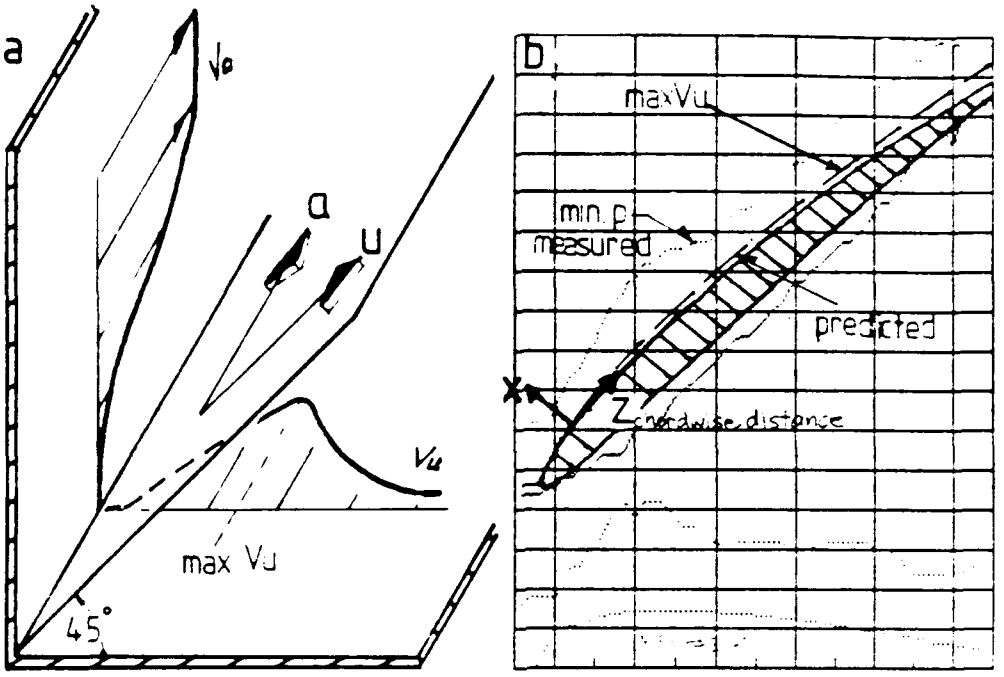

Fig. 4.1-4 (a) Schematic of velocity profiles of Barclay (1982) for flow in a streamwise corner (b) Comparison of locus of outward flow from Barclay with minimum pressure line in compressor.

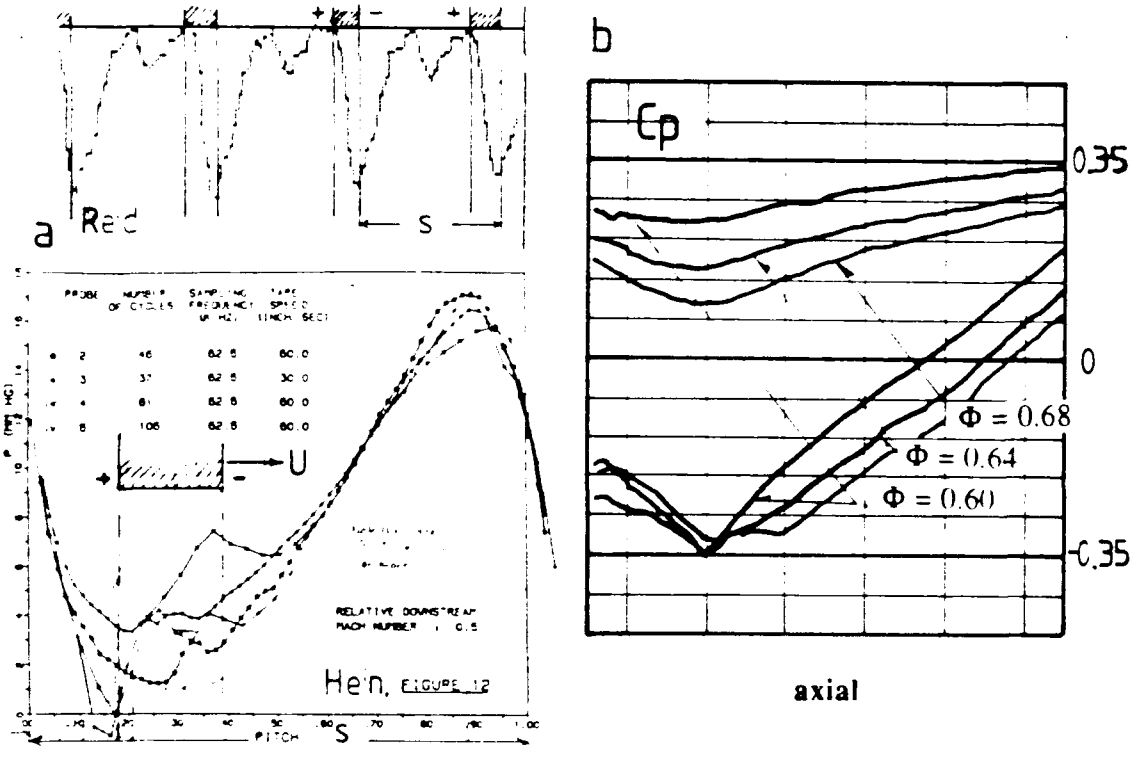

Fig. 4.1-5 (a) Minimum pressure line locations in data of Heinemann (1985) and Reid (1987) (b) Change in pressure distributions relative to far field pressure datum with incidence.

4.1.2 The Passage Flow

In contrast to the behavior of the region between the blade suction side and the minimum pressure locus, the passage side of the pattern's behavior was basically consistent with the passage average incidence condition and resembled two-dimensional cascade flow in character. The main differences were observed near the leading edge around the basin region and along the diagonal cross passage gully.

4.1.2.1 Net Circulation of Blade Tip, Clearance and Wall Flow

The ensemble average pressure measurements in this program were repeatable to an extremely high level of detail in the pressure traces. Small ripples in the traces repeated spatially to within 2 to 3 hundredths of pitch and to less than 2.5% levels in amplitude for the same passage. The confidence in the location of the blade, the minimum etc. is quite high in the tangential direction. The observations consistently locate the pressure minimum about 0.1 of pitch away from the suction side of the blade. The blade tangential thickness is about 0.1 of pitch at maximum thickness. For the balance of the spacing (0.8) the pressure monotonically increases with various notches and ripples until just before the pressure side (0.03 of pitch). This means that roughly 0.77/0.90 = 0.85 of the passage is approximating the cascade conditions.[70]

Calculated distributions of the blade loading from the two-dimensional solution showed reasonable agreement with the pressure minimum to maximum levels (measured from the minimum line or locus to the pressure-side blade edge) of the passage. The calculated loadings and the corresponding test data are compared in Figure 4.1-6(a). Allowing for the pressure relief at the leading edge on the suction side, grid sensitivity and similar computational concerns, the computations predict what the blade loading should be (for a zero clearance condition). A comparison of measured blade edge pressures to those of the two dimensional prediction shows (Figure 4.1-6(b)) that the pressure across the blade, however, is significantly lower than predicted. In this case pressure-side magnitudes were in reasonable agreement between the calculation and data, but the measured suction side pressures are higher than predicted. *From this comparison it would seem, to a first order, that the two-dimensional cascade circulation effectively acts some distance off the blade suction surface (i.e., around the blade and fillet).* This phenomenon suggests, in the context of the clearance vortex models, in the literature, that the clearance is not changing the two-dimensional circulation around the blade end, but rather altering the amount or proportion of the tip passage flow experiencing it.[71]

These results should be noted in the context of the ratio of shed circulation to bound circulation of a cascade blade determined by Yaras et al. (1991, Part II, Fig. 4) as a function of tip gap and wall speed. Their measurements were made in relatively low turning turbine cascade with a moving wall. Motion of the wall relative to the blade reduced the circulation detected in the passage at zero speed by 65%, at engine equivalent speeds, for a clearance of e/c = 0.025. The overall effect was an observed shed circulation to bound circulation ratio of 0.15 for that clearance and speed combination. That is, 85% of the bound circulation was not detected in the downstream flow. Although the wall motion was toward the pressure side (i.e., a

[70] Perceiving the flow field in this manner suggests formulating models in terms of blade spacing. Such an approach was taken by Smith (1970), where a staggered spacing was introduced to normalize the clearance dimension in accounting for flow changes with clearance.

[71] Correlating of blade lift fall-off, based on surface pressure distributions, with circulation shedding at the tip does not seem to be supported by the present measurements. The blade surface is not sensing the full circulative effect of the blading and tip flow on the passage throughflow.

turbine), the results resemble those of the present study. Their results show that the circulation retained at the tip (based on measurements down stream of the cascade, Part II, Fig. 4) increased, while the blade loading decreased (based on blade measurements, Part I, Fig 10), as wall speeds were increased.

4.1.2.2 Corner Separation and the Basin

Corner Separation When compared to the two-dimensional solution, a consistent feature of the suction side pressure distribution is the relief of pressure near the leading edge. As this location on the suction side corresponds to the minimum pressure of the two-dimensional distribution, it is also the location of maximum under-expansion of the *relative* leakage flow. That is, the difference between the pressure of the gap pressure gradient acting over a short tangential thickness and the passage two-dimensional blade-to-blade minimum pressure value will be large (Fig. 4.1-6(b)). At the same location the incidence condition will be extreme (due to the almost tangential relative velocity) and the low development length Reynolds Number on the blade will favor a 3-D separation following Barclay's analysis of flow in a streamwise corner. With the potential for either radially inward flow (toward the lower pressure inboard on the span) or flow outward on the plane of symmetry (3-D separation) or tangential flow in the wall motion direction, it is most likely there is a wedge of recirculating flow in the corner contributing to the pressure relief. The competing corner separation flows are presented schematically in Figure 4.1-7.

Similar observations are made in an experimental and computational study of the suction side corner separation conducted by Goto (1991) in a mixed flow impeller. Computational cases shown in his paper (Fig. A.1 and A.2) for the leading edge region with a small clearance show reversed flow (i.e., flow moving forward along the casing) consistent with a flow separation in the corner region. Goto attributes substantial thickening of the case wall boundary layer to these reverse flows which (he states, p. 9) are induced by the tip leakage.

The shearing conditions in the corner correspond with the *WS* derivation of Sec. 2.2 if the wall shear factor is considered to represent the ratio of tangential to axial shear. In the corner this ratio likely to be extreme. The situation is also consistent with the description developed by Chen et al. (1988) for vortex filament generation and its direction on the suction side. They argue that a separation bubble situated in the leading edge suction corner initiates or promotes experimental observations of the vortex development. Their description was shown to be related to the *WS* factor derived in Sec. 2.2 by the analysis of Sec. 2.2.3. It is clear these considerations and their correlation potential become more important near stall. In the present discussion, they largely aid in understanding the flow pattern. Previous discussion has indicated the losses involved in a vortex filament motion are probably small. The major work changes seem to be related to the pressure loading.

Low Pressure Basin Centered in the basin, the lowest pressure's downstream location may therefore be thought of as pressure relief of what would otherwise be a lower pressure upstream. As incidence increases, the low pressure basin region seems to "flow" upstream into the leading edge corner. However, the center of the low pressure basin is consistent with a constant pressure gradient in the gap acting over the tip tangential thickness; i.e., where the blade is thickest, the edge pressure is lowest. If the suction-side edge pressure is inversely proportional to the tangential thickness, the pressure basin position should correspond to the maximum tangential thickness. The basin position data confirm this reasoning. Pursuing this line of thinking, the proportion of over and under pressure matching should change along the blade with clearance change and the basin bowl would tend to move aft with increasing clearance.

This trend is best demonstrated in Fig. 3.7-4(b) and is shown schematically in Fig. 4.1-6(b).

Yaras et al. (1989, Figs. 7 and 8) show blade loading and the case wall pressure patterns for a turbine cascade with a stationary wall. There is a strong similarity in both suction side pressure distribution relief at the leading edge and in the presence of a low pressure basin on the case wall near the blade maximum thickness. Unlike the present compressor data, their basin lies almost wholly in the gap (i.e., under the blade)[72] and the minimum pressure locus, while passing through the basin, moves away from the suction side when it passes out into the passage. Storer and Cumpsty (1990, Fig. 4) show similar results (i.e., a pressure basin under the blade with minimum pressure at the suction edge, Fig. 4.1-2(c)) in a large scale compressor cascade and also calculate the same flowfield with a Navier-Stokes code. Inoue and Kuroumaru's (1988, Fig. 8) measurements show the basin moving aft, while always including maximum tangential thickness for all cases except the largest clearance case (e/b = 0.056). At this clearance condition the whole pressure pattern alters, suggesting a major change in flow structure.[73] The largest clearance case measured where the pattern (observed in the present study) persists in their data was at e/b = 0.034. This suggests the present data have a practical range of implementation.

4.1.2.3 Cross Passage Pressure Gully (Vortex Filament)

The cross passage gully behavior did not seem to be consistent with a passage vortex. In a rotor, the resultant net secondary flow would be expected to depend on, at least, wheel speed, turning and boundary layer properties. The cross passage gully formation, on the other hand, seems to be only mildly affected by turning and appears to be primarily a consequence of the corner condition near the leading edge.[74]

The exit to the cross passage gully region of the passage has been examined in great detail by Lakshminarayana, Zaccaria and Marathe (1991). They conducted surveys at 4% and 64% of chord downstream of a rotor of a single stage with inlet guide vanes (at $\Phi = 0.51$) using a miniature five hole probe in the tip region. This probe provided radial velocity components near the case wall. Surveys were conducted from 0.9 to 0.9925 of radius (i.e., radially inward from e/b = 0.015). These measurements led the authors to conclude a strong shear layer interaction occurs as the relative leakage flow traverses the passage case wall. They concluded (p. 4) that there was no evidence of a vortex in the location where high losses were identified (Fig. 20). They state (p.11) that,

---

[72] See footnote to Eqn 4(3) regarding suction pressure estimation.

[73] The condition also corresponds to a high curvature condition for the clearance flow as discussed in Sec A 1 1. The tangential distance from the blade tip to the curved wall divided by gap height (L/e) in this case approaches 8.

[74] Graham's (1985) water tunnel visualizations and data in a turbine cascade with a moving wall provide another simulation to examine in terms of vorticity due to the tunnels spanwise pressure gradient approximating the centrifugal field in the passage. The e/b = 0.006 case with the end wall stationary is the closest case to the present compressor test range (e/b = 0.006). This case shows the *lowest* ratio of tip divided by mid span loading for all the stationary clearances examined, including a sealed tip (Fig. 20), and marks the onset of clearance vortex formation (Fig. 19) in the passage. The Cp distribution (Fig. 14) bears a resemblance to the present compressor data, allowing for the acceleration in the cascade. In the figures presented, there does not seem to be distinct evidence of a cross passage vortex coming off the tip for Graham's "thin" blade section at small clearances. Translating these observations, in a high turning and accelerating cascade, to the compressor situation is hard to justify, beyond noting that any vortex is weak to non-existent at a similar test condition.

"The leakage flow emanating from the gap travels farther into the passage, mixing with the mainstream closer to the pressure surface. This sets up substantial radial outward flow near the suction surface as well as near the interaction region. ... This is contrary to the phenomena observed in cascades, where the vortex tends to roll up near the suction side, causing considerable losses and flow separation."

The angle of the initial and very visible low pressure region of the gully in the compressor varies slightly in position and angle with changing incidence, Fig. 3.6-6. Beyond the initial extension the gully tends to move around as if the flow above the gully is detached. The overall impression is that the gully reflects a vortex filament starting at the corner separation, partially crossing the passage and stretching close to the wall and then lifting away.[75]

The gully moves forward in the passage with stator relative position corresponding to high incidence and large bulges of the minimum pressure locus into the passage occur at this condition. This seems to be consistent with Chen et al.'s (1988) arguments discussed previously. The observable intensifying of the gully near maximum blade tangential thickness as clearance increases (Fig. 3.7-3(a)) seems to be due to conditions changing at the leading edge rather than the result of *relative* leakage further downstream along the suction side. The gully peters out rather than strengthening as the accumulated leakage (mixing-out) increases.

4.1.2.4 Effect of Upstream Stator Flow

If the pressure traces representing the blade-to-blade relative pressure field are compared for all the different stator relative positions along the stator suction side, the flow has a pulsatile character. The chordwise pressure difference, between the basin starting position and the trailing edge, fluctuates nearly 33% of the nominal dynamic pressure (q) in the passage. Most of this change takes place on the leading side of the basin. Changes in the region from the minimum locus to the pressure side are much smaller in terms of passage q. This difference can be correlated quite directly with the expected behavior of a non-uniform flow (blade-to-blade) passing from the stator into the rotor. The pressure changes are shown using a test case in Figure 4.1-8. For the condition near the design *passage average* incidence, the clearance flow is minimally affected by the pulsating suction-side pressure field (see Fig. 3.7-1(b)). *This is a confirmation, to some extent, of the argument (of Chen et al. (1988)) that pressure driven leakage is not a significant factor in the tip gap flow at small clearances.* The situation at higher passage average incidence (Fig. 3.7-1(a)) is not so straightforward. This contour pattern shows a new flow mode developing and should be explored further.[76]

The general conclusion reached from the stator relative measurements was that the suction side flow underwent chordwise pressure gradient changes and that these cyclic excursions had minimal effect on the tip clearance flow (at throughflows above peak power). In terms of losses, however, the situation is less clear. It seems a more or less stable *relative* leakage condition along the chord is interacting with a pressure gradient varying cyclically along the chord. This suggests the flow velocity (W) is cyclically varying above the *relative* leakage, particularly above the basin.

---

[75] Inoue and Kuroumaru (1988) show this vortex filament strengthening with increasing clearance in their measurements

[76] It should be recalled from Sec. 3.2.1 that the stator solidity is 0.62 (i.e. low) at the case wall and the blade inter-row spacing is not large. How to interpret the pattern changes in 3.7-1(a) is not clear with the data on hand. Further measurements are needed to define the flow situation. As the flow condition is approaching stall, additional measurements were not pursued in this study

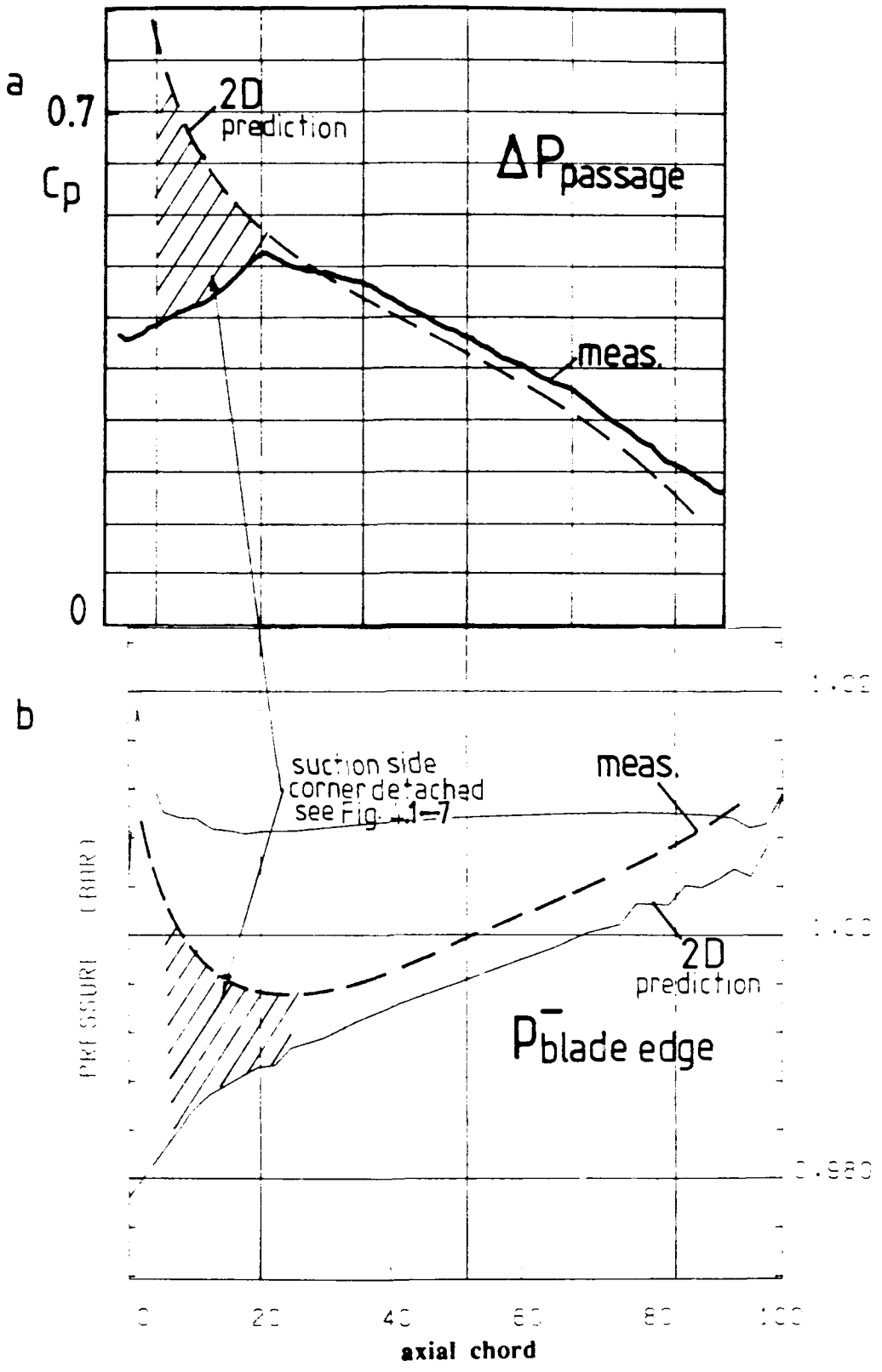

Fig. 4.1-6 (a) Comparison of predicted (Q3D, App. B.7) two-dimensional blade loading and the measured minimum to maximum pressure difference in the passage. (b) Comparison of the measured suction side pressure level compared to the Q3D prediction. The suction side pressure is higher than predicted.

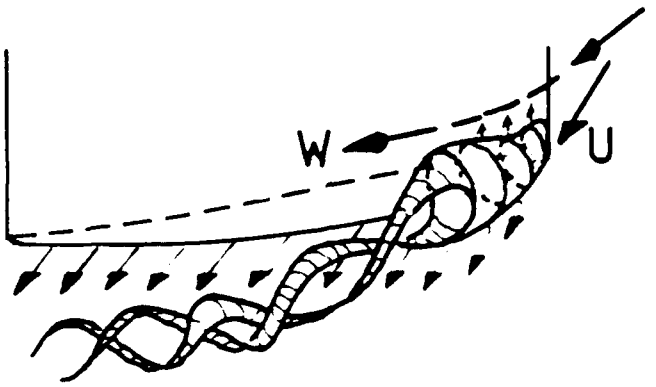

Fig. 4.1-7 Schematic of the corner separation and vortex filament shedding from the corner separation based on the present results. The behavior strongly resembles that shown by Goto (1991) in computations of the flow in the leading edge corner of a mixed flow impeller.

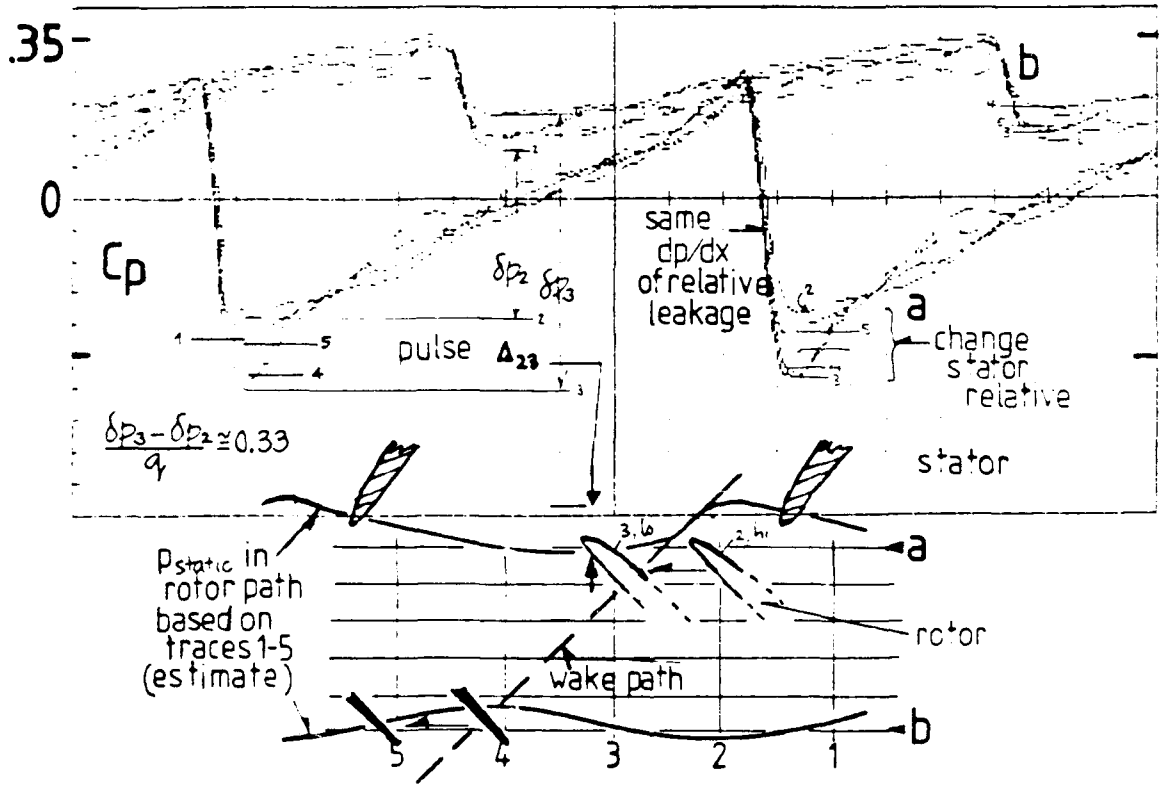

Fig. 4.1-8 Pressure pulsations on the suction side of the blade and interaction with the *relative* leakage.

4.2 Stage Flow

The preceding section focussed on the details of the flow structure in the tip and wall corner region of the passage. This region of the flow is the main concern in terms of mechanism identification for tip clearance loss. To complete the discussion, the corner flow details are considered in the context of the stage and its performance. It should be noted that the results in this study were generated in an embedded stage.

Embedded vs. Isolated Rotor Flow The visualization results indicated the presence of a second rotor eliminates a trailing edge corner separation in the first stage stator at the case wall. The separation seem to occur in the stator unless it is followed by a rotor. The presence of a second rotor also seems to force the flow to more nearly approximate the design conditions in terms of *passage average* distributions. Consideration of the results should recognize that the measured flow was a reasonable approximation to the design flow, which was developed from a strip theory. The losses, however, were larger than predicted by the design method.

4.2.2 Efficiency Decrement Predictions

The result of a clearance change from e/b = 0.0035 to e/b = 0.006, in terms of blade surface pressure loading at the tip shown in Figs. 3.5-2 and 3.5-3, has a very small impact on the two stage efficiency. This is not consistent with the projected efficiency change for a small clearance increment at a small clearance level (Sec. 2.1). The efficiency change at constant power is expected to be large, see Figure 4.2-1. The change observed in the efficiency was consistent with the detailed pressure measurements, i.e., the input power (blade tip loading) decreased while the passage circulation and flow rate remained relatively constant. This suggests the power input reduction was offset by increased losses. If the losses continue to increase as clearance increases they will begin to overtake the tip unloading which is reducing the power input in the present data. It can be seen in the e/b = 0.006 case of Fig. 3.7-3(b) and -4(b) that there is not much tip unloading left to be exploited, i.e., the suction edge pressure will increase to the pressure edge value. After this crossover the efficiency would be expected to decline.

It is doubtful in the present case that this situation can be construed as evidence of an optimum clearance condition that might exist in all compressors. While Storer (1989) observes a similar "optimum" clearance in his cantilevered stator testing using mixed out losses, the present author is somewhat wary of claiming optimum conditions. The present behavior might be argued to be more like a deadband at small clearances. The reasons for this proposition include (a) the trend of all the low speed compressors to droop to lower efficiency sensitivity at small clearances (see Fig. 2.1-5) (b) the large spanwise losses across the outer span in this compressor and its relatively low stage efficiency[77] and (c) its symmetric velocity diagram which unloads the tip. That is to say, whereas the rapid decrease in Inoue's free vortex rotor efficiency is consistent with higher loading at the tip, the present symmetric stage has a lower loading and a correspondingly smaller under expansion mismatch at the tip.

In principle, the correlation developed in Sec. 2.1 was indicative of the tip loss trend rather than a prediction tool. It is the present authors impression the trend found by

---

[77] The situation might be put in the context of the clearance change not making a bad compressor worse. See comments of Sec. A.1.4 regarding initial level of efficiency. It should be noted that negligible efficiency changes for small clearance changes has been detected previously. Robinson (1982, Figs. 16-17 Compressor B) shows such behavior in a high speed six stage machine at full and part speed.

that method is still a valid indication of the loss development process over a wide range of clearance.

4.2.2 Prospects For Stage Performance Improvement

The prospects for improved stage performance, based on the results of the present study, are summarized below. Schematics of the design changes discussed are shown in Figure 4.2-2.

End Wall Section Profile Design A profile design approach can be formulated for the tip section based on the present study results. Under conditions of constant chordwise clearance, increasing the thickness distribution at the tip could reduce losses by minimizing pressure mismatch between the passage design requirement (two-dimensional strip theory) and the gap flow conditions, Eqn. 4(5). Increased thickness would, on the other hand, lower suction side pressure. However there is possibly a benefit in searching for a better matching. Thickening the blade only near the leading edge to extend gap pressure gradient and lower suction-side edge pressure may have a pay-off by simply reducing the pressure relief in the tip corner.

Improved Performance by Case Wall Geometry Design A wavy shape, contour or trench on the wall in the axial direction would have similar consequences to varying thickness. The trend suggested by the experimental data is to reduce the clearance in order to lower suction side pressure for a fixed section profile. This is obviously mechanically undesirable, however, trenches and slots are known to produce this type of effect. Wisler and Beacher (1986) detected a slight performance improvement using a line-on-line blade tip over a sloped trench which deepened toward the leading edge. Applying the present gap gradient results; this would unload the forward part of the blade and load up the aft of the section (for a given tip profile thickness distribution). Their flow is somewhat different, however, due to the rearward facing step down into the trench. This step should lower any shear layer into the trench and alter the separation in the leading edge corner. As has been pointed out previously, knowing what the *desirable* pressure distribution ought to be is a fundamental problem.

There is some potential to contour the wall *circumferentially* to better match pressures in concert with the stator outflow periodicity. But, ripples on the wall would also lead to a time varying clearance with possibly undesirable tone noise. In general the gap flow is likely to be under expanded, which will require a tighter clearance to improve the pressure matching. As the desired trend is toward better matching at larger clearances, circumferential contouring would probably be undesirable.

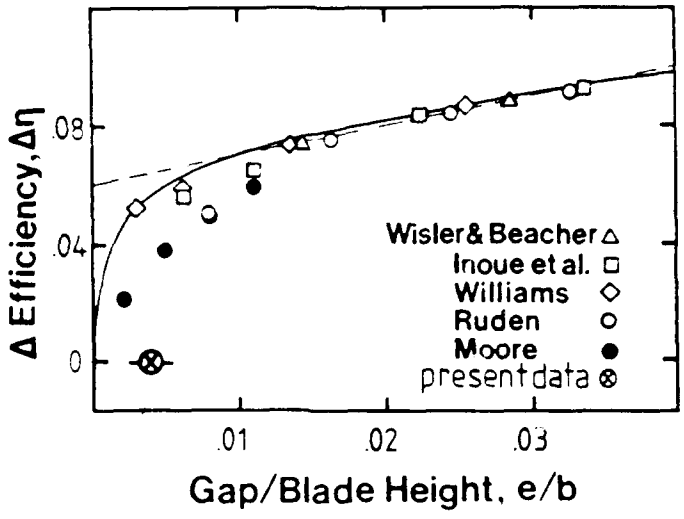

Fig. 4.2-1 Efficiency decrement prediction (of Sec. 2.1) compared to the present experimental results.

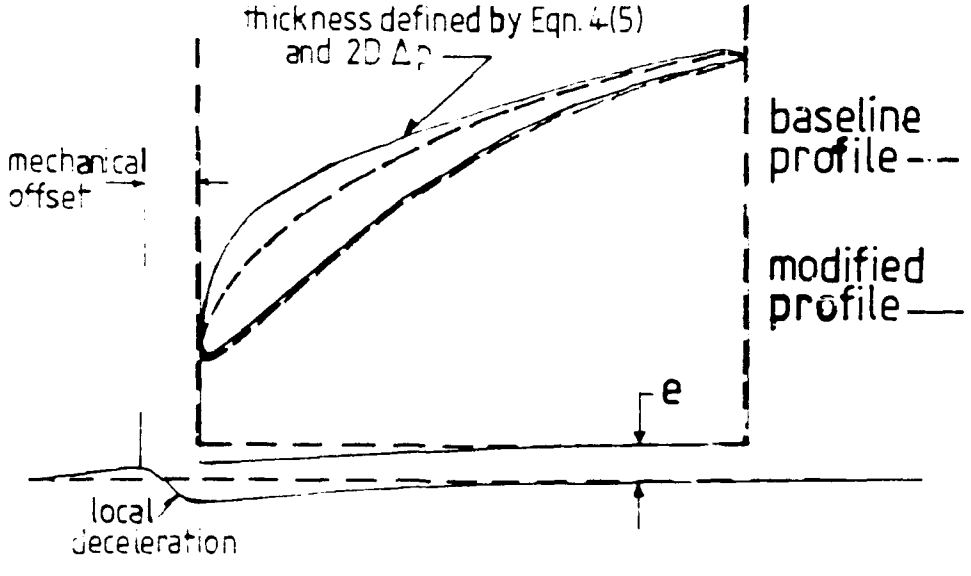

Fig. 4.2-2 Schematic of design modifications to improve performance based on present results.

4.3 Flow Models and Mechanisms

The primary knowledge problem with tip clearance flow, it was argued in Part 1, lies at the mechanism(s) level. Improved resolution of whether (one of) gap leakage, tip local vorticity generation or boundary layer characteristics dominate the entropy production was seen to be required. Alternatively, the means by which they interact or combine to produce inefficiencies needs to be understood more thoroughly before the models can be improved.[78]

In the process of this discussion, the present author has tried to reconcile the experimental and analytical results of this study in a manner which identifies the more promising modelling approaches. Before proceeding to the discussion, some comments on the general picture developed from the experiment and analysis are set out below.

The discussion of the literature of Part 1 posed a number of questions that should be applied to the results of any study. Issues addressed included:

(1) are the experimental results generally applicable and how do they compare to other detailed data,

(2) is new information brought to bear on the mechanism issues raised in past analysis or prior entropy modelling and

(3) do the results lend themselves to incorporation in a strip theory additive loss model.

The results of the analysis and experiments from these particular perspectives are addressed below.

It should be noted throughout that the experimental results gathered in this study are for small clearances, $e/b < 0.006$, compared to typical machinery levels of e/b from 0.015 to 0.025. These data were acquired intentionally because measurements at larger clearances could always be made in future phases of the experiment. Fortunately, some of the small clearance measurements made in the study (to date) can be compared with the small clearance measurements of other researchers who have explored larger clearance ranges. Consequently, questions about the generality of the flow can be addressed with reasonable confidence using the data on hand and previous studies. This approach was taken using Inoue and Kuroumaru's (1988) measurements, which included near wall velocities and wall pressures, made in a highly expanded stage of free vortex design without inlet guide vanes. They measured the flow over a generous clearance range and their data permits flow characteristics, observed to be in common, to be traced to larger clearances. Lakshminarayana et al. (1982 Parts I and II) permit comparisons to be made at one clearance with a solid body stage having inlet guide vanes. Their measurements include pressure distributions on the blade surfaces, close to the tip, and turbulence intensity data in the passage above the wall. Robinson (1982) presents a quantitative analysis of detailed data measured by Anderson at Cambridge and Hunter and Cumpsty (1982) which permits spanwise or passage average information to be considered. These studies

[78] A consideration identified in the Part 1 was the relevance of new information for blade design or machinery optimization. Models based on better understood and defined mechanisms should be additive so 2-D strip theory design or section prediction loss estimation procedures to be of practical utility in stage design.

allow a three dimensional composite to be developed for comparison with the present experimental results.

The data of Inoue and Kuroumaru (1988) show a remarkably similar qualitative pattern of tip-wall flow to the present passage average wall pressure results. The main, and immediately noticeable, dissimilarity lies in the location of the passage pressure minimum gully relative to the blade suction side. The present experimental results show the minimum lying some distance off the suction side. Inoue and Kuroumaru's (1988) data show the pressure minimum lying close to or under the suction side blade edge along the passage, Figure 4.3-1. The patterns are otherwise similar in contour shape and placement. It should be recalled from the analysis in Part 2 that the *WS* factor for the two machines is very different. Table 2.2-1 shows Inoue's stage with a *WS* of 200 compared to the present stage's design *WS* at 1450. Movement of the position of the suction minimum away from the blade suction side in a higher *WS* machine is consistent with a physical interpretation of the *WS* factor (Sec. 2.2).

A most important phenomenon detected in the present experiment, which could not be inferred from Inoue and Kuroumaru's (1988) data or their discussion, is the almost *constant passage pressure difference distribution* or tangential loading on the bulk of the fluid passing through the passage *as clearance changes*. Figures 3.7-3(b) and 3.7-4(b) show a substantial change in blade edge pressure loading (0.28 C_{pu} falling to 0.18 C_{pu} as clearance increases from near zero to e/b = 0.006). The passage loading remains steady, however, at 0.37 to 0.38 C_{pu} (see also Fig. 4.1-5(b)). This implies the blade tip section does not do all of the work on the fluid and it is the blade force plus the wall shearing motion (in the relative frame) that is regulating the pumping (if the gap is small). A corollary to this observation would suggest that major (in a cascade sense) suction side geometry or profile changes or on-tip treatments for the blade would have minimal to slight impact on the pumping performance. This observation may explain Wisler's (1977) performance insensitivity to significant changes of his blade profile at the tip.

A third key point that emerges from the experimental results is the observation that the *pressure level changes due to a clearance change* are uniform with a slight tapering off toward the trailing edge along the blade length, i.e., they do not appear to be much different where tangential loading is greatest, see Fig. 3.7-2(b). The pressure level changes also occur close to the blade and have disappeared, to a large degree, by the distance of the minimum pressure gully away from the suction side. This would suggest the gap is effectively "sealed" (i.e., unresponsive to passage conditions) in terms of *pressure driven* leakage.[79] Chen et al. (1988 p. 4) observed from examination of Inoue's 1986 larger clearance data and other sources that the "sealing of the clearance becomes stronger as the flow rate decreases." While such a trend with flow rate was not detected in the present test results (compare top and bottom panel of Fig. 3.7-2(b)), it was clear that the *higher blade loading regions did not appear to pass more flow than any other chordal region*. The tangential static pressure gradient under the blade decreased in strength, and roughly uniformly, as the clearance was increased and this change has been examined in more detail in Sec. 4.1.1.1 and Figure 4.1-2(b).

In terms of the overall questions being addressed, the following general comments could be made:

---

[79] The difference in pressure loading on the blade between the two clearances in Fig 3.7-2 (b) has an extremely weak correlation with the pressure loading ramp applied to the blade itself. Doubling the pressure loading has negligible effect on the differential in pressure patterns for the two clearances.

General Applicability of Observations The fact that the averaged wall pressure patterns in the *second* stage of this two stage, solid body rotation machine correspond to the patterns observed in Inoue's essentially *"isolated"* free vortex rotor, and the fact that both sets of measurements differ similarly from the predicted two-dimensional blade-to-blade pressure distributions, provides some confidence that the mechanisms observed are generally applicable.[80] The two passages differ mainly in aspect ratio. Inoue has also varied solidity with consistent results, so an experimental basis can be demonstrated to exist, at a detailed level, for assuming a clearance change causes similar flow effects in all passages.[81] The stator relative data from this study suggest (except for the lower flow rate, higher passage average incidence case) that the near wall flow structure is not altered appreciably by stator wakes or a periodic non-uniform inflow condition. This observation provides passage average tip modelling with a much firmer experimental basis for near design conditions than it has had previously.

New Information on Mechanisms The pressure minimum locus' location off the blade for this high *WS* stage and the constant passage tangential loading with changing clearance provide new factors to consider in terms of the identification and modelling of entropy production (see the more detailed discussion following).

In addition, the *stator relative* results at the highest *passage average* incidence case (near peak power) show a very strong cross passage tangential formation starting to develop in the passage at certain stator relative locations. This pattern exhibits behavior qualitatively in character with the description of the inception of incidence driven rotating stall advanced in Chen et al. (1988).[82]

Strip Theory Additive Loss Modelling The well known tip local blade unloading or pressure distribution change associated with a clearance increase needs to be re-examined in the context of the present results. The unloading in pressure is confined to a very narrow zone under and just outside the blade suction side edge in the present data. This result has significant model development potential as the zone of pressure change is a fillet-like region in the suction-side to wall corner. The effect of this flow zone is similar to lowering the blade camber. As camber change can be handled relatively easily in a strip theory design technique there is some potential to model this local flow.

4.3.1 Modelling Losses in the Near Wall Flow Region

If the flow structure identified so far is considered in terms of entropy increase, a mixture of processes can be identified. These can be summarized as follows:

(1) A *relative* leakage flow having a pressure gradient determined by the tip speed and gap size. The relative leakage may be under expanded when compared with the blade-to-blade pressure field further inboard on the blade span when it issues into the passage.

---

[80] Within a context of the parameters identified so far in the analysis of Part 2

[81] This has generally been assumed in most clearance studies due to the general consistency of the observations in linear cascades. This assumption more or less flows over to rotating machines even though their pressure gradients are defined by more variables and therefore are, in the general case, more variable. This point was discussed in Moyle (1981, p 4). In this case the comparison is being made between two sets of detailed measurements. The data are also average in two different senses. One by virtue of an isolated rotor flow and the other by coalescing a series of stator relative pressure patterns into an average.

[82] This aspect of the data has not been pursued further in the present discussion due to the emphasis on efficiency, however the present author suspects it is consistent with a vortex filament nature of the cross passage flow and a coupling between a local incidence change and a clearance change in the leading edge region at the tip.

(2) A fillet region of low total pressure flow, most likely circulating in a horseshoe pattern, situated above the higher velocity *relative* leakage flow along the suction side.

(3) A region of separation in the leading edge suction-side corner which generates a vortex filament seen crossing the passage diagonally.

(4) A cyclic fluctuation in the suction-side chordwise pressure gradient which is most pronounced along the forward part of the basin and resembles a wedge like high pressure zone cycling in the passage.

(5) A apparent displacement of the throughflow away from the suction-side toward the pressure side presumably due to flow deceleration along the suction-side. The displaced flow is acted upon by roughly the same pressure loading calculated for the two-dimensional blade-to-blade loading.

Of these facets of the flow structure, (1)-(4) have the potential to increase the flow entropy. (5) is more of a blockage effect, i.e., the tangential force acts on a lesser proportion of the flow due to the action of (1)-(4).

The prospects of modelling all of these mechanisms and accounting for their entropy increases are not good. Point (1) for example, could be approached by modifying a simple pressure dump momentum balance to include the experimentally observed boundary conditions. Similarly, Point (5) provides a basis for allocating different loss behavior to different section of the passage and calculating the combined entropy increase. Points (2),(3) and (4) above are much more difficult to model.

In the process of reviewing the measurements, one forms an impression that the flow structure is the result of a number of weakly interacting or independent mechanisms whose combination forms a net loss. Efficiency changes involve consideration of the operating point of the stage as well as the losses, and for the test results on hand it appears that blade tip loading falls while passage tip loading remained stable. This would result *increased* efficiency for the stage at constant speed and throughflow. However, if the in-flow losses increased near the tip due to (2)-(4) above, the "pumping" efficiency improvement would be undermined by these increasing losses. The net efficiency observed is thus a combination of several factors. Further unloading of the tip may not be available to offset losses at larger clearances (there is not much tip loading left at the e/b = 0.006 clearance in Fig. 3.7-3/4(b)) and the stage efficiency would be expected to fall off. Storer (1989) observes similar behavior in mixed-out losses for a stator cascade as clearance is increased.

In introducing the analyses of Part 2, it was noted that the equation of motion suggested several sources may produce the total pressure gradients associated with tip clearance losses. As all losses are ultimately frictional in an adiabatic system, where the most dissipation occurs and how the loss is transported or develops needs to be modelled. In this regard the following points could be deduced from the test data.

4.3.3.1 Viscous Dissipation

Frictional losses in gap appear to be relatively small and any shear must have been concentrated on the blade end or blade side of the gap. Although total pressure loss in the *relative* leakage due to a simple pressure dump expansion would be high, the total *relative* leakage flow is approximately 0.006 of total flow for the e/b = 0.006 clearance, i.e., small. This proportion of the loss would grow as clearance increased. The blade end shear would be expected to remain constant with increased clearance.

4.3.3.2 Decay of Streamwise Vorticity

The cross passage gully appears to decay or the related flow moves away from wall with downstream flow. The gully also strengthens with increasing clearance but not intensely. The growth of the cross passage pressure depression and associated tip unloading occur while the efficiency of the compressor improves slightly. This suggests a vortex growth or strengthening (as suggested by the cross passage pressure depression increase) is not in itself a sufficient condition to produce increased inefficiency. A trading off or balance seem to be struck at each clearance level.

4.3.3.3 Unsteady (Pulsative) Effects

In the clearance range tested in the present program the *relative* leakage did not appear to be affected by or coupled to the pulsations (of Fig. 4.1-8) generated by motion relative to the stator. This might not be the case at larger clearances.

4.3.2 Tip Flow Mechanisms

How or whether gap leakage, tip local vorticity generation or boundary layer characteristics produce losses in the tip region has been identified as a major issue in this subject. From and examination of the present experimental data the pressure gradient of the gap due to *relative* leakage and its attendant shear seem to dominate the flow field. Unlike earlier proposals, the leakage is not found to be due to the blade pressure loading forcing flow through the tip gap, but rather the relative motion of blade. Arguments emphasizing tip local vorticity generation based on decreasing tip pressure loading would seem to be a consequence of determining the lift coefficient from the blade surface C_P distribution rather than the effective pressure loading from blade-to-blade noted in these results. A summary schematic of the tip flow mechanisms identified in the present study are shown in Figure 4.3-2.

The influence of the wall boundary layer could not be deduced from the experiments conducted. Inoue commented that the result of changing boundary layer thickness on the near wall tip flow structure was minimal in his experience.[83] However, in the context of boundary layer mechanisms, it should be noted that *boundary layer thickness normalized by spacing* might *correlate* the minimum pressure locus offset quite well, if the minimum pressure locus position were to depend only on boundary layer thickness. However, note that in addition, such a method will work reasonably well if the minimum pressure locus position depends on *WS* because the method involves spacing. This point is worthy of further experimentation.

Other Observations At some clearance level, one can speculate, the *relative* leakage must be large enough to disrupt the circulation of blade outer span extending to the wall or at least disrupt its effect on the passage throughflow. Based on Inoue and Kuroumaru (1988) this would seem to occur at e/b > 0.035. This e/b level is at the upper end of practical interest, so the many facets of the flow at the wall which have been discussed in this section are all at play in the range of realistic clearances.

[83] This comment is based on measurements that have not been published to date. The observation is significant in the present work as it supports the proposition that the minimum pressure locus location depends physics modelled by the WS factor rather than boundary layer thickness.

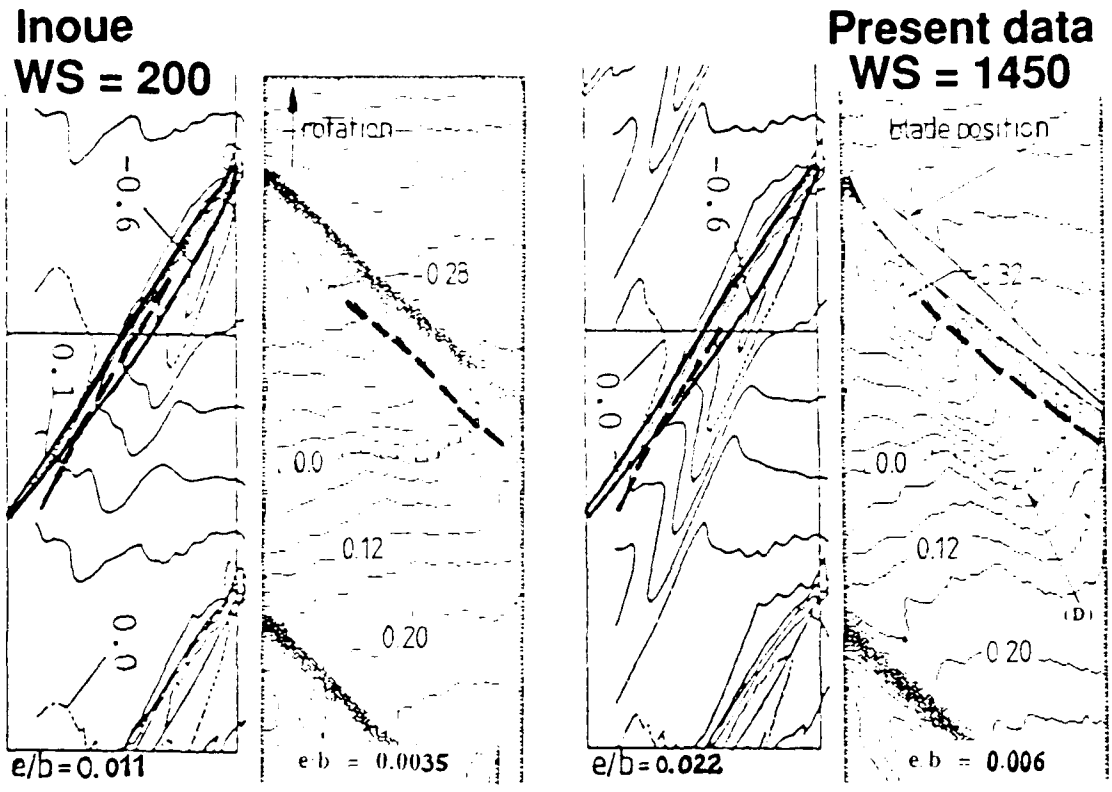

Fig. 4.3-1 Comparison of wall pressure minimum locii from the present study and those of Inoue and Kuroumaru (1988) in a low *WS* compressor.

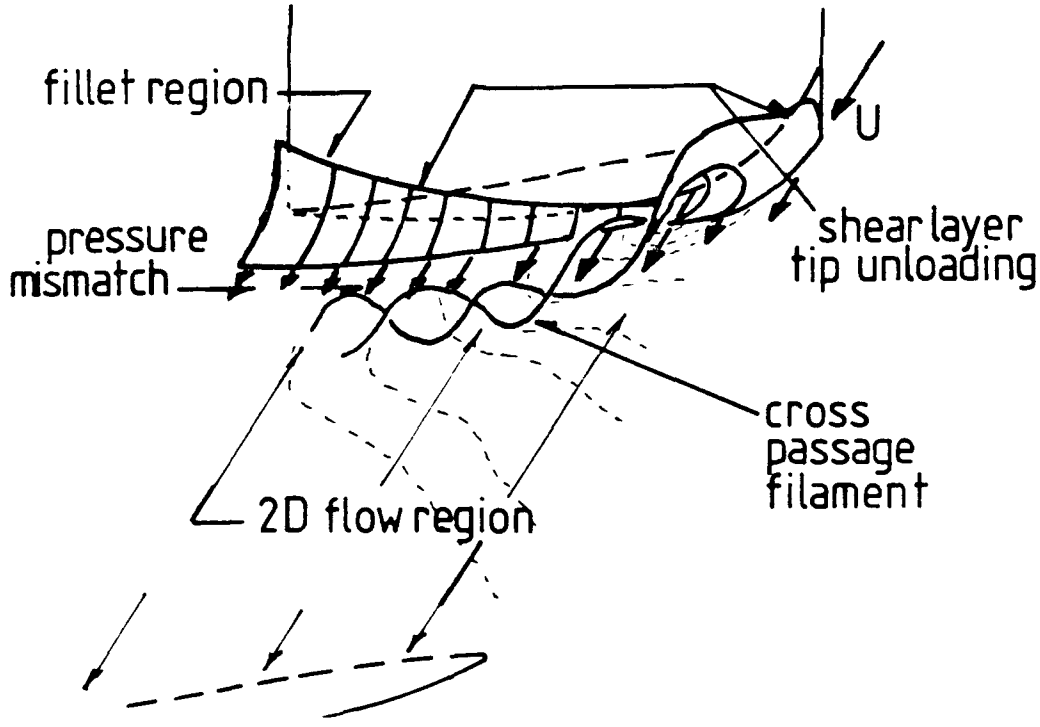

Fig. 4.3-2 Summary of mechanism(s) in the tip-wall corner identified by the present study.

4.4 Discussion Summary

As an experimental study over a wide range of geometries could not be attempted in this program, the following items were chosen (Sec. 1.5) for experimental emphasis in the present study:

(1) Obtaining more intersections of performance data and detailed measurements to contribute to the data base, particularly at small clearances, i.e., $0.002 < e/b < 0.01$. In this study the detailed wall pressure measurements could be correlated with the known, overall compressor performance.

(2) Exploration of the blade-to-blade flow changes due to the stator proximity (wakes) on the rotor tip flow near the case wall.

(3) Acquiring skin friction or wall shear measurements on the case wall.

4.4.1 Experimental Observations

To a large degree, these objectives were realized in the program and contributed to the results of the experimental study which, after discussion, are summarized below:

(1) The measurements at the wall indicated that the absolute flow is stagnant in the interval between the blade suction side and the minimum pressure line running outboard of the suction side. In the relative frame this is equivalent to flow passing under the blade at wall speed and in the secondary flow frame (where a tangential component of velocity is subtracted from the relative flow) is equivalent to a *zero or low velocity* outward flow from the suction side toward the minimum pressure line. In other words there was *no evidence of significant pressure driven leakage flow* in the basin region of the pattern. The low pressure basin would appear to be due to the wall dragging low energy fluid away from the blade at wall speed or, alternately, the absence of passage flow fluid penetrating into the tip wall corner aft of the peak suction basin. Other measurements suggest the stagnant fluid region moves with the blade.

(2) The pressure gradient in the tip gap closely approximated a Couette flow under conditions where the flow was stationary in the absolute frame and the wall shear level was negligible. This might be thought of as resembling the starting condition of a Couette flow (Sec. 4.1.1). The layer of flow that performed in this manner was found to form near the blade side of the gap and was a very small proportion of the whole tip gap. The thin layer was found to adjust the pressure loading on the suction side at the tip (Sec. 4.1.1.2).

(3) The blade edge loading was consistent with the gap pressure gradient acting over the distance of the blade tangential thickness rather than either the calculated two dimensional blade pressure distribution or a pressure driven leakage flow in the gap.

(4) A locus of minimum pressure extending from leading edge to trailing edge of the blade lay approximately one (maximum) tangential thickness off the suction side. The pressure difference between the minimum locus pressure and the blade pressure side was in fair agreement with the calculated two dimensional blade pressure distribution, except for a region of pressure relief near the leading edge (Sec. 4.1.2.2). The minimum pressure magnitude in the passage was noted to be fixed relative to the far field pressure in the test section.

(5) The tip *relative* leakage flow pattern was independent of the stator relative position of the rotor (local incidence conditions) provided passage average incidence was not large. At larger passage average incidence conditions the *relative* leakage pattern shows some interaction with the local incidence and the flow pattern began to alter significantly.

4.3.2 Unresolved Issues / Further Study

In the process of reviewing the experimental results and analysis, a number of the results have been identified that seem worthy of further investigation. These items have been summarized below:

(1) The consistent magnitude of the peak minimum pressure in the passage on the minimum pressure locus over a wide range of incidence and clearance conditions is unresolved. This phenomenon requires a physical explanation as the pressure seems to a datum for the whole tip flow.

(2) The suction-side corner pressure relief and probable separation or recirculation is not adequately resolved. The potential for an end bend or thickness increase to alter the suction-side leading edge corner flow should be examined in the context of the other identified features of the flow structure.

(3) The (corner separation) origins of the vortex filament nature of the cross passage flow and the *quid pro quo* between an incidence change and a clearance change in the leading edge region at the tip need further clarification. The peak minimum pressure constancy (1 above) also seems to be *common* to the similarity in behavior of clearance changes and tip local (rather than passage average) incidence changes at high incidence. This aspect of the flow should be explored further, particularly its relationship to stall inception.

(4) The flow stability criteria at the wall should be examined further in conjunction with the tip gap pressure unloading in the context of stall. Examination of the wall curvature at the tip gap (App. A.1.4) resulted in the recognition that the flow may be Taylor-Goertler unstable under certain curvature conditions and these conditions can lead to increased vorticity production on the case wall near the tip gap. The influences of this phenomenon on tip clearances losses were not fully defined in this study and they are a suggested area for further research.

(5) Methods of incorporating the pressure unloading due to gap size into a design system in terms of either thickness distributions for the tip profile or leakage corrections to the blades tip stagger angle.

4.4.3 Models and Mechanisms

The results and discussion lead to several observations about the mechanisms and modelling of the tip flow in the prior literature. These can be summarized as follows:

(1) The wall pressure on the suction side, away from the blade, was found to decrease to a minimum pressure (except for a small region at the leading edge) consistent with the two dimensional inviscid flow expected for the blade. This was equivalent to the two dimensional passage flow being displaced from the suction side of the blade along the tip. Such behavior suggests models or methods including blade *spacing* are more likely to reflect the mechanisms at work than methods based on blade profile parameters or blade dimensions.

(2) Blade suction surface unloading (inferred from the wall pressures) typical of previous studies was also observed in the present experiment. However, in the current experiments the unloading was in good agreement with a pressure gradient due to a shear layer blocking the gap and acting over the distance of the blade tangential thickness. This suggests the blade edge pressure could be modelled from the pressure gradient in the gap, blade thickness and gap size.

(3) The circulation of the blade extended to the wall as if the flow were two dimensional but not coincidentally with the blade surfaces. Tangential forces or lift coefficients determined at the tip using pressures on the blade surface would be unlikely to represent the actual circulation around the blade and fillet flow region. It is frequently proposed in the literature that a significant amount of circulation is shed at the tip (based on blade pressures). The present data suggests that much of circulation remains bound to the tip plus fillet region and earlier models might be adjusted to reflect this behavior.

(4) The fundamental flow structure at the wall appeared to be defined by the blade motion relative to the wall. Changes in passage incidence, stator relative position and tip clearance gap appeared to interact with this basic structure but not cause any fundamental change in its character. This suggests modelling for the gradient (2 above) could be developed in terms of wall and blade motion parameters.

Some of the results from the experimental study are peculiar to the NPS compressor and its blading. However, the results show low pressure areas extending along the suction side of the rotor blade, but lying away from the blade surface. Pressure contours indicate the the tangential loading at the tip is lower than predicted by two dimensional calculations, however, the predicted loading is observed between the lowest pressure's path in the passage and the the blade pressure side. The results suggest a viscous or shearing layer, due to the blade relative motion, is generated on the blade side of the tip gap. This layer modifies the inviscid relative flow field and produces an unloading on the blade tip.

Comparison with other studies (and other studies confirmations of the findings of this study) suggest the general features of the flow identified and discussed in this study are to be found in other compressors.

Part 5

Conclusion

At the outset of this study, a broad review of tip clearance effects in axial flow compressors was conducted to assess the range of passage designs previously tested. This review indicated that, although there had been considerable prior work on the subject and a reasonable accumulation of experimental data, the physical understanding of the tip local flow conditions was not resolved in terms of the proposed mechanisms. Numerous models and correlations of clearance change phenomena had also been developed in the past, but predictions of behavior based on these models frequently conflicted due to their independent derivation and calibration. A need to isolate what is, in fact, a consistent manifestation of a tip clearance effect was also noted in reviewing the literature. Given this situation, rather than try to verify or expand the models, emphasis in the study was placed on compilation and analysis of the prior test data with a view to mechanism identification or reconciliation. Flow measurement in a multistage machine was also emphasized. The principal conclusions of the present study were:

(1) Loss changes due to tip clearance changes only depend on the clearance dimension at the tip (Sec. 2.1). The rate of the dependence of efficiency changes at constant power on gap size was found to be independent of compressor configuration, passage geometry or tip speed. This suggested the losses originate where the geometry is very similar in all compressors. The corner close to the blade tip and case wall was considered to be the most likely site since its geometry varies little from compressor to compressor.

(2) The presence or absence of tip vortex formations in the passage secondary flow pattern near the case wall correlates well with the ratio of inertial (due to rotation) to viscous forces in the rotor passage (Sec. 2.2). This led to the further conclusion that a tip clearance vortex is not essential to the production of tip losses but rather reflects the nature of the passage flow in which the loss process of (1) takes place.

(3) From static pressure measurements at the case wall of a second stage rotor it was observed that the tangential loading at the tip was lower than predicted by two dimensional calculations, however, the predicted loading was present between the lowest pressures in the passage and the blade pressure side (Sec. 4.1.2). From these results it was concluded that a low energy and probably separated fillet of flow lies along the tip and decreases the blade surface loading.

(4) The results also show the lowest pressures in the passage extending along the rotor suction side, but lying away from the blade. Based on these results and additional wall shear measurements, it was concluded that an intense shear layer was present in the tip gap due to motion of the blade relative to the case wall (Sec. 4.1.1). This thin layer issued from the tip gap into the passage flow in the relative frame. The layer's interaction with the passage flow was the probable reason for the separated fillet and the likely origin of the losses (1) associated with tip clearance changes.

Comparison and reconciliation of the present analyses and experiments with other studies (and other studies confirmations of the findings of this study) suggest common flow behavior exists in several machines and the conclusions of this study can be applied widely to the analysis of tip clearance flows in axial compressors.

Part 6

References

Barclay, W. H., "Flow in Streamwise Corners Having Large Transverse Curvature," AIAA 82-4120 and *AIAA Journal*, p. 726, May 1982.

Beitler, R. S., Saunders, A. A., and Wanger, R. P., "Fuel Conservation through Active Control of Rotor Clearances," AIAA-80-1087, July 1980.

Beknev, V. S., "The Investigations of the Stage of the Axial Flow Compressor Designed with due Regard for Losses with Blade Height," Thermal Engineering (in Russian), Jan. 1961.

Beknev, V. S., "Some Problems of The Improvement of Axial Flow Compressor Performances," XIIIth. Annual International Gas Turbine Conference and Products Show, Washington D.C. Mar. 1968.

Benser, W. A., "Transonic Compressor Technology Advancements", Fluid Mechanics, Acoustics and Design of Turbomachinery - Part II, Symposium held at Pennsylvania State University, edited by B. Lakshminarayana, NASA SP-301, 1974, p. 598.

Bettner, J. L., and Elrod, C., "The Influence of Tip Clearance, Stage Loading and Wall Roughness on Compressor Casing Boundary Layer Development," ASME 82-GT-153, 1982.

Betz, A., in: *Hydraulische Probleme*, p. 161, VDI-Verlag, Berlin, 1926 (Discussion of model in Vavra (1960)).

Bhargava, R. and Raj., R. S., "Near Wall Flow Parameters in the Blade End-Wall Corner Region," ISABE 89-7136, 1989.

Bhargava, R., Raj., R. S. and Boldman, D. R., "Wall Shear Stress Measurements in Blade End-Wall Corner Region," ASME 87-GT-181, 1987.

Bindon, J. P., "The Measurement and Formation of Tip Clearance Loss," *ASME Journal of Turbomachinery*, July 1989, Vol. 111 p. 257, and ASME 88-GT-203, 1988.

Brasz, J. J., "Investigation into the Effect of Tip Clearance on Centrifugal Compressor Performance," ASME 88-GT-190, June 1988.

Brown, G. L., "Theory and Application of Heated Films for Skin Friction Measurement," Proc. 1967, Heat Transfer and Fluid Mechanics Institute, Stanford Univ. Press, pp. 361-381, 1967.

Cat, T. V., "A Preliminary Investigation of Pressure Distribution on Casing Near Tips of An Axial Flow Compressor," Honors Thesis, Dept. of Civil and Mechanical Engineering, University of Tasmania, Feb. 1977.

Chen, G. T., Greitzer, E. M., Tan, C. S., and Marble, F. E., "Similarity Analysis of Compressor Tip Clearance Flow Structure", ASME 90-GT-153, June 1990.

Chen, Y. N., Haupt, U. and Rautenberg, M., "The Vortex-Filament Nature of the Reverse Flow on the Verge of Rotating Stall," ASME 88-GT-120, 1988.

Cumpsty, N. A., "Annulus Wall Boundary-Layer Measurements in a Four Stage Compressor," ASME 85-GT-61, Mar. 1985.

Dean, R. C. Jr., "The Influence of Tip Clearance on Boundary-Layer Flow in a Rectilinear Cascade," Gas Turbine Laboratory MIT, Cambridge, Massachusetts, Report No. 27-3, Dec. 1954.

Dishart, P. T., and Moore, J., "Tip Leakage Losses in a Linear Turbine Cascade," ASME 89-GT-56, June 1989.

Dring, R. P., Joslyn, H. D., and Hardin, L. W., "Compressor Rotor Aerodynamics - An Analytical and Experimental Investigation," United Technologies Research Center, UTRC-15, March 1980.

Dring, R. P., Joslyn, H. D., and Hardin, L. W., "An Investigation of Axial Compressor Rotor Aerodynamics," ASME 81-GT-56, Mar. 1981.

Dring, R. P., Joslyn, H. D., and Wagner, J. H., "Compressor Rotor Aerodynamics," Presented at AGARD-PEP Specialists' Meeting 61-A, Viscous Effects in Turbomachinery, June 1983.

Dunavant, J. C., "Cascade Investigation of a Related Series of 6-Percent-Thick Guide-Vane Profiles and Design Charts," NACA-RM L54I02, 1954.

Engeda, A., Strate, W. P., and Rautenberg, M., "Correlation of Tip Clearance Effects to Impeller Geometry and Fluid Mechanics," ASME 88-GT-92, June 1988.

Fabri, J., and Reboux, J., "Effect of Outer Casing Treatment and Tip Clearance on Stall Margin of a Supersonic Rotating Cascade," ASME 75-GT-95, 1975.

Fickert, B., "The Influence of Radial Clearance of the Rotor on the Compressor Efficiency, Part C of "The Influence of Physical Dimensions and Flow Conditions on Compressor Characteristics," Bureau of Ships 338, pp. 95-108, 1946.

Freeman, C., "Effect of Tip Clearance on Compressor Stability and Engine Performance," in: *von Karman Institute for Fluid Dynamics, Lecture Series No. 5*, "Tip Clearance Effects in Axial Turbomachines," Apr. 1985.

Gallus, H. E., Grollius H., and Lambertz J., "The Influence of Blade Number Ratio and Blade Row Spacing on Axial-Flow Compressor Stator Blade Dynamic Load and Stage Sound Pressure Level," ASME 81-GT-165, May 1981.

Goto, A., "Study of Internal Flows in a Mixed Flow Pump Impeller at Various Tip Clearances Using 3D Viscous Flow Computations", ASME 90-GT-36, June 1990.

Goto, A., "The Effect of Tip Leakage Flow on Part Load Performance of a Mixed Flow Pump Impeller", ASME 91-GT-84, June 1991. To be published in the *ASME Journal of Turbomachinery*.

Graham, J. A. H., "Investigation of a Tip Clearance Cascade in a Water Analogy Rig," ASME 85-IGT-65, 1985.

Gundy-Burlet, K. L., Rai, M. M. and Dring, R. P., "Two-Dimensional Computations of Multi-Stage Compressor Flows Using a Zonal Approach," AIAA 89-2452, July 1989.

Hah, C., "A Numerical Modeling of Endwall and Tip-Clearance Flow of an Isolated Compressor Rotor," ASME Gas Turbine Conference and Exhibit, Houston, Texas, 85-GT-116, Mar. 18-21, 1985,

Hararika, B. K. and Raj, R. S., "An Investigation of the Flow Characteristics in the Blade Endwall Corner," NASA CR 4076, July 1987.

Hatch, J. E., Giamati C. C., and Jackson R. J., " Application of Radial Equilibrium Condition to Axial-Flow Turbomachine Design Including Consideration of Change of Entropy With Radius Downstream of Blade Row," NASA RM E54A20, Apr. 1954.

Heinemann, H-J., "High-Speed Data Acquisition and Reduction for Wall Static Pressures Derived within the Passage of a Rotating Annular Turbine Cascade," Proceedings of the Eighth Symposium on Measuring Techniques for Transonic and Supersonic Flows in Cascades and Turbomachines, Oct. 1985, Universita Degli Studi Di Genova, Dec. 1986.

Henneke, D. K., "Active and Passive Tip Clearance Control," in: *von Karman Institute for Fluid Mechanics, Lecture Series No. 5*, "Tip Clearance Effects in Axial Turbomachines," Apr. 1985.

Herzig, H. Z., Hansen, A. G., and Costello, G. R., "A Visualization Study of Secondary Flows in Cascades," National Advisory Committee for Aeronautics, Washington, Fortieth Annual Report, Report 1163, in Vol. Report Nos. 1158-1209, pp. 147-197, 1954.

Holman, F. F., and Kidwell, J.R., "Effects of Casing Treatment on a Small, Transonic Axial Flow Compressor," ASME 75-WA/GT-5, July 1975.

Honami, S., Shizawa, T., and Takahama, M., "Behavior of the Leg of the Horseshoe Vortex around the Idealized Blade with Zero Attack Angle by Triple Hot-Wire Measurements," ASME-GT-?, 1988.

Hunter, I. H., and Cumpsty N. A., "Casing Wall Boundary Layer Development through an Isolated Compressor Rotor," *ASME Journal of Engineering for Power*, Vol. 104, pp. 805-818, 1982.

Inoue, M., Kuroumaru, M., and Fukahara, M., "Behavior of Tip Leakage Flow Behind an Axial Compressor Rotor," ASME 85-GT-62, 1985.

Inoue, M., Kuroumaru, M., and Fukahara, M., "Behavior of Tip Leakage Flow Behind an Axial Compressor Rotor," *ASME Journal of Engineering for Gas Turbines and Power*, Vol. 108, pp. 7-14, 1986.

Inoue, M., and Kuroumaru, M., "Structure of Tip Clearance Flow in an Isolated Axial Compressor Rotor," ASME 88-GT-251, June 1988.

Koch, C. C., and Smith, L. H., Jr., "Loss Sources and Magnitudes in Axial-Flow Compressors," *ASME Journal of Engineering for Power*, p. 411, July 1976.

Koch, C. C., "Stalling Pressure Rise Capability of Axial Flow Compressor Stages," *ASME Journal of Engineering for Power*, Vol. 103, pp. 645-656, 1981.

Lakshminarayana, B., and Horlock, J. H., "Leakage and Secondary Flow in Compressor Cascades," British A.R.C. Report and Memorandum 3483, 1967.

Lakshminarayana, B., "Methods of Predicting the Tip Clearance Effects in Axial Flow Turbomachinery," *ASME Journal of Basic Engineering*, pp. 467-482, Sept. 1970.

Lakshminarayana, B., Pouagare, M. and Davino, R., "Three Dimensional Flow Field in the Tip Region of A Compressor Rotor Passage - Part I: Mean Velocity Profiles and Annulus Wall Boundary Layer- Part II: Turbulence Properties," ASME 82-GT-11 and ASME 82-GT-234, 1982.

Lakshminarayana, B., Murthy, K. N. S., Pouagare, M. and Govindan, T. R., "Annulus Wall Boundary Layer Development in a Compressor Stage, Including the Effects of Tip Clearance," presented at the AGARD PEP Specialists Meeting 61A "Viscous Effects In Turbomachines", Copenhagen, Denmark, June 1983.

Lakshminarayana, B., Sitaram, N., and Zhang, J., "End-Wall and Profile Losses in a Low Speed Axial Flow Compressor Rotor," *ASME Journal of Engineering for Gas Turbines and Power*, Vol 108, pp. 22-31, Jan. 1986.

Lakshminarayana, B., and Murthy, K. N. S., "Laser Doppler Velocimeter Measurement of Annulus Wall Boundary Layer Development in a Compressor Rotor," ASME 87-GT-251, June 1987 and *ASME Journal of Turbomachinery*, Vol 110, pp. 377-385, Jul. 1988.

Lakshminarayana, B., Zaccaria, M., and Marathe, B., "Structure of Tip Clearance Flow in Axial Compressors," ISABE 91-7144, Tenth ISABE Conference, Nottingham, U.K., Sep. 1991.

Lieblein, S., "Analysis of Experimental Low-Speed Loss and Stall Characteristics of Two Dimensional Compressor Blade Cascades," NASA RM E57A28, 1957.

Ludwig, L. P., "Gas Path Sealing in Turbine Engines," AGARD-CP-237, Apr. 6-7 1978.

Mahler, F. H., "Advanced Seal Technology," AFAPL-TR-72-8, 1972.

Maki, M., and Moyle, I. N., "Aircraft Energy Management System, Phase I - Vol. 1. Lockheed L1011," Transport Canada Research and Development Center, Report TP 1314, May 1978.

McDougall, N. M., "A Comparison Between the Design Point and Near stall Performance of an Axial Compressor," ASME 89-GT-70, June 1989.

Mellor, G. L., Jr., "Shear Flow in Bends - Report of Research Activities, 1953-1954, Theoretical Consideration of Secondary Flow," Gas Turbine Laboratory, Report No. 27-2, MIT, Dec. 1954.

Moore, R. D., and Osborne, W. M., "Effects of Tip Clearance on Overall Performance of Transonic Fan Stage With and Without Casing Treatment," NASA TM-X-3479, Feb. 1977.

Moore, R. D., "Rotor Tip Clearance Effects on Overall Blade-Element Performance of Axial-Flow Transonic Fan Stage," NASA TP-2049, Sept. 1982.

Morphis, G. and Bindon, J. P., " The Effects of Relative Motion, Blade Edge Radius and Gap Size on the Blade Tip Pressure Distribution in an Annular Turbine Cascade with Clearance," ASME 88-GT-?, 1988.

Moyle, I. N., "Feasibility and Cost Benefits of Trimming the USAF F-4/J79 Fleet to a Computed Thrust," U.S. Air Force Flight Test Center, Edwards AFB, California, AFFTC-TR-79-35, 1979.

Moyle, I. N. and Zebner, H., "Multistage Compressor - Installation of Cast Epoxy Blades," Naval Postgraduate School, Monterey, California, Turbopropulsion Lab. TN 80-06, Oct. 1980.

Moyle, I. N., "Multistage Compressor - Initial Measurements with One Stage of Symmetrical Blading," Naval Postgraduate School, Monterey, California, Turbopropulsion Lab. TN 80-09, Oct. 1980.

Moyle, I. N., "Progress Report - Multistage Axial Compressor Program on Tip Clearance Effects," Naval Postgraduate School, Monterey, California, Report NPS-67-81-01CR, Aug. 1981.

Moyle, I. N., "Multistage Compressor - Survey of Literature on Tip Clearance and Blade Tip Flow Effects in Axial Turbomachines," Naval Postgraduate School, Monterey, California, Turbopropulsion Laboratory, Technical Note 81-01, Sep. 1981.

Moyle, I. N., "Single Stage Compressor Test Baseline for a Symmetric Blading," Naval Postgraduate School, Monterey, California, NPS-67-86-003/CR, December 1986.

Moyle, I. N., "Analysis of Efficiency Sensitivity Associated with Tip Clearance in Axial Flow Compressors," ASME 88-GT-216, June 1988 and synopsized in the *ASME Journal of Turbomachinery*, Vol 112, pp. 795-6, Oct. 1990.

Moyle, I. N., "Influence of the Radial Component of Total Pressure Gradient on Tip Clearance Secondary Flow in Axial Compressors," ASME 89-GT-19, June 1989.

Moyle, I. N., Walker, G. J. and Shreeve, R. P., "Stator Averaged, Rotor Blade-to-Blade Near Wall Flow in a Multistage Axial Compressor With Tip Clearance Variation," ASME 91-GT-30, June 1991. To be published in the *ASME Journal of Turbomachinery*.

Murthy, K. N. S., and Lakshminarayana, B., "Laser Doppler Velocimeter Measurement in the tip region of a Compressor Rotor," AIAA 84-1602, June 1984 and *AIAA Journal*, Vol. 24, pp. 807-814, May 1986.

Peacock, R. E., "Blade Tip Gap Effects in Turbomachines - A Review," Naval Postgraduate School, Monterey, California, NPS-67-81-016, Nov. 1981,

Peacock, R. E., "A Review of Turbomachinery Tip Gap Effects, Part 1: Cascades," *Intl. Jrnl. Heat and Fluid Flow*, Butterworth and Co. Ltd., Vol. 3, No. 4, pp. 185-194, Dec. 1982.

Peacock, R. E., "A Review of Turbomachinery Tip Gap Effects, Part 2: Rotating Machinery," *Intl. Jrnl. Heat and Fluid Flow*, Butterworth and Co. Ltd., Vol. 4, No. 1, pp. 3-16, Mar. 1983.

Peacock, R. E., "Turbomachinery Tip Gap Aerodynamics - A Review," ISABE 89-7056, 1989.

Pouagare, M., Lazarus, K. and Weingold, W. P., "Tip Leakage Reduction Through Tip Injection In Turbomachines," AIAA-86-1746, 1986.

Rai, M. M., "Navier Stokes Simulations of Rotor Stator Interaction using Patched and Overlaid Grids," AIAA 85-1519-CP, 1985.

Rai, M. M., "Three-Dimensional Navier-Stokes Simulations of Turbine Rotor-Stator Interaction; Part II - Results," *AIAA Journal of Propulsion*, Vol 5, No. 3, pp. 312-319, May-June 1989.

Rains, D. A., "Tip Clearance Flows in Axial Flow Compressors and Pumps," California Institute of Technology, Hydrodynamics and Mechanical Laboratories, Report No. 5., June 1954.

Reeder, J. A., "Tip Clearance Problems in Axial Compressors (a Survey of Available Literature)," Union Carbide Corp., Oak Ridge Gaseous Diffusion Plant, Report No. K-1682, Jan. 4, 1968.

Reid, L., Private correspondence and discussion of wall pressure and wall shear measurements made by Reid in a single stage at 11,500 RPM, November 1987.

Roberts, W. B., Serovy, G. K., and Sandercock, D. M., Design Point Variation of 3-D Loss and Deviation for Axial Compressor Middle Stages, " ASME 88-GT-57, June 1988.

Robinson, C. J., "A Review of the Effect of Rotor Tip Clearance on Axial Compressor Performance," Rolls-Royce plc, RCR 90830, Jan. 1982.

Ruden, P., "Investigation of Single Stage Axial Fans," NACA TM 1062, Apr. 1944, (originally published in 1937 in German).

Schlachter, W., "Investigation of Tip Clearance Effects in Axial Compressor Stages," Naval Postgraduate School, Monterey, California, Dec. 1, 1971.

Schlachter, W., "Calculations for Axial Compressor Blading with Uniform Inlet Enthalpy and Radial Enthalpy Gradient," Naval Postgraduate School, Monterey, California, NPS-67-81-008, May 1981.

Schlichting, H., "*Boundary Layer Theory*," McGraw-Hill Book Co., Inc. English Edition, 1955.

Schmidt, M. J. P., Agnew, B. and Elder, R. L., "Tip Clearance Flows - Part I, Experimental Investigation of an Isolated Rotor, Part II, Study of Various Models and Comparison with Test Results, " Eighth ISABE Conference, Cincinnati Ohio, June 1987.

Schulz, H. D., Gallus, H. E., and Lakshminarayana, B., "Three Dimensional Separated Flow Field in the Endwall Region of an Annular Compressor Cascade in the Presence of Rotor-Stator Interaction, Part I - Quasi-Steady Flow Field and Comparison with Steady State Data, Part II Unsteady Flow and Pressure field," ASME 89-GT-76 and ASME 89-GT-77, June 1989.

Sedille, M. M., "Compresseurs Axiaux. Influence du Jeu," *Des Comptes Rendus Des Seances De L'Academie Des Sciences*, Seance du 5 Juin, p.1789, 1939.

Senoo, Y., and Ishida, M., "Pressure Loss Due to the Tip Clearance of Impeller Blades in Centrifugal and Axial Blowers," *ASME Journal of Engineering for Gas Turbines and Power*, Vol. 108, pp. 32-37, Jan. 1986.

Senoo, Y., "Pressure Losses and Flow Field Distortion Induced by Tip Clearance of Centrifugal and Axial Compressors," *JSME International Journal*, Vol. 30, No. 261, pp. 375-385, 1987.

Senoo, Y. "Mechanics on the Tip Clearance Loss of Impeller Blades", ASME 90-GT-37, June 1990.

Sharma, O. P., and Butler, T. L., "Predictions of Endwall Losses and Secondary Flows in Axial Flow Turbine Cascades," ASME Journal of Turbomachinery, Vol. 109, pp. 229-236, Apr. 1989.

Smith, L. H., Jr., "Static Pressure Gradients caused by Secondary Flow," General Electric, Aircraft Gas Turbine Division, Evendale, No. R55AGT360, Jul. 15, 1955.

Smith, L. H., Jr., "The Effect of Tip Clearance on the Peak Pressure Rise of Axial-Flow Fans and Compressors," ASME Symposium on Stall, New York, Dec. 4-5, 1958,

Smith, L. H. Jr., "Casing Boundary Layers in Multistage Axial-Flow Compressors," *Flow Research On Blading*, Elsevier Publishing Co., New York, 1970.

Storer, J. A., "The Interaction between Tip Clearance Flow and the Passage Flowfield in an Axial Compressor Cascade," ISABE 89-7024, 1989.

Storer, J. A., and Cumpsty, N. A., "Tip Leakage Flow in Axial Compressors", ASME 90-GT-127, June 1990.

Tarigar, M., "Development of a Boundary Layer Control Device for Tip Clearance Experiments in an Axial Compressor," M.Sc. Thesis, Naval Postgraduate School, Monterey, 1988.

Vavra, M. H., *Aerothermodynamics and Flow in Turbomachines*, John Wiley and Sons Inc., New York, 1960.

Vavra, M. H., "Aerodynamic Design of Symmetrical Blading for Three-Stage Axial Flow Compressor Test Rig," Naval Postgraduate School, Monterey, California, NPS-57-VA70091A, Sep. 1, 1970.

Vavra, M. H., Pucci, P. F., Schlachter, W., "Redesign of the Low Speed Three Stage Axial Flow Compressor Test Facility," Naval Postgraduate School, Monterey, California, NPS-57-Va73121A, Dec. 1973.

von Karman Institute for Fluid Dynamics, Lecture Series, No. 5, "Tip Clearance Effects in Axial Turbomachines," Apr. 1985.

Waddell, J. A., "Evaluation of the Performance and Flow in an Axial Compressor," Naval Postgraduate School, Monterey, M.Sc. Thesis, Oct. 1982.

Williams, A. D., "The Effect of Tip Clearance Flows on Performance of Axial Flow Compressors," California Institute of Technology, Pasadena California, A.E. Thesis, 1960.

Wisler, D. C., "Core Compressor Exit Stage Study, Volume I - Blading Design," General Electric Company, NASA CR-135391, Dec. 1977.

Wisler, D. C., "Aerodynamic Effects of Tip Clearance, Shrouds, Leakage Flow, Casing Treatment and Trenching in Compressor Design - Blading Design in the Endwall Region," in: *von Karman Institute for Fluid Dynamics, Lecture Series, No. 5*, "Tip Clearance Effects in Axial Turbomachines," Apr. 1985.

Wisler, D. C., and Beacher, B. F., "Improved Compressor Performance Using Recessed Clearance (Trenches) Over the Rotor," AIAA-86-1745, June 1986.

Wu, C-H., and Wolfenstein, L., "Application of Radial-Equilibrium Condition to Axial-Flow Compressor and Turbine Design," NASA TN 1795, Jan. 1949.

Wu, C-H., "A General Theory of Three-Dimensional Flow in Subsonic and Supersonic Turbomachines of Axial-, Radial- and Mixed Flow Types, NASA TN 2604, 1952.

Wu, C-H., and Wu, W., "Analysis of Tip Clearance Flow in Turbomachines," Polytechnic Institute of Brooklyn, Gas Turbine Laboratory, Report No. 1, July 1954.

Yamamoto, A., Takahara, K., Nouse, H., Mimura, F., Inoue, S. and Usui, H., "An Experimental and Analytical Study of Blade Tip-Clearance Effects on an Axial-Flow Turbine Performance," NAL, Japan, Report TR-466T, Jan. 1982.

Yaras, M., Yingkang, Z. and Siolander, S. A., "Flow Field in the Tip Gap of a Planar Cascade of Turbine Blades," ASME 88-GT-29, Jun. 1988.

Yaras, M. I, and Sjolander, S. A., "Losses in the Tip-leakage Flow of a Planar Cascade of Turbine Blades," AGARD-CP-469 (Paper 20), 1989.

Yaras, M. I., and Sjolander, S. A., "Prediction of Tip-Leakage Losses in Axial Turbines", ASME 90-GT-154, June 1990.

Yaras, M. I., and Sjolander, S. A., "Effects of Simulated Rotation on Tip Leakage in a Planar Cascade of Turbine Blades; Part I Tip gap Flow", ASME 91-GT-127, June 1991. To be published in the *ASME Journal of Turbomachinery*.

Yaras, M. I., Sjolander, S. A., and Kind, R. J., "Effects of Simulated Rotation on Tip Leakage in a Planar Cascade of Turbine Blades; Part II Downstream Flow Field and Blade Loading", ASME 91-GT-128, June 1991. To be published in the *ASME Journal of Turbomachinery*.

Yeo, P. H., "Review and Evaluation of a Turbomachinery Throughflow Finite Element Code," M.Sc. Thesis, Naval Postgraduate School, Monterey, June 1989.

Part 7

Appendices

A.1 Flow Field Considerations

The instantaneous flow in an axial compressor is truly complex. It encompasses many large and small scale fluid motions in the space of the machine and also in time as the components move with respect to each other.[84] Through assumptions, which idealize the averaged features of the flow or blading (irrotationality, incompressibility and an infinity of blades), engineering approximations to the averaged flow on axisymmetric surfaces can be implemented in an essentially two dimensional manner. By using test data from linear cascades to replace much of the information lost through simplification of the averaged equations, a workable system to design machines can be developed from the axisymmetric approximation and some considerations of the force equilibrium in the radial direction. Comprehensive descriptions and elaboration of such "strip-theory" design systems are published in two well known compilations; Aerodynamic Design of Axial Compressors (1965) and The Aerothermodynamics of Aircraft Gas Turbine Engines (1978).

While such a strip system can produce acceptable designs, it involves the assumption that the cascade or two dimensional flow idealization holds for each blade element across the span. This assumption is known to be an approximation, even in cascades, and the design method becomes less accurate or reliable close to the bounding walls of the passage.[85] The blade tip clearance, at the hub or case wall, is in a region of the flow field that experiences large gradients in total pressure and circulation along with scraping, leakage and local skewing, shear and separation. Despite the evident flow complexity, the average flow quantities (and angles) are known to be repeatable, in a design sense, near the walls.

This means that the average performance can be modelled and improved understanding of the flow may lead to improved design. The following section therefore considers the flow field in an average sense in examining the tip clearance in the flow.

A.1.1 Geometry of the Passage

The geometry of a turbomachine passage is usually described with a system of parameters based on two dimensional cascade testing of aerofoil sections, Figure A.1-1. This convention influences how the flow in the machine is perceived *(even when the cascade conditions no longer hold).* For example, a passage of unit solidity and unit aspect ratio has as much wetted wall area as it has wetted aerofoil area. If this passage is unshrouded, one wall is moving at wheel speed relative to the blades. The wall motion is also an influence on the blade flow near the tip. In this situation it is questionable whether incidence, deviation, camber or stagger can be applied to a profile with the same interpretation as in a two dimensional flow[86].

---

[84] A general description of the flow field is possible conceptually or mathematically (Wu, 1952; Yavra, 1960) in terms of differential equations. However, in order to have tractable equations for the system, the general vectorial description is substantially simplified by averaging in time and space. The detailed information lost by these averaging processes is replaced with boundary conditions, forces, etc. and is discussed in detail by Adamczyk (1985).

[85] Also, in bladings where appreciable radial gradients of circulation exist or in situations where the radial gradients of total pressure become large across the span; the "strip-theory" methods traditionally have become unreliable. This problem is a subject of active research and improved agreement between experimental data and calculations, by use of consistent averaging of the flow quantities, was recently reported by Dring and Oates (1989).

[86] Studies prior to 1970 typically rely on a velocity diagram for the blade tip which has been modified to reflect the presence of a tip gap, e.g., Mager (19**).

The ability to compare blade tip profiles and gap levels on a proportional basis is also more complicated in a passage. In this case, the wall local geometry does not only scale in proportion to the cascade dimensions but also with radius (R). The case wall also turns flow passing through the tip gap away from the direction normal to the gap by the gap dimension (e) within some distance (l) from the blade tip, see Fig. A.1-1. The ratio of l/e shown in Fig. A.1-1 varies as $(2R/e - 1)^{0.5}$ and is indicative of the curvature of the tip flow due to the presence of a wall. If l/e is large the flow is effectively rectilinear near the tip gap (i.e., streamline curvature effects should have a minimal effect on the gap flow). If one assumes the tip flow effects are influenced by wall curvature at, for the sake of example, any l/e less than 10, then including the effects of hub-to-tip ratio (*HR*), it can be shown that curvature is significant for $e/b > 0.02/(1-HR)$. If $HR = 0.5$, any clearance level greater than $e/b = 0.04$ would be influenced by the wall curvature. An e/b level of 0.04 is not uncommon for $HR = 0.5$ stages evaluated experimentally. Values of l/e are can be as low as 8 in the experimental data to be discussed later. The influences of wall curvature are discussed in more detail in App. A.3.1.

Exploring the similarity of passages without considering curvature, it is clear that a rough geometric similarity (in a cascade sense) is achieved when solidity, aspect ratio and stagger angle are the same for different scales of passage. An alternative view to the familiar cascade convention is also shown on the right of Fig. A.1-1. In this schematic the concept of a staggered spacing (g) is shown. The staggered spacing characterizes both the diffusive area ratio of the passage and also the blade spacing normal to the chord. As a leakage flow, free from any viscous effects, would be expected to decelerate across the staggered spacing in the blade-to-blade pressure gradient, the staggered spacing is a characteristic dimension of the leakage flow diffusion. This case wall layer, crossflow perception of the passage flow has led certain authors, notably Smith (1970), to normalize clearance effect data by staggered spacing rather than chord, blade thickness or blade height.[87] For the purposes of this study the present author has adopted a convention of using the tip radius, as the length dimension, and passage descriptive parameters to define other dimensions. This convention has the advantage of generalizing the tip local dimensions in terms of the passage geometry parameters. The definitions used are as follows;

$a = R(1-HR)/AA$	axial chord
$b = R(1-HR)$	blade height or span
$c = R(1-HR)/AR$	blade chord
$s = R(1-HR)/(AR.\sigma)$	blade spacing or pitch
$g = R(1-HR)/(AA.\sigma)$	staggered spacing

so that the set {R: *HR*, *AR*, σ, *AA*} defines the shape of the overall passage. The ratio *AA*, the axial aspect ratio, is essentially a substitute for the cosine of the stagger angle.

---

[87] There has been some debate in the literature whether any one of these dimensions has more physical significance in normalizing the clearance gap (e), particularly Hunter and Cumpsty (1982, p. 10) and Cumpsty (1985, p. 5 Conclusion 3). Despite their opposition to use of staggered spacing no new or preferred alternative normalizing dimension, for correlating wall boundary layer thicknesses or efficiency change, was advanced in their discussions. Almost every dimension of the passage has been used to normalize clearance gap in past work on this subject, without clearly superior correlation.

Note that σ = c/s = a/g in this system of definitions. This system is used for its *convenience* when comparing different compressor passage shapes. All parameters are defined in terms of tip dimensions. The tip gap has also been routinely normalized by blade height or span (b) in the present study.

Using this system of definitions, comparison of the variety of passages where end wall or tip conditions have been experimentally changed is instructive. The experiments are shown in Figure A.1-2 using the axial aspect ratio (AA = b/a) and solidity (σ) to correlate the data. Lines of constant (b/g) are shown on the plot to indicate the degree of wall wetted surface in the passage. Several patterns are evident in the test scatter.

(1) The solidity range of the test data is not widely spread from unity with an axial aspect ratio range of one to four around a solidity of one. This allows a comparison of aspect ratio at constant solidity.

(2) Limited multistage data are available and only in the higher aspect ratios.

(3) The (b/g) ratio of 2.0 has the widest range of solidities and axial aspect ratios for comparison of staggered spacing normalization.

The passage blade normal cross-sections, sections and wall "footprints" are also shown beside the axes to indicate the variety of passages this diagram represents. From this information we can conclude that the tests available in the open literature only permit a limited number of systematic comparisons of passage geometry influences for any proposed correlation of tip clearance effects. The sparseness of the database of tests is discussed in Sec. 1.3.3.

A.1.2 Flow in the Stage

The primary flow in a stage is commonly characterized by the fluid hub-to-tip velocity diagrams. The basis for developing these diagrams is the pressure radial equilibrium condition on a fluid element in the inter-blade spaces. By selecting two radial distributions from a choice of work input per blade element, axial velocity or tangential velocity, the third can be defined by applying the radial equilibrium condition.

The velocity diagrams defined by these distributions specify the fluid turning required of each blade element. Empirical data from cascade testing has been organized to specify the fluid turning in terms of camber and thickness distribution for flow conditions of minimum loss angle of attack. By using cascade data, for each blade element, the stage can be fully specified and its performance estimated. Similar techniques can be used to determine the off-design performance.

The simple description of the flow and blading design process, above, has been substantially elaborated in practice by the use of digital computers to perform passage average and blade-to-blade fluid dynamic computations of the stage performance. However, for most research and understanding purposes the significant flow effects can be described with the simple equilibrium techniques.

For example, if a design approach is selected where specific work input is uniform across the span and the whirl distribution is specified in the general form

$$V_u(r) = A.(r_m/r) + B + C.(r/r_m) \qquad A(1)$$

then a wide range of stage velocity diagrams can be analyzed under common throughflow conditions. Results of this type of analysis from Vavra (1960, p. 458)[88] are shown in Figure A.1-3. It can be seen that substantially different case wall velocities are produced by the different whirl distributions for *roughly* the same turning at the tip. Clearly the magnitude of the *average* pressure difference from pressure to suction side at the blade tip will be lower for the symmetric blading, with a solid body whirl distribution, than for the free-vortex distribution. This situation is defined by the velocity diagram rather than the blade profile section selected for the tip.

Whirl distribution therefore produces a first order effect in considering tip clearance and case wall flow. *The average blade-to-blade pressure difference (tangential loading) at the tip can vary significantly (approximately 20%), depending on whirl distribution, for the same throughflow and wheel speed.* The whirl most strongly impacts the "tip leakage driven by pressure difference" arguments and flow models discussed in (Sec. 1.1.2). The whirl also produces other flow effects. For example, changes in axial velocity across a non-free-vortex blading produce much stronger radial flows near the case wall than would be the case in a free-vortex design.

The fact that the form of the spanwise velocity distributions, for a given throughflow, determines the end wall pressure gradients and differences greatly complicates the interpretation of compressor test data. This whirl effect needs to be considered in addition to the geometric similarity of App. A.1.1 when flow comparisons are made in different stages.

A.1.2.1 Secondary Flows in the Passage

The classical description of a secondary flow in a curved duct is developed from considerations of the spanwise gradient of the inflow velocity profile. The presence of a gradient causes a rotation of the near wall flow as the it is turned in the duct. Typically the spanwise gradient is associated with the velocity gradient of the end wall boundary layer. This wall flow is presumed to coexist with a uniform core flow region. A schematic of the cascade effect is shown in Figure A.1-4.

For any real flow of a fluid, from one blade row into another, the situation is further complicated by velocity gradients from wakes of upstream rows, an imposed gradient from any non-free vortex whirl distribution and velocity defects from any corner separations that might exist immediately upstream of the passage. The idealization of two secondary opposed vortices at each case wall may be overwhelmed or grossly modified in a real stage flow. In addition, in a rotating row of an unshrouded compressor blade there is a counter motion of the wall and a centripetal force acting on the fluid in the relative frame. All of these effects need to be equilibrated in the passage flow and their manifestation in a secondary flow pattern is by no means simple to interpret.

As an example of this equilibration effect, it can be seen in Fig. A.1-4 that the flow on the case walls of the stationary cascade will be from the pressure to the suction side of the passage. *In a rotating annular cascade* with a finite number of blades there will be an *opposed* motion in the flow induced by the passage rotation. The passage eddy produced in the relative frame induces a fluid motion from suction to pressure side at the tip wall. The motion in one direction is the consequence of the turning and viscous influences in the wall boundary layer and the opposite motion is due to the response of

[88] Vavra's analysis is based on earlier analyses of a similar type by Wu and Wolfenstein (1949). Considerations of this type led Vavra to suggest the study of tip clearance changes in symmetric bladings. The blading investigated in Part 3 of the present study is of the symmetric type.

the potential flow to the rotation. The resultant net secondary flow can be seen to depend on, at least, wheel speed, turning and boundary layer properties in the particular stage.

A.1.2.2 Boundary Layers/Near Wall Total Pressure Distribution

Viscous layers are present on all the surfaces in the passage and have an influence on the enure flow. The layers of principal interest in tip clearance analyses are:

Blade Surface Layers and Spanwise Flow Unlike two dimensional aerofoil or cascade boundary layer analyses where considerations of layer thickness, surface pressure or velocity distributions and drag predominate; tip clearance related blade surface boundary layer studies are three dimensional and concerned with transverse flow in the layer. Radially outward transverse flow in the blade surface boundary layer which results in a net spanwise flow over the blade needs to be considered in the flow picture of the tip gap and wall corner. A number of studies of the three dimensional layers on blades have been conducted over the years with a variety of conclusions. Recently Smith (1989) concluded from a numerical study, reconciled with his own (earlier) experiments, that the amount of fluid passing into the tip wall corner is a very small proportion of the total flow entering the tip wall corner from the annulus wall boundary layer (0.004 increasing to 0.037 near stall). His results are consistent with the stronger emphasis placed on case wall layers in tip clearance and stall studies, when boundary layers are being considered.[89]

Case (Annulus) Wall Layer(s) In an analogous manner to the concept of a secondary flow discussed above, the simple concept of a case wall boundary layer undergoes a substantial transformation when applied in a series of stages. The use of the concept of a boundary layer has developed from the resemblance of the near wall passage average axial velocity profiles to those of a conventional two dimensional boundary layer (Mellor and Wood, 1970). When the blade-to-blade velocity field is examined, however, it is clear that a typical blade row *exit* flow, *near the wall*, has a wide variation in kinetic energy. There is a typically lower total pressure (loss core) toward the pressure side of the passage and a throughflow magnitude on the suction side. Because the radial distribution of the average of the blade-to-blade velocity profile has the form that resembles a boundary layer, it is possible to calculate thicknesses and trace their development through the stage or machine. Similarly blockage factors and related quantities can be determined (Dring, 1985/9). It is important to stress these quantities are passage averaged.

At the blade local level of flow detail, these thickness averages are much more difficult to interpret or apply to the blade profile (see Wisler's (1985) discussion or Fig. 1.3-4). The concept of the case wall boundary layer also takes on the character of a near wall total pressure distribution in both radial and circumferential directions at the blade local level. The direction of the wall boundary layer velocity also becomes highly skewed relative to the blade. This effect is shown schematically in Figure A.1-4. The skewing results in a very rapid change in blade relative flow direction near the wall. The total pressure distribution near the wall will be examined in more detail in Part 2, Sec. 2.2.

A.1.2.3 Axial Spacing, Interaction and Matching

A description of the flow in the blade passages does not complete the picture of the stage flow. The interblade spacings figure significantly in the tip-case wall flow character. The axial spacing of the blade rows has a strong influence on the

[89] Note, however, that the effects of spanwise flows may be included or modelled in inviscid analyses, notably Rains (1954) and Lakshminarayana (1970).

circumferential distribution of velocities entering each blade row. The blade trailing edge wakes diffuse with increasing axial spacing and the influence of each blade row's pressure field upon another is diminished. Large axial spacings also tend to permit a radial equilibrium distribution of spanwise static pressure to be restored in the flow.

In a typical stage, blade spacings are small (5 - 15% of axial chord) and significant pressure field interactions[90] are observed between the blades. Koch (1981, Fig. 6) provides some correlative data on the pressure rise losses associated with spacing. Furber (1985) reports a peak pressure rise at an axial spacing of 4% of blade chord in a spacing variation study. The spacing was varied from 1 to 33% chord. The magnitude of improvement seems similar to Koch's data. It was of interest to note no change in efficiency was observed over the range of 1-33% spacing to chord tested by Furber.

The overall collection of the spacing effects, in concert with the primary passage blade flow angles, secondary and clearance effects, is generally referred to as the "*matching*" problem. In essence, the stage (compounded with upstream and downstream stages) arrives at a flow condition which is unique to the blading and duct environment in which it operates. An excellent demonstration of how the flow in a stage is defined by its environment is given by Longley and Hynes (1989). They forced a stage, which stalled in isolation, to operate stably by placing two unstalled stages downstream of the one that stalled and throttling the whole system below the stalling flow of the first stage. Usually any minor change in arrangement of the clearance, duct or stages "rematches" the whole flow field. Accounting for this phenomenon in the case of changing the (design) tip clearance can require redesign or restaggering of all the blade rows in a machine to reoptimize the overall design. This practice is mentioned by Mikolajczak and Pfeffer (1976, Sec. 2.2).

The principal problem matching presents in investigating tip clearance effects is the difficulty of isolating any increased losses caused by a clearance change from additional inefficiencies caused by poor flow matching in the system. Isolated rotor test baselines are useful in this regard. If a rotor, tested in isolation, is then configured as a stage it is conceptually possible to deduce the magnitude of the matching effects. This approach was adopted in a multistage test program by Dring (1983), unfortunately overall performance changes with clearance levels were not reported.

A.1.2.4 Control Volume Considerations

Another relatively subtle flow field issue arises in quantitative analysis of experimental data or the use of experimental measurements for tip flow loss estimation. From the discussion of "matching" above, it should be clear that the fluid energy within the rotor may or may not be recovered in the stator or following blading. In defining a control volume for flow analysis in a machine with multiple blade rows, it is not at all straightforward to apply detailed survey probe measurements to an overall performance measure. Conversely, integral measurements derived from a machine control volume are difficult to allocate or relate to a smaller, internal control volume where detailed measurements might be made or predictive models applied.

Test Section System Response Similarly, it is generally not safe to assume that, for example, increased losses at the rotor tip will translate into a proportional decrease in

[90] Gallus et al. (1981) describe a number of pressure field interaction and profile loading changes with spacing and blade number variation. Schulz et al. (1989) recently demonstrated the influence of periodic upstream wakes on an annular cascade flow in conjunction with a clearance change. The effect of the periodic wake disturbances noticeably reduced corner separations relative to the baseline flow.

overall system performance. Such a situation might only be true in the special case of an isolated rotor, and then, only when the rotor does not adjust its overall flow field distribution to reflect the increased losses. An overall flow redistribution may also occur in the rotor due to the nature of its duct system rather than any blade profile effect. Such system response shifts are particularly difficult to identify in experimental data.

This problem is most likely to arise when *models* for the flow at the tip are applied or calibrated by using overall machine performance data. Corrections for matching of the stages or system response shifts are noticeably ignored or absorbed in model constants in much of the comparison of predictions to test data. Generally speaking, it is difficult to experimentally isolate the clearance effects within the behavior of the whole system in any set of data.

A.1.2.5 The Experimental Basis for Modelling

In the description of the experimental research (Sec. 1.3) the studies were organized from the perspective of test configurations (Z parameter). The reason for this approach originates in Fig. 1.1-3. The flow field structure in the first rotor is clearly different from the second. Consequently, a description following Z was the preferred approach to organizing the data.

In order to account for the tip local flow or tip clearance effects in any blade row of a machine with passage flows like that of Fig. 1.1-3, any model would, at first sight, need to describe the whole field. This field is evidently complex and difficult to describe quantitatively. To avoid dealing with such a complex field description, tip clearance models are invariably formulated in such a way that the model quantitatively accounts for a difference between two passage flow conditions. If we assume the flow field in any passage, on average, is defined completely by a set of parameters and a clear dependence exists between some subsets with respect to others such that

$$\{\text{dependent subsets}\} = F(\{\text{independent subsets}\})$$

then the typical tip clearance modelling approach can be applied. Consider a simple example, $\{y\} = F(\{a,b,e\})$, and a known dependence

$$y = a.e + b$$

with two sets of experimental results $\{y\} = F(\{a,b,e\})$ and $\{y'\} = F(\{a,b,e'\})$ we can very quickly conclude from the difference of y and y' that

$$y - y' = a.e + b - a.e' - b = a.(e-e')$$

$$\Delta y = a.\Delta e$$

This problem formulation approach underlies almost all non-computational, quantitative tip clearance correlation or modelling. The difficulty encountered in proposing clearance effect descriptions is that the equivalent of {a,b} involves 15 to 20 parameters (i.e., it is a multivariable problem) in a situation where F is unknown. The nature of the equivalent of "a" in $\Delta y = a.\Delta e$ is a very basic question in this subject.

Even within this differential method, application of the experimental data in developing a model can involve major differences in philosophy concerning the information (field representation) value of the data. Some of these distinctions are fundamental and should be mentioned in case they are not obvious to the reader.

With few exceptions, clearance experiments have been conducted on particular compressor geometries, which we can designate as A, B, C, ...etc., by *only* varying the tip gap parameter (e/b). The resulting measurements capture the steady flow behavior of a series of slightly different compressors, A', A", A"'..., B', B", B"'... and so on, over ranges of speed (Ω) and throughflow (Φ) for each A, B,... etc. compressor. Omitting fluid property variations at the compressor face, one set of measurements (A') represents the tip local flow situation for

$$\{\Omega,\Phi\},(e'/b),\{Z,R\},\{AR,HR,\sigma,AA\},\{\text{blading geom.}\},\{\text{wall geom.}\}$$

independent parameters, where only the set $\{\Omega,\Phi\}$ has been varied. The dependent parameters of the compressor control volume are power (P) and pressure rise (Π). The blading and wall geometry parameter sets {blading geom.},{wall geom.} are discussed in Sec. 1.4. Their details are not essential to this discussion and have been collapsed to {tip geom.} below. Many experiments are also conducted on constant speed throttle lines so Ω can also be dropped and power coefficient (P) becomes a torque coefficient (M). Thus A', A", A"' represent flow situations for

$$\{\Pi',M'\} = F_{A'}(\{\Phi\},(e'/b),\{Z,R,AR,HR,\sigma,AA,\text{tip geom.}\}_{A'})$$

$$\{\Pi'',M''\} = F_{A''}(\{\Phi\},(e''/b),\{Z,R,AR,HR,\sigma,AA,\text{tip geom.}\}_{A''})$$

$$\{\Pi''',M'''\} = F_{A'''}(\{\Phi\},(e'''/b),\{Z,R,AR,HR,\sigma,AA,\text{tip geom.}\}_{A'''})$$

where $F_{A'},F_{A''},F_{A'''},\ldots$ imply a correlation. A similar process can be applied for compressor B giving $F_{B'},F_{B''},F_{B'''}$. The *major philosophical differences arise* in treatment of this collection of F's, i.e., $F_{A'},F_{A''},\ldots F_{C'},F_{C''}$ and so on.

Researchers who wish to develop improved machinery tend to perceive the F's as functionals containing information about optimization. They usually compare F's for different passages $\{AR,HR,\sigma,AA\}$ at otherwise similar conditions {Z,R} and construct and conduct experiments accordingly. Their perception is fundamentally *relative* and a major issue is *comparability* of the data. This philosophy underlies a lot of industrial testing where a good deal of attention is paid to the test facility and its consistency from test to test.

Investigators attempting to model the physics for the tip flow perceive these data as a representation of a universal or unique flow description, F, valid for (all) A, B, C... etc. In this case, the problem is then posed as one of proposing a reasonable physical model of or approximate expression for F and validating it with the available $F_{A'},F_{A''},\ldots F_{C'},F_{C''}$. This perception is fundamentally *absolute* or *mechanistic*. The approximate expression is usually constructed in terms of differences from a reference condition, such as zero clearance or two dimensional flow, and becomes relative, only, due to the difficulty of formulating the complete F expression (as discussed above). A major issue in this perception is *representativeness* of the data.

These distinctions in treatment and concerns with the data need to be recognized in the tip clearance literature. Each approach has its own problems. The point to be noted is that the experimental data is not exclusively generated for the purpose of developing models and in some cases is not well suited to use in model development.

A.1.3 Flow in the Tip-Wall Corner

The local conditions near the tip of a blade moving in a case wall boundary layer encompass the convergence of a number of conventional boundary conditions at one location in the passage. Secondary flows develop in the passages of annular cascades when variations of radial velocity exist across the blade span (Lieblein, 1951 p. 3.6). These secondary flows form shear surfaces in the blade wakes which correspond to the formation of a sheet of trailing vortices. The strength of the trailing vorticity is related to the spanwise loading variation and the magnitude of the radial velocity variations across the wakes from pressure to suction side.

Conditions at the case walls near the blade tip dictate, however, that there be zero radial velocity while there is also a non zero value of lift on the blade. That is, measured blade surface pressure distributions indicate non-zero values of lift. Consequently, the concept of maximum circulation shedding at the blade ends (analogous to a finite aerofoil) are unlikely to be representative of flow conditions where the radial velocity must be zero and blade and endwall boundary layers are acting. The axial and circumferential velocity also tend to zero as the wall is approached, in the boundary layer, so the trailing vorticity will also vanish at the wall.

At the same location, the blade wake in the relative frame needs to adjust to the case wall conditions in the absolute frame. The blade tip lift (static pressure distribution) condition also has to adapt to the scraping motion of approaching fluid. Resolution of a compatible local flow condition with the blade surface flow and overall throughflow is also required in addition to accommodating any upstream blade wakes which are being carried through the rotor. This adjustment must also take place with negligible radial flow at or near the wall, as mentioned above.

Generally speaking, this type of situation is a good candidate for a flow separation somewhere in the immediate vicinity of the converging requirements. Separation or an equivalent region of flow recirculation introduces a much higher degree of uncertainty in terms of analysis and design. The high probability of a separation-reattachment feature in the tip-wall corner flow is worthwhile noting at this point in the discussion. Exploration of a flow mechanism of this type was noticeably absent in the compressor literature prior to 1989 and has only received recent attention in cascades.[91]

In terms of design flexibility to cope with the flow situation described, the machinery options are limited. It is well known that the flow in and around the tip clearance gap is time varying in the passage frame and that, without enormously increased mechanical complexity, the blade section profile can only be designed in a time average sense. When considering the wall geometry and the relative motion, it is clear that wall geometries which regulate the flow, in the relative frame, either via the wall contour or

---

[91] Schulz (1989) and Storer (1989) discuss the consequences of a fluctuating flow and tip clearance changes, respectively, on the presence of a mid chord to trailing edge separation observed in annular and linear cascades modelling stators. Both periodic fluctuations and small clearance increases from a sealed tip reduced the separated zone and improved the flow. Larger clearance increases degraded the flow. Neither inflow was skewed. Rai (1989) describes some computational difficulties encountered with the presence of a separation region due to tip clearance when modelling an experimental turbine stage. The separation was eliminated by reducing the clearance gap in the computation from e/h = 0.014 (the experimental value) to 0.004.

surface can be designed with lower complexity. The major options, however, are profile shape, blade tip treatment, wall control[92] and suction or blowing.[93]

It can be seen from this outline of the flow conditions in the tip wall corner that the design problem is not at all straightforward at the detailed or local flow level.

A.1.4 Gap Flow/Flow Stability on Curved Walls

At an even closer proximity to the tip gap and case wall other physical considerations arise. These are, particularly, the flow in the gap and the flow on the *curved* wall which forms one boundary of the gap flow:

Gap Flow The local geometry and boundary conditions in the gap can be approximated in several ways. A very convenient approximation to the geometry is to consider the flow in an analogous manner to a parallel flow between (infinite) flat plates or in a gap between two rotating concentric cylinders. In such cases analytical solutions for parallel flows can be applied to the gap flow. The most widely applied approximation is the Couette flow. Schlichting (1955 pp. 61-69) provides a number of relevant solutions. The Couette solution, however, only accounts for the effects of streamwise pressure gradient on the velocity profile. This situation applies to a tip gap flow when the thickness of the blade is large relative to the gap height. In this case, the flow still only roughly approximates a *two dimensional ideal.* Using such an idealization also neglects wall curvature and the typically small thickness-to-gap ratio of compressors, however, it is a useful bench mark or reference flow in terms of analysis. How well Couette flow solutions represent the flow is examined in more detail in Part 4.

Flow Stability on Curved Walls A less noted geometric feature of the tip clearance flow is the curvature of the wall bounding one side of the gap. It was noted in App. A.1.1 that the curvature of the tangential streamline in the tip-wall corner scales with tip radius independently of cascade parameters. This fact is of some relevance to tip flows if it is noted that, for a fixed tip speed (U_t) and gap size (e), the wall curvature determines the Taylor viscous stability of the in-gap flow. Schlichting (1987 p. 526) describes the Taylor stability criterion. If the Taylor Number for a tip gap is determined, assuming t/e large, then

$$Ta = (\rho U_t e/\mu)(e/R)^{0.5} = (\rho U_t a/\mu) AA(1 - HR)^{0.5}(e/b)^{1.5}$$

For typical compressor conditions, i.e., $\rho U_t a/\mu = 5x10^5$ and an $AA(1 - HR)^{0.5}$ of approximately unity, then the instability vortex onset ($Ta > 41.3$) occurs at e/b = 0.002 and laminar to turbulent transition ($Ta > 500$) occurs at around e/b = 0.01. As e/b = 0.01 is at the lower bound of practical clearance levels, it can be seen that the flow inside the gap provides *favorable conditions* for (turbulent) Taylor vortex production. The tip gap would then act as site of continuous vortex generation as the blade moves over the case wall.

---

[92] As aerocompressors experience a wide range of thermal and stress induced clearance changes while operating, the gap dimensions can be actively (in addition to passively) tuned in certain segments of the flight envelope. Beitler et al. (1980) have proposed an active clearance control system using selective heating and cooling of core compressor walls. The concept involves controlling the clearance to achieve the optimum performance in different flight segments. Their trade-off study shows a net gain in performance for an engine using such a system.

[93] Pouagare et al. (1986) describe the outcome of fluid injection through the tip end of an isolated, untwisted aerofoil in a wind tunnel. Their study was exploratory with a view to reduction of tip leakage flow and losses by blowing the tip end to effect a seal. Their results were mixed and there were difficulties in finding a suitable injection scheme.

In the passage outside the gap, the *absolute* flow over the case wall is also consistent with the formation of Goertler vortices at some curvature. In a similar manner to the derivation above, the absolute flow angle of an unstable wall flow can be determined from the stability limit given by Schlichting (1987 p. 533) and the usually known passage parameters and case radius dimension. This means that the flow over a curved case wall can develop a vortical structure independently of any vortices the tip gap might produce.

The influence of the curvature of the wall bounding the tip gap is therefore more subtle in terms of initiation of vortical flows in the passage than the often stated "the roll-up of the tip leakage forms vortex" argument. Both the Taylor and Goertler criteria indicate the flow undergoes a transition as $1/R^{0.5}$ increases, thus as machine radii decrease (or as the flow direction becomes more circumferential) the prospect of vortex sheets in the wall flow increases. The transitional nature of the flow should be noted as some compressors used for tip clearance experiments have been quite small, while, the range of radii that have been experimentally addressed, overall, is relatively large (see Table 1.3-1). Consequently, the wall flows in the experimental machines will be distributed over different regimes of flow stability and tendency to vortex production.

A.1.5 Flow Field Issues Summarized

From this overview of the flow field and its interaction with tip seal clearance, the reader can see that there are numerous factors to be considered in a general analysis of the flow. The leading physical points made in this section are summarized below:

(1) The geometry of the passage, in which the tip clearance resides, can vary a great deal in terms of wetted wall area and tip local wall curvature with respect to the tip clearance gap height (App. A.1.1 and App. A.1.3).

(2) For a given wheel speed, work input distribution and throughflow, the whirl distribution determines the degree of tip tangential pressure loading and also the blade relative velocity magnitude and direction at the tip element sections (App. A.1.2).

(3) The amount of inviscid turning required of the blade element sections in conjunction with the amount of viscous drag on the wall area and the local wall curvature will influence the secondary flow pattern near the tip (App. A.1.3, A.1.4).

(4) Upstream case wall boundary layers and wakes will modify the flow in the tip region. The strength and impact of the case wall layers and wakes will depend on axial spacing, number of stators and their matching to the flow (App. A.1.2.3).

(5) Measurable changes in the flow due to tip seal changes, particularly efficiency or loss quantities, may be difficult to allocate between the clearance effects, changes in characteristics of the machine and the test facility response to flow changes. Changes in these quantities may also be difficult to attribute to a particular blade element's performance (App. A.1.2.4).

The flow field and the points above need to be recalled when the data base of available tests is examined in the following section on experimental observations. Comparisons of the performance of one test compressor to another, in terms of clearance, at least require these aspects of the flow field to be reconciled with any firm conclusions.

References (see also Part 6)

Adamcyzk, J. J., "Model Equation for Simulating Flows In Multistage Turbomachinery," ASME 85-GT-226, Mar. 1985.

Aerodynamic Design of Axial Compressors, NASA Special Publication SP-36, U.S. Dept. of Commerce, Technical Information Service N65-23345, 1965.

Dring, R. P., and Oates, G., "Through Flow Theory for Non-axisymmetric Turbomachinery Flow, Part I - Formulation, Part II - Assessment," ASME 89-GT-304 and ASME 89-GT-305, June 1989.

Furber, S. B., "The Effect of Very Low Axial Clearance on the Performance of an Axial-Flow Compressor Stage," *Jrnl. of Fluid Mechanics*, Vol. 159, p. 477-485, Oct. 1985.

Mikolajczak, A. A., and Pfeffer, A. M., "Methods to Increase Engine Stability and Tolerance to Distortion," AGARD ?, p. 7-1 to 7-17, 1976.

Lieblein, S., "Secondary Flows In Annular Cascades and Effects of Flow in Inlet Guide Vanes," NASA RM E51G27, 1951.

Longley, J. P., and Hynes, T. P., "Stability of Flow through Multistage Axial Compressors," ASME 89-GT-311, June 1989.

Mellor, G. L., Wood, G. M., "An Axial Compressor End-Wall Boundary Layer Theory," ASME Gas Turbine Conference and Products Show, Brussels, Belgium, Paper No. 70-GT-80, May 24-28, 1970.

Schlichting, H., "*Boundary Layer Theory*," McGraw-Hill Book Co., Inc. Seventh Edition, 1987.

Smith, G. D. J., "Radial Boundary Layer Flow on an Axial Compressor Rotor Blade," ISABE 89-7057, 1989.

The Aerothermodynamics of Aircraft Gas Turbine Engines, G. Oates, Ed., AFAPL-TR-78-52, 1978.

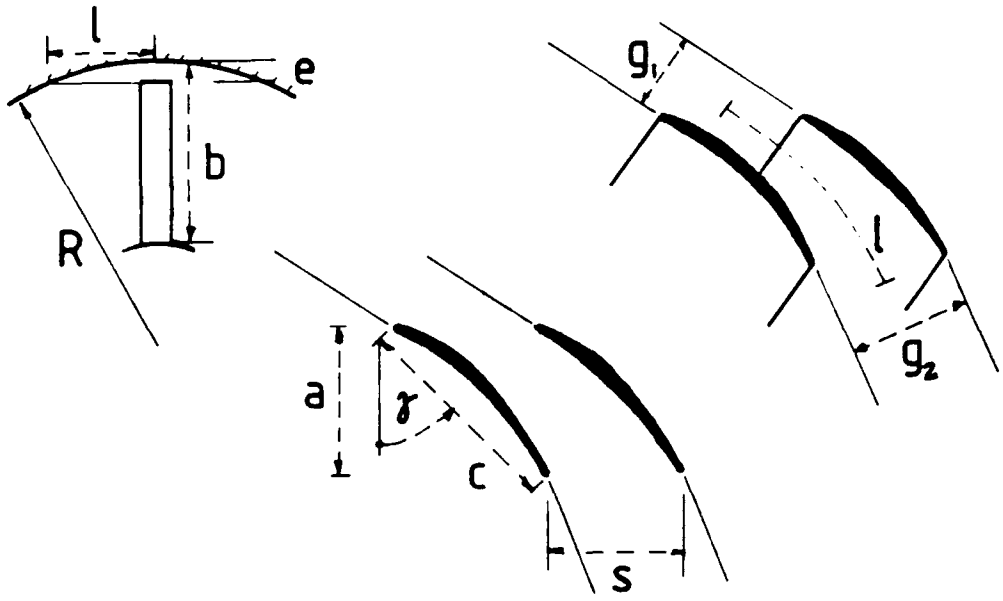

Fig. A.1-1 Convention used to describe the passage shape in a stage and the wall footprint and curvature characterization.

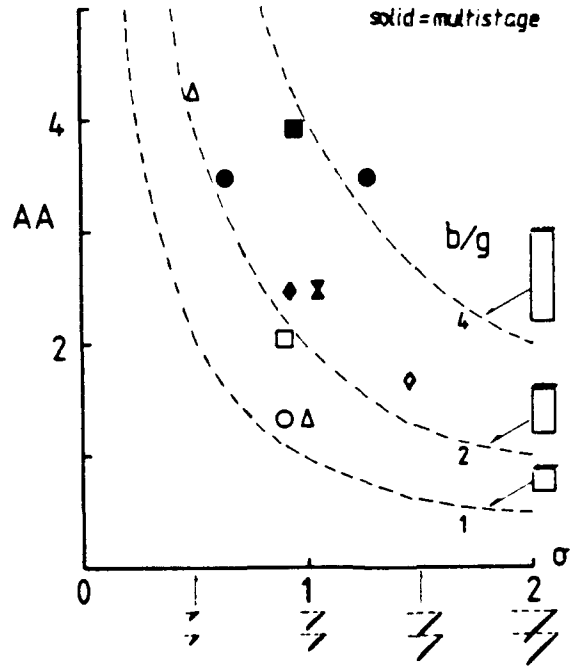

Fig. A.1-2 Comparison of experimental compressor passage shapes used for a variety of studies in the literature.

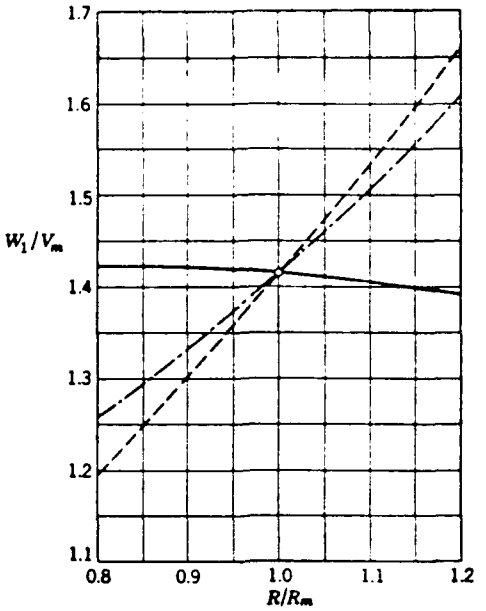

. Relative Velocity W_1 ahead of Rotor Blades of Axial Flow Compressor Stage with 50% Reaction at Mean Radius R_m. ———Symmetrical blading. — · — Constant flow angle α_1. — — — Free-vortex flow.

Fig. A.1-3 The effects of whirl distribution on spanwise velocity and tangential pressure loading for symmetric and free vortex blading, from Vavra (1960).

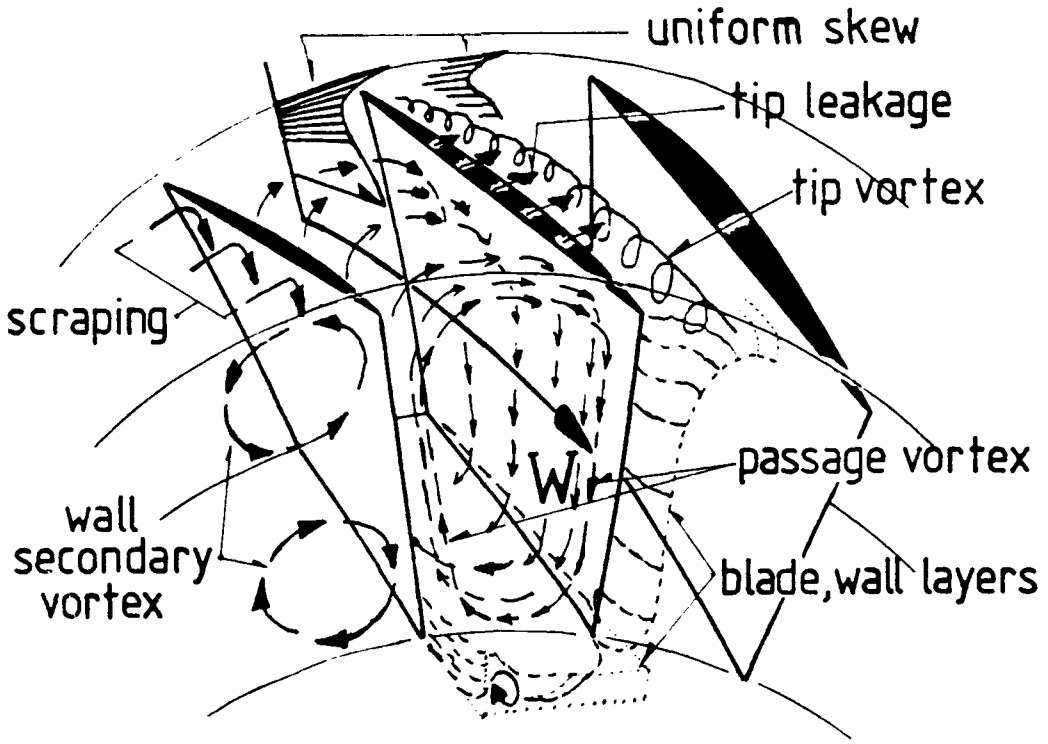

Fig. A.1-4 Schematic diagram of the secondary flow motions produced in the passage by different effects including skew.

A.2 Definitions of Efficiency

A concern which arises frequently in the tip clearance literature involves the definition of efficiency to be used in describing the entropy changes in the flow as tip clearance is varied. The most commonly used measures of efficiency are adiabatic (or isentropic) and polytropic. The adiabatic efficiency definition compares the work done on the fluid to the energy input of the pressure rise process. It is based on the fact turbomachines are effectively adiabatic and that the work done in an adiabatic process can be determined from the process end points regardless of the degree of reversibility. For a steady flow process per unit mass

$$T.ds = dh - v.dP \qquad A(2)$$

from state 1 to state 2, with negligible initial or final kinetic or potential energies, the work input (W_{flow}) to an incompressible fluid is given by $v_1(P_2-P_1)$ or $(P_2-P_1)/\rho$. The adiabatic efficiency can then be defined very simply as

$$\eta = W_{flow} / E_{input}$$

and this expression can be transformed to a rate efficiency

$$\eta = \Phi\Pi/P \qquad A(3)$$

For a perfect (compressible) gas where $v = RT/P$ and $dh = C_p dT$ the entropy change can be found by integration of A(14) above. In this case the reversible work between two pressure levels is usually used to define the efficiency. As an adiabatic reversible process is isentropic $W_{reversible}$ can be found from integration of A(2) when $ds = 0$. The isentropic efficiency is defined as

$$\eta_{is} = W_{\text{reversible from T1,P1 to P2}} / E_{input}$$

Due to the differences in state equations, η is generally not equal in magnitude to η_{is}. The polytropic efficiency is based on the assumption that the equivalent process between the end states can be connected by a reversible process with heat addition. The efficiency defined using a polytropic process is often called the "infinitesimal stage" or "zero pressure rise" efficiency. The polytropic efficiency can be defined as

$$\eta_p = W_{\text{reversible(polytropic) from T1,P1 to P2}} / E_{input}$$

It can be thought of as an isentropic efficiency corrected for the effect of pressure ratio. It should be noted that much of the stage testing in clearance effect studies has been conducted at pressure ratios close to unity. In this case the efficiencies above have similar (but not exactly the same) magnitudes. However, it is relevant to note that efficiency *decrements* are commonly used to gauge clearance effects. The differences in *decrements*, due to definition of the efficiency, are much smaller than differences between the efficiency *magnitudes* due to definition at a similar pressure ratio. The differences in the decrements, due to definition, are usually insignificant for analysis purposes when studying tip effects.

The reader should note that adiabatic efficiency has generally been applied to data in the present study due to its input-output definition.[94] The distinction, however, is largely academic in most of the discussion due to the use of decrements or changes in efficiency in what is effectively constant pressure ratio testing. *It is more important to note that, whichever efficiency is used, it is applied to a particular control volume when determined (see App. A.1.2.4)*

Loss/Efficiency and Blockage/Work Transfer Distinguishing two different measures of flow *quality* in the performance evaluation of a turbomachine passage flow field is also important in the modelling and flow field interpretation. The first is the mechanism of loss production or entropy increase of the fluid associated with the actual energy transfer from the blading to the fluid or vice versa. The flow quality is defined in terms of loss coefficients or efficiency. The second description involves the idea of an equivalent obstruction having had an effect on work transfer in the passage. This concept is normally called blockage. Blockage is a conceptual measure of obstruction. It is used to relate the actual work transfer effected due to the actual fluid flow when compared to a desired, ideal (or unobstructed or analytically possible) work transfer that should occur in the passage.

Clearance effects are usually quantified in terms of efficiency *decrements* or entropy or loss *increments* at the machine or stage level rather than blockage in the models examined so far. If one looks for more localized methods of describing the tip gap effects, the physical interpretation of blockage seems to be a good way to model or account for tip local entropy increases. Put very simply the blockage level might be considered to reflect the fact that there is a spanwise entropy distribution in the fluid entering any stage. However, Mellor (1953) proposes an alternative description in terms of a total pressure (enthalpy) distribution near the wall approaching the stage.

Either can be used as the basis for physical interpretation[95] of the tip effects. However, due to the interpretive issues involved with blockage, it is desirable to maintain a clear distinction between loss and blockage descriptions in any model development or computational analysis. From the discussion of the "strip theory" idealization in App. A.1, it is clear there is some uncertainty involved in defining the work transfer that should occur in the passage. Approaches to tip clearance effect description that rely on a flow model typically involve specific assumptions in this area, whereas correlations (discussed below) do not.

References (see also Part 6)

---

[94] These definitions of efficiency have been included in the thesis to support the general use of adiabatic efficiency differences when making comparisons of clearance effects in different stages. In a number of discussions there has been insistence on the part of others that polytropic efficiency must be applied when considering efficiency changes due to clearance. By definition polytropic efficiency is useful for standardizing blading performance or projecting blading performance over a range of pressure ratios. Theoretically it is the most appropriate efficiency to use in stage comparisons where reheat needs to be considered. Having considered this fact, use of polytropic efficiency has not been preferred in this study. Due to the difficulties of identifying or isolating efficiency changes due to tip clearance, it is not always certain the observed results exclusively relate to the stage aerodynamics or reheat assumed in the definition.

[95] However, it seems to be characteristic of the wall flow that boundary layer thicknesses based on momentum grow slowly or stabilize in a multistage machine while thicknesses based on temperature tend to continually increase through the machine. This observation suggests pursuit of entropy (loss rate) correlations for phenomena induced by tip gap variation might be more instructive than blockage approaches in terms of physical insight. Hatch et al (1954) provide an example of calculations including a cumulative loss approach based on entropy gradient.

B.1 Flow Quality in the Test Section and Facility

Initial measurements on the low speed compressor test rig showed substantial scatter in flow measurements for repeated testing of the same configuration. An analysis of the data showed that the accuracy level of signals acquired was not satisfactory for a clearance study. Further work to improve the flow stability and improve the measurement quality has been set out in the attachment. The results were of general interest in terms of test facility development.

B.1.1 Flow Stability and Uniformity

An important consideration in upgrading the overall, or combined, accuracy of the measurements was the actual stability and uniformity of the flow. The measurement system scanner and Scanivalves required a time interval of roughly one minute to switch through all the channels and record the measurements. Rapid or non-uniform fluctuations of the flow in the test section could distort the measurements and provide erroneous information.

B.1.1.1 Stability

Observations with a linearized hot wire in the compressor inlet (just upstream of inlet guide vanes) showed that flow conditions in the test section were unsteady and that instrumentation and data acquisition should be developed to account for an unsteady flow. Hot wire readings showed an oscillation with a nominal velocity of 8 units fluctuating from 7 to 9 units in periods of 5 - 10 sec. This represented velocity changes of the order of 12.5% and dynamic pressure fluctuations of 25%. A small part of this variation could be attributed to inlet air temperature variability. However, it appeared that fluctuations of at least 5% velocity in the test section were also detectable on the Scanivalve and differential transducer measurements.

There were three probable sources of such fluctuations. The first was a small pressure differential between inlet and exhaust of the compressor tunnel. Reviewing the compressor static-head, flow characteristic, it was possible to show the sensitivity of the test section dynamic pressure to static pressure rise was roughly 9.0 for a single stage. Thus a 2.5 mm (0.1 in) water pressure fluctuation from end-to-end of the tunnel would produce a 23 mm (1.0 in) fluctuation in dynamic pressure in the compressor test section. For a particular flow point where the total dynamic pressure was 162 mm, the 2.5 mm fluctuation was capable of producing a 14% change in dynamic pressure or roughly 6.7% of velocity.

Secondly, any fluctuation in pressure recovery in the diffuser would produce a similar result. Measurements of fluctuations in diffuser static pressure rise using a close coupled differential transducer showed fluctuations over a range of 5 mm (0.2 in) at 86 mm (3.3 in) of diffuser pressure rise. This pulsation could account for part of the observed tunnel fluctuations. Any oscillation in a separated zone in the diffuser could generate the pulsation. It should be noted this outcome would only be slightly altered with increased throttle due to the sensitivity being dependent on the compressor pumping characteristic. However, more stages should substantially increase the characteristic slope and thus reduce the sensitivity.

A third factor was observed at the inlet nozzle plane. Smoke puffed into the inlet mesh enclosure showed a strongly swirling motion in the inflow at the nozzle throat. This strongly resembled a ground effect vortex being sucked into the inlet. The excitation this vortex might produce at the compressor face appeared to be at a much higher frequency than the 5 to 10 sec. fluctuation observed. The general form of the observed

gusting is shown on Figure B.1-1, where repeated samples of the compressor-face radial rake dynamic pressure are plotted. Repeated samples of the ensemble averaged flow (i.e., the average of the data of Fig. B.1-1), however, were indistinguishable from one to another.

Similarly, data taken at different times indicated the average flow was stable. This strongly suggested an end-to-end pressure mismatch or a very low frequency rotating separation in the diffuser. It had previously been noted that the compressor face flow angle fluctuated with a similar period and that a fence and trips to produce a uniform separation on the diffuser cone greatly reduced this apparent yawing of the flow. Sealing of the diffuser cone to eliminate any back flow into the test section also seemed to reduce the fluctuations. A consequence of these observations was the realization that the simple arrangement of an inlet, a low pressure rise stage and an exhaust diffuser would inherently be very sensitive to external conditions.[96] The fluctuation would also increase with increasing hub-to-tip ratios in the test section.

In the particular case of this test rig, having the inlet nozzle outside the building was seen to aggravate the problem. Wind effects on the building itself could induce larger variations than might be encountered if the whole tunnel was inside the building.

B.1.1.2 Uniformity

The uniformity of the flow was initially addressed in terms of circumferential uniformity. The radial flow distribution became an issue of stability later in the measurement program and it became clear that the fluctuations in the axial velocity involved radial non-uniformity of the flow. Once trips had been installed in the diffuser, the circumferential uniformity of the flow, measured by yaw angles in the passages, greatly improved and yaw balanced probes remained balanced indefinitely. In the inlet, probes mounted anywhere in the 0-90 deg measurement sector indicated similar average total pressure readings and it was apparent that there was no significant (non-periodic) circumferential variation in the flow. Radial uniformity, however, was only demonstrated with very long averages of readings and there was appreciable variation of radial distributions of axial velocity measured in short time intervals.[97]

B.1.2 Repeatability

A number of repeatability issues arose in the program. One concern was the repetition of test sequences for different builds of the test section and the degree of consistency of flow path geometry from one build to another. Another issue was the repeatability of measurements of the flow from one test condition to another.

B.1.2.1 Blading and Test Section Builds

Each build is assigned a roman numeral and the builds are referred to throughout the report by these designations. Different blade sets were used for some builds. Each set used as a row is assigned a number subscript. In order to distinguish different blade sets by position, in the discussion, rotor and stator blade positions are referred to as R1, R2 or R3 and S1, S2 or S3 and blade sets by subscripts where appropriate. Thus $R1_2$ refers to the second set of rotor blades in position 1, IA_2 refers to the second set of

---

[96] This strongly recommended the approach of having an auxiliary fan in the circuit and higher throttle resistance to substantially steepen the system head-flow characteristic for a single stage or isolated rotor test configuration.

[97] This unsteadiness, in conjunction with the stability of the flow angles, suggested the tangential velocities adjusted in concert with the axial velocities and that the radial fluctuations were coupled to effects discussed under stability (above).

type A inlet guide vanes and $E1_2$ refers to the second set of vanes in exit guide vane position 1. Table B.-1 correlates compressor blading by position, set and build.[98]

Table B.1-1

Test Section Build Summary. Blade Sets used in each Row are denoted by subscripts.

Position	I	R1	S1	R2	S2	R3	S3	E1	E2
Build I		IA_1	R_1	S_1					E_1
Build II	IA_2	R_2	S_2					E_2	
Build III	IA_2			R_3	S_3	R_2	S_2	E_2	

B.1.2.2 Flow Repeatability

In order to conduct the measurement program in a fundamentally time varying flow environment, it was necessary to average extensively as data were recorded. Each channel and pressure line was assigned an individual sample size to record a single data value. The data acquisition procedure was subsequently developed to process an ensemble average, of each channel, for all the signals acquired. The ensemble sample size was re-evaluated as stages were added to the test section to define the minimum ensemble number, and thus time, to acquire stable data. In addition, the pressure datum used for Scanivalve differential pressure measurements was placed in the test section at the lowest static pressure available. This configuration reduced differential pressure data sensitivity to the fluctuations and reduced the measurement scatter appreciably.

B.1.3 Measurement Considerations

A major consideration was the axisymmetric quality of the measurements to be taken. This encompassed the circumferential uniformity of the flow and the blade tip gaps and the wakes from struts and supports. In addition the signal discrimination and averaging that would be necessary in the data acquisition was a consideration.

B.1.3.1 Circumferential Uniformity

Due to the limited number of survey ports in the compressor casing and the mechanical arrangement of the casing halves, surveys of the circumferential uniformity of the whole flow were not possible. Point surveys in certain locations indicated acceptable levels of uniformity. For experimental purposes it was assumed data measured at different circumferential locations could be correlated.

The blade tip gap was enlarged to the different gap levels by mounting a grinding wheel on the compressor case and slowly moving the blades past the wheel. The grinding wheel axis was aligned parallel to the compressor axis and the wheel was dressed using a fixture aligned to the axis. The resulting tip gap was uniform from leading to trailing edge of the blade irrespective of any stagger misalignment error of the blading. Blade-to-blade uniformity of the resulting gaps was measured using a dial

[98] The blade/vane sets showed very slight differences in flow angles or flow character. These differences could be attributed to both manufacturing variations and installation or alignment differences with each build. Generally the magnitude of the variations were small and were considered negligible for experimental purposes. Consequently, the blade set designations are only used in Table B.1-1 of the report in order to provide a record of the sets installed in each row position. Individual blade positions in the row were not maintained from build to build or recorded.

gauge in one of the circumferential survey slots when the case was closed. Tip clearance uniformity was within ±0.038 mm (±0.0015 in) of the nominal gap dimension. The grinding arrangement and fixtures are shown in Figure 3.4-2.

B.1.3.2 Strut Wakes

The upstream face of the compressor test section was preceded by the rotor bearing housing which was supported by six substantial struts. The struts had a uniform aerofoil section and were aligned axially. The wakes from these struts were convected into the test section and could introduce an unwanted disturbance in the measurements.

After the strut wakes had traversed several blade rows it was very difficult to know their precise position or influence on the measurements. Consequently, measurements downstream of the inlet guide vane row and the first rotor were scrutinized for wakes but diligent strut wake tracking was not attempted after the first blade row due to the extended circumferential stretching of the wake filament in subsequent rows.

Based on approximations to transit streamlines through the blading, the wake locations at each survey plane were estimated and the bearing housing was positioned to minimize strut interference on each build. The struts were placed in the same positions for each of the Build III A-B clearance tests. Tests using the boundary layer spires, which could be rotated circumferentially relative to a probe, as a circumferential distortion showed the blade-to-blade wall pressure measurements were not affected by upstream distortion. However, the strut wakes originated much closer to the test stage and their influence on the detailed measurements was difficult to establish.

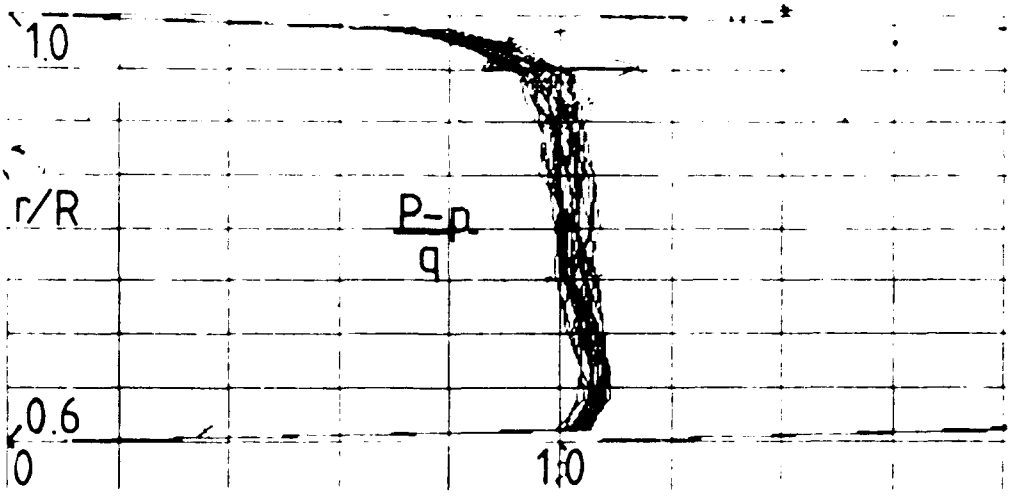

Fig. B.1-1 Repeated samples in a five minute period of compressor-face total pressure, showing the degree of fluctuation in the pressure.

B.2 Instrumentation and Measurement Uncertainty

B.2.1 Low Response Instrumentation

The low response instrumentation was used to measure overall flow conditions in the test section (the operating point) and the radial distribution of the passage average flow between the blade rows.

Reference measurements of inflow temperature and dew point were needed to determine compressor face density. Shaft torque and angular velocity were to used to define power input and wheel speed. The torquemeter was calibrated statically using a known moment. The system used to determine the angular velocity of the shaft was calibrated with a squarewave generator which provided pulses at a known frequency. Stage average temperature rise and the blade passing frequency derived from high response pressure fluctuations were used to confirm the shaft torque and speed sensors performed accurately when the shaft was rotating.

The pneumatic instrumentation used in the program was customary for routine compressor testing and consisted of wall static tappings, commercial Pitot static, Kiel, cobra, yaw and five hole sensors for pressure, angle and velocity sensing. A list of the probe types and their characteristics is set out in Table B.-1.

Table B.2-1

Summary of Test Program Pneumatic Probe Complement and Application. (Pt. indicates measurement made at a single radial-circumferential point)

Probe Tip Type	Size (in)	Qty	Application
Impact Tube	.062	20	Pressure (Radial Rake P & Q, fixed)
Kiel (NPS made)	.062	11	Pressure (Circ. Rake R, surveys)
Kiel	.062	4	Pressure (Pt. Mean line Exit, fixed)
Cobra	.062	3	Pressure/yaw (Pt. S, U, V, survey)
Pitot Static	.062	1	Vel/pressure, (Pt. Mean line fixed)
Five Hole	.125	3	Vel/yaw/pitch (Pt. X, Y, Z, surveys)

Because the operating point and single port pneumatic probes were conventional they have not been described in detail in this document. The fabrication and calibration of the circumferential rake is reported in Moyle, 1980. The multiport probes were calibrated in a free jet or a small wind tunnel. Their tip calibrations were fitted and stored as polynomial surfaces or functions following methods which have been described in Appendix B.3.

The pneumatic pressures were measured with Scanivalves. The Scanivalve actuators were driven by the data acquisition controller and the pressure measured with a 0.170 bar (2.5 psig) differential pressure transducer. The transducers were calibrated using a water manometer and a variable pressure source. The reference pressure in the circuit was placed at the lowest pressure case wall static location in the test section to enhance measurement accuracy and repeatability. The Scanivalve zero offset was measured at the beginning and end of each sweep. This tare was used to adjust pressures for zero drift. Usually it was extremely small, of the order of 1 mm (0.04 in) of water. The calibration pressure was also recorded in each sweep to confirm the calibration of the transducer was consistent. The transducers were packaged to stabilize temperature

drift and were shielded from direct sunlight which was found to induce a small thermal calibration shift. Pressure lines were periodically leak checked or replumbed as the duration of the program required routine maintenance of the equipment. This general arrangement gave repeatable and verifiable pressure data throughout a test and from one test to another

B.2.2 High Response Instrumentation

A systematic variation of tip clearance in the embedded stage provided an opportunity to survey the flow consequences, within the passage, of clearance changes on the blade-to-blade time-average flow field relative to the stator. By using high response sensor elements and a timing signal from the rotor, the sensor output could be correlated relative to blade position and time averaged.

A plate arrangement was developed for the circumferential survey slots which would permit this type of survey and averaging. The plate is shown in Figure 3.3-3. In this arrangement, a plate in the wall over the rotor was drilled to allow axial and circumferential movement of either a wall pressure transducer or a wall shear stress sensor. At the rotor exit a slant wire/film velocity sensor or an impact pressure transducer could be mounted to allow different radii to be traversed and provide a blade-to-blade survey of the rotor exit velocity or pressure field. By moving the sensors circumferentially, wake convection influences could be examined and the end of the passage (bounding the tip gap being studied) could be surveyed.

Phase Lock System The blade-to-blade measurement phase-lock on the rotor was achieved by triggering the acquisition system using a magnetic (flux-gap) sensor. A timing wheel on the shaft with a single hole provided a one-per-revolution pulse in magnetic flux. This pulse was fed to a signal generator which produced a shaped pulse (square wave) which in turn triggered a stroboscope facing a viewing port above the other rotor (i.e., the rotor not being studied). An inscribed blade on this rotor was coarsely timed to be visible through the Plexiglass viewing port by moving the flux sensor relative to the shaft timing wheel. By phase shifting the shaped pulse using the signal generator, the scribed mark on the blade tip could be finely positioned with respect to a grid scribed in the Plexiglass. The grid position was known precisely and provided the spatial reference in the absolute frame. The phase shifted shaped pulse rise was used to trigger both the data acquisition sequence and fix the blade position on the grid. Spatial errors due to twist or other backlash between the timing wheel on the shaft and the blade tip were avoided in this arrangement.

This phase lock scheme permitted the blade edge positions to be fixed without any reference to the acquired signal. Independent spatial resolution capability for the blade edges was considered to be essential for locating the position of the scraping, pressure side induction and suction downwash expected to be observed in the near wall flow.

Probes and Their Resolution The sensors used to acquire blade-to-blade data are summarized below with their leading characteristics, Table B.-2. In terms of flow resolution, the probe dimensions were small compared to the passage dimensions and good resolution of flow features could be expected in the passage. However, some of the sensor dimensions were nominally of the order of the tip dimensions (esp. near the blade trailing edge) and measurements on the case wall under (or in) the tip gap were not expected to be able to spatially resolve the flow for all probe tips. Hence all sensors provided good temporal resolution at the tip based on the blade maximum thickness, but good spatial resolution was *generally* restricted to within length scales of the order of the passage width.

Table B.2-2

Type and Characteristics of High Response Sensors.

Probe Tip Type	Size (in)	Qty	Application
Flush Kulite	0.093	1	B-B Wall static press. survey
Capped Kulite	0.093	1	B-B Wall shear survey
Impact Kulite	0.093	1	B-B Exit total press. survey
Slant Wire/Film	0.001	1	B-B Exit Vel/yaw/pitch (W, survey)

Details of the high response sensor calibrations, frequency response analysis and sensitivity to pressure, temperature and other gradients are attached in App. B.4 and B.5. The Attachment also discusses spatial resolution in more detail. Overall, the high response instruments and associated electronics were able to meet the measurement response requirements in a machine with a nominal blade passing frequency of 805 hz. The survey configurations used are discussed in Part 3, Sec. 3.4.

B.2.3 Data Acquisition System

Data acquisition was accomplished with either a Hewlett Packard 9845 controller or a later 9000/300 controller and a 98032A interface bus. Acquisition systems on the bus included a digital voltmeter, system voltmeter, scanner and Scanivalve control unit.

The controller directed a programmable acquisition sequence (sweep) over the set of sensors connected to the scanner and stored the data on magnetic tape or disk. The probe sensor field included pressure transducers, radial position and yaw angle potentiometers and thermocouple junctions. Speed, torque and similar operating data were acquired in the same manner with strain or frequency transducers. The probes were positioned manually, balanced and then a data channel sweep recorded their position.

Pneumatic and related low frequency data was processed through the digital voltmeter and ensemble averaged. Hot wire (or film) and Kulite data was processed in a similar fashion through the system (high speed analog to digital) voltmeter. The high speed data sampling was triggered by the pulse from the timing wheel fitted on the compressor shaft, phase shifted, to fix the blade's spatial reference, as discussed previously.

A summary of the processes and programs used on the HP 9845 are described in Moyle (1980). Most of the software was upgraded to be HP 9000/300 compatible without significant change in acquisition philosophy (Moyle, 1990). The system provided a flexible and reliable data acquisition procedure. It was limited, however, in high speed acquisition capability to 5000 readings per second due to system voltmeter capabilities. Consequently, all blade-to-blade ensemble survey data was acquired once per revolution using the precise timing capabilities of the system voltmeter to delay (in 1 μsec increments) then hold and read a voltage with respect to the shaped trigger signal.

B.2.4 Instrumentation and Measurement Uncertainty

Pressure difference was the principal measurement in the program and was used extensively to establish or derive other quantities. These were primarily velocity and loss quantities in the flow field. By using Scanivalves the same pressure transducer was used for the majority of the low response measurements and bias error was not a

significant component of uncertainty when the pressure difference data were used to establish derived quantities. High response measurements of unsteady flow quantities required more elaborate calibrations and verifications on a channel by channel basis.

The derived quantities were typically formulated in terms of a function of pressure difference normalized by a reference pressure based on wheel speed and compressor face density. Consequently, bias errors were significant only when the instrument, used to measure a reference quantity, was altered in the measurement program. Bias errors would be significant if the data were used in comparison with data from other experimental sources. The precision of the measured quantities were, therefore, of primary concern in this program and uncertainty has been expressed in terms of precision of the derived quantities. Table B.2-3 sets out the precision of the primary measurements. Precision is defined using the methods of Abernathy (1973, pp. 1-7).

Table B.2-3

Precision of Primary Measurements from Calibration.

Measurement/Quantity	Sensor/Calibration	Prec.(±% pt.)
Pressure Difference	Scanivalve/Micromanometer	0.1
Absolute Pressure	Barometer	0.015
Absolute Temperature	J/T Thermocouples/NBS#561	0.05
Wheel (Shaft) Speed	1/Blade pulse/Oscilloscope	0.006
Shaft Torque	Torquemeter/Static Moment	0.4
Dew Point Temp	EG&G Humidity Analyzer	0.03
Probe Radial Posn.	Vernier Scale	0.15
Probe Angular Posn.	Digital Level/Vernier Scale	0.66

It is noteworthy that the Scanivalves acquire pressure data sequentially while the data are processed as if they were acquired at the same instant of time or as if the flow was absolutely steady. In fact, the compressor hunts continuously for the operating point in response to changes in inlet air temperature (typically ±1 degK (±2 degF), end-to-end duct pressure variations (2.5 mm (0.1 in) of water) due to external wind conditions and to some degree its own flow field. Over a period of 60 seconds a typical pressure channel will fluctuate slightly. This period was typically less than the two to three minutes required to cycle the Scanivalve through all the channels. Consequently, an alternative measure of uncertainty was provided by the repeatability of the processed data for a (nominally) constant throttle screen resistance. To the extent that the screens were kept clean and free of debris, comparison of repeated measurements of derived quantities provided an estimate of the measurement uncertainty which included the effects of flow shifts, averaging and data processing. These data are set out in Table B.2-4.

Table B.2-4

Uncertainty of Flow Quantities from Repeated Measurement.

Derived Quantity	Comment or Range	% pt.
Flow Coefficient	$\Phi = 0.7$	0.6
Pressure Coefficient	$\Phi = 0.7$	0.5
Efficiency (Low Φ)	$\Phi < 0.7$	1.2
Efficiency (High Φ)	$\Phi > 0.7$	0.6

Comparison of the uncertainties derived by these methods showed that the repeatability precision of derived quantities was generally of the order of (or less than) the calculated precision.

References (see also Part 6)

Abernathy, R. B., "Uncertainty in Gas Turbine Measurements - Handbook," AEDC TR 73-5, 1973.

Moyle, I. N., "Multistage Compressor - Data Acquisition System." Naval Postgraduate School, Monterey, California, Turbopropulsion Laboratory Note 80-07, Oct. 1980.

Moyle, I. N., "Multistage Compressor - Data Acquisition System and Reduction Software." Naval Postgraduate School, Monterey, California, Turbopropulsion Laboratory Note 90-02, Oct. 1990.

B.3 Pneumatic Probe Sensor Calibration and Measurement

B.3.1 Probe Pressure Coefficients

The probe calibration technique is developed from the general considerations of a pressure coefficient as a non-dimensional pressure. Following Shreeve and Anderson (1976), the pressure coefficient (Cp_j) can be defined as

$$Cp_j = (p-p_j)/(2pkM^2) \qquad B(1)$$

Where (p_j) is an indicated pressure on the probe and (p) is the local static pressure. For a probe immersed in air moving relatively at Mach No. (M), with Reynolds No. (R_e), oriented with a yaw (θ) and a pitch (ϕ) to the flow

$$Cp_j = f\,(M, R_e, \theta, \phi) \qquad B(2)$$

A pressure coefficient difference $Cp_{ij}=(Cp_i-Cp_j)$ is also a function of these parameters and similarly ratios and other combinations of the coefficients are functions of (M, R_e, θ, ϕ). Expanding the expression of B(1) for a difference Cp_{ij}

$$Cp_{ij} = (p_i-p_j)/p_i.(p_i/p_t).(p_t/p)/(2kM^2) = f\,(M, R_e, \theta, \phi) \qquad B(3)$$

It can be seen that if (p_i) is chosen to be a pressure equal to the stagnation pressure of the flow indicated on the probe (p_1) then

$$(p1-p_j)/p1 = (p_t/p1).(p/pt).\ 2kM^2\ .f\,(M, R_e, \theta, \phi) \qquad B(4)$$

This basic expression is primary to the application of a probe as a flow and direction sensor.

It can be seen that differences and ratios of differences of pressure are all functionally described by the same flow variables. While in principle it is desirable to treat Mach No. and Reynolds No. as independent variables, in a simple calibration of a single probe in a flow tunnel or free jet, they cannot be independently varied. Consequently Reynolds Number effects were ignored. A non-dimensional velocity $X^2 = V^2/(2C_pT_t)$ was used as the independent variable. In this form

$$p/p_t = (1-X^2)^g \quad ; \quad 2kM^2 = g.X^2/(1-X^2)$$

where $g = k/(k-1)$ and

$$(p_1-p_j)/p_1 = g.(p_t/p_1).X^2(1-X^2)^{(g/k)}.\ f(M,R_e,\theta,\phi) \qquad B(5)$$

A final consolidation is made with either the assumption that $p_1 = p_t$ or that p_t/p_1 also is a function of X,θ and ϕ. For practical purposes the distinction is not critical as most calibration methods correlate the coefficient to X, θ and ϕ directly, i.e.,

$$(p_1-p_j)/p_1 = F(X, \theta, \phi) \qquad B(6)$$

Where the function (F) absorbs all of the sub-functional influences of (p_t/p_1), (f) and the velocity relationships.

B.3.2 Coefficient Surface Functions as a Calibration

The purpose of the calibration of a probe is to relate the measured local surface pressures on the probe to the condition that would be present without the probes intrusion into the calibration flow. Thus when measuring an unknown flow, the probe should alter the measurement environment in a similar manner to that in which it was calibrated. Under this condition, its local surface pressures can be used as an indication of the flow velocity and direction in the measurement environment. This is a subtle point. It is often difficult to ascertain that the probe is in a similar environment to the one in which it was calibrated. Proximity of the probe to surfaces, or exposure to wakes and shear flows in the measurement environment that were not present in the calibration flow can alter the form of (F) above. Hence, an implicit assumption in the following discussion is that (F) will hold in the measurement environment.

For a cylindrical five hole probe, pressure coefficient combinations can be defined conveniently as

$$Z_x = (1 - (1 - (p_1-p_{23})/p_1)^{(1/g)})^{0.5} = F_x(X, \theta, \phi)$$

$$Z_y = (p_2 - p_3)/(p_1 - p_{23}) = F_y(X, \theta, \phi)$$

$$Z_p = (p_4 - p_5)/(p_1 - p_{23}) = F_p(X, \theta, \phi)$$

where p23 = (p2 + p3)/2
and p1, p2, p3, p4, p5 are the port pressures

B(7)

Using these coefficients, which roughly correlate with velocity, yaw and pitch, and if it is possible to find functions (C_i), below

$$X = C_x(Z_x, Z_y, Z_p)$$
$$\theta = C_y(Z_x, Z_y, Z_p)$$
$$\phi = C_p(Z_x, Z_y, Z_p) \qquad B(8)$$

which satisfy B(6), above, over the range of X, θ, ϕ of interest, then the functions C_i represent a calibration of the probe. In general, the functions C_i are surfaces and can be found by surface fitting techniques if Z_x, Z_y and Z_p are known over the X, θ, ϕ range.

B.3.2.1 Least Squares, Polynomial Surface Fitting

Several general methods can be used to fit the surfaces of B(7). The most straightforward is a least squares fit of an arbitrary polynomial of the form

$$C_i (Z_x, Z_y, Z_p) = \Sigma_l \Sigma_m \Sigma_n \; c_{lmn} . Z_x^{\,l} . Z_y^{\,m} . Z_p^{\,n} \; ; \; i = x,y,p \qquad \text{B(9)}$$

Realizing a satisfactory fit (i.e., finding c_{lmn}) of a highly curved surface may require a very large number of closely spaced data points and a high order of the (l,m,n) exponents, however, some degree of approximation is possible to any arbitrary surface with this basic functional form of C_i. If the probe can be balanced in yaw while surveying a flow field, the general form of the equation B(8) is considerably simplified. In this case ($Z_y = 0$) and B(8) becomes

$$C_i (Z_x, Z_p) = \Sigma_l \Sigma_n \; c_{ln} . Z_x^{\,l} . Z_p^{\,n} \; ; \; i = x,p \qquad \text{B(10)}$$

A scheme to solve for the c_{ln} of B(10) was developed by Zebner (1980) and has been used in this study to calibrate several probes. This scheme requires a formal, ordered accumulation of test data in sets of velocity, yaw and pitch in its method of reduction for the calibration terms c_{ln}. It was not extended to three dimensions due to its relatively inflexible ordered solution scheme. However, it is possible to solve directly for the c_{lmn} to any order for an arbitrary assembly of calibration points if B(9) is expressed in the matrix form

$$\left| \begin{matrix} N \times 3 \\ [X_1\ \theta_1\ \phi_1] \\ . \\ . \\ [X_N\ \theta_N\ \phi_N] \end{matrix} \right| = \left| \begin{matrix} N \times o \\ [\,1\ Z_x\ Z_y\ Z_p\ Z_x Z_y\ \ldots Z_x^{\,l} Z_y^{\,m} Z_p^{\,n}\,]_1 \\ . \\ . \\ [\,1\ Z_x\ Z_y\ Z_p\ Z_x Z_y\ \ldots Z_x^{\,l} Z_y^{\,m} Z_p^{\,n}\,]_N \end{matrix} \right| \begin{matrix} o \times 3 \\ [c_x\ c_y\ c_p] \end{matrix}$$

where N is the number of test points
and $o = (l+1)(m+1)(n+1)$

B(11)

This form is the equivalent of the matrix equation

$$X = Z.C \qquad \text{B(12)}$$

with the general solution for C (Luenberger, 1969 p. 83 Theorem 1)

$$C = [\,Z^T.Z\,]^{-1}.Z^T.X \qquad \text{B(13)}$$

Consequently, the coefficients of B(8), c_{lmn}, can be found rapidly with a computer from B(12) by formulating the problem in the form of B(10). The algorithm for B(12) is extremely compact and once C has been determined, the form of B(11) can be used (as an inner product; x = z.C) to determine X, θ and ϕ for any measurement row

vector (z). This solution form is a considerable simplification of the calibration representation problem. Graphical calibration methods, Bryer and Pankhurst (1971), in comparison require a large number of graphs, each with graphed functions of [X θ ϕ],[Z_x Z_y Z_p] stored for the probe. In the formulation described the matrix C of equation B(12) contains the complete functional form for the probe.

Application to Calibration of Cylindrical Five Hole Probes Either this method or that of Zebner were applied to the calibration of United Sensor DA-120 probes in either (respectively) the enclosed calibration jet described in Moyle (1986) or the free jet discussed by Neuhoff (1981). Both jet tunnels allowed the probes to be pitched and yawed to the reference flow. Typical calibration data is shown in Figure B.3-1 for the velocity, pitch and yaw coefficients as a function of yaw angle.

As probes used in the program were calibrated by both methods, the techniques are referred to as the balanced yaw and variable yaw methods and are compared in Table B.3-1.

Table B.3-1

Comparison of Calibration Techniques.

	Balanced Yaw	Variable Yaw
Calibration Variables	X,ϕ	X,θ,ϕ
Probe Coefficients	Z_x,Z_p	Z_x,Z_y,Z_p
Least Squares Method	Zebner	Moyle
Calibration Flow	Free Jet	Enclosed Jet
Cal. Constants/Variable	16-30	6-24
Const. Data Stored as	Array (l.m)	Vector (l.m.n)
Order of Coefficients	(Z_x^2,Z_p)	(Z_x,Z_y,Z_p)
X Velocity	(4,2)	(1,3,2)
θ Yaw	-	(1,3,2)
ϕ Pitch	(3,3)	(0,3,2)
Fit Accuracy (Nominal)		
X Velocity (%) @ 100 m/s	±0.5	±1.5
θ Yaw (deg) ±20 deg	-	±0.5
ϕ Pitch (deg) ±35 deg	±0.75	±1.5

The accuracy data indicated that the inclusion of the additional yaw variable or using the probe in a fully three dimensional mode increased the error bands. The highest order of each coefficient also provides an indication of the complexity of the surface fit. Note that the Zebner fit uses Z_x^2 as the primary velocity fitting term. This was not found to improve the variable yaw data fit. As the formulation of the C_i of B(7) can be arbitrary in the functional form of the coefficient terms, several forms were examined. These included Reynolds Number correlating terms ($X + X^{0.5}$) and inviscid pressure distribution corrections to the Z terms. These inviscid corrections were consistent with the yaw variation of the pressure coefficient on circular cylinders. No significant

improvement in accuracy could be obtained. Pitch angle accuracy had the largest error band, as shown in the table above.[99]

References (see also Part 6)

Bryer D. W. and Pankhurst R. C., "*Pressure Probe Methods for determining Wind Speeds and Flow Direction*," National Physical Laboratory, U.K. 1971. The Campfield Press, St. Albans, England.

Luenberger, D. G., "*Optimization by Vector Space Methods*," John Wiley and Sons, Inc., 1969.

Moyle I. N., "Design and Development of a Probe Calibration Wind Tunnel," Naval Postgraduate School, Monterey, California, Turbopropulsion Laboratory Note 85-01, Dec. 1986.

Moyle I. N., "Single Stage Compressor Test Baseline for a Symmetric Blading," Naval Postgraduate School, Monterey, California, NPS-67-86-003/CR, December 1986.

Neuhoff F., "Calibration and Application of a Combination Temperature and Pressure Probe for Velocity and Rotor Loss Distribution Measurements in a Compressor," Naval Postgraduate School, Monterey, California. NPS 67-81-03CR, 1981.

Shreeve R. P., Anderson D. J. and Olson J. A., "Calibration and Application of Multiple Sensor Pneumatic Probes for Velocity Determinations with Corrections for Boundary Effects," AIAA 78-1198.

Zebner H., "Procedure and Computer Program for the Approximation of Data (With Application to Multiple Sensor Probes)," Naval Postgraduate School, Monterey, California. NPS 67-80-001CR, Aug 1980.

[99] These results raised some questions about the general applicability of multi-dimensional probe calibrations in complex measurement environments over wide angle ranges. It was apparent in the data that modest oblique orientations (pitch-yaw combinations) considerably expanded the prediction error bands over the data set. The error increase was partly due to the measurement uncertainty introduced by an additional variable, however the results also suggested that the very tight error bands that can be demonstrated in balanced yaw calibrations may not be valid indications of overall error in shear or non uniform static pressure flow measurement situations. This is an issue in turbomachinery passage and interblade row measurements where a probe, normally calibrated in a uniform flow, is used with the expectation that its accuracy will be consistent with the calibration accuracy. In situations where a large oblique condition can be expected on the probe, partial or piecewise calibrations may be better than attempting to calibrate the whole surface in one set of surface constants. Generally, a probe will show some multi-valued region in its characteristic as angle range is increased. As this is a fundamental physical characteristic, the inversion problem (i.e., using pressure coefficient to determine velocity and angles) is an intractable problem unless a piecewise fit, or some alternative correcting procedure, is developed.

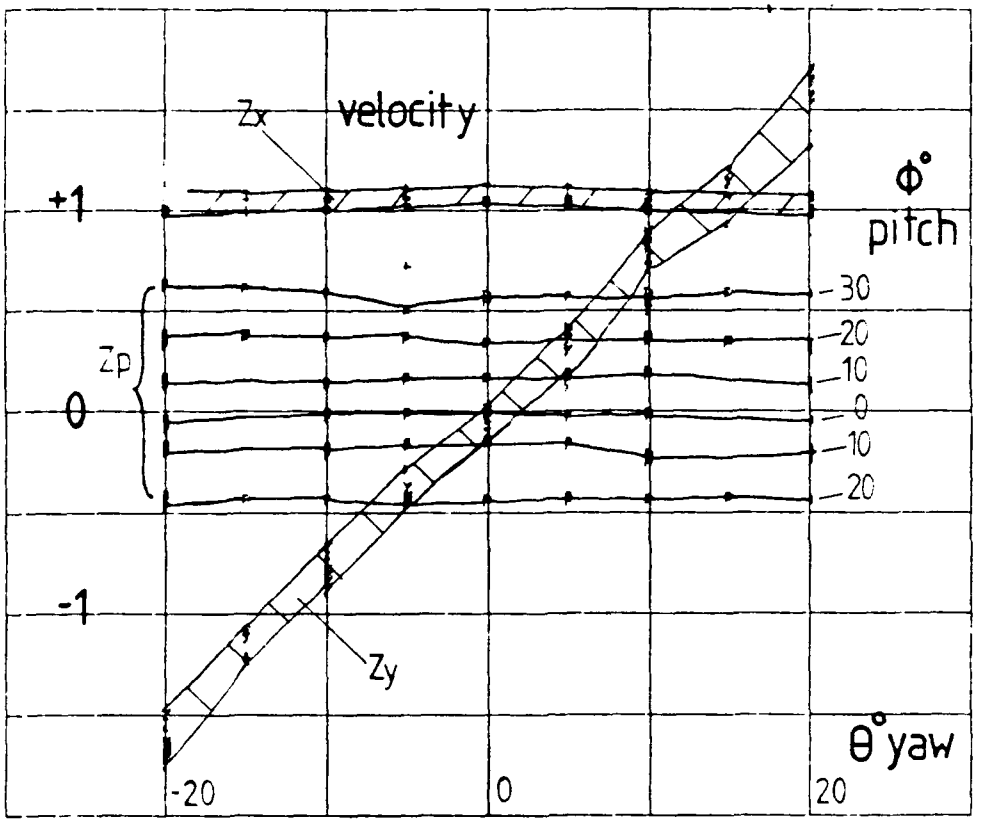

Fig. B.3-1 Calibration data collected for a cylindrical probe over four velocities and seven pitches plotted as coefficients as a function of yaw angle.

B.4 Hot Wire Sensor Calibration and Measurements

Measurements with a slant hot wire (or film) were expected to made in the compressor by fixing the probe sensor on a radial shaft and inserting the probe from the case wall into the flow between the blade rows. The probe tip could then be yawed through a wide range of angles. Using a velocity coordinate system aligned with the wire, the relative velocities normal (W_n), bi-normal (W_b) and parallel to the wire (W_p) could be transformed into the compressor absolute frame (V_a, V_u, V_r) by inverting the matrix transformation

$$W = A.V$$

where the matrix A is defined as

$$\begin{vmatrix} \cos(Y).a & -\sin(Y).a & b \\ \sin(Y) & \cos(Y) & 0 \\ -\cos(Y).b & \sin(Y).b & a \end{vmatrix}$$

where (a) and (b) are the sine and cosine of the wire slant angle, respectively and (Y) is the probe yaw angle relative to the axial direction in the absolute frame.

The effective velocity (W_e) relative to an ideal wire or film is given by

$$W_{e2} = W_{n2} + W_{b2} + kW_{p2} = W^T K W$$

For a non-ideal wire on conducting support prongs, misalignment, stem, interference and other real phenomena in a duct flow may be defined by a calibration function of the form

$$c(y,p) = W_e^{\,2} - V^T A^T K A V$$

where (y) is the flow yaw direction relative to the probe, (p) is the flow pitch direction relative to the probe stem and K is an unknown sensor coefficient matrix, which has the form below for an *ideal* probe

$$\begin{vmatrix} 1 & 0 & 0 \\ 0 & 1 & 0 \\ 0 & 0 & k \end{vmatrix}$$

It can be seen that asymmetry of the probe, bowing of the wire and similar bias of stem effects can be accommodated in the coefficients of the matrix (K). The more precisely (K) is known, the smaller c(y,p) becomes.

B.4.1 Calibration Method

In a known flow of velocity V, components of velocity relative to the probe can be generated by yawing and pitching the probe at known angles (y,p) to the flow. As the matrix (A) is defined by setting Y = y and the V vector is known from

Va	V.cos(p)
Vu	V.sin(y)
Vr	V.sin(p)

then by using K above and the W_e^2 measured by the anemometer unit, then $c(y,p)/W_e^2 = 1 - V^T A^T K A V/W_e^2$ and assuming $c(y,p)/W_e^2 = \Sigma_l \Sigma_m C_{lm} y^l . p^m$

C_{lm} of the surface defined can be found by two dimensional least squares fitting if $c(y,p)/W_e^2$ is defined over a wide range of yaw and pitch angles. Storing the C_{lm} provides a calibration of the probe.

B.4.2 Determining Unknown Velocities

An unknown velocity can be established by recording W_e^2 over a range of yaw angles (Y) at the unknown flow condition. Applying a procedure where successively improved estimates of y,p are made from the measurements using a Newton-Raphson method, then the velocity can be determined to some tolerance. If N yaw conditions are recorded (Y_j, j = 1- N) and the unknown yaw, pitch and velocity are defined as $Y^\#$, $P^\#$ and $V^\#$ then the identity

$$0 = 1 - V^T A^T K A V/W_e^2 - c(y,p)/W_e^2$$

in the form of (N) error equations

$$e_j = 1 - V_j^T (A^T K A)_j V_j / W_{ej}^2 - \Sigma_l \Sigma_m C_{lm} . (Y_j - Y^\#)^l . P^{\#m}$$

where V_j is given by Vj

$$\begin{vmatrix} Va & V^\#.\cos(P^\#) \\ Vu & V^\#.\sin(Yj - Y^\#) \\ Vr & V^\#.\sin(P^\#) \end{vmatrix}$$

provides the basic algorithm. By combining the errors as

$$e^2 = \Sigma_j e_j^2 \quad j = 1 - N$$

improved estimates of $Y^\#$,$P^\#$ and $V^\#$ can be sought from an initial condition and

$$Y^\#_{i+1} = Y^\#_i - e^2_i/(de^2/dY^\#)_i$$
$$P^\#_{i+1} = P^\#_i - e^2_i/(de^2/dP^\#)_i$$
$$V^\#_{i+1} = V^\#_i - e^2_i/(de^2/dV^\#)_i$$

The criterion for convergence can be set by iterating to e^2 less than a small value. By choosing a range of Y's spanning the probable value of Y the method is known to converge.

B.4.3 Data Acquisition and Processing

The data acquisition process was expected analogous to the case wall pressure measurement. The signal for two blade passages was sampled at 100 increments per rotor passage, for up to six yaw orientations of the sensor, at each radial position of the probe tip. A fixed number of radial positions (15) could then be interpolated over a radial span of 50 mm (2 in) divided into 60 increments. This arrangement resulted in 60 by 200 matrices for post processing, analysis and presentation.

B.5 Case Wall Sensors and Measurements

In examining the literature on tip clearance effects in axial compressors it was noted that while the wall is a major aerodynamic surface near the tip, very limited data is available about the conditions on the wall relative to the moving rotor passage. This seemed to be a logical subject to explore further in the context of this study particularly after the work of Bettner and Elrod (1982) varying wall roughness under the rotor. In this study it seemed more appropriate to try and define the shear stress and pressure field near the wall in the rotor passage and the flow conditions near the wall exiting from the passage. Consequently instrumentation was developed to survey the wall shear and static pressure relative to the blade.

A direct method of acquiring these data was to measure the wall shear using a hot film or buried wire sensor flush with the wall and to use a semiconductor pressure transducer mounted in a similar fashion. With suitable timing, prior calibration and data reduction, both blade-to-blade shear and static pressure could be measured. However, sensor output is not easily interpreted in unsteady flows of this kind and further analysis was required to size the sensors and ensure their suitability for the measurements envisaged. The following sections describe the sensor considerations in terms of the unsteady flow.

B.5.1 Case Wall Static Pressure Measurements

Calibration and verification of the case wall pressure sensor measurement and response mainly focussed on the sensor response. The Kulite XCS-093-1D high response transducer was calibrated by applying a known pressure to the back (non sensing) side of the differential diaphragm. The calibration accuracy was 0.25 mmw (0.01 inw). The transducer was ranged in a similar manner using a reference back pressure at the beginning and end of each acquisition period. Thermal drift was of the order of was 2.5 mmw (0.1 inw). Full-scale range for the *signal pressure* was 0 to 250 mmw (0 to 10 inw).

The transducer was flush mounted with an "M" type screen inside a brass sleeve in a stainless steel wall plug. The plug was inserted into thirty holes in the case wall insert plate. The wall plug could be rotated in the hole. Tolerances on the whole plate and plug assembly were very tight and the holes were honed to accept the plugs. The plugs were recessed into the holes in later testing to assess the effect of poor seating in the holes.

B.5.1.1 Characteristics and Response of the Sensor

Position and alignment of the plug had minimal effect on the signals recorded:

Rotation Turning the plug through 360 deg in six increments had no visible effect on the pressure traces recorded.

Recessing Recessing the sensor plug up to .3 mm (0.0125 in) in five increments into the wall only changed the shape of the pressure side of the pressure trace. The suction side was not affected. Plug seating didn't affect the suction (pressure minimum) trace and hence minimum position. The expected seating error was of the order of 0.05 mm (0.002 in). The pressure traces were negligibly affected by this amount of recessing.

The averaged traces recorded by the system were repeatable to a high degree. Individual traces recorded with an oscilloscope showed considerable variation from

one to another and the continuous signal from the sensor was analyzed for possible resonances:

Repeatability Repeated samples (5) of the wave form for one probe position (hole) produced exactly the same trace over a four hour period. The data were very (almost exactly) repeatable.

Spectral Analysis Spectral analysis of the energy content of the waveform from the transducer shows only rapidly attenuating peaks at harmonics of blade passing frequency. The peaks at 4.8, 5.6 and 6.4 khz were slightly higher than their neighbors, but inconsequentially so. There was no peak indicative of any significant resonance.

Sensor resolution was of some concern in the study due to the need to define the blade edges (i.e., the clearance gap) precisely. Calculated temporal resolution of the probe was very high. Spatial resolution was lower but acceptable.

Temporal Resolution If the blade thickness is used as the wavelength of the flow feature of interest, then the temporal resolution required of the probe is 8 khz. This was an order of magnitude lower than the sensor response of 100 khz claimed by the manufacturer. Due to the sharp edged pressure correlation with blade edge position (discussed below), the sensors temporal response was accepted to be of the order claimed by the manufacturer.

Spatial Resolution Spatial resolution of the probe is about 4.5 mm of the 95 mm blade pitch (4.75% of pitch) based on sensor diameter. The probe diameter was 2.4% of pitch. This was not extremely high resolution, however, the minimum pressure locus (of particular interest) was about 15-20% of pitch on average from the pressure maximum or two resolution intervals from the suction side. The blade edge position measurements suggest the spatial resolution of the probe was more like 1% of pitch, i.e., the sensor effective area was much smaller than its mechanical diameter.

Blade Edge Position Measurements to check the blade edge position and timing system used a rubbing strip of tape on the pressure side of the blade. The tests showed the blade edge was located within 0.01 of pitch of theoretical position in the (timed) window moving in the relative frame. This was the highest resolution of the timed divisions of the pitch, i.e., 100 readings per passage. These measurements instilled considerable confidence in the system's spatial accuracy.

Unsteady performance of the sensor was acceptable and the screen was altered to see if the measurements were affected. This had a minimal impact on behavior. The results of Heinemann's (1986) systematic comparison of five wall pressure sensor tips in the same configuration were also similar at low Mach Number (i.e., < 0.5). The similarity of sensor behavior to Heinemann provided additional confidence in the sensors fidelity and suitability to the application.

B.5.2 Wall Shear Measurements Using Buried Wire or Film Gauges

Wall shear measurements were initially attempted with commercial hot film gauges. These probes were theoretically capable of making measurements on the case wall. Analyses conducted are summarized below.

B.5.2.1 Sensitivity of Surface Wire (Film) Gauges to Pressure Gradients

For design conditions in the stage the average pressure gradients ($dp^{\#}/dx$) in the axial and circumferential direction can be determined from Vavra (1970), Table X, using the stage static pressure coefficients and the change in whirl

$$(dp^{\#}/dx)_{ax} = 1.075;\ (dp^{\#}/dx)_{per} = 2.878$$

thus the total gradient is nominally (with $r_t/r_m = 1.25$)

$$dp/dx = (3.072)(1.25) = 3.84$$

Following Brown's (1967) development of an expression for wall shear stress including a pressure gradient, it is possible to determine the ratio of the shear stress with a pressure gradient to that of no pressure gradient (τ_w/τ_{w0}) in terms of the sensor effective width (W_e), local fluid conditions (P_r, N_u, R_{et}) and the pressure gradient. This relation is given by

$$\tau_w/\tau_{w0} = 1 + 0.1461.(P_r/N_u^2).R_{et}^2.(W_e/r_t)^3.(dp/dx)$$

for the nominal conditions $P_r = 0.7$, $N_u = 20$, $R_{et} = 0.5\times10^5$ and $dp/dx = 3.84$ the expression above becomes

$$\tau_w/\tau_{w0} - 1 = 2.45\times10^8.(W_e/r_t)^3$$

for the condition that

$$\tau_w/\tau_{w0} - 1 < 0.01;\ \text{then}\ (W_e/r_t)^3 < 4.08\times10^{-12}$$

and thus for $r_t = 457.2$ mm (18.0 in)

$$W_e < 0.157 \text{ mm}$$

Thus, provided the effective width (or diameter) of the wire gauges are less than 0.157 mm (0.006 in) the influence of pressure gradients, of the order indicated, can be neglected. As wire gauges have actual wire widths (W) or diameters of 0.005 - 0.010 mm the effective wire diameter may be of the order of 15 - 30 times the actual wire diameter. Data from Brown indicates the effective width of his surface film to be three times ($W_e = W\lambda$, $\lambda = 3$) its dimensional width (W) and consequently a 15 - 30 allowance for effective width was considered very conservative.

As buried wire gauges of the Murthy and Rose (1978) type were proposed for use in the study, with wire diameters of 0.005 mm (0.197×10^{-3} in), the effects of pressure gradients in the passage on the measurement's accuracy were expected to be negligible.

B.5.2.2 Attenuation of Wall Shear Signal in a Fluctuating Flow

In a fluctuating flow the surface wire or film gauge response to the fluctuating shear level is affected by the thermal conduction lag of the substrate. Generally this reduces or attenuates the actual signal from the sensor compared to its steady state response.

The effect is described and analyzed in Bellhouse and Schultz (1967). They completed an analysis which relates the indicated fluctuating shear level, using the steady calibration, (τ_{ls}) to the actual shear fluctuation, (τ_l). The forms of the gain equations $G\tau(\omega) = (\tau_l/\tau_{ls})$ given are

$$G\tau(0) = 1$$

$$G\tau(\omega) = K_{gl}.(1/(1 + j\omega T_l)$$

for low frequencies and for high frequencies

$$G\tau(\omega) = K_{gh}.\ 1/(j\omega T_h)^{3/2}$$

The K_g functions were only dependent on the sensor effective width factor while the time constants were given by the square of the boundary layer momentum thickness (θ) and thermal diffusivity of the fluid (κ). The time constant term is given by

$$T = \theta^2/\kappa = 9/4.(W\lambda)^2/(N_u^{\ 2}.\kappa)$$

For $N_u = 20$, $\kappa_{air} = 20.75 \times 10^{-9}$ (ft^2/s) and $\lambda \cong 3$, the first break frequency is

$$\omega_l = 1/T_l = 2.71 \times 10^5/(3W)^2$$

It can be seen that for very small wires W=0.005 mm (0.197×10^{-3} in) the break frequency is very high. The analysis suggests that provided small wire dimensions are used and frequencies are greater than zero but substantially less than ω_l then establishing K_{gl} would permit use of the steady state calibration (adjusted by K_{gl}) over the frequency range indicated.

The compressor blade passing frequency at 1620 RPM was 810 hz and this suggested a flat frequency range of 800 - 8000 hz would provide adequate response.

B.5.2.3 Calibration of the Response of a Thin Film Sensor

Efforts with films and buried wires were stopped when the sensor output in an unsteady flow was examined. The unsteady (ac) signal was found to be a minute fraction of the total (dc) signal. Most of the dc signal was due to conductive heat transfer into the substrate. Acquiring signals of this type was quite difficult with the existing high speed System Voltmeter in terms of offset and digitization. Discussion with Reid (1987) indicated sensitivity with alignment was low. When considered along with limited signal discrimination capability and the response lag due to the substrate soaking, the films were not practical with the existing equipment.

B.5.3 Wall Shear Measurements Using Fence Pressure Sensors

Due to the difficulties with films in terms of signal acquisition, pressure difference fence sensors were explored. Wall plugs with an abrupt step (0.254 mm, 0.010 in high) between two static tappings placed in the corners of the plug surface and step were found to have good response and directional sensitivity. The height and width of the step were reduced systematically with good response. A similar design was then tested with a forward facing step fixed to the mesh of a Kulite transducer. This

arrangement had a single slit (approximately 0.05 mm, 0.002 in wide) at the abrupt step corner opening into the transducer cavity through the screen mesh. The forward step design had good directional sensitivity. Although lack of symmetry prevented reversal checks which are commonly used to verify the behavior of unsteady sensors, its unidirectional sensitivity made it unambiguous in sensing direction. Minimum output was detected at 180 deg to maximum output. These sensors gave proportional output with zero offset and tracked the near wall impact pressure with the same characteristics as the wall static pressure sensor described above. Data were very repeatable.

Preliminary, uncalibrated measurements were made with these probes. The sensor were not calibrated because the abrupt step was made of 0.127 mm (0.005 in) Magic Tape and was found to degrade with time. More durable materials were much more difficult to fabricate to the minute dimensions and this problem proved to be a major source of delay in acquiring complete surveys. The preliminary measurements were extremely useful, however, as the shear level under the blade tip and further into the passage turned out to be negligible. The zero point (i.e., zero output) was the only known point on the sensor calibration characteristic and appreciable regions of the output trace were at zero output. These results have been discussed in Part 4.

References (see also Part 6)

Bellhouse, B. J. and Schultz, D. L., "Determination of Mean and Dynamic Skin Friction, Separation and Transition in a Low Speed Flow with a Thin Heated Element," *Jrnl. Fluid Mechanics*, Vol. 24(2) pp. 379-400, 1966.

Bettner, J. L., and Elrod, C., "The Influence of Tip Clearance, Stage Loading and Wall Roughness on Compressor Casing Boundary Layer Development," ASME 82-GT-153, 1982.

Brown, G. L., "Theory and Application of Heated Films for Skin Friction Measurement," Proc. 1967, Heat Transfer and Fluid Mechanics Institute, Stanford Univ. Press, pp. 361-381, 1967.

Heinemann, H-J., "High-Speed Data Acquisition and Reduction for Wall Static Pressures Derived within the Passage of a Rotating Annular Turbine Cascade," Proceedings of the Eighth Symposium on Measuring Techniques for Transonic and Supersonic Flows in Cascades and Turbomachines, Oct. 1985, Universita Degli Studi Di Genova, Dec. 1986.

Murthy, V. S. and Rose, W. C., "Buried Wire Gage for Wall Shear Stress Measurements," NASA Ames Research Center X th. Aerodynamics Testing Conference, Apr. 1978.

Reid, L., Private correspondence and discussion of wall pressure and wall shear measurements made by Reid in a single stage at 11,500 RPM, November 1987.

Vavra, M. H., "Aerodynamic Design of Symmetrical Blading for Three-Stage Axial Flow Compressor Test Rig," Naval Postgraduate School, Monterey, California, NPS-57-VA70091A, Sep. 1, 1970.

B.6 Variation of Case Wall Boundary Layer Thickness

Prior studies of case wall phenomena in axial compressors have emphasized and even parameterized tip gap related effects in terms of case wall boundary layer displacement thickness. From a consideration of the flow near the wall it is clear that the length scales of the two dimensions are similar. Consequently, in this program, the case wall boundary layer thickness was considered a parameter of the tip flow study.

As it was possible to artificially thicken the wall layer upstream of the compressor test section, an array of spires was developed for insertion into the throttle housing. The throttle section was two duct diameters upstream of the compressor-face bullet. This provided a rapid method of thickening the wall layer and considerably more test configuration flexibility than wall roughness elements. Use of this approach required the spires to be sized empirically to achieve the desired thickness.

In order to determine boundary layer thickness required at the compressor inlet face and the corresponding size of downstream spire elements, surveys were conducted at design flow coefficient (0.64) to define the unthickened boundary layer profile. The nominal displacement thickness upstream of the inlet guide vanes was 1 mm (0.04 in) The surveyed profile power term was far from the 1/7 - 1/8 considered to be normal in a turbulent layer and was consistent with the local acceleration into the test section bulking the profile near the case wall. The measurement data is summarized in Table B.6-1.

Table B.6-1

Boundary Layer Profile Survey Results at the Compressor Test Section Inlet Face.

$$u/U = (y/\delta)^n$$

	Upstream Duct	Test Section Inlet
δ	25 mm (1.0 in)	16 mm (0.65 in)
n	0.156	0.0677

B.6.1 Gap-to-Thickness Selection

In selecting a thicker boundary layer level at the compressor-face, it was desirable that the ratio of nominal clearance to boundary layer displacement thickness repeat for a larger clearance condition in later testing. The rationale for this parametric consistency was the need for experimental evaluation of the effect of the tip gap-to-thickness ratio (e/δ_1) on the losses. This would be particularly interesting, should there be any similarity in the flow with this ratio or a discernable trend over a wide ratio range.

Using gap-to-blade height (e/b) from other studies as an indicator of a desirable test range and the minimum clearance possible as the initial clearance, the following design goals, set out in Table B.6-2, were established for the gap and the boundary layer thickness.

Table B.6-2

Boundary Layer Displacement Thickness at the Compressor-Face for Selected Clearances.

Blade Height b = 182.9 mm (7.200 in)
Staggered Spacing g = 72.3 mm (2.847 in)

Clearance Gap				Face Displacement Thickness	
				Unthickened	Thickened
e (in)	e (mm)	e/b (-)	e/g (-)	e/δ_1 (-)	e/δ_1 (-)
0.020	0.508	0.003	0.007	0.488[1]	0.093[2]
0.108	2.743	0.015	0.038	2.634	0.500[1]
0.288	7.315	0.040	0.101	7.024[2]	1.333

Note:

[1] e/δ_1 is the same for two different e/g ratios

[2] e/δ_1 range spans two orders of magnitude, i.e., 0.1 - 10.0

The data were not expected to predict the effective displacement thickness that would result in the stages of the compressor. However the selection allowed sizing of the boundary layer generator spires for the thickened flow condition.

B.6.2 Boundary Layer Thickening Spire Design

Using data from Tables B.6-1 and B.6-2 it was possible to establish the nominal required displacement thickness (δ_1) in the duct upstream of the compressor section.

Using a design value of (δ_1) of 5.5 mm (0.22 in) for the thickened condition required the compressor-face height (δ) to be 87.1 mm. This translated into an upstream duct thickness of δ = 134 mm (5.28 in). Using the data of Standen (1972) for half width spires in a rectangular tunnel used for atmospheric boundary layer simulation, a half width spire height of 203 mm (8.0 in) was estimated to be required to generate the desired profile upstream of the test section.

As Standen's spires were developed for a rectangular tunnel, an adjustment was made to the spire profile to correct for the cylindrical flow in the compressor duct. The corrections applied were based on retaining the same blockage proportion on each axisymmetric surface as had been present in the rectangular duct. The theoretical and design spire geometries are shown in Figure B.6-1. The fabricated geometry was further simplified for ease of machining. In order to avoid possible resonance due to wakes from the spires with the thirty (30) blade rotor, twenty nine (29) spires were used with a nominal base arc of 99 mm (3.90 in). This slightly modified the spire blockage near the base arc viz-a-viz Standen's data.

B.6.3 Flow due to Boundary Layer Thickening Spires

Surveys at the compressor face showed the spire wakes did not fully mix out in the distance from the throttle housing to the compressor face. The spires therefore produced a circumferentially distorted flow at the inlet section. Although the radial velocity profile was influenced by the distribution of upstream spire resistance, the boundary layer thickness did not seem to be increased relative to the annulus core flow. A description of the surveys and boundary layer properties are described in Tarigan (1988). A number of remedies, including redesigning the spire shape, were considered. However, the approach of obtaining parametric scaling of the boundary layer was shelved due to the time expected to be involved in further development.

References (see also Part 6)

Standen, N. M., "A Spire Array for Generating Thick Turbulent Shear Layers for Natural Wind Simulation in Wind Tunnels," LTR-LA-94, National Aeronautical Establishment, NRC Canada, May 1972.

Tarigan, M., "Development of a Boundary Layer Control Device for Tip Clearance Experiments in an Axial Compressor," M.Sc. Thesis, Naval Postgraduate School, Monterey, 1988.

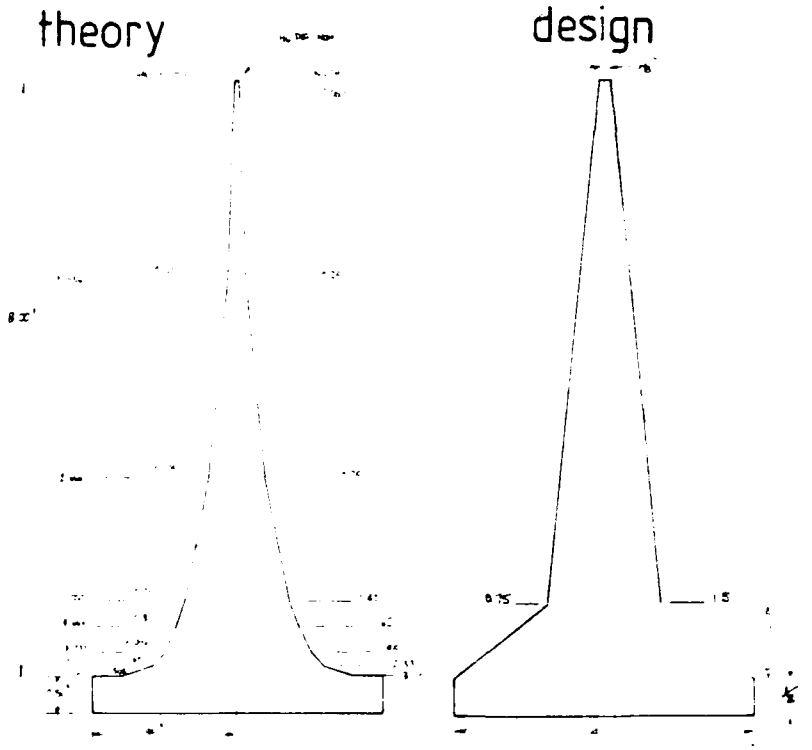

Fig. B.6-1 Theoretical and design spire profile used to generate a thick boundary layer upstream of the compressor face.

B.7 Computational Predictions of the LSMSC Flow

The flow measurements from the low speed multistage compressor gathered in the program, could be used to evaluate the flow calculations made by computer codes developed for the purpose of predicting flow fields and refining the design of turbomachinery. A variety of computational schemes are available which address the flows prediction at different levels of complexity. The levels vary from single passage flow solutions (Katsanis, 1977) to passage average models of multiple blade rows (discussed in Hirsch, 1984) to extremely complex solvers of the unsteady flow in rotating and stationary blade rows (Rai, 1987).

The available data from the measurement program were of the passage average type. In particular blade rows, blade-to-blade average data were also generated. These data could be predicted by the multiple blade row, passage average type of calculation code and a version of a code developed by Hirsch (1979) called Q3D was used for comparison with the data. Because comparisons between the measurements and a code prediction were not the primary objective of the program, this discussion essentially identifies areas of major discrepancy. Measurements of a flow field involve some element of uncertainty and, similarly, computations involve idealizations of the test hardware geometry and a large range of model, algorithmic and numerical efficacy concerns. Consequently, identifying areas where major discrepancies were detected was seen to be productive, but resolution of why the discrepancies exist was considered beyond the scope of the present comparison. It should be noted that the basic criterion for the comparison was the present author's judgement of what constituted a significant deviation in the data. Attention was focussed on the flow angles, velocities and pressure levels.

B.7.1 The Q3D Program

The operation of the Q3D program is described by Hirsch (1983). A user's guide by Schulz (1984) and a discussion of comparison on cascade blading by Schulz et al. (1984) are available. The program can produce both passage average and blade-to-blade flow field data for multiple blade rows in a variety of geometric or turbomachinery configurations. As the program can produce *all* the data of generally accepted interest in terms of blade and compressor (average) performance at a prescribed throughflow, only a small amount of the data could be compared with the experiment.

B.7.1.1 Comparison of Build I/II Data and the Code Predictions

Code predictions for the design flow ($\Phi = 0.64$), a low and an open throttle condition were produced with and without the endwall boundary layer (EWBL) option active. The EWBL option includes a near wall calculation region (grid) which produces a more refined solution of the overall flow field. As the measurements discussed in this report principally deal with the design flow condition for a single stage of the symmetrical blading, only that condition was examined in detail. The trends observed at the design condition were also evident in the code predictions at the higher and lower flow conditions. It is expected that the comments made for the design flow would be applicable to the other conditions.

Inlet Guide Vane Exit/ Rotor Inlet Flow predictions of the Q3D code did not demonstrate the underturning surveyed in the compressor. As this condition was a major obstacle in establishing an adequate row-to-row comparison baseline in the test program, it was surprising, that the code did not show this flow feature. The blading

was modelled at the average throughflow level (not blade-to-blade) and it was thought a more detailed calculation might improve the prediction. However, this calculation mode was not exercised until the later work of Yeo (1989, Fig. 25).

Rotor Exit/Stator Inlet This flow station was generally in reasonable agreement between the data, design and prediction.

Stator Exit/Duct The flow at this station predicted better than at the inlet guide vane exit and showed a region of presumed stall or separation that was deduced from measurements and streak data near the tip wall corner. Comparing the computed incidence from the rotor onto the stator showed a significant trend toward stalling incidence which probably promoted the separation. This data was not confirmed by the survey probe in the rotor exit, however, and there was some (unresolved) question whether the code prediction and data agreement was produced for the right reasons in this (stator outer case wall) region.

B.7.1.2 Comparison of Build III Data and The Code Predictions

A more comprehensive Q3D prediction of the compressor flow was conducted by Yeo (1989) with mixed results. The code was not able to predict the measured *slope* of the static-to-static pressure rise as a function of flow (i.e., off-design) once it had been "tuned up" to match the design flow. As this characteristic involves relatively straightforward measurements, Yeo's (1989, Figs. 23 and 25) results and discussion of the problems of reconciling computed flows to basic measurements is instructive. Two dimensional blade-to-blade pressure distributions from the "tuned up" design point computation have been compared to experimental data in Part 3.

References (see also Part 6)

Hirsch, C. and Warzee G., "An Integral Quasi-3D Finite Element Calculation Program for Turbomachinery Flow," *ASME Journal of Engineering for Power*, Vol 101, pp. 141-148, Jan 1979.

Hirsch, C., "Computer Program for Turbomachinery Flows, Finite Element Method - Users Guide," May 1983.

Hirsch, C., "Computational Models For Turbomachinery Flows," Naval Postgraduate School, TR NPS67-84-022, 1984.

Katsanis, T., and McNally, W. D., "Revised FORTRAN Program for calculating Velocities and Streamlines on the Hub-Shroud Midchannel Stream Surface of an Axial, Radial, or Mixed Flow Turbomachine or Annular Duct," NASA TN D-8430, Mar. 1977.

Rai, M. M., "Unsteady Three-Dimensional Navier Stokes Simulations of Turbine Rotor-Stator Interaction," AIAA 87-2??8, 1987.

Schulz, H. D., "Guide to Using the Finite Element Code Q3DFLO-81 on the NPS IBM 370," Naval Postgraduate School, Turbopropulsion Laboratory TN 84-01, June 1984.

Schulz, H. D., Neuhoff, F., Hirsch, C., and Shreeve, R. P., "Application of Finite Element Code Q3DFLO-81 to Turbomachinery Flow Fields," Naval Postgraduate School, TR NPS67-84-005PR, 1984.

Yeo, P. H., "Review and Evaluation of a Turbomachinery Throughflow Finite Element Code," M.Sc. Thesis, Naval Postgraduate School, Monterey, June 1989.

C.1 Symmetrical Stage Design Aerodynamics

The detailed design of the symmetric stage is set out in a design report by Vavra (1970). Leading characteristics of the design are described in the following sections. Data from the design report and the off-design analysis, Vavra et al. (1973), have been included to provide a summary description of the blading and its design performance.

C.1.1 Blading Design and Off-Design Flow

The design velocity diagram for the symmetric blading is shown in Figure C.1-1(a) and the modified version for off-design performance estimation in Fig. C.1-1(b). The spanwise distribution of design flow conditions is set out in Table C.1-1.

Table C.1-1

Spanwise Distribution of Symmetric Blading Design Flow Data.

		Rotor					Stator				
r/r_t	φ	W'_1	β_1	$\Delta\beta$	D_R	σ_R	V'_2	α_2	$\Delta\alpha$	D_S	σ_S
(-)	(-)	(-)	(°)	(°)	(-)	(-)	(-)	(°)	(°)	(-)	(-)
0.60	0.70	0.86	35.08	27.83	.250	1.06	0.96	31.04	22.57	.424	1.22
0.70	0.68	0.86	37.47	24.54	.305	0.98	0.92	35.09	20.12	.415	1.01
0.80	0.65	0.85	40.00	20.32	.356	0.92	0.87	39.88	18.60	.407	0.85
0.90	0.61	0.84	43.78	15.76	.402	0.92	0.87	39.88	18.60	.400	0.72
1.00	0.54	0.82	48.59	09.63	.427	0.85	0.78	52.45	17.36	.376	0.62

A noticeable consequence of the design philosophy and method developed by Vavra is the selected stator tip wall solidity, (0.62). While the calculated losses were low for this solidity, a degree of flow turning control onto the subsequent rotor was sacrificed.

By assuming a loss correlation as a function of blade incidence angle and using the modified diagram of Fig. C.1-1(b), the compressor flow-pressure rise characteristic, shown in Figure C.1-2, was generated. This characteristic is referred to as the "design characteristic" for the compressor throughout the discussion. The design method was based on the assumption of axisymmetric stream flow surfaces. Corrections for streamline curvature were applied in the design calculations.

C.1.2 Blade Section Profiles

The blade profiles for the rotor and stator were developed from a circular arc camber line and a C-4 thickness distribution which was slightly flattened at the leading edge. The thickness distribution is set out in Table C.1-2.

Table C.1-2

Percent Thickness Distribution for Modified C-4 Circular Arc Profiles used for Symmetric Blading.

			leading edge radius				12.0				
			trailing edge radius				6.0				
x/c	1.25	2.50	5.00	7.50	10.0	15.0	20.0	30.0	50.0	70.0	90.0
y/t	16.8	19.1	26.8	32.4	37.0	43.5	47.3	50.0	45.7	40.5	16.0

The blade profile data, developed from the velocity diagram requirements, is shown in Table C.1-3. The shape of the blade profiles across the span for the stage and guide vane are shown in Figure C.1-3.

Table C.1-3

Spanwise Distribution of Symmetric Blading Geometric Design Data.

b = 183 mm (7.20 in)

	Rotor				Stator			
r/r_t	γ	ξ	c/b	t/c	γ	ξ	c/b	t/c
(-)	(°)	(°)	(-)	(-)	(°)	(°)	(-)	(-)
0.60	15.71	40.48	.333	.125	16.07	29.26	.361	.065
0.70	20.30	37.42	.361	.098	21.10	29.28	.347	.076
0.80	25.56	32.54	.389	.076	26.21	31.44	.333	.087
0.90	32.19	26.34	.417	.068	31.20	36.91	.319	.100
1.00	40.96	16.00	.444	.062	34.71	47.58	.306	.114

Inlet guide vane sections used are referred to as IA and IB. The IA and the exit guide vane sections were developed using circular arc camber lines and thickness distributions of Table C.1.1. The IB blade set was not used in the present clearance variation tests.[100] Two sets of IA bladings were made. The fabrication method differed, resulting in thicker trailing edges on the second set. The two bladings are referred to as IA_1 and IA_2 respectively. Varying the stagger of the IA_2 vanes in an attempt to improve the turning is reported in Waddell (1982). The IA_2 set was used in the tip clearance variation testing. The specific blade sets used in the program are set out in Table B.1-1.

C.1.3 Profile Loss Estimation

In considering compressor performance variation due to tip clearance changes, the *design* spanwise loss coefficient distribution was of particular interest. The design performance estimate was based on loss correlations described in Vavra (1970). The *design* spanwise distributions of the loss coefficients and pressure rise are shown in Figure C.1-4. These distributions are discussed later in the report are included to complete the summary of the stage design aerodynamics.

C.1.4 Blading Fabrication and Fidelity to Design

The blades were fabricated by casting an aluminum filled epoxy resin in room temperature vulcanizing (RTV) silicone rubber molds. The mold was laid up with a small aluminum collar to provide a machined reference face for socketing into the compressor case and hub. A steel reinforcing shank, attached to a threaded rod was also cast into the matrix to complete the blade. Some of the blades were additionally reinforced with a very lightweight glass cloth and a carbon fibre shank to strengthen the root. Details of the technique are described in Moyle (1981).

The RTV mold halves were cast from a single master blade for each blade type. This blade was milled from solid aluminum and hand polished. The coordinates of the

[100] The IB design flow objective was identical to the IA blading, however, an A4K6 section following Dunavant (1954) and a different design method was used to try and achieve the design rotor in-flow condition. The IB blading development is discussed in Moyle (1986).

surface contours were generated from the design stagger, camber and thickness data of Vavra 1970. The section centroids were stacked on a radial line.

Cast blades were sectioned and compared with the design profile data. Generally, the leading and trailing edge contours did not precisely match the design due to their small radii and dimension. The remainder of the section could be produced precisely. Overall the blading fidelity to design was good and the blades showed no evidence of untwisting or dimensional change with time.

References (see also Part 6)

Moyle, I. N., "Multistage Compressor - Fabrication Molds and Casting of Epoxy Blades," Naval Postgraduate School, Monterey, California, Turbopropulsion Lab. Note 81-03, Oct. 1981.

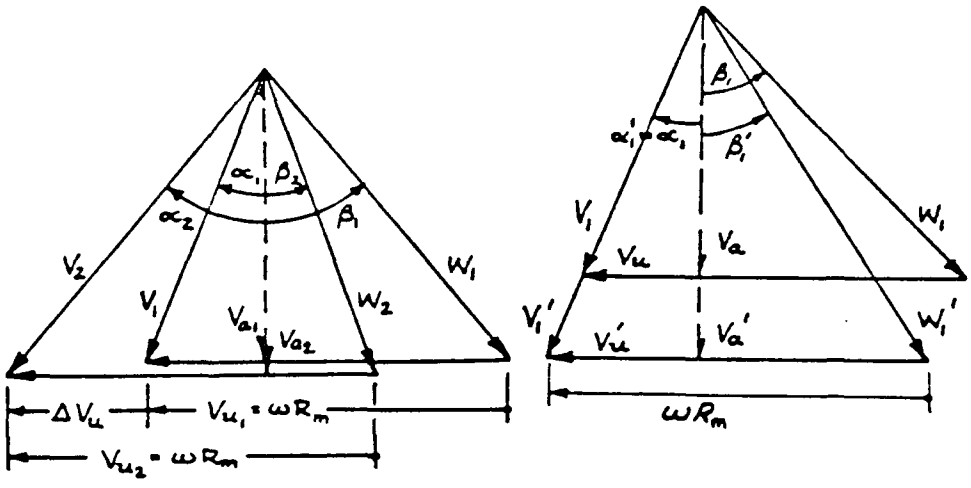

Fig. C.1-1 (a) Design velocity diagram for the symmetric blading. (b) Modified velocity diagram for off-design conditions in the symmetric stage (from Vavra, Pucci and Schlachter (1973)).

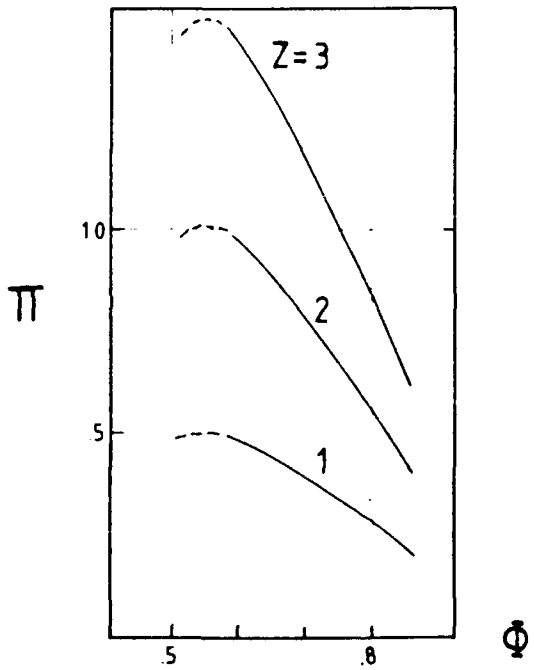

Fig. C.1-2 Stage design pressure rise flow rate characteristic based on off-design velocity diagram and loss correlation for different numbers of stages (Z).

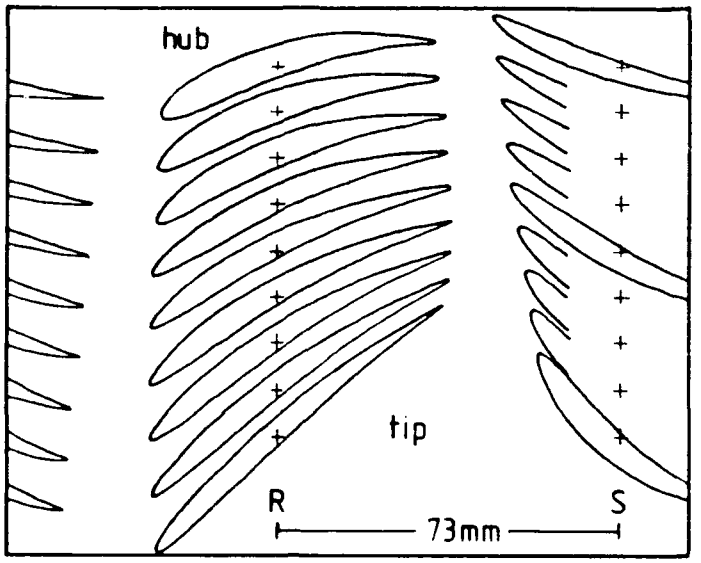

Fig. C.1-3 Rotor and stator section profiles on cylindrical surfaces from hub to tip.

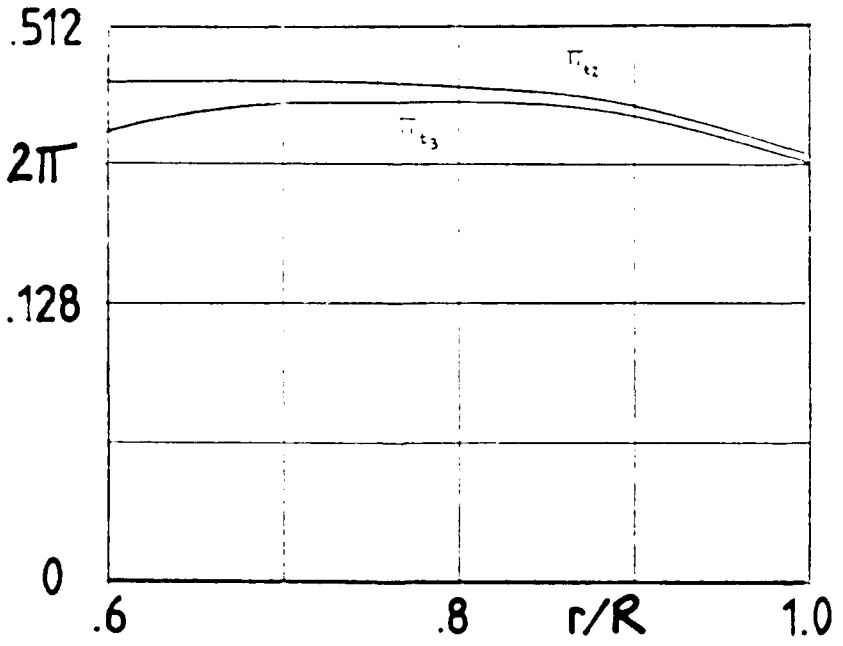

Fig. C.1-4 Spanwise distributions of pressure coefficient based on design loss coefficient distribution.

INITIAL DISTRIBUTION LIST

1. Commander
   Naval Air Systems Command
   Washington, DC 20361
   Attention: Code AIR 530T 1
   Code AIR 536T 1
   Code AIR 5004 1

2. Office of Naval Research 1
   800 N. Quincy Street
   Arlington, VA 22217
   Attention: Dr. Jack Hansen

3. Commanding Officer 1
   Naval Air Warfare Center
   Aircraft Division, Trenton: PE-31
   250 Phillips Blvd.
   Princeton Crossroads
   Trenton, NJ 08628-0176
   Attention: G. Mangano

4. Commanding Officer 1
   Naval Air Development Center
   Warminster, PA 19112
   Attention: AVTD

5. Library 1
   Army Aviation Material Laboratories
   Department of the Army
   Fort Eustis, VA 23604

6. Dr. Arthur J. Wennerstrom 1
   AFWAL/POTX
   Wright-Patterson AFB
   Dayton, OH 45433

7. Air Force Office of Scientific Research 1
   AFOSR/NA
   Bolling Air Force Base
   Washington, DC 20332
   Attention: MAJ. Daniel B. Fant

8. National Aeronautics and Space Administration
   Lewis Research Center
   21000 Brookpark Road
   Cleveland, OH 44135
   Attention: Chief, Internal Fluid Mechanics Division 1
   Library 1
   N. Sanger MS 5-11 1
   J. Adamcyzk MS 5-11 1

9. General Electric Company — 1
TIC, N-32
1 Neumann Way
Cincinnati, OH 45215

10. Library — 1
Pratt and Whitney Aircraft Group
P.O. Box 2691
West Palm Beach, FL 33402

11. Library — 1
Pratt and Whitney Aircraft Group
East Hartford, CT 06108

12. Library — 1
Curtis Wright Corporation
Woodridge, NJ 07075

13. Library — 1
AVCO/Lycoming
550 S. Main Street
Stratford, CT 06497

14. Library — 1
Teledyne CAE
Turbine Engines
1330 Laskey Road
Toledo, OH 43612

15. Library — 1
Williams International
P.O. Box 200
Walled Lake, MI 48088

16. Allison Gas Turbine Division — 1
General Motors Corporation
P.O. Box 420
Indianapolis, IN 46206-0420
Attention: Dr. R.A. Delaney

17. Library — 1
Garrett Turbine Engine Company
111 S. 34th Street
P.O. Box 5217
Phoenix, AZ 85010

18. Professor J.P. Gostelow — 1
School of Mechanical Engineering
The New South Wales Institute of Technology
New South Wales
Australia

19. Dr. G.T. Walker — 1
Civil and Mechanical Engineering Department
The University of Tasmania
Box 252C
GPO Hobart, Tasmania 7110
Australia

20. Professor F.A.E. Breugelmans — 1
Institut von Karman de la Dynamique des Fluides
72 Chausee de Waterloo
1640 Rhode-St. Genese
Belgium

21. Professor Ch. Hirsch — 1
Vrije Universiteit Brussel
Pleinlaan 2
1050 Brussels
Belgium

22. National Aeronautics and Space Administration
AMES Research Center
Moffett Field, CA 94035
Attention: Library — 1

23. Dr. John Denton — 1
Whittle Laboratory
Department of Engineering
Cambridge University
England

24. Library — 1
ONERA
29 Ave. de la Division Leclerc
92 Chatillon
France

25. Professor D. Adler — 1
Technion Israel Institute of Technology
Department of Mechanical Engineering
Haifa 32000
Israel

26. Dr. P.A. Paranjpe — 1
Head, Propulsion Division
National Aeronautics Laboratory
Post Bag 1700
Bangalore - 17
India

27. Professor Leonhard Fottner — 1
Department of Aeronautics and Astronautics
German Armed Forces University
Hochschule des Bundeswehr
Werner Heisenbergweg 39
8014 Neubiberg near Munich
Germany

28. Professor Dr. Ing. Heinz E. Gallus — 1
Lehrstuhl und Institut feur Strahlantiebe
und Turbourbeitsmashinen
Rhein.-Westf. Tech. Hochschule Aachen
Templergraben 55
5100 Aachen
Germany

29. Dr. Ing. Hans-J. Heinemann — 1
DFVLR-AVA
Bunsenstrasse 10
3400 Geottingen
Germany

30. Dr. H. Weyer — 1
DLR
Linder Hohe
505 Porz-Wahn
Germany

31. United Technologies Research Center
East Hartford, CT 06108
Attention: Dr. R.P. Dring — 1

32. Director, Gas Turbine Laboratory — 1
Aeronautics and Astronautics Department
31-265 Massachusetts Institute of Technology
Cambridge, Massachusetts 02139

33. Dr. B. Lakshminarayana — 1
Professor of Aerospace Engineering
The Pennsylvania State University
233 Hammond Building
University Park, PA 16802

34. Mr. R.A. Langworthy — 1
Army Aviation Material Laboratories
Department of the Army
Fort Eustis, VA 23604

35. Mechanical Engineering Department
Virginia Polytechnic Institute and
State University
Blacksburg, VA 24061
Attention: Professor W. O'Brien 1
Professor H. Moses 1
Professor J. Moore 1

36. Professor T.H. Okiishi 1
Professor of Mechanical Engineering
208 Mechanical Engineering Building
Iowa State University
Ames, Iowa 50011

37. Dr. Fernando Sisto 1
Professor and Head of Mechanical
Engineering Department
Stevens Institute of Technology
Castle Point
Hoboken, NJ 07030

38. Dr. Leroy H. Smith, Jr. 1
Manager, Compressor and Fan
Technology Operation
General Electric Company
Aircraft Engine Technology Division
DTO Mail Drop H43
Cincinnati, OH 45215

39. Dr. W. Tabakoff 1
Professor
Department of Aerospace Engineering
University of Cincinnati
Cincinnati, OH 45221

40. Mr. P. Tramm 1
Manager, Research Labs
Detroit Diesel Allison Division
General Motors
P.O. Box 894
Indianapolis, IN 46206

41. Defense Technical Information Center 1
Cameron Station
Alexandria, VA 22314

42. Naval Postgraduate School
Monterey, CA 93943-5000
Attention: Professor M.F. Platzer (AA/Pl) 1
Turbopropulsion Laboratory (AA/Sf) 10
Library 2
Research Administration (08) 1

43. EXOTECH PTY. LTD. 2
2625 Cabot Court
Fremont, CA 94538-1405
Attention: Dr. I. N. Moyle